



INSA



SAPIENZA
UNIVERSITÀ DI ROMA

N°d'ordre NNT : 2022LYSEI009

THESE de DOCTORAT DE L'UNIVERSITE DE LYON

opérée au sein de

Institut National des Sciences Appliquées de Lyon

En cotutelle internationale avec

La Sapienza - Università di Roma

Ecole Doctorale N° 162

Mécanique, Energétique, Génie Civil, Acoustique (MEGA)

Spécialité: Génie Mécanique

Soutenue à huis clos le 28/02/2022, par :

Alessandro Lazzari

Vibrational and frictional aptitude of C/C materials in presence of a rheological and physico-chemical active interface

Devant le jury composé de :

Bueno, Marie-Ange	Professeure	Université de Haute-Alsace	Présidente
Meziane, Anissa	Professeure	Université de Bordeaux	Rapporteuse
Renouf, Mathieu	Chargé de Recherche	Université de Montpellier	Rapporteur
Baillet, Laurent	Professeur	Université Grenoble Alpes	Examineur
Gadiou, Roger	Professeur	Université de Haute-Alsace	Examineur
Akay, Adnan	Professeur	Bilkent University	Examineur
Saulot, Aurélien	Professeur	Insa de Lyon	Directeur de thèse
Massi, Francesco	Professeur	Sapienza University of Rome	Directeur de thèse
Dubois, Sandra	Ingénieure	Safran Landing Systems	Invitée

Département FEDORA – INSA Lyon - Ecoles Doctorales

SIGLE	ECOLE DOCTORALE	NOM ET COORDONNEES DU RESPONSABLE
CHIMIE	<u>CHIMIE DE LYON</u> https://www.edchimie-lyon.fr Sec. : Renée EL MELHEM Bât. Blaise PASCAL, 3e étage secretariat@edchimie-lyon.fr	M. Stéphane DANIELE C2P2-CPE LYON-UMR 5265 Bâtiment F308, BP 2077 43 Boulevard du 11 novembre 1918 69616 Villeurbanne directeur@edchimie-lyon.fr
E.E.A.	<u>ÉLECTRONIQUE, ÉLECTROTECHNIQUE, AUTOMATIQUE</u> https://edeea.universite-lyon.fr Sec. : Stéphanie CAUVIN Bâtiment Direction INSA Lyon Tél : 04.72.43.71.70 secretariat.edeea@insa-lyon.fr	M. Philippe DELACHARTRE INSA LYON Laboratoire CREATIS Bâtiment Blaise Pascal, 7 avenue Jean Capelle 69621 Villeurbanne CEDEX Tél : 04.72.43.88.63 philippe.delachartre@insa-lyon.fr
E2M2	<u>ÉVOLUTION, ÉCOSYSTÈME, MICROBIOLOGIE, MODÉLISATION</u> http://e2m2.universite-lyon.fr Sec. : Sylvie ROBERJOT Bât. Atrium, UCB Lyon 1 Tél : 04.72.44.83.62 secretariat.e2m2@univ-lyon1.fr	M. Philippe NORMAND Université Claude Bernard Lyon 1 UMR 5557 Lab. d'Ecologie Microbienne Bâtiment Mendel 43, boulevard du 11 Novembre 1918 69 622 Villeurbanne CEDEX philippe.normand@univ-lyon1.fr
EDISS	<u>INTERDISCIPLINAIRE SCIENCES-SANTÉ</u> http://ediss.universite-lyon.fr Sec. : Sylvie ROBERJOT Bât. Atrium, UCB Lyon 1 Tél : 04.72.44.83.62 secretariat.ediss@univ-lyon1.fr	Mme Sylvie RICARD-BLUM Institut de Chimie et Biochimie Moléculaires et Supramoléculaires (ICBMS) - UMR 5246 CNRS - Université Lyon 1 Bâtiment Raulin - 2ème étage Nord 43 Boulevard du 11 novembre 1918 69622 Villeurbanne Cedex Tél : +33(0)4 72 44 82 32 sylvie.ricard-blum@univ-lyon1.fr
INFOMATHS	<u>INFORMATIQUE ET MATHÉMATIQUES</u> http://edinfomaths.universite-lyon.fr Sec. : Renée EL MELHEM Bât. Blaise PASCAL, 3e étage Tél : 04.72.43.80.46 infomaths@univ-lyon1.fr	M. Hamamache KHEDDOUCI Université Claude Bernard Lyon 1 Bât. Nautibus 43, Boulevard du 11 novembre 1918 69 622 Villeurbanne Cedex France Tél : 04.72.44.83.69 hamamache.kheddouci@univ-lyon1.fr
Matériaux	<u>MATÉRIAUX DE LYON</u> http://ed34.universite-lyon.fr Sec. : Yann DE ORDENANA Tél : 04.72.18.62.44 yann.de-ordenana@ec-lyon.fr	M. Stéphane BENAYOUN Ecole Centrale de Lyon Laboratoire LTDS 36 avenue Guy de Collongue 69134 Ecully CEDEX Tél : 04.72.18.64.37 stephane.benayoun@ec-lyon.fr
MEGA	<u>MÉCANIQUE, ÉNERGÉTIQUE, GÉNIE CIVIL, ACOUSTIQUE</u> http://edmega.universite-lyon.fr Sec. : Stéphanie CAUVIN Tél : 04.72.43.71.70 Bâtiment Direction INSA Lyon mega@insa-lyon.fr	M. Jocelyn BONJOUR INSA Lyon Laboratoire CETHIL Bâtiment Sadi-Carnot 9, rue de la Physique 69621 Villeurbanne CEDEX jocelyn.bonjour@insa-lyon.fr
ScSo	<u>ScSo*</u> https://edsciencessociales.universite-lyon.fr Sec. : Mélina FAVETON INSA : J.Y. TOUSSAINT Tél : 04.78.69.77.79 melina.faveton@univ-lyon2.fr	M. Christian MONTES Université Lumière Lyon 2 86 Rue Pasteur 69365 Lyon CEDEX 07 christian.montes@univ-lyon2.fr

*ScSo : Histoire, Géographie, Aménagement, Urbanisme, Archéologie, Science politique, Sociologie, Anthropologie

Acknowledgements

This thesis work has been carried out in collaboration between the Sapienza University of Rome and the INSA of Lyon. I would firstly like to thank these institutions, for having made this research project possible, and the French National Association of Research and Technology (ANRT), for its support to this work through the CIFRE convention N. 2018/1016.

I want to express my sincerest gratitude and warmest thanks to my Italian and French supervisors, Prof. Francesco Massi and Prof. Aurélien Saulot, without whom the completion of this work would have been impossible. Their valuable guidance and advice allowed me to overcome any obstacle and attain the most challenging objectives. I would like to express a special thanks to Francesco Massi, whose commitment to research and admirable attitude to support his students and collaborators, at the human and professional level, inspired me towards the past three years. I also would like to thank Sandra Dubois, who gave me the opportunity to work on such an intriguing research project, and Anne Bessette, for her advice and contribution to this thesis work.

I also sincerely thank the reviewers, Prof. Anissa Meziane and Dr. Mathieu Renouf, for their comments and valuable insights. My sincere thanks also go to all the committee members, for having made my PhD defense an enjoyable moment of discussion and constructive exchange.

A special thanks also goes to all researchers, professors and friends that I had the opportunity and pleasure to meet during these years at the DIMA. Among them, I would like to express my deep gratitude to Davide, for his timely suggestions and valuable support and Ilaria, for the pleasant time spent together in the laboratory and for her meaningful help during this journey. My warmest thanks also goes to Francesco, Livia and Matteo, for all the fun moments and the stimulating discussions.

I would also like to extend my heartfelt thanks to all colleagues and friends at the LaMCoS. Among them, I would like to mention Tudor, Adriana, Gregorio, Samy, Pierrick, Martial, Loïc, Lucas, Valentin, Olivier, Nathalie, Marjolaine, Anaïs, Georges, Fan, Sarra and Benoit. With them, I felt at home.

A special thanks also goes to Amandine, for her kindness and precious assistance in the laboratory.

Last but certainly not least, I would like to thank my family, without whom none of this would have been possible. This thesis is dedicated to them.

Cotutelle agreements

ACCORD DE COOPERATION POUR LA MISE EN ŒUVRE D'UNE COTUTELLE DE THESE

L'Université de Rome "La Sapienza" ayant son siège à Rome (Italie), Piazzale Aldo Moro 5, représentée par son Recteur Professeur Eugenio GAUDIO agissant en-qualité et en vertu des pouvoirs qui lui sont conférés d'une part

ET

L'INSA de LYON, représenté par Monsieur Eric MAURINCOMME, Directeur de l'établissement, agissant en-qualités et en vertu des pouvoirs qui lui sont conférés, d'autre part

Pour la partie italienne :

- Vue la délibération du Sénat Académique du 2 octobre 2003 ;
- Vue la Loi 240/2010 art. 19 – dottorato di ricerca;
- Vu le D.M. 45/2013 relatif aux normes en matière de doctorat de recherche ;
- Vu le Règlement de l'Université en matière de doctorat de recherche ;

ET

Vu pour la part française :

- Vu le code de l'éducation, notamment ses articles L.612-7, L. 613-1, D. 613-3, D. 613-6, D613-18 et D613-19 ;
- Vu le code de la recherche, notamment son article L.412-1 ;
- Vu le décret n° 2015-127 du 5 février 2015 portant approbation des statuts de la communauté d'universités et établissements « Université de Lyon »
- Vu l'arrêté du 25 mai 2016 fixant le cadre national de la formation et les modalités conduisant à la délivrance du diplôme national de doctorat
- Vu la charte du doctorat de l'Université de Lyon avec avenant INSA Lyon
- La convention cadre franco-italienne entre la Conférence des Présidents d'Université (CPU) et la Conferenza dei Rettori delle Università Italiane (CRUI) sur la reconnaissance des diplômes et validation des titres universitaires signée en date 18 janvier 1996;
- La convention cadre franco-italienne entre la Conférence des Présidents d'Université (CPU) e la Conferenza dei Rettori delle Università Italiane (CRUI) sur la co-tutelle de thèse signée le 13 février 1998;

désireux de contribuer à l'instauration et/ou au développement de la coopération scientifique entre équipes de recherche italiennes et étrangères en favorisant la mobilité des doctorants, sont convenu(e)s des dispositions suivantes :

Titre I – Modalités administratives

Art. 1 – L'Université de Rome "La Sapienza" et L'INSA de Lyon désignées ci-après "les établissements", décident dans le respect des lois et des règlements en vigueur dans chacun des pays et/ou établissements, d'organiser conjointement une cotutelle de thèse au bénéfice de l'étudiant désigné ci-après:

Prénom et nom : Alessandro LAZZARI

Spécialité : Ingenieur Mécanique – Doctorat en Meccanica Teorica ed Applicata

Sujet de thèse : **Aptitude / capacité vibratoire surfacique des matériaux C/C en présence d'une couche « 3/1 »**

La vibration induite par un contact frottant est une problématique ancienne, mettant en jeu plusieurs disciplines comme la tribologie, la mécanique vibratoire ou la mécanique de la rupture. Une branche importante des problématiques scientifiques et industrielles est liée aux instabilités vibratoires engendrées par les contacts. Dans plusieurs disciplines et champs d'applications, l'analyse et les contrôles des instabilités de contact est un sujet au cœur de la recherche actuelle. Ces phénomènes vibratoires, souvent non désirés car avec des répercussions négatives, sont les résultats des différents phénomènes physiques ayant lieu à l'échelle du contact et à celle du système, et dont les couplages complexes nécessite une phase de compréhension. Dans ce contexte, ce travail de thèse propose l'analyse et la reproduction des instabilités vibratoires induites par le contact sera couplée avec l'analyse des phénomènes physicochimiques en surface, qui caractérisent le comportement en frottement des matériaux composite C-C.

➤ Contexte de l'étude :

o Conditions de financement :

Le doctorant est salarié dans le cadre de la convention de formation par la recherche CIFRE n° 2018/1016 (France)

o Calendrier préliminaire du projet de recherche est indiqué pour les trois années :

La première année sera dédiée à un état de l'art détaillé dans la littérature liée aux différentes thématiques du projet (vibrations induites par le frottement, instabilités de contact, physicochimie des composites CC, ...). Pendant cette phase, le doctorant sera amené à prendre en main différents outils d'analyse en dynamique (instrumentation de mesure, post-processing des signaux, ...) et en tribologie (microscopes optique et électronique, spectroscope, ...).

La deuxième année une partie substantielle des travaux de thèse portera sur la reproduction et l'analyse de la propension des matériaux C-C à engendrer des instabilités vibratoires. Différentes campagnes d'essais seront reproduites. En parallèle des essais et analyses expérimentales une modélisation numérique sera développée pour la reproduction de la dynamique (génération et propagation d'ondes) locale au contact, en liens avec les essais expérimentaux.

La troisième année les différents résultats sur banc d'essais, avec les corrélations entre i) réponse en frottement macroscopique, ii) réponse vibratoire et iii) réponse physicochimique des interfaces, permettront une synthèse pour la corrélation des phénomènes locaux au contact avec des variables macroscopiques à l'échelle du système. En outre, un résumé final, une écriture du manuscrit et une soutenance de thèse sont prévus.

o Les modalités d'encadrement, de suivi de la formation et d'avancement du doctorant :

Les rencontres avec les directeurs de thèse (Francesco MASSI et Aurélien SAULOT) auront une périodicité d'une fois toutes les deux semaines minimum. Tout le long de la durée de la

thèse le doctorant produira des rapports et présentations intermédiaires pour le suivi du travail. Chaque année, une présentation en face du collège des professeurs du doctorat en « Meccanica Teorica ed Applicata » est obligatoire pour l'inscription à l'année suivante.

o Conditions matérielles de réalisation du projet :

Le projet sera développé principalement sur les sites du LaMCoS de l'INSA de Lyon et du département DIMA de l'Université de Rome La Sapienza. Les bancs d'essais, déjà présents dans le locaux des deux établissements, seront dédiés à l'exécution des campagnes expérimentales, Une ordinateur et les licences des codes numériques nécessaires seront mise à disposition du doctorant.

Les principes et les modalités administratives et pédagogiques de cette cotutelle sont définis par le présent accord.

Art. 2 - La durée de préparation de la thèse est normalement de trois ans. La durée de préparation du doctorat peut être au plus de six ans.

Un avenant sera rédigé au moins 6 mois avant la date de fin prévue initialement. Des périodes de recherche alternées auront lieu dans chacun des établissements. Le calendrier et la durée des séjours seront détaillés à l'article 8 de la présente convention. La durée minimale de préparation effectuée dans un établissement ne peut normalement être inférieure à une année. La durée prévue pour la préparation de la thèse en cotutelle est de 3 ans, à partir de l'année scolaire 2018/2019.

Art. 3 - La préparation de la thèse s'effectue par périodes alternées, à peu près équivalentes, dans chacun des deux établissements partenaires. La durée de ces périodes sera déterminée de commun accord par les deux directeurs de thèse.

Art. 4 – Le doctorant est inscrit en thèse dans chacun des deux établissements co-contractants sous le régime de la collaboration internationale à partir de l'année universitaire **2018-2019**.

Le doctorant sera inscrit administrativement dans chacun des deux établissements dès que toutes les conditions nécessaires à son inscription seront réunies.

Le doctorant est inscrit en thèse de doctorat de l'Université de Lyon, opéré au sein de l'INSA Lyon, au sein de l'Ecole Doctorale MEGA à compter de la rentrée universitaire 2018-2019.

Art.5 – Le doctorant acquitte, chaque année, ses droits d'inscription dans un des établissements. Il est exempté de ces droits dans l'autre établissement. Sur la durée de la thèse, le doctorant doit obligatoirement s'acquitter de ses droits d'inscription au moins une fois dans chaque établissement; l'acquittement desdits droits est une condition de validité de la cotutelle internationale. Le doctorant doit fournir chaque année les justificatifs d'inscription, s'ils existent, en doctorat à l'établissement pour lequel il en est exonéré.

Art.6 – Le doctorant est soumis à la réglementation en vigueur sur la couverture sociale dans le pays où il acquitte les droits d'inscription. Dans celui où il est exonéré, il doit justifier également d'une couverture analogue, et doit en produire les justificatifs au moment de son inscription administrative dans chaque établissement. Il s'engage par ailleurs à souscrire une « responsabilité civile vie privée » obligatoire en France. Ces assurances conditionnent l'inscription administrative.

Une assurance couvrant ses déplacements entre les deux pays est par ailleurs vivement conseillée.

Art.7 – Lors de son inscription, le doctorant devra fournir les justificatifs relatifs à ses ressources, à sa couverture sociale ainsi qu'à son assurance relative aux accidents du travail, dans chacun des pays,

Conformément à la Charte du Doctorat de l'UdL avec avenant INSA, un revenu minimum pendant les périodes de séjour en France, conforme à celui mentionné dans la Charte du doctorat conditionne l'inscription en doctorat à l'INSA Lyon. Ce revenu doit être au moins équivalent au SMIC.

Dans le cas où le doctorant serait dans l'incapacité de présenter les justificatifs de financement nécessaires à son inscription, l'INSA Lyon pourra prononcer de plein droit la résiliation de la présente convention.

Art. 8 – Pour les périodes d'études effectuées en France et pour la soutenance, le doctorant bénéficie de l'ensemble des dispositions de l'arrêté du 7 août 2006 susvisé, et de la charte des thèses de l'INSA de Lyon.

Titre II – Modalités pédagogiques

Art. 1 – Le travail de thèse de l'étudiant sera réalisé sous la supervision commune de deux directeurs de thèse :

- Francesco MASSI (Professeur au Dipartimento di Ingegneria Meccanica e Aerospaziale), directeur de thèse à l'Université "La Sapienza" ;
- Aurélien SAULOT (Maître de conférences, HdR, au Laboratoire de Mécanique des Contacts et des Structures), directeur de thèse à l' INSA de Lyon ;

qui s'engagent à exercer pleinement la fonction de tuteurs de la candidate ainsi qu'à formuler chacun un avis écrit sur la thèse de Doctorat.

L'avis favorable des deux Directeurs de Thèse est une condition nécessaire à l'admission à l'examen final.

Art. 2- La thèse donnera lieu à une soutenance unique, reconnue par les deux établissements concernés. La soutenance aura lieu à l'INSA de Lyon. Le jury de soutenance est composé sur la base d'une proportion équilibrée de membres de chaque établissement désigné conjointement par les établissements contractants et comprend, en outre, des personnalités extérieures à ces établissements. Il comprendra au moins quatre membres et au maximum huit, dont la moitié au moins sont des personnalités extérieures aux établissements signataires de la cotutelle. Les autres membres sont désignés sur la base d'une proportion équilibrée de membre de chaque établissement désigné conjointement par les établissements contractants. La parité homme/femme devra se conformer aux conditions requises par les deux établissements contractants. Conformément à l'arrêté du 25 mai 2016, "le directeur de thèse participe au jury, mais ne prend pas part à la décision". Le directeur de thèse, comme les co-encadrants, n'ont pas à sortir pendant les délibérations, ils peuvent prendre part aux discussions préliminaires mais doivent s'abstenir lors de la délibération et du vote final.

Art. 3 - La thèse sera rédigée et discutée en Anglais. Elle comportera un résumé substantiel rédigé en Français et en Italien.

Art. 4 – En cas de rapport favorable du Jury, chacun des deux établissements s'engage à conférer le titre de docteur de recherche pour la même thèse.

L'Université de Rome "La Sapienza" s'engage à conférer le grade de docteur de recherche en Meccanica Teorica e Applicata.

L'INSA de Lyon s'engage à conférer le grade de docteur de recherche en Mécanique.

Art. 5- Lorsque le doctorant doit valider des formations complémentaires (scientifiques ou visant à son insertion professionnelle), les établissements (l'Ecole Doctorale MEGA pour l'INSA LYON) préciseront les modalités de reconnaissance mutuelle de ces formations, en accord avec les directeurs de thèse et le doctorant. Les Obligations de formation en cas de cotutelle pour l'ED MEGA sont les suivantes :

- 6h de formation scientifique

- 2 séminaires

-12 h de cours parmi les cours de l'université de Lyon au niveau formations transversales.

Titre III – Conclusions

Art. 1 – L'étudiant est tenue de respecter les règlements et les usages de l'établissement d'accueil.

Art. 2 – Par l'intermédiaire de leurs directeurs de thèses respectifs, les établissements signataires s'engagent à se communiquer toutes les informations et la documentation utiles à l'organisation de la cotutelle de thèse faisant l'objet du présent accord.

Art. 3 – Les modalités de présentation, de dépôt et de reproduction de la thèse seront établies dans chaque pays dans le respect de la réglementation en vigueur.

La protection du sujet de thèse, ainsi que la publication, l'exploitation et la protection des résultats issus des travaux de recherche du doctorant dans les deux établissements signataires seront assujetties à la réglementation en vigueur et assurées conformément aux procédures spécifiques à chacun des pays impliqués dans la cotutelle.

Sur demande, les dispositions concernant la protection des droits de propriété intellectuelle pourront faire l'objet de protocoles ou de documents spécifiques.

Art. 4 – Le présent accord entre en vigueur à partir de la date de signature du représentant légal de chaque établissement signataire et le reste jusqu'à la fin de l'année universitaire au cours de laquelle la thèse ou les travaux seront soutenus. Dans le cas où l'étudiant ne serait pas inscrite dans l'un et/ou l'autre des établissements signataires, ou bien renoncerait par écrit à poursuivre, ou bien n'est pas autorisée à poursuivre la préparation de sa thèse en vertu de la décision de l'un au moins des deux directeurs de thèse, les deux établissements signataires mettront fin conjointement et sans délai, aux dispositions du présent accord.

Art. 5 – Le présent accord est rédigé en six exemplaires originaux, dont trois en italien et trois en française, faisant également foi.

Roma, li _____

Pour le Recteur de l'Université
La Sapienza de Rome



Il Coordinatore del Dottorato di Ricerca
Antonio CARCATERRA

[Handwritten signature of Antonio Carcaterra]

Il Co-direttore di tesi
Francesco MASSI

[Handwritten signature of Francesco Massi]

Le Doctorant
Alessandro LAZZARI

[Handwritten signature of Alessandro Lazzari]

Villeurbanne, li 1^{ER} février 2019

Pour le directeur de l'INSA de Lyon
Florence POPOWYCZ
Directrice Adjoint de la Recherche
Et des Etudes Doctorales

Le Responsable de l'Ecole Doctorale
Jocelyn BONJOUR

Le Directeur du laboratoire
Daniel NELIAS

Co-directeur (s) de thèse
Aurélien SAULOT



[Handwritten signatures of Jocelyn Bonjour and Aurélien Saulot]

Résumé

De nos jours, l'intérêt croissant pour les composites carbone-carbone (C/C), dans un nombre important de contextes industriels, a conduit à une augmentation importante des travaux de recherche visant à étudier de tels matériaux. Les composites en C/C étant utilisés dans plusieurs applications industrielles, telles que les freins à disque hautes performances, un nombre considérable d'études se sont concentrés sur leurs propriétés tribologiques. Néanmoins, malgré le grand nombre de travaux traitant de ce sujet, très peu de recherches ont été menées à ce jour sur la relation entre la réponse en frottement des matériaux en C/C et l'apparition de vibrations instables induites par frottement, en fonction des principaux paramètres de contact (par exemple, vitesse de glissement, température, pression de contact, etc.). Cependant, comprendre et prédire l'apparition de phénomènes vibratoires indésirables, qui se produisent lors du contact de glissement des composites en C/C, est l'un des plus grands défis à relever pour améliorer les performances de freinage.

À cet égard, l'étude des vibrations induites par le frottement implique de multiples domaines scientifiques, et ceci compte tenu notamment des caractéristiques physico-chimiques complexes des composites en C/C et de la forte influence des conditions d'exploitation sur la réponse de frottement de tels matériaux. De plus, l'impact significatif du troisième corps sur leur comportement tribologique nécessite une connaissance approfondie des mécanismes rhéologiques affectant le coefficient de frottement et l'apparition d'instabilités dynamiques de contact.

Dans ce cadre de recherche, la présente thèse de doctorat a pour objectif d'étudier et de caractériser l'apparition de vibrations instables induites par frottement entre matériaux en C/C, et ceci pour différentes conditions de contact. Le comportement en frottement, et sa relation avec l'apparition d'instabilités dynamiques, a été étudié sur des tribomètres linéaires visant à caractériser des éprouvettes en C/C dans des conditions aux limites contrôlées. Des bancs d'essais spécialement conçus ont permis d'étudier la réponse tribologique et vibratoire d'échantillons en C/C, portée sur le rôle de la température (jusqu'à environ 500 °C) mais aussi de la vitesse de glissement et de l'environnement d'essai. Des informations significatives, jusqu'à présent absentes de la littérature, concernant la nature et les principales caractéristiques des instabilités dynamiques causées par les matériaux en C/C en contact glissant, sont présentées dans ce travail. De plus, des modèles numériques ont été développés, afin d'étudier les principales caractéristiques des différents phénomènes vibratoires. À cet égard, le présent travail propose une nouvelle approche, basée sur l'analyse du déphasage entre les signaux vibratoires, afin de distinguer l'apparition d'un couplage modal ou d'une instabilité due au gradient négatif frottement-vitesse, ainsi que la coexistence des deux phénomènes.

Une attention particulière est également portée sur le rôle du troisième corps et son apport rhéologique. L'effet des contaminants métalliques et non métalliques a été étudié en détail et des échantillons de matériaux en C/C, avec des particules contaminantes sur la surface de friction, ont été testés dans des conditions aux limites contrôlées. La relation entre la contribution rhéologique à la réponse en frottement et l'apparition d'instabilités dynamiques en présence de conditions aux limites distinctes a ensuite été étudiée. Les résultats obtenus ont permis d'élaborer différents scénarios décrivant le comportement tribologique des matériaux en C/C et l'apparition de vibrations instables induites par frottement, en tenant compte de la rhéologie du contact lors du freinage.

Cette thèse de doctorat a été réalisée en collaboration entre l'Université La Sapienza de Rome, au Département d'Ingénierie Mécanique et Aérospatial (Rome, Italie) et l'Institut National des Sciences Appliquées (INSA) de Lyon, au laboratoire LaMCoS (Lyon, France).

Riassunto

Al giorno d'oggi, il crescente interesse per i materiali compositi in carbonio-carbonio (C/C), impiegati in un numero significativo di contesti industriali, ha portato ad un notevole incremento di lavori di ricerca finalizzati allo studio di tali materiali. Essendo i compositi in C/C utilizzati in molte applicazioni industriali, quali ad esempio i freni a disco ad alte prestazioni, un numero considerevole di studi è incentrato sulle loro proprietà tribologiche. Tuttavia, nonostante la grande quantità di lavori che trattano tale argomento, ad oggi poche informazioni sono reperibili sulla relazione tra la risposta tribologica dei materiali in C/C e l'insorgenza di vibrazioni instabili indotte dall'attrito, in funzione dei principali parametri di contatto (ad esempio, velocità di scorrimento, temperatura, pressione di contatto, ecc.). Ciò nonostante, comprendere e prevedere il verificarsi di fenomeni vibrazionali indesiderati, che si verificano durante il contatto strisciante dei materiali compositi in C/C, è una delle maggiori sfide al fine di migliorarne le prestazioni.

A questo proposito, lo studio delle vibrazioni indotte dall'attrito coinvolge molteplici discipline, soprattutto considerando le complesse caratteristiche fisico-chimiche dei compositi in C/C e la forte influenza delle condizioni operative sulla risposta d'attrito di tali materiali. Inoltre, l'impatto significativo del terzo corpo sul loro comportamento tribologico richiede una profonda conoscenza dei meccanismi reologici, che ne influenzano il risultante coefficiente di attrito e il verificarsi di instabilità dinamiche di contatto.

All'interno di questo quadro di ricerca, la presente tesi di dottorato si propone di indagare e caratterizzare l'insorgenza di vibrazioni instabili indotte dall'attrito nei materiali compositi in C/C, in diverse condizioni di funzionamento. L'evoluzione dell'attrito e la sua relazione con il verificarsi di instabilità dinamiche sono stati studiati su tribometri lineari, volti a caratterizzare provini in C/C, in condizioni al contorno controllate. Tali banchi prova, appositamente progettati, hanno permesso di studiare la risposta d'attrito e vibratoria dei provini in C/C, con particolare attenzione al ruolo della temperatura, fino a circa 500 °C, della velocità di scorrimento e dell'ambiente di prova. In questo lavoro vengono presentate informazioni significative, finora mancanti in letteratura, riguardanti la natura e le principali caratteristiche delle instabilità dinamiche causate da materiali in C/C in contatto strisciante. Inoltre, sono stati sviluppati modelli numerici allo scopo di indagare i diversi fenomeni vibratorii. A tale proposito, il presente lavoro propone un nuovo approccio, basato sull'analisi dello sfasamento tra i segnali vibrazionali, al fine di distinguere l'insorgenza di accoppiamento modale o instabilità dovuta al gradiente negativo attrito-velocità, nonché la coesistenza di entrambi i fenomeni.

Particolare attenzione viene posta anche al ruolo del terzo corpo e al suo contributo reologico. L'effetto di contaminanti metallici e non metallici è stato studiato in dettaglio e provini di materiali in C/C, con specifiche particelle contaminanti depositate sulla superficie di attrito, sono stati testati in condizioni al contorno controllate. È stata quindi indagata la relazione tra il contributo reologico alla risposta d'attrito e l'insorgenza di instabilità dinamiche in presenza di condizioni al contorno distinte. I risultati ottenuti hanno consentito di sviluppare diversi scenari che descrivono il comportamento tribologico dei materiali in C/C e l'insorgenza di vibrazioni instabili dovute all'attrito, tenendo conto dell'effettiva reologia del contatto durante la frenata.

Questa tesi di dottorato è stata svolta in collaborazione tra l'Università La Sapienza di Roma, presso il Dipartimento di Ingegneria Meccanica e Aerospaziale (Roma, Italia) e l'Institut National des Sciences Appliquées (INSA) di Lione, presso il laboratorio LaMCoS (Lione, Francia).

Abstract

Nowadays, the growing interest in carbon-carbon (C/C) composites, in a significant number of industrial contexts, has led to a major increase of research works aimed to investigate such materials. Being C/C composites used in many industrial applications, such as high-performance disc brakes, considerable numbers of studies focus on their tribological properties. Nevertheless, despite the large amount of works dealing with this topic, very few researches have been carried out so far on the relationship between the C/C frictional response and the onset of unstable friction-induced vibrations, as a function of the main contact parameters (e.g. sliding velocity, temperature, contact pressure, etc.). However, understanding and predicting the occurrence of undesired vibrational phenomena, taking place during frictional contact of C/C composites, is one of the greatest challenges in order to improve the overall braking performance.

In this regard, the study of friction-induced vibrations involves multiple scientific fields, especially considering the complex physiochemical characteristics of C/C composites and the strong influence of the operating conditions on the frictional response of such materials. Moreover, the significant impact of the third body on their tribological behavior requires a deep insight of the rheological mechanisms affecting the friction coefficient and the occurrence of contact dynamic instabilities.

Within this research framework, the present PhD thesis aims to investigate and characterize the onset of unstable friction-induced vibrations of C/C materials, under different contact conditions. Their frictional response and its relationship with the occurrence of dynamic instabilities have been investigated on linear tribometers aimed to characterize C/C specimens, under controlled boundary conditions. The specifically designed test benches have allowed studying the frictional and vibrational response of C/C samples, with particular attention on the role of temperature, up to almost 500 °C, sliding velocity and test environment. Meaningful information, so far missing in the literature, concerning the nature and the main characteristics of the dynamic instabilities caused by C/C materials in frictional contact, are presented in this work. Moreover, numerical models have been developed, in order to investigate the main features of the different vibrational phenomena. In this respect, the present work proposes a novel approach, based on the analysis of the phase shift between vibrational signals, in order to distinguish the onset of mode coupling or negative friction-velocity slope instabilities, as well as the coexistence of both phenomena.

Particular attention is also given to the role of the third body and its rheological contribution. The effect of metallic and non-metallic contaminants has been investigated as well, by contaminating the frictional surface of C/C material samples, tested under controlled boundary conditions. The relationship between the rheological contribution to the frictional response and the onset of dynamic instabilities in presence of distinct boundary conditions has been then investigated. The obtained results have allowed developing different scenarios describing the C/C tribological behavior and the occurrence of unstable friction-induced vibrations, taking into account the rheology of the contact during braking.

This PhD thesis has been carried out in collaboration between the Sapienza University of Rome, at the Department of Mechanical and Aerospace Engineering (Rome, Italy) and the Institut National des Sciences Appliquées (INSA) of Lyon, at the laboratory LaMCoS (Lyon, France).

Keywords: C/C materials, Friction-induced vibrations, Contact instabilities, Contact rheology

Summary

Introduction

Chapter 1

C/C composite materials and friction-induced vibrations

1.1	Carbon-Carbon materials	11
1.1.1	Generalities on sp^2 carbon materials	11
1.1.2	C/C material manufacturing process	13
1.1.3	Tribological and physicochemical properties of C/C materials	15
1.1.3.1	Tribological triplet and rheology of a contact	15
1.1.3.2	Tribology and surface chemistry of sp^2 carbon materials	17
1.1.3.3	Physicochemical properties of C/C third body and wear debris	21
1.1.3.4	Influence of the metallic impurities on carbon materials	23
1.1.3.5	Numerical tribology of C/C composites	24
1.1.4	Concluding remarks	26
1.2	Dynamic instabilities in dry frictional contacts	26
1.2.1	Overview on friction-induced vibrations	28
1.2.1.1	Stable friction-induced vibrations	29
1.2.1.2	Unstable friction-induced vibrations	29
1.2.2	Frictional contact instabilities	31
1.2.2.1	Mode coupling and complex eigenvalue analysis	31
1.2.2.2	Negative Friction-Velocity Slope instability	33
1.2.2.3	Macroscopic stick-slip instability	36
1.2.3	Thermally driven instabilities on C/C materials	38
1.3	PhD positioning	40

Chapter 2

Experimental characterization under controlled boundary conditions

2.1	Experimental setup and signal analysis	43
2.1.1	Dedicated test bench	43
2.1.2	C/C material specimens	45
2.1.3	Measurement protocol and definition of the boundary conditions	47
2.1.4	Analysis of the outputs	50
2.2	Frictional and vibrational characterization	54
2.2.1	Role of temperature and imposed velocity profile	54
2.2.2	Comparison between MAT1 and MAT2	58
2.2.3	Comparison between MAT4 and MAT5	60
2.2.4	Overall discussion on tested materials (variable velocity tests)	63
2.2.5	Analysis of constant velocity tests	66
2.3	Experimental tests under controlled atmosphere	68
2.3.1	Description of the setup	68
2.3.2	Experimental protocol	70
2.3.3	Discussion of the results	72
2.4	Concluding remarks	77

Chapter 3

Experimental and numerical identification of unstable friction-induced vibrations through phase shift

3.1	Experimental Analysis	81
3.1.1	Setup and measurement protocol	81
3.1.2	Variable velocity test	86
3.1.3	Constant velocity tests	89
3.2	Numerical Analysis	91
3.2.1	Finite element analysis of the unstable modes	92
3.2.1.1	Numerical model	92
3.2.1.2	Analysis of the experimental unstable modes	94
3.2.2	Numerical analysis through a lumped-parameter model	98
3.2.2.1	Description of the model	98
3.2.2.2	Complex eigenvalues analysis	100
3.2.2.3	Transient analysis	103
3.2.2.4	Lumped-parameter model with non-linear contributions (i.e. stick-slip and detachment)	107
3.4	Concluding remarks	111

Chapter 4

Experimental analysis of the C/C material response with different third bodies

4.1	Materials and methods	114
4.1.1	C/C material with either Ox or Oy coatings	114
4.1.2	C/C material coated with Ox/Oy mixtures	116
4.1.3	Experimetal protocol	119
4.2	Main experimental outcomes	120
4.2.1	Third body with either Ox or Oy contaminants	120
4.2.1.1	Discussion on variable velocity tests	120
4.2.1.2	Discussion on constant velocity tests	124
4.2.2	Third body with Ox/Oy mixtures	126
4.2.2.1	Discussion on variable velocity tests	127
4.2.2.2	Discussion on constant velocity tests	131
4.3	SEM/EDX analysis on C/C material with 8Ox2Oy and 2Ox8Oy	132
4.4	Concluding remarks	136

Chapter 5

General conclusions

5.1	Original contributions	139
5.1.2	Analysis of the C/C frictional and vibrational response under controlled boundary conditions	139
5.1.3	Numerical characterization of the dynamic instabilities	143
5.1.4	C/C material response in presence of O_x and O_y on the contact interface	144
5.2	Overall scenario	147
5.2.1	Frictional and vibrational response for $T < 300$ °C	147
5.2.2	Frictional and vibrational response for $T > 300$ °C: role of the third body and rheology of the contact	148
5.3	Future works	153

References

Annexes

I.	SEM/EDX analysis of C/C material specimens	170
II.	Comparison between <i>sliding</i> and <i>static heating</i> tests	172

- III. Comparison between first and fourth day of the preliminary protocol 174
- IV. Comparison between C/C specimens coated with a lower amount of Ox and Oy 174

Introduction

Over the past decades, carbon fiber-reinforced carbon composites, also known as carbon–carbon (C/C) composites, have offered significant advantages in many industrial applications, compared to other more conventional materials or advanced ceramics [1]. Their excellent thermo-mechanical properties, even under harsh operational conditions, have made these materials widely used in a variety of engineering fields [2, 3]. In particular, low weight, high tribological performance and long service life of such composites have favored their widespread use as brake materials for high-speed vehicles [2].

In recent years, the growing interest in C/C brakes from many industrial manufacturers has led to wide-ranging research and development activities, aimed to investigate their main tribological features and further improve braking performances [2-4]. As outlined in many works dealing with such materials, the complex physicochemical characteristics of C/C composites affect strongly their tribological behavior [5-8]. More specifically, as a function of the operating conditions (e.g. temperature, sliding speed, environment, contact pressure, etc.), research studies have shown the occurrence of different frictional and wear regimes [5, 9-11]. The mechanisms underlying these phenomena involve several research fields and require a multidisciplinary approach to be studied and understood. Over time, the joint effort of different scientific domains, aimed to investigate the frictional response and the physicochemical features of C/C materials, has shed light on such complex scenarios and has allowed enhancing knowledge on this subject.

Nevertheless, most of the works dealing with C/C composites, in braking applications, have been primarily focused on the effect of contact parameters on the friction coefficient behavior and wear rate. As a result, in the literature, very few research studies aimed to investigate the vibrational response of C/C materials during sliding contact, under distinct boundary conditions [12]. However, the mutual interaction between the complex frictional behavior of C/C composites and the system dynamic response can often result in self-excited friction-induced oscillations, which can affect the proper functioning of the mechanical system, leading to annoying noise and vibrations. This subject requires, therefore, further investigation.

Among the main mechanisms leading to unstable friction-induced vibrations, the onset of dynamic instabilities due to negative friction-velocity gradient and mode coupling, both of them resulting from the interaction between the system dynamics and the frictional response of the material, have been the subject of many research works [13-17]. Moreover, both these phenomena can be associated also to the occurrence of macroscopic sick-slip vibrations, when the frictional and dynamic response of the system is favorable [17-20].

Despite the number of studies carried out on unstable friction-induced vibrations, in real industrial problems, it is often challenging to determine the nature of the observed dynamic instabilities, especially in presence of complex tribological scenarios, such as for C/C composites. In this respect, understanding the mechanisms leading to the undesired vibrational phenomena underlies the development of effective counter-measures and the necessary design improvements to stabilize the system.

In the literature, significant lack of knowledge concerns also the effective role of the rheology, during frictional contact of C/C materials, in both their frictional and vibrational response. Despite recent works have broaden knowledge on the third body and wear debris physicochemical features of carbonaceous materials [21-23], there is still need for a better understanding of how

carbon particles and metallic/non-metallic contaminants in a real frictional interface can affect the overall macroscopic response.

In this context, the following thesis aims to provide an overview of the prevailing frictional and dynamic phenomena of C/C materials in frictional contact, taking place under different operating conditions and in presence of specific contaminants affecting the rheology.

First, the extensive literature on C/C materials and the main mechanisms leading to unstable friction-induced vibrations are presented in Chapter 1. In this section, generalities on C/C materials, including their manufacturing process and their tribological and physicochemical main features are discussed. Moreover, an overview of friction-induced vibrations and the main frictional contact instabilities (i.e. mode coupling, negative friction-velocity slope, stick-slip) are presented as well.

Then, in order to investigate in further detail the tribological behavior of C/C materials under well-controlled boundary conditions, samples machined from C/C brake discs are tested on specifically designed test benches (Chapter 2). The frictional and vibrational responses of the specimens are studied under a wide temperature range (up to 500 °C) and for different sliding velocities. Particular attention is paid to the effect, on the material response, of metallic and non-metallic contaminants taking part in the rheology of the contact. As a function of the boundary conditions and the contaminating particles, the evolution of the friction coefficient and the onset of unstable friction-induced vibrations are analyzed in detail. Moreover, the frictional and vibrational response of C/C specimens is investigated in different atmospheres, characterized by either air or a low oxygen environment.

Once having identified the operative conditions leading to the unstable friction-induced vibrations, an in-depth analysis of the retrieved dynamic instabilities is carried out in Chapter 3. Both experimental and numerical analyses are performed in order to identify the instability scenarios and retrieve useful features for distinguishing them. For this purpose, experimental tests are carried out on C/C specimens under controlled boundary conditions and through a specifically dedicated protocol. A finite element analysis is also performed in order to investigate the unstable modes identified in the experience. Moreover, a lumped-parameter numerical model is developed with the aim of reproducing the different dynamic instabilities and analyzing the vibrational response. The analysis of the phase difference between the recorded signals is the proposed tool for distinguishing the phenomena leading to the unstable vibrations.

The last part of the thesis (Chapter 4) is devoted to the analysis of the frictional and vibrational response of C/C specimens, in presence of specific contaminants on the contact interface. Different coatings are deposited on the contacting surfaces of C/C specimen pairs in order to study the material response with diverse third bodies.

The impact of the rheology into the occurrence of different tribological behaviors of the tested material, as well as the close relationship with the onset of unstable vibrations, is then discussed in detail. Moreover, SEM/EDX analyses are carried out for characterizing the third body and further investigate the mechanisms leading to different tribological and dynamic response of the tested materials.

Lastly, a concluding section (Chapter 5) presents and synthesizes the main contributions provided by the present work. Overall scenarios, as a function of the investigated contact parameters (primarily temperature and sliding velocity) and the third body, are proposed. Perspectives for future works are presented as well.

Chapter 1

C/C composite materials and friction-induced vibrations

The main focus of the present work is the characterization of the tribological and vibrational response of C/C materials. Approaching this subject requires a thorough investigation of both the principal features of C/C materials and the main mechanisms underlying the onset of friction-induced vibrations. Therefore, the following sections provide first an overview of the literature concerning C/C materials, and their tribological properties, and then describe the main works dealing with the vibrational scenarios observed in dry contacts.

1.1 Carbon-Carbon materials

Carbon-Carbon materials are a class of composites consisting of carbon fibers embedded in a carbonaceous matrix. The development of these materials combines the advantages of a carbon fibrous reinforcement, such as high specific strength and stiffness, with the high refractory properties of a graphite-like structure [1]. The structural constituents of C/C composites belong to the family of sp^2 carbon materials, essentially characterized by stacks of parallel layers of carbon atoms, each forming a two-dimensional hexagonal network [24, 25].

In the following, the main structural characteristics of sp^2 carbon materials are discussed. Then, an overview of the manufacturing process and the main tribological and physicochemical features of C/C composites is presented.

1.1.1 Generalities on sp^2 carbon materials

In nature, carbon exists in different allotropic forms. Among them, the better known are graphite and diamond. A different state of hybridization of carbon atoms distinguishes these two allotropic forms. In a diamond, the hybridization state of s and p orbitals lead to a tetrahedral arrangement of the carbon atoms (sp^3 hybridization). On the other hand, graphite has planar hexagonal bonds and each carbon atom has a state of hybridization sp^2 . Because of the sp^2 hybridization, only three of the four carbon valence electrons are saturated in the plane. The free valence electrons of each plane form delocalized electrons, which can provide good electrical conductivity along the carbon layers. The bonds between atoms of the same layer are covalent (bond energy of almost $520 \text{ kJ}\cdot\text{mol}^{-1}$), while the bonds holding together the planes are much weaker and characterized by Van Der Waals electrostatic forces (bond energy of almost $10 \text{ kJ}\cdot\text{mol}^{-1}$) [26, 27].

The lamellar structure of graphite, presented in Figure 1.a, gives rise to carbon layers called basal plane surfaces or graphitic planes (or even graphene planes), while their edges are called prismatic surfaces. As shown in Figure 1.b, the carbon atoms located at the edge of the plans are characterized by two different configurations, the "zig-zag" or "arm-chair" geometry [27].

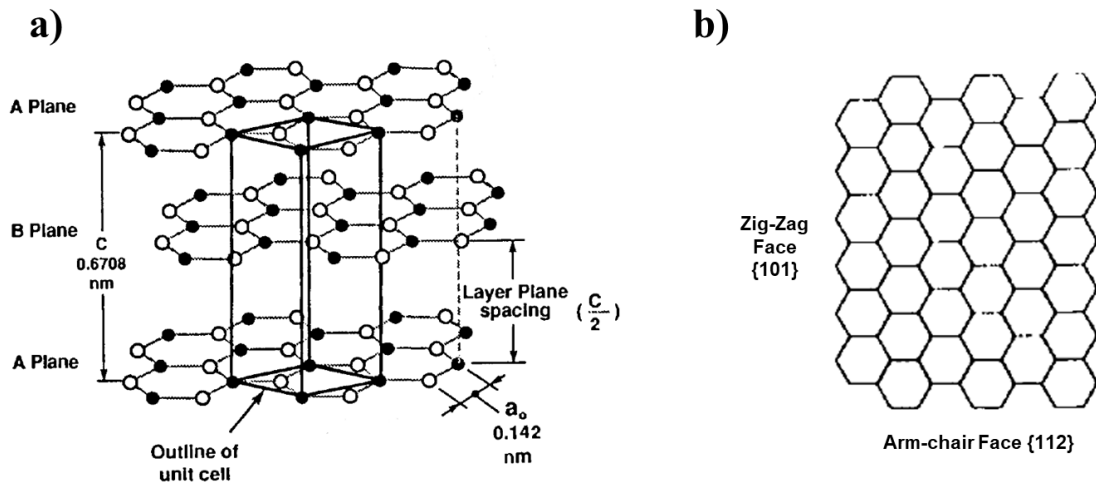


Figure 1 a) Crystal structure of hexagonal graphite; b) Zig-Zag and Arm-chair configurations of carbon edge sites. Adapted from [27].

In the ideal hexagonal graphite structure, the graphitic planes are arranged in ABAB stacking sequence. The interatomic distance between coplanar C atoms is 0.142 nm while the distance between each planar layer is equal to 0.335 nm [27, 28]. The carbon atoms characterizing the prismatic surfaces have covalent bonds only with two other carbon atoms. As a result, free valence electrons lead to dangling bonds functioning as active sites and capable of interacting with hydrogen, carbon or heteroatoms [29, 30]. Any fracture not parallel to a base plane, initiated for instance under the effect of mechanical stress, reveals such prismatic surfaces, characterized by a surface energy much higher than that of the base planes (5 J/m^2 for the prismatic plane but only 0.11 J/m^2 for the basal plane [27]).

Moreover, it should be remarked that the real structure of graphite diverges from the ABAB orderly arrangement described above for pure hexagonal graphite. The presence of structural defects, such as vacancies, stacking faults, disclinations and dislocations, leads to other active sites, where reactions with gases or vapors occurs preferentially [4, 8, 10].

In this respect, it has been observed that the prismatic surfaces and the defects of the basal planes constitute privileged sites for the chemisorption of oxygen groups [31, 32]. The oxygen functions chemisorbed on the surfaces of carbon materials are primarily involved in gasification reactions, occurring at temperatures higher than $400 \text{ }^\circ\text{C}$. The mechanisms at the basis of this phenomenon are characterized by a first adsorption of oxygen molecules, followed by a rearrangement of surface oxygen complexes and a desorption of CO and CO₂ [33]. A higher presence of active sites, favoring the adsorption of oxygen, leads to a higher reactivity of the carbon materials in an oxidizing environment [34]. Moreover, in a gasification reaction, the desorption of CO and CO₂ results in the creation of other active sites characterized by dangling bonds, that can either form another C-C bond, by reacting with another dangling bond, or remain free. The tribological implications related to the presence of dangling bond in carbon materials will be discussed in {1.1.3}.

Among the main features of graphite, lightweight and excellent refractory properties are worthy of mention. A density of around 2.26 g/cm^3 and a sublimation temperature, at atmospheric pressure, of about $3700 \text{ }^\circ\text{C}$ characterize this material [27].

The anisotropy of the graphite lamellar structure strongly affect its thermo-mechanical properties. Because of the strong covalent bonds between atoms in the plane, and the weak Van der Waals interlayer interactions, the in-plane Young's modulus is almost equal to 1060 GPa, while the transversal Young's modulus is only 36.5 GPa [35, 36]. Graphite is also characterized by a low coefficient of thermal expansion (CTE) along the in-plane layers, which ensure a dimensional stability over a large temperature range. In particular, the in-plane value of the CTE is negative between 25 °C and 400 °C, and it is approximately equal to $1 \cdot 10^{-6} \text{ } ^\circ\text{C}^{-1}$ at 1000 °C. However, a larger CTE can be observed along the orthogonal direction of the layers, where the crystal structure presents Van Der Waals forces. In this case the CTE ranges from $2.8 \cdot 10^{-5}$ to $3 \cdot 10^{-5} \text{ } ^\circ\text{C}^{-1}$ between 25 °C and 1000 °C [37].

In addition to graphite, the family of sp^2 carbon materials includes a large variety of carbon materials characterized by a different degree of crystalline perfection. Graphene layer stacks disoriented by random rotations, along their ternary axis, lead to the so called “turbostratic” arrangement. A turbostratic lattice structure is typical for non-graphitic carbons. C/C composites can be considered as a heterogeneous mixture of graphite and non-graphitic carbon, since they are usually characterized by carbon fibers with a high degree of graphitization in a pyrocarbon matrix [24, 25, 38].

In C/C materials, some of the above-mentioned characteristics of graphite are inherited and improved. The making process of such composites is described in the following.

1.1.2 C/C material manufacturing process

Composites are best defined as materials in which two or more non-miscible constituents, with a different structure, are brought together to produce a new material whose overall performance and resultant properties are improved, compared to the individual constituents. Typically, composites consist of a fibrous reinforcement embedded in a matrix, which gives cohesion and bind the fibers together. In the case of C/C composites, both the reinforcement and the matrix are in carbon, but their structures are different [1, 24].

The reinforcement of a C/C material consists of carbon fibers made from the pyrolysis of a precursor under controlled atmosphere. The properties of the carbon fibers depend on the adopted precursor. Nowadays, the most widely used precursors, especially for disc brakes, are the polyacrylonitrile (PAN) fibers. The carbon fibers used in C/C composites and stemming from the heat treatment of PAN fibers are called “ex-PAN” carbon fibers.

The manufacture of ex-PAN carbon fibers is carried out in several stages and can lead to two different categories, namely High strength (HS) and High modulus (HM) carbon fibers. Figure 2 describes the process for obtaining HS and HM ex-PAN carbon fibers.

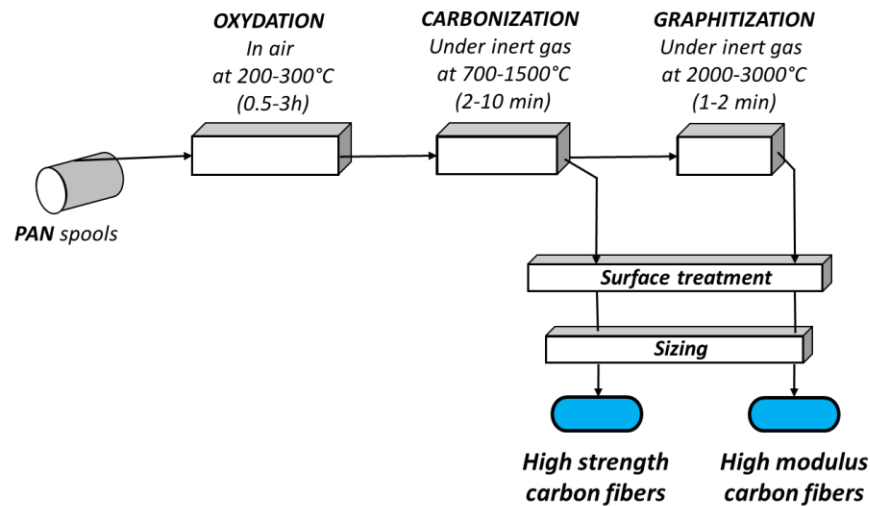


Figure 2 Manufacturing process of ex-PAN carbon fibers.

As shown in Figure 2, PAN fibers are first grouped in spools and then spun for the heat treatments. The process leading to carbon fibers involves an initial oxidation stage, a carbonization and a graphitization treatment. First, the oxidation process is carried out at a temperature between 200 and 300 °C, in air. During this phase, the PAN filaments change from a polymeric state (white color) to an infusible and thermally stable state (black color). The oxidation is an essential stabilization stage of the PAN fibers, as it allows the subsequent thermal processing without collapse of the fibers or loss of microstructural orientation.

The following step is the carbonization, carried out under inert atmosphere, usually nitrogen or argon, at a temperature between 700 and 1500 °C. During this operation, fundamental changes in both chemical composition and physical properties occur. Around 50% by weight of the fibers is volatilized as gases, essentially derived from carbon and nitrogen, and the polyaromatic planes, characterizing the fiber microstructure, are further aligned with respect to the fiber axis. After this process, high strength carbon fibers, with a Young's modulus between 200 and 250 GPa, are obtained.

A further possible step is the graphitization, which is necessary only to obtain carbon fibers of intermediate ($E = 250 \div 400$ GPa) or high ($E = 400 \div <600$ GPa) elastic modulus. During this operation, carbonized fibers are stretched and subjected to a temperature between 2000 and 3000 °C, under inert atmosphere. At the end of this phase, the fibers contains more than 99% of carbon and a further orientation of the microstructure is obtained [1, 39, 40].

It should be remarked that the Young's modulus increases with temperature while the strength reaches its maximum during the carbonization stage, at a temperature of around 1400 °C [1, 24]. Carbon fibers derived from the process described above are usually woven in appropriate directions to tailor specific properties. In [41], different carbon fiber architectures have been investigated. It has been shown that the fiber architecture drastically affects both composite strength and deformation characteristics. Moreover, the woven composites behave more consistently and show less variation of properties, compared to non-woven composites.

Once the fibrous structure is realized, a pyrocarbon matrix is deposited through chemical vapor infiltration (CVI). This process is characterized by the synthesis of carbon by high-temperature ($\approx 1000-1400$ °C) dehydrogenation of a light hydrocarbon (methane, propane) penetrating by

diffusion and convection through the porous network of the preform. Different deposition conditions can lead to different types of pyrocarbons, which are differentiated by their microstructure [42].

Overall, the final properties of C/C composites are affected by multiple combinations of fiber and matrix characteristics, responding to various applications for which C/C materials are intended. Among the most remarkable properties, C/C composites are characterized by low density (from 1.3 to 2.5 g/cm³), high tensile strength (up to 900 MPa) and Young's modulus (up to 300 GPa), high thermal conductivity (from 20 to 150 W/mK) and thermal shock resistance (150-170 W/mm), low CTE (from -2 to 2*10⁻⁶ K⁻¹) and preserved, or even improved, thermo-mechanical properties up to 2000 °C. Compared to conventional graphite, mechanical properties are superior. C/C composites are in fact manufactured for withstanding damage and minimum delamination crack growth [3, 24]. In the following, the tribological characteristics of these composites is also discussed.

1.1.3 Tribological and physicochemical properties of C/C materials

C/C materials are involved in many industrial applications where their tribological response underlies the good performance of the mechanical system. As a result, in the last few years, many research works have been carried out in order to study the frictional response of such materials. In the following, the main tribological features of C/C are described. Nevertheless, before delving into the friction behavior of C/C composites, key concepts defining the tribological contacts are presented.

1.1.3.1 Tribological triplet and rheology of a contact

Frictional contacts involve considerable complexities requiring a multi-physical and multi-scale approach. The study of the tribological behaviour of two generic bodies in contact has gradually moved from considering only the bulk of the media in contact to a more comprehensive interfacial approach, where the particles circulating within the contact zone play an essential role. This innovative concept was introduced first by Godet and further developed by Berthier, who added complementary notions such as the “tribological triplet”. According to this approach, a tribological problem is simultaneously affected by the bodies in contact, called “first bodies”, the material at the interface separating them, called “third body”, and the mechanism connecting the components in frictional contact [43-47]. A diagram of the tribological triplet is shown in Figure 3.

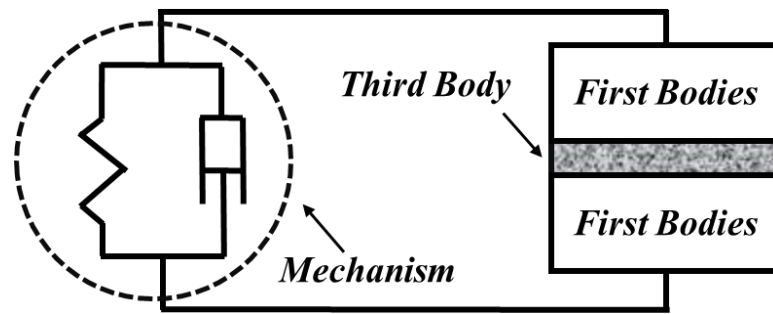


Figure 3 Diagram of the tribological triplet of a tribo-system.

In a tribo-system, such as the one depicted in Figure 3, the physicochemical nature, the geometrical characteristics and the topography of the first and third bodies are prominent factors. Moreover, the first bodies sustain the working conditions, such as load or sliding mode, imposed by the mechanical system. Regarding the third body, it consists of particles trapped in the contact and separating the contact surfaces of the first bodies. In the case of non-lubricated friction, the third body is generated in situ by the detachment of first body particles during friction [25, 29]. In a contact, the volume and the superficial parts of the third body can be considered as accommodation sites, i.e. where the speed gradient and the stress distribution between two rubbing surfaces is accommodated. According to Berthier [46], other possible accommodation sites are the mechanism itself, the bulk of the first bodies and the “extreme surface” of the first bodies. He also identified different modes of accommodation, e.g. the elastic deformation, the fracture (crack propagation), the shearing and the rolling mode. The combinations of a site and a mode are referred to as “accommodation mechanisms”.

The effect of particles lying in the contact interface and the rheology of the third body have a strong impact into the overall response of the frictional contact. In this respect, Berthier [46] introduced the concept of “tribological circuit”, which defines the different flows of particles coming in and out of the contact. Figure 4 shows a schematic representation of the flows of matter characterizing a tribological circuit.

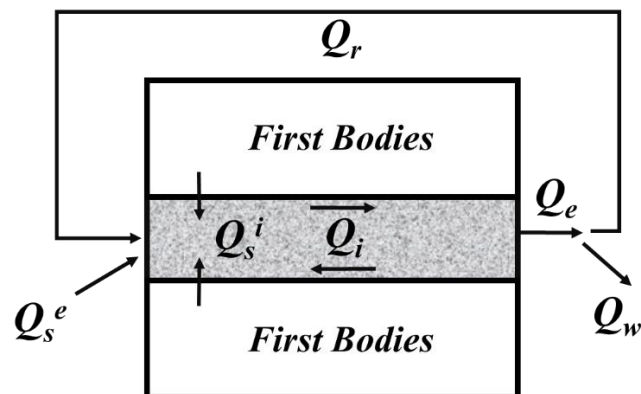


Figure 4 Flows of particles moving in and out the contact zone and defining the tribological circuit.

The internal source flow, Q_s^i , is caused by the detachment of first body particles during frictional contact. It results in the natural formation of the third body. The external source flow, Q_s^e , is due to the external particles entering the contact interface. It also takes into account, for instance, artificial lubricants introduced in the contact. The internal flow Q_i is the overall flow of particles circulating between the first bodies. On the other hand, Q_e is the flow of particles ejected from the contact. Part of this flow is definitely lost by the contact and leads to wear, Q_w , while the remaining part, Q_r , is reinjected into the contact and takes part again in the accommodation mechanisms within the third body. A mass equilibrium of the system imposes that the amount of particles of third body per unit of time has to be equal to the difference between the source flow, composed of Q_s^i and Q_s^e , and the wear rate Q_w [47, 48].

The study of the tribological behavior of C/C materials requires considering the overall tribosystem and the rheology of the contact, as outlined above. Moreover, it should be remarked that for sp^2 carbon materials also the environment of the contact plays a non-negligible role, as it can strongly affect the physicochemical behavior of the first and third bodies. An insight into the main tribological features of these materials is then provided.

1.1.3.2 Tribology and surface chemistry of sp^2 carbon materials

Sp^2 carbons are known for being excellent solid lubricants. In the first place, this characteristic was attributed to the weakly bonded graphitic layers of their lattice structure, which shows a low resistance to shear stress [49]. However, scientific evidence, such as the strong increase of the friction coefficient in vacuum conditions or inert atmosphere, have proved a more complex scenario.

Pioneering studies about the role of gaseous environment, in the frictional behaviour of graphite, have been carried out by Savage [50-52]. He showed that the lubricant properties of graphite are not only related to the crystal structure alone, but depends on adsorption films, especially water, covering the frictional surface and providing a lower cohesion at the contact interfaces. Moreover, by using a tribometer consisting of a graphite pin on disc, he observed the existence of two different frictional regimes conditioned by the gaseous environment. A low friction regime, i.e. friction coefficient lower than 0.2, and a high friction regime, characterized by a friction coefficient between 0.5 and 0.8 and heavy wear. The latter was always observed in vacuum or in presence of an inert atmosphere (nitrogen). Tests carried out by Savage showed that a low friction regime and an almost null wear rate can be always obtained at ambient temperature with condensable vapors (e.g. water, methanol, pentane, heptane or more complex organic molecules as glycols) if a sufficient vapor pressure is provided. The limit pressure is specific for each tested vapor.

A more comprehensive theory was proposed by Lancaster [53-55]. During frictional contact, in normal water-containing environment, basal planes are damaged and high-energy active sites are exposed. A low friction regime is possible only if the active sites, which favor the adhesion of the contact surfaces [56], are neutralized by water molecules. He proposes a mechanism whereby the adsorbed vapor, on the neighboring basal planes of graphite, acts as a “reservoir” from which water molecules migrate to neutralize newly exposed dangling covalent bonds. The transition to a high friction regime occurs when the ratio between the partial pressure of water vapor and the saturation water pressure, in literature referred to as P/P_0 , decreases below a threshold value, which depends on both the environment and the contact temperature. Being the amount of water

adsorbed depending on the ratio P/P_0 , the transition to a different friction regime can be caused by either changing the amount of vapor, affecting P , and/or altering the temperature, which affects P_0 . In particular, for natural graphite, Lancaster [55] mentioned the existence of a critical contact temperature, of almost 150-180 °C, above which the water adsorbed on the surface of the graphite is completely desorbed and no longer able to neutralize the active sites caused by the frictional contact.

Yen investigated in more detail the influence of water vapor and oxygen on the tribological behaviour of sp^2 carbon materials [25, 57]. He carried out friction tests under controlled atmosphere and low sliding speed (to minimize frictional heating), through a pin-on-disk apparatus. The experiments were conducted at atmospheric pressure in wet (50% RH) and dry (100 ppm of H_2O) nitrogen environment, and in wet and dry air. The results obtained for graphite are presented in Figure 5.

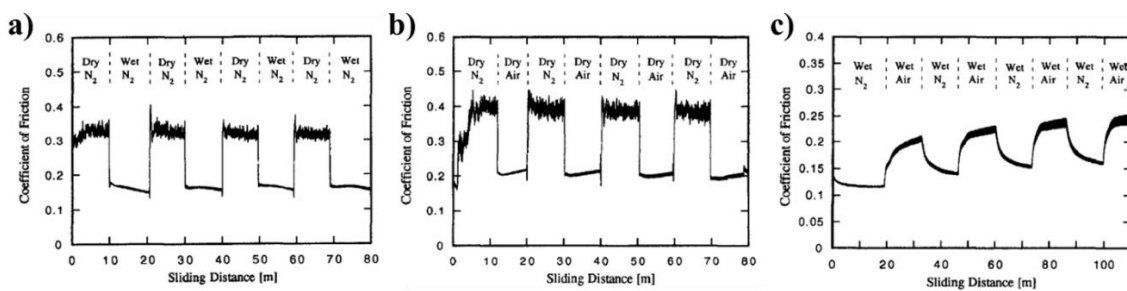


Figure 5 Influence of the environment on the graphite friction coefficient. a) Cycles of wet and dry nitrogen environment; b) Cycles of dry nitrogen and dry air environments; c) Cycles of wet nitrogen and wet air environment. Adapted from [25].

As shown in Figure 5.a, alternated friction cycles, under dry and wet inert atmosphere, demonstrated that a low friction regime is possible only in presence of moisture in the environment, i.e. wet nitrogen, confirming that water vapor acts as a lubricant for carbonaceous materials. Moreover, the effect of water vapor is reversible, as the friction immediately increases and decreases from a dry to a wet environment. The role of oxygen is instead investigated in Figure 5.b and Figure 5.c. Cycles of dry nitrogen and dry air show that oxygen in air acts as a lubricant, leading to low friction regime. Oxygen is in fact known to form oxygen groups on the graphite surface that can favor the adsorption of water molecules. In turn, water molecules can function as secondary adsorption sites for other water molecules, leading to coalescing clusters and the formation of a continuous adsorbed phase [58]. As a result, even in dry air environment, a small amount of water vapor and the presence of oxygen can lead to a low friction regime. However, as shown in Figure 5.c, under low friction regime the introduction of oxygen (wet air) can also lead to an irreversible increase of the friction coefficient with the increase of the sliding distance. Yen attributed the phenomenon to an increase of the real contact area due to oxygen-induced tribochemical wear [25, 59].

The work carried out by Yen and Ishihara [7, 25] has shown that water vapor and oxygen play a similar role on the tribological behaviour of C/C composites and other sp^2 carbon materials. In particular, it has been observed that C/C materials exhibit a low friction regime in ambient air and a high friction regime under a dry nitrogen atmosphere. The oxygen still shows a lubricating effect, even if less effective than water vapor. In fact, under dry air, a progressive increase of the

friction coefficient due to the presence of oxygen is observed. Moreover, it has been noted that for C/C materials in dry nitrogen environment, a small amount of moisture (100 ppm of H₂O) can prevent the high friction regime, which has been observed only after that the surface of the C/C pin has been flattened in air by wear.

The influence of water vapor on C/C materials was also studied by Chen et al. [8]. They investigated, on a disc-on-disc setup, the effect of different relative humidity on the frictional response of C/C composites. It was observed that a higher relative humidity delays, or even prevents, the transition from a low friction regime to a high friction regime, for any speed of rotation. Moreover, after the transition, higher friction coefficients and wear rates were observed in the lower humidity environment. In another work, Chen et al. [60] showed that higher sliding speeds, leading faster to higher contact temperature, result in shorter sliding distance at which the transition, from a low to a high friction regime, occurs. According to [61], also an increase of the contact pressure can bring forward the transition to high friction regime.

The effect of both temperature and sliding speed on the tribological behaviour of C/C materials has been also studied by Gomes et al. [5]. By means of a pin-on-disc test bench, they showed that room temperature condition and low sliding speed lead to low wear, while direct or frictional heating involve a strong increase of wear and surface degradation, characterized by an extensive fiber and matrix fracture.

More recently, the mechanisms behind the occurrence of the friction transition, in the literature referred to as “dusting” (strong ejection of detached particles similar to dust), have been studied by Gouider et al. [6, 24]. They investigated the frictional response of C/C materials using a pin-on-disc tribometer equipped with a mass spectrometer, in order to analyze the gas exchange close to the contact. As shown in Figure 6.b-d, a sudden increase of CO₂ in the atmosphere composition has been observed when the abrupt increase of friction coefficient occurs.

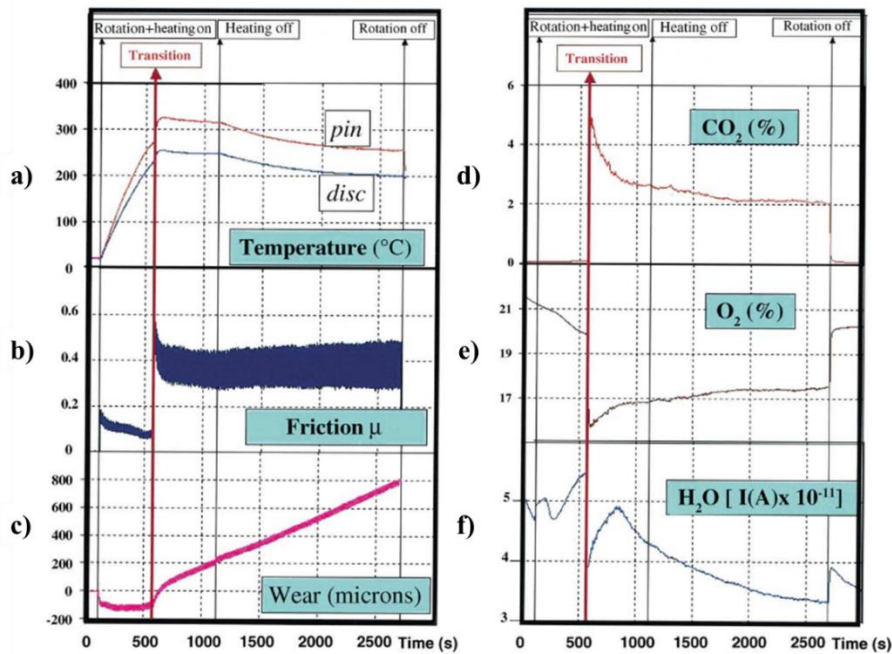


Figure 6 Mass spectrometry during C/C composite friction in a pin-on-disc setup [6]. a) pin and disc temperatures; b) friction coefficient; c) wear; d) CO₂ (%); e) O₂ (%); f) H₂O (partial pressure). More detailed information about the study in [6].

Concurrent with the production of CO₂, during the transition an almost equal, but opposite, decrease of O₂ is observed (Figure 6.e). The consumption of H₂O is also shown in Figure 6.f. This phenomenon suggests a gasification reaction induced during the frictional interaction. The release of CO₂ and the consumption of O₂ and H₂O, with sudden variation in the friction coefficient, is systematically coupled with a significant detachment of particles. The scenario proposed by Goudier et al. [6, 24] and Kasem et al. [9, 22] describes the friction transition as a function of both physico-chemical and mechanical actions on the tribo-system. Specifically, any parameter that may lead, directly or indirectly, to a considerable detachment of particles from the first bodies (source flow of the third body) allows the formation of dangling bonds. If the third body source flow is sufficiently high to allow the formation of a large number of dangling bonds, and the surrounding environment does not allow for an immediate total saturation of them, then adhesive interactions in the contact increase significantly and the sudden increase of friction coefficient occurs. Before the dusting event, Figure 6.f shows that the increase in temperature increases the water vapor desorption from the contact. Consistently with previous outcomes in the literature [34, 37], the accommodation mechanisms, which drive friction and wear in a contact, lead to an increase of the source flow Q_s^i . The particle detachment increases as well, up to the dusting phenomenon. The continuous consumption of O₂ and the CO₂ released into the atmosphere, after the transition, indicates that the oxidation process lasts as long as the high friction regime is preserved. Moreover, gasification can promote mechanical wear by weakening the surface of the first bodies, and thus contribute to wear (Figure 6.c) and generation of third body, as observed in [62, 63].

The works carried out by Rietsch et al. [23, 64] made it possible to study the influence of gaseous environments and temperature on the tribochemical phenomena occurring on the contact interface of carbon materials. In agreement with the scenario described above, they have shown that the generation of third body is directly related to the production of dangling bonds, resulting from the rupture under mechanical stress of the carbon covalent bonds. In [23], by means of a planetary ball milling, they observed that the friction regime depends on a kinetic competition between the deactivation of the dangling bonds by the contact atmosphere and the creation of interfacial carbon-carbon bonds generating adhesion.

The effect of the main parameters discussed in this section (i.e. environment, temperature and rheology of the third body) on the friction coefficient (μ) and wear of sp^2 carbon materials is summarized in Table 1.

			<i>Friction</i>		<i>Wear</i>	
			$\mu \leq 0.2$	$\mu > 0.2$	Low	High
<i>Environment</i>	Air	Wet	✓		✓	
		Dry	✓		✓	
	N ₂	Wet	✓		✓	
		Dry		✓		✓
<i>Temperature [T] (in air)</i>	Room Temperature		✓		✓	
	T > \approx 200-300 °C			✓		✓

Table 1 Friction coefficient and wear of sp^2 carbon materials as a function of the environment and temperature condition.

The strong impact of the third body, on the macroscopic frictional behavior and the wear rate, has encouraged researches in the physicochemical and structural characteristics of the C/C wear debris. The work of Rietsch et al. [65] suggested, for instance, that the third body main features are very similar to those of the wear debris ejected during the frictional contact. An overview of the main results on this subject is then presented in the following.

1.1.3.3 Physicochemical properties of C/C third body and wear debris

First studies on C/C wear debris were carried out by Hutton et al. [66]. They simulated taxiing and landing aircraft braking and collected samples of wear debris in each test. It was shown that wear debris is characterized by significant differences with respect to the first bodies. Under both cold taxiing and landing conditions, it consists of a disordered carbon phase, due to shear deformation of the pyrocarbon matrix, and presents fragments of ex-PAN fibers. They also investigated very high-energy operating conditions, such as the rejected take-off braking, and showed that in this case a graphitic tribofilm is formed, as a result of the high interface temperature and energy involved in braking.

Later, Peszynska-Bialczek et al. [67] observed that wear debris of C/C materials, collected from aircraft braking test simulations (carried out at 25% and 100% of normal landing energy), presents a significant amount of physisorbed water and oxygenated groups. Their decomposition in CO and CO₂ during thermogravimetry analysis led to a loss up to 13 wt% at 1000 °C.

François et al. [68, 69] investigated, through temperature-programmed desorption, the spectra of C/C debris samples collected from taxiing braking simulations. The spectra of CO₂, CO and H₂O were similar to those shown in the literature for most oxidized activated carbons. Moreover, the C/C wear debris were richer in oxygen compared to the debris obtained by slowly sawing an untested C/C disc (representing the composition of the C/C material bulk). In particular, being the amount of thermally desorbed oxygen higher than that necessary to cover the whole specific surface area (i.e. the total surface area of a material per unit of mass) of the wear debris samples, the author hypothesized that oxygen groups are also located in the particle bulk. Overall, a mass loss, by thermogravimetry analysis, up to 10 wt% and a specific surface area not greater than 200 m²/g have been observed.

In a later work, Pevida et al. [70], investigated the C/C wear debris of two materials with different structural order in order to study the effect of the graphitization. Both the wear debris presented an amorphous structure and up to 10 wt% of oxygen content. The specific surface area (almost 180 m²/g) has been found similar as well.

Consistent results have been found by the work of Rietsch et al. [21]. For different energy breaking, they observed a strongly divided C/C wear debris with morphological and physicochemical characteristics similar to the activated carbons. They also measured an active surface area (i.e. the sum of the areas of the active sites located at the edges of the graphitic planes and on the defects of the basal planes [71]) of almost 30 m²/g and a specific surface area up to 400 m²/g (higher than that retrieved by François et al. [68] and Pevida et al. [70]). By means of temperature-programmed desorption and mass spectrometry, a significant desorption of CO and CO₂ (Figure 7.b) has been observed, compared to the desorption spectra of C/C bulk material powder (Figure 7.a).

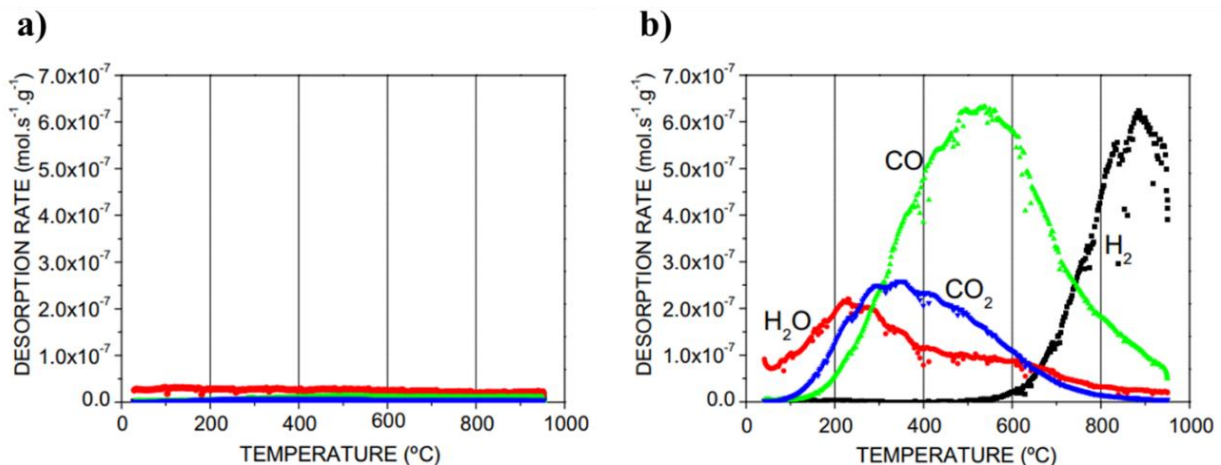


Figure 7 Gas desorption spectra obtained through temperature-programmed desorption coupled with mass spectrometry. a) Gas desorption rate of bulk material powder b) Gas desorption rate of C/C wear debris. More detailed information in [21].

As can be seen in Figure 7.b, a peak of desorbed H₂O is observed around 300 °C and it can be attributed to the water physisorbed on the surface of the debris. Moreover, an important amount of hydrogen is also released for temperature higher than 600 °C. The authors speculate that it could be due to chemical reactions between the carbon surface and the water present in the atmosphere.

In [22], Kasem et al. have shown that the production of CO₂ observed in the friction regime transition [6, 9, 24] is strongly linked to the amount and size of the particles constituting the third body at different temperatures.

The literature on the phenomena underlying the tribological response of C/C materials presented until now does not consider the presence of impurities that can be included, deliberately or not, into carbon materials. A contamination of metallic or alkaline earth oxides can have a strong impact on the thermal and frictional behavior of such materials. Therefore, the following section provides a brief overview on this subject.

1.1.3.4 Influence of the metallic impurities on carbon materials

In the literature, metallic impurities affecting the oxidation process of carbon materials have been the subject of many research works [72-75]. In [74], McKee et al. investigated the behavior of refractory metal borides, carbides, nitrides and silicides dispersed on graphite up to 1000 °C, in air. The study, carried out by thermogravimetry analysis, showed that even small amounts of these finely dispersed materials can strongly affect the reactivity of graphite at high temperatures. In particular, it was observed that compounds consisting of metals of the Group III-IV are rapidly oxidized below 1000 °C. The effect of these oxides on the gasification kinetics of graphite varies depending on the catalytic properties of such metal oxides. While vanadium and molybdenum oxides favor the carbon oxidation, compounds of metals such as zirconium, titanium, aluminum, silicon and niobium form stable and non-reducible oxides that have little, or absent, catalytic activity on graphite oxidation.

Later, Yamaguchi et al. [75] observed that refractory oxides, such as Al₂O₃ or ZrO₂, can affect the oxidation of graphite. In particular, it was shown that the presence of Al₂O₃ accelerates the graphite oxidation, while ZrO₂, TiO₂ and MgO have an inhibiting effect. The authors attributed the different behavior of the oxides to their propensity to donate or accept electrons from graphite.

Within this context, it should be observed that the role of metallic impurities has been approached in general by a physicochemical point of view, without accounting for the effective rheological role of such more or less hard particles at the real contact interface. Moreover, because the rheology of a particle compound affects also its physicochemical interaction with and within the interfaces, further investigations should be oriented on experimental and numerical tribological tests, where the third body of C/C materials is produced and analyzed in-situ.

All the outcomes presented so far, concerning the rheological and physicochemical characteristics of C/C materials in frictional contact, have been obtained through experimental approaches. In the following, the main numerical studies related to the tribological behaviour of C/C composites are shown as well.

1.1.3.5 Numerical tribology of C/C composites

In the literature, friction, damage and wear of C/C materials have been investigated through numerical models aimed to understand the influence of their structure in the tribological response.

As shown in {1.1.2}, C/C materials are characterized by a complex structure consisting of a pyrocarbon matrix with carbon fiber reinforcement. Moreover, the needle-punching process, common in aircraft disc brakes, leads to vertical inclusions characterized by rearranged fibers crossing the layers of the C/C preform [76]. In order to model such a composite, a possible approach in the literature provides for the use of a representative elementary volume of material at a mesoscopic scale (i.e. in between the macro and microscopic scales). A first attempt to model and understand the contact mechanisms of C/C composites at the mesoscopic scale was carried out by Peillex et al. [77]. They developed a two-dimensional finite element model (FEM) consisting of vertical heterogeneities embedded in a matrix (representing the C/C composite) rubbing on a rigid surface, as shown in Figure 8.

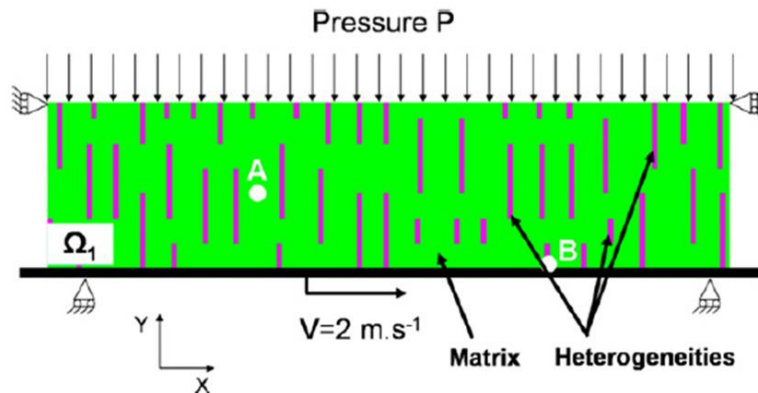


Figure 8 Heterogeneous model of a C/C composite. Adapted from [77].

This model allowed investigating the stress and strain fields in the material with different morphologies, i.e. different distribution of the heterogeneities. In [77], Peillex et al. applied the homogenization theory in order to develop a homogeneous model with equivalent characteristics of the heterogeneous one. It has been observed that, for some values of the applied pressure, the homogenous and the heterogeneous models differ in terms of instability friction regimes. These instabilities consist of local adhesion, sliding, detachment phases at the nodes in contact, during the overall frictional interaction, and are at the basis of the local vibrations propagating in the first bodies [78]. Their results highlight the prominent role of the “contact dynamics” in friction problems and suggest that the heterogeneities and the material volume close to the contact interface strongly affect the frictional response.

The work of Mbodj et al. [78, 79] validated the previous assumption. In particular they observed that the friction instability regimes are closely dependent on the distribution of the vertical inclusions in the close proximity to the contact surface. She also investigated the contact between a composite and a deformable surface and the contact between two composites. The influence of the porosity in the representative elementary volumes has been investigated as well.

Despite the many advantages provided by the finite element method, a strong limitation of this approach is that the behavior of the third body cannot be simulated and the rheology of the contact remains unknown. In order to overcome this issue, a different approach is provided by the discrete element method (DEM). The main advantage of this numerical analysis is that wear is no longer represented only by local or global laws (such as the Archard's law), but it is described by particles showing the rheology and the evolution of the third body. Champagne et al. [80], developed a DEM model to investigate the behavior of C/C composites in frictional contact. They investigated the role of the vertical inclusions and the evolution of the third body in order to obtain a predictive approach in terms of friction and wear. The model provided for two distinct continuum and discrete mediums, characterizing the first and the third bodies respectively. The formers were modelled through a cohesive zone model (CZM) while the latter involved an unilateral cohesive contact law, in order to simulate the interactions of the detached particles between them and with the first bodies. The simulations, carried out under a normal force and a shear velocity between the first bodies, highlighted two different phases. First, a transient phase where the damage of the first bodies in frictional contact accumulate. Then, a steady state phase where the establishment of a third body layer (which becomes the main site of accommodation of the relative velocity between the first bodies) leads to stabilized friction and damage.

It was observed that a heterogeneous material exhibits a much higher damage with respect to a homogenous one. This result emphasizes the importance of explicitly modelling the heterogeneities in the materials and their strong influence in the frictional response.

Different geometries of the representative elementary volume were adopted to study the effect of the vertical inclusion length and distribution. The obtained results showed that longer inclusions, reaching the contact interface, increase the damage, at steady state, of the first bodies. On the other hand, the presence of shorter heterogeneities reduces the amount of global damage by allowing a quick establishment of a protecting third body layer. Therefore, the less is the energy required to brake the interface between the matrix and the inclusions, the lower overall damage has been achieved. The model proposed by Champagne et al. [80] also investigated the effect of different cohesive third bodies. For a given time of simulation in the transient regime, higher cohesion led to greater global damage.

Further studies on the thermal phenomena taking place in a frictional contact have been carried out by Rivière et al. [81]. They observed that higher temperatures are strongly localized within the third body. They also noticed that a higher cohesive force of the third body particles leads to higher damage. A thicker third body due to such higher damage is responsible for an increase in the number of contacts and, therefore, a higher maximal temperature deviation. However, the authors highlighted that after a threshold value, higher values of the cohesive force can lead to a decrease of the maximum temperature. In fact, beyond a certain value, cohesive force of the third body can lead to a strong increase of damage and friction coefficient. This results in a third body layer sufficiently thick, so as to favor heat conduction between the third body particles. Moreover, it was observed that shear velocity has a significant impact on the contact temperature, as it is responsible for the increase of collisions between the particles. Therefore, an increase in sliding velocity leads to higher heat generation and contact temperature.

As highlighted by the large amount of research works on the topic, the mechanisms at the basis of the tribological behavior of carbon materials, with or without metallic impurities, are a complex subject. An in depth investigation of the frictional and vibrational behavior of systems, with sliding interfaces in C/C materials, requires a good understanding of the role of both the

first and third bodies, as well as the mechanism dynamics and the environment/boundary conditions.

1.1.4 Concluding remarks

As shown so far, C/C composites offer excellent thermo-mechanical properties. These characteristics make them an essential resource in many industrial applications, especially for high-performance disc brake systems.

Being composed of sp^2 carbon constituents, their tribological behaviour is strongly affected by the physicochemical features of a graphite-like structure. The presence of active sites, due to structural defects and dangling bonds, can lead to two different friction regimes characterized by a low friction coefficient (lower than almost 0.2 and negligible wear) and a high friction coefficient (generally greater than 0.3 and with a high wear rate).

The different friction regimes seem the result of a kinetic competition between the deactivation of the dangling bonds, by means of the contact atmosphere, and the creation of interfacial carbon-carbon bonds generating adhesion between the first bodies. The saturation of the dangling bonds, in a wet air environment, is attributed to the interaction of the active sites with oxygen, which forms oxygenated groups on the surface, and water contained in the contact atmosphere. According to a widely accepted mechanism proposed by Lancaster [10, 53-55], the water physisorbed on the graphitic basal planes acts as a 'reservoir', from which water molecules migrate to deactivate the dangling bonds generated by the frictional interaction. Oxygenated groups act as nucleation sites of water clusters on the carbon surface and promote, therefore, the establishment of a low friction regime.

Beyond a critical temperature, the water molecules are desorbed from the graphite surface. The "reservoir" no longer feeds the newly exposed active sites and adhesive and abrasive phenomena lead to high friction coefficient and high wear. At a local contact temperature higher than 400 °C, gasification reactions occur. This phenomenon promotes mechanical wear by weakening the surface of the first bodies.

The strong sensitivity of the C/C frictional response to the environment and to the characteristic parameters of the contact often results in a hard to predict behavior of the friction coefficient. The occurrence of dynamic instabilities, due to the evolution of the friction coefficient under different boundary conditions and to the wave generation and propagation within brake materials and components, is a major issue in many industrial applications. In the next chapter, an overview of the stable and unstable friction-induced vibrations is provided.

1.2 Dynamic instabilities in dry frictional contacts

In dry contact scenarios, the relative motion between two components of a mechanical system produces contact and friction interactions. Such interactions, macroscopically observed by a

normal and frictional force resultant, consist of an overall distribution of local microscopic mechanical and physicochemical interactions. The dynamic response of a system to such distributed interactions is known as friction-induced vibration [82-85]. The occurrence of this ever-present phenomenon in frictional contacts gives rise to different system vibrational responses (either stable or unstable [16, 86-88]), characterized by both a different amplitude and a different frequency spectrum. In this regard, the work carried out by Di Bartolomeo et al. [89] has shown how the vibrational response at the scale of the system dynamics is related to the elastic energy, which is released by local ruptures/impacts at the contact interface and propagates in the form of acoustic waves. Low-energy waves decay rapidly because of the material damping, while waves of relevant magnitude propagate until the boundaries of the mechanical system leading to friction-induced vibrations. The occurrence of this phenomenon, resulting from the mutual interaction between the local contact dynamic excitation and the system response, in specific conditions, can become relevant in terms of structural integrity and may lead to safety issues or maintenance requirements [17, 90].

The complexity of this topic engages multiple scientific fields and, during the last decades, a significant amount of experimental, theoretical and numerical works have been developed to investigate the dynamic excitation coming from the contact [16, 86, 87, 91-94].

Because of the wide range of involved phenomena and applications, a specific classification of friction-induced vibrations is difficult to be defined. In the literature, a possible approach to discriminate different behaviors of the friction-induced vibrations has been proposed as a function of the degree of coupling in the friction pairs [88, 95, 96]. Akay, in [88], classifies the driving mechanism of friction-induced vibrations in two major categories depending on the nature of the contact, i.e. weak or strong.

Weak contacts are characterized by the propagation of waves produced by the impacts of the local asperities of the contact surfaces. Each component of the friction pair responds to the excitation at its own natural frequencies, almost independently of the other body in contact. The vibrational response associated to this type of contacts is usually characterized by a low amplitude aperiodic signal, with a broadband frequency range spectrum and peaks in correspondence of the eigenfrequencies of the bodies in contact. Such frictional condition produces the so-called roughness noise [88, 95].

On the other hand, strong contacts produce a more complex scenario, as they can modify the dynamics of the whole mechanical system. In this case, the friction pair gives rise to a coupled dynamics, strongly affected by the main contact parameters (e.g. contact pressure, contact stiffness, sliding velocity, temperature, materials properties). Under such condition, dynamic states characterized by high amplitude oscillations of the vibrational response or abrupt motions can arise [88, 95]. These phenomena are called unstable friction-induced vibrations. The onset of dynamic friction instabilities is undesired in the vast majority of industrial applications and they often lead to noise issues or damage of the mechanical system [97-99]. As a result, the understanding of the conditions leading to frictional instabilities is of great importance in several fields of research concerning for instance brake systems, wheel/rail contacts, machining tools, prosthesis, earthquakes, etc.

In the following, stable and unstable vibrations caused by frictional contact scenarios are discussed. Then, previous outcomes on friction-induced vibrations in mechanical system with C/C frictional material, under different boundary conditions, are presented.

1.2.1 Overview on friction-induced vibrations

1.2.1.1 Stable friction-induced vibrations

The main mechanism driving the stable vibrational response is due to the local interaction of the asperities of the surfaces in contact [100, 101]. As shown in Figure 9, the mechanical process responsible for this phenomenon has its origin at the scale of the surface asperities, which determine random impacts and ruptures hindering the motion and exciting the dynamics of the mechanical system.

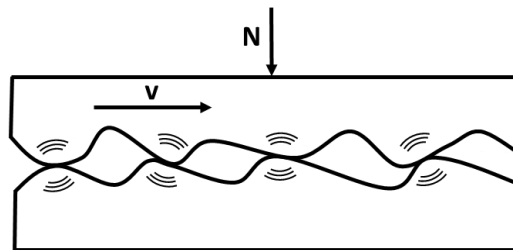


Figure 9 Schematic representation of local random impacts and ruptures of the surface asperities during sliding motion of two bodies in frictional contact.

The frictional interaction of solids having rough surfaces is responsible for the typical wideband noise characterized by a low sound level, in the literature referred to as friction noise or roughness noise (to underline the primary cause). In this respect, an analysis of the relation between the SPL (sound pressure level), characterizing the friction noise, and the surface roughness has been carried out by Othman et al. [102], through an experimental setup consisting of a stylus sliding on frictional surfaces of different materials. It has been observed a linear increase of the SPL for higher surface roughness, regardless of the material. The fundamental mechanics at the origin of radiated noise, in a weak contact condition, have been studied by H. Ben Abdelounis et al., in [101]. The authors assert that the friction noise depends on the topography of the surfaces in contact, the sliding speed and “the dynamics of the surfaces”. With regard to the latter, for light load, they hypothesize that the natural modes of the contacting bodies are much stiffer than the contact stiffness resulting from the superposition of all contact spots. As a result, the frictional response is not affected by the increase of rigidity due to the contact and the bodies behave as if they were completely uncoupled.

Even if this stable friction-induced vibrations are common in weak contacts, a stable behavior of the vibrational response can be also observed in case of strong contacts, depending on the parameters of the mechanical system and the coupling conditions. In this respect, Di Bartolomeo et al. [95] investigated a system characterized by two beams in contact, sliding under imposed boundary conditions, with the aim of studying the friction noise under both weak and strong contacts. It has been shown that, increasing the normal load, the RMS value (root mean square value) of the vibrational response decreases until a range after which it starts rising, as shown in Figure 10.

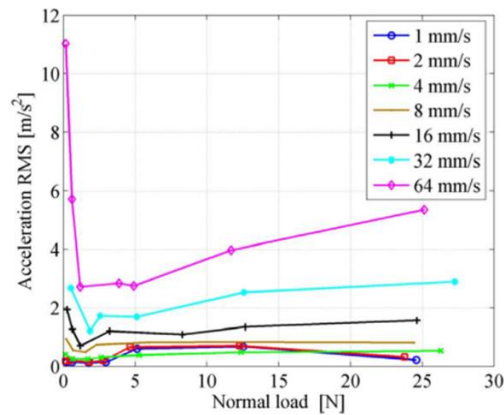


Figure 10 Acceleration RMS of stable friction-induced vibrations measured as a function of the normal load and sliding velocities of two beams in frictional contact. Further information about the study in [95].

This behavior is related to the dynamic coupling degree between the contacting bodies. As long as there is a condition of weak contact, the vibrational response of the beam is almost independent of the other beam in contact and it is characterized by larger oscillations. Increasing the normal load, the system approaches a more constrained configuration reducing the amplitude of vibrations. After attaining a critical range of normal load, the system becomes strongly coupled and it responds according to its coupled dynamics. From this point, a further increase of the normal load, as well as of the sliding velocity, results in higher power injected in the contact and therefore in a higher vibrational amplitude (except for the highest loads, where the roughness plasticization decreases the vibration amplitude).

In strong contact condition, where the coupled dynamics can lead to unstable friction-induced vibrations, it has been observed, in [103], that the friction noise can provide a source of broadband dynamical excitation, triggering the onset of an unstable mode and leading to frictional instability. In particular, after comparing the friction noise and the propensity to dynamic instability for the same system with different frictional materials, it has been observed that the energy content associated to the friction noise can be considered as an index of the contact excitation from the interface.

It is therefore clear that a coupled dynamics (e.g. typical of brake and clutch systems), due to strong contact conditions, changes significantly the frictional and vibrational scenario. Even if a stable vibrational response is generally possible, strong contacts can often lead to unstable friction-induced vibrations, which is described in the following section.

1.2.1.2 Unstable friction-induced vibrations

In the last decades, many efforts have been put in the study of unstable friction-induced vibrations. The prediction and control of dynamic instabilities due to the frictional contact has been the object of several research works aimed to study these phenomena, through experimental, theoretical and numerical approaches [16, 104-106]. However, despite the vast number of studies on the subject, the occurrence of unstable friction-induced vibrations is still a current issue in many industrial applications. In most cases, the onset of these dynamic instabilities can in fact

be a source of deleterious effects on the performance and functioning of mechanical systems, leading often to wear, structural damage, fatigue and noise emission. A review of the main mechanisms proposed in the literature, concerning unstable friction-induced vibrations and noise emissions, has been carried out by Ibrahim [83, 107].

A significant part of the literature dealing with dynamic instabilities due frictional contacts is related to the analysis of NVH (Noise, Vibration, and Harshness) brake issues. During braking, part of the energy involved in the process is in fact converted in vibrational energy, resulting in undesired sound irradiation and degradation of both the braking system and a number of other components of the vehicle. According to [108], aircraft brakes tend to respond at lower frequencies, up to 300 Hz, while automotive and rail brakes often lead to noise characterized by a much higher frequency content (often over 500 Hz). Hoffman and Gaul [90] provided a review of different classes of unstable friction-induced vibrations caused by brakes.

Because of the wide range of involved phenomena related to friction instabilities, a complete review would be very extensive and beyond the scope of this work. In the following, three of the main instability mechanisms, widely investigated in the literature, are discussed more in detail:

- **Mode coupling.** This phenomenon is generally acknowledged as one of the main causes of self-excited vibrations induced by the frictional forces [104, 105, 109, 110]. The onset of this dynamic instability is due to two vibration modes of the system, close in frequency, coupling through friction forces and leading to an unstable mode of the mechanical system. On equal parameters of the system, it has been observed that self-excited friction induced vibrations due to mode coupling arise when the kinetic friction coefficient is higher than a threshold value (lock-in) [16, 111]. This vibrational phenomenon results in harmonic vibrations at the frequency of the unstable mode, exponentially increasing up to a limit cycle, where non-linear contributions limit the further growth of the oscillation amplitude.
- **Negative friction-velocity slope.** A decrease of the friction coefficient with the increase of the relative velocity in a frictional contact is considered as a possible root mechanism of destabilizing effect, leading to dynamic instability [112, 113]. The decreasing behavior of the friction force during braking can in fact lead to negative apparent damping and be responsible for the unstable vibrational response [114].
- **Macroscopic stick-slip.** This friction instability is characterized by alternate phases of sticking and slipping motion, leading to impulsive excitation of the mechanical system. Ramps and abrupt drops of the tangential contact force characterize the typical saw-tooth behavior of the frictional response. The stick-slip instability is considered the responsible mechanism of a multitude of phenomena related to different fields. Examples of stick-slip can be found in geodynamics [115, 116], in music instruments [117], in articular cartilage [118] and in a huge number of mechanical systems including, for instance, hydraulic actuators [119] or disc brakes [17, 120, 121].

1.2.2 Frictional contact instabilities

1.2.2.1 Mode coupling and complex eigenvalue analysis

Over the last decades, the mode coupling dynamic instability has received considerable attention. The occurrence of this phenomenon is considered as one of the most prominent issues in industrial applications. In automotive brake systems it is considered to be the main responsible for brake squeal noise emissions.

In 1972, North carried out a pioneering study in which this mechanism has been described [122]. He demonstrated that the onset of friction instabilities can be caused by the coupling of at least two modes of the mechanical system. In particular, he has shown that a change in a system parameter can bring two initially separated eigenfrequencies to get closer to each other towards the same frequency (lock-in point). The instability arises when the two structural modes coalesce, leading to the same imaginary part of the eigenvalues and opposite in sign real parts. A positive sign of the real part of an eigenvalue leads to the unstable vibrational response characterized by the exponential growth of the vibration amplitude. The unstable mode of the system is due to a non-symmetric contribution to the system stiffness matrix given by the frictional forces, which makes the system not conservative and allows energy to be transferred from the frictional interface to the vibrational motion. Hoffmann et al., in [15], have shown that energy can flow through the friction force, which acts as a link between the normal motion to the contact surface and the parallel one. As a result, in order to obtain an energy transfer different from zero, a shift in time between the tangential and normal oscillations to the contact is necessary.

In a later work [123], Hoffmann and Gaul investigated the role of the structural damping in the mode coupling instability. It has been proved that different values of the structural damping, assumed as linear viscous, can bring a stable system to become unstable. As a result, structural damping cannot be considered as a secondary effect that can be neglected to a first approximation. Further studies on the effect of damping on the mode coupling instabilities have been carried out by Sinou and Jèzèquel [104]. A simple non-linear two-degrees-of-freedom numerical model has been used to prove that there exists, in some cases, an optimal structural damping ratio between the modes of the system which decreases, as a function of the friction coefficient, the unstable region.

Minimal models consisting of at least two degrees of freedom and describing the mode coupling instability are largely spread in the literature [15, 104, 124, 125]. In [126], Popp shows some examples of 2 DoF models where geometrical effects and non-conservative restoring forces influence the stability of the system. In [127], Brunetti et al. have shown a more complex lamped-parameter model, consisting of 6 DoF. The effects of the friction forces on the stability of the system have been investigated through complex eigenvalue analysis (CEA), firstly described by North [122, 128], as a function of the friction coefficient. Even for a constant friction coefficient, non-conservative friction forces lead to the unsymmetric stiffness matrix, which can lead to an unstable vibrational response of the system if the friction coefficient exceeds a threshold value. Despite the large number of works studying the mode coupling through minimal models, it is still difficult to predict the onset of a squeal phenomenon only by relying on such models, especially when dealing, for instance, with real industrial brake systems. In recent years, a combined numerical and experimental approach has been often adopted to study the occurrence of squeal. Many works have been carried out by means of a pin-disc configuration to investigate the lock-in phenomenon and predict the occurrence and the characteristics of the instability [129-

131]. In [132], Allgaier et al. investigated the mode lock-in through a pin-disc apparatus and a finite element model, with the primary objective of determining which friction model and which modelling details are necessary to simulate the lock-in phenomenon. In [133], Tuchinda et al. showed that the dynamic instability occurs when a mode of the free pin approaches a mode of the free disc. The friction coefficient at which the lock-in occurs is indicated as first critical coefficient of friction. The study shows the presence of a second critical value of the friction coefficient, previously unobserved, where the unstable mode resulting from the coupling of the disc and pin modes splits back in two stable modes, if the friction coefficient exceeds such a value. This behavior has been called by the authors “locking-out”. In [134], Massi and Giannini presented an experimental analysis on a beam-on-disc setup aimed to correlate the modal damping distribution and the squeal propensity. The experimental evaluation of the lock-in point has been carried out by adding a lumped mass at one side of the beam, so that its natural frequency approaches the disc frequency, until both the modes coalesce. Addition of layers of rubber between the substructures of the system allowed varying the modal damping. It has been observed that a non-homogeneous distribution of the damping can increase the squeal propensity. In particular, it has been shown that the larger the ratio between the modal damping of the two coalescing modes, the larger the propensity of the system to develop squeal. A parametrical analysis with respect to the value of the added mass was also pursued, through CEA, in the numerical model developed in a later paper [135]. Figure 11.a shows the eigenvalue evolution as a function of the added mass and Figure 11.b the respective locus plot.

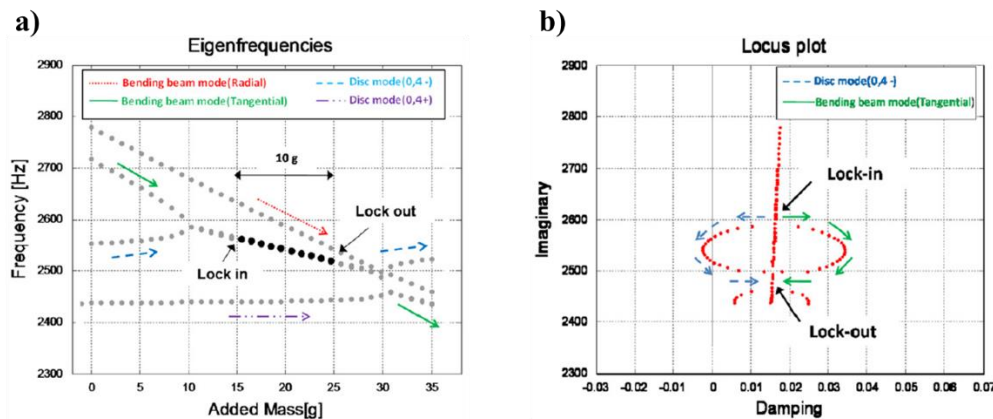


Figure 11 Complex eigenvalue analysis in a beam-on-disc numerical model: a) Evolution of the system eigenvalues as a function of the added mass on the beam. b) Locus plot as a function of the modal damping. More specific information in [135].

It can be noted that after the locking-in, one eigenvalue moves toward the negative damping half-plane, leading to the squeal unstable vibrational response, while the other one moves to the positive damping half-plane. By increasing further the mass, also the locking-out can be observed. The numerical reproduction of the experimental results highlighted the increase of the coalescence trend due to an inhomogeneous distribution of the added damping, while a homogeneous distribution of damping reduces the mode coupling propensity.

While most of the works dealing with the mode coupling instability are focused on automotive brakes and clutches, further works have investigated such phenomenon in aeronautic C/C brake systems.

In [92], Sinou et al. investigated the onset of whirl vibrations occurring under operational braking with a constant friction coefficient. More specifically, the onset of this unstable vibration, ranging between 200 and 300 Hz, is primarily due to a mode coupling phenomenon favored by the offset angle between the brake rod and the housing. The stability of the system, described with 15 degrees of freedom, has been studied by determining the eigenvalues of the Jacobian matrix of the system at the equilibrium points. Coalescing imaginary parts of the eigenvalues have been observed at around 250 Hz (onset of the mode coupling leading to the whirl vibration). With equal parameters, it has been shown that increasing the brake pressure it is possible to prevent the occurrence of the instability. However, the whirl instability cannot be avoided if the friction coefficient is higher than a threshold value.

It has been also observed that a low friction coefficient, offset angle and brake pressure can promote the stability of the system. However, these conditions can be hardly achieved in real applications. Lastly, it has been shown that the stiffness of the torque plat of the disc brake plays an important role on the stability of the system. In fact, specific intervals of stiffness values can avoid the mode coupling. On the other hand, increasing or adding damping on one part of the mechanical system can promote the onset of the dynamic instability.

In [93], the non-linear dynamical behavior of the whirl vibration has been investigated through the center manifold approach and rational fractional approximations. This procedure has allowed reducing the dimension of the original system and avoiding time-consuming numerical integration to obtain the time-history response and, consequently, the limit cycle amplitudes. A good agreement has been found between the proposed approach and the standard fourth-order Runge–Kutta algorithm for the solution of the non-linear system.

In the literature, some studies have been also focused on biomechanical applications, concerning for instance hip endoprosthesis systems. Experimental studies show that certain configurations can lead to self-excited dynamic instabilities, leading to exponentially growing oscillations that asymptotically tend to a limit cycle with significant amplitude. Even in this case, a computationally efficient approach to study the onset of the instability is the complex eigenvalue analysis [136].

The studies mentioned above accounted for a constant friction coefficient, whose value is determinant for the occurring of the mode coupling instabilities. Nevertheless, another well-known mechanism responsible for self-excited friction-induced vibrations is related to the decrease of the friction coefficient while increasing the relative velocity at the contact. A discussion on this further dynamic instability is presented in the following.

1.2.2.2 Negative Friction-Velocity Slope instability

First insights, correlating a squeal sound, in a drum brake, and a dynamic friction coefficient decreasing with the increase of the sliding speed, are found in a work of Mills [137], in 1938. Similar conclusions have been drawn, in later works, by Sinclair [138], in 1955, and by Fosberry and Holubecki [139], in 1961.

A simple mechanical system consisting of a mass-damper-spring oscillator on a moving belt, shown in Figure 12, can be used to describe this phenomenon.

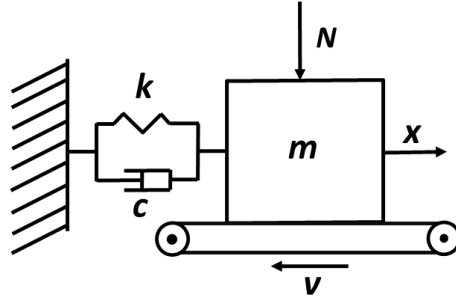


Figure 12 A single DoF spring-mass-damping system model on moving belt.

The friction coefficient μ is modeled as a linearly decreasing function of the relative velocity at the contact interface and it reads:

$$\mu = \mu_s - \alpha v_{rel}$$

Where μ_s is the static friction coefficient, v_{rel} is the relative velocity, defined as $v_{rel} = v - \dot{x}$, and the friction velocity slope is equal to α . The equation of motion describing the system can be written as follows:

$$m\ddot{x} + c\dot{x} + kx = \mu N$$

That leads to:

$$m\ddot{x} + (c - \alpha N)\dot{x} + kx = N(\mu_s - \alpha v)$$

It can be seen that if $\alpha N > c$ the system has an “apparent” negative damping that brings to the onset of a self-excited dynamic instability.

Shin et al., in [140], investigated numerically the occurrence of a negative friction-velocity gradient instability through a 2 DoF model representing a brake pad and a disc. Both the pad and the discs are modelled as single modes connected by a friction interface, which is pre-stressed by an external normal contact force N representing the brake pressure. Even in this case, the friction coefficient decreases linearly (slope equal to α) with the increase of the relative velocity at the contact interface. The stability analysis of the system, for various conditions, shows that the αN term, acting again as a negative damping contribution, should never be greater than $\min(c_1, c_2)$ for a stable condition, where c_1 and c_2 are the damping coefficient of the pad and the disc. This result also demonstrates that, in presence of a negative-friction velocity slope, a homogenous increase of damping on both the pad and the disc can prevent the onset of the friction instability.

In [141], Kang investigated the dynamic instability of a sliding oscillator subjected to a non-linear friction force. The friction coefficient is modelled in this case as an exponentially decreasing function of the relative sliding velocity. He observed that the negative slope of the friction coefficient is a destabilizing factor and the speed of the sliding belt in contact with the oscillator influences the dynamic instability. Specifically, he showed that in presence of a negative friction-velocity gradient the positive real part of the system eigenvalues increases if the velocity of the belt decreases.

Ouyang et al. [142] investigated the effect of the negative friction-velocity slope in an elastic system, consisting of two spring-dashpots in the transverse and in-plane directions, rotated around an annular disc. It has been observed that the presence of the negative friction-velocity

relationship, together with the in-plane stiffness and damper, is a source of initiation of additional resonances.

If the works cited above give an overview of the main features of such kind of instability, in the literature, several other works, both for dry and lubricated contacts [17, 113, 142-144], have focused on the effect of negative friction-velocity gradients, in different mechanical systems, bringing either to harmonic oscillation or stick-slip.

In fact, in the literature, a sliding friction coefficient decreasing with the velocity is also considered as one of the main causes of stick-slip phenomena [17, 19, 143, 144]. The onset of this frictional instability and its main features are described in the following paragraph.

1.2.2.3 Macroscopic stick-slip instability

The macroscopic stick-slip friction instability is a phenomenon consisting of two different states of motion, namely a sticking and a sliding phase. During the sticking phase, the static friction force, between the elastic media in contact, does not exceed the maximum static friction capacity. In this phase, the two contact surfaces stick and the asperities deform elastically. When the sliding occurs the two bodies return in relative motion and the asperities deform plastically [107]. As a result, a growth of the friction force during the sticking is observed, followed by a sudden drop in the slipping phase, where all the stored elastic energy is released. This behavior can lead to strong vibrations of the system due to the impulsive excitation. The shifting between the sticking and sliding status can interest either the overall surface (macroscopic stick-slip) or localized areas of the interface.

Moreover, it should be kept in mind that in a real physical system the switch between a status to another cannot be a discontinuity.

The initiation of the sliding motion has been the object of research works aimed to explain the dominant mechanisms behind the rupture of the sticking interface and its relationship with the global dynamics. Rubinstein et al. [145] showed that a sequence of crack-like precursors precede the onset of the sliding motion. It has been observed that these precursors are initiated at a shear level lower than the static friction threshold and arrest before traversing the entire contact interface. Lately, it has been demonstrated that the presence of isolated micro-slip events prior to the occurrence of the macro-slip phase acts as a source of propagating waves. When a sufficient number of micro-slips occurs at almost the same time, they release enough energy to sustain a slip pulse propagation. These slip pulses behave as precursors. When an increasing number of precursors are triggered and their distance of propagation augments, an extensive rupture occurs and a macro-slip is observed. The superficial rupture and the resulting propagating waves excite the system and lead to the impulsive vibrational response characteristic of the macroscopic stick-slip phenomenon [89].

While the nucleation mechanism described by Rubinstein, and in several other works [89, 146-148], allows the macroscopic stick-slip phenomenon also with a constant macroscopic friction coefficient, in the literature, the onset of a stick-slip motion in a sliding contact has been often attributed to a difference between the static and the kinetic friction coefficients. In particular, a decrease in the kinetic friction coefficient with increased sliding velocity (negative friction-velocity slope) is thought to be the major responsible for this friction-induced instability [17, 107, 144, 149]. In 1940, Blok [149] stated that the essential condition for the stick-slip friction instability to arise is the decrease of the frictional force with the increasing sliding speed. Moreover, further studies on the subject have shown that the increase of the friction coefficient

near zero sliding speed imposes a minimum critical velocity under which stick-slip is observed [150, 151]. Singh [152] presented a theoretical and experimental study on this critical velocity and demonstrated the influence of parameters such as the difference between static and kinetic friction coefficient, damping, stiffness, and sliding mass. Jang et al. [121] investigated a number of brake friction materials characterized by different material compositions. The specimens showing less negative friction-velocity slope were also characterized by a lower propensity to creep groan (noise emission in brake systems related to stick-slip [153]).

The effect of the boundary conditions and main system parameters on the stick-slip friction instabilities has been investigated in many research works [17, 19, 154-156]. Behrendt et al. [18], showed that the macroscopic sliding velocity can be considered as a key parameter separating different regimes of resulting dynamics. A numerical model consisting of an elastic brake pad sliding at different constant velocities over a rigid surface, under constant load, has been studied by finite element analysis. As shown in Figure 13.a, a velocity-dependent friction coefficient has been implemented.

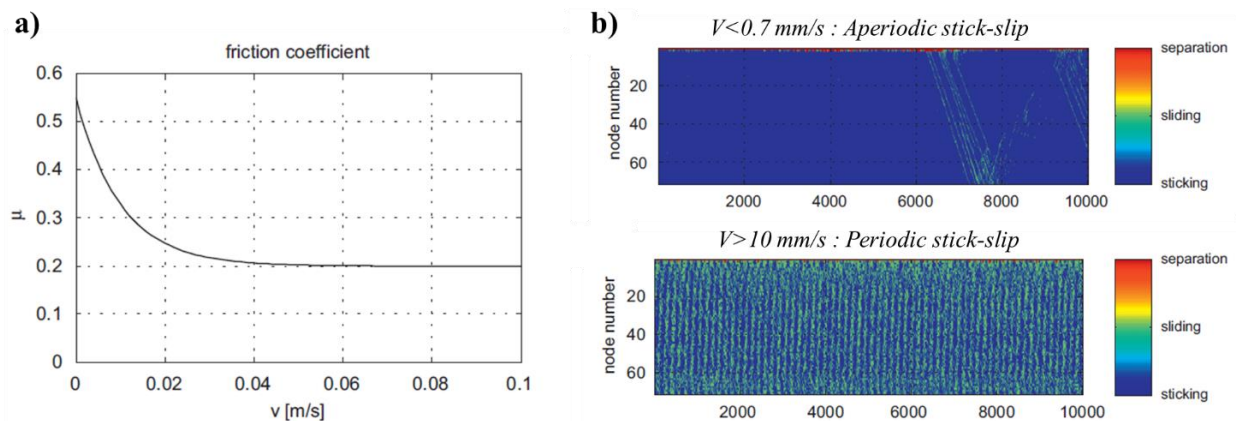


Figure 13 Numerical study on stick-slip motion: a) Velocity-dependent friction law of the contact interface; b) Contact states during stick-slip motion for two different sliding speed regimes ($V < 0.7$ mm/s, $V > 10$ mm/s). More information about the numerical simulation in [18].

Figure 13.b shows the different contact states during a stick-slip motion for two regimes of sliding velocity. It has been observed that, for sliding velocities close to zero, the slip phenomena are not synchronized with the structural vibration, resulting in an aperiodic stick-slip motion. However, for slightly higher velocities, the stick-slip phenomenon depends strongly on the structural vibration properties. As a result, a periodic macroscopic stick-slip regime, characterized by the frequency of a structural mode, can be observed.

Yoon et al. [120] showed the effect of different loads, speeds, and contact stiffnesses into brake-induced stick-slip. They observed an increase of the stick-slip oscillation amplitude with a higher load and a decrease with a higher sliding speed. The smaller intensity and period of the stick-slip instability, when increasing the sliding velocity, supports the extinction of stick-slip at higher sliding speeds. Moreover, it has been shown that a lower contact stiffness reduce the intensity and period of the stick-slip oscillation.

Fuadi et al. [157] proposed a map to predict the onset of stick-slip phenomena leading to creep groan in braking applications. The study has been carried out both experimentally, by means of a caliper-slider setup, and numerically, through a 2 DoF model. The experimental diagram, shown

in Figure 14, has been developed as a function of a stiffness ratio Ks , defined as the ratio between the stiffness of the structure and the one of the contact, and a dimensionless index Ls , comprised of the main parameters affecting the stick-slip phenomenon.

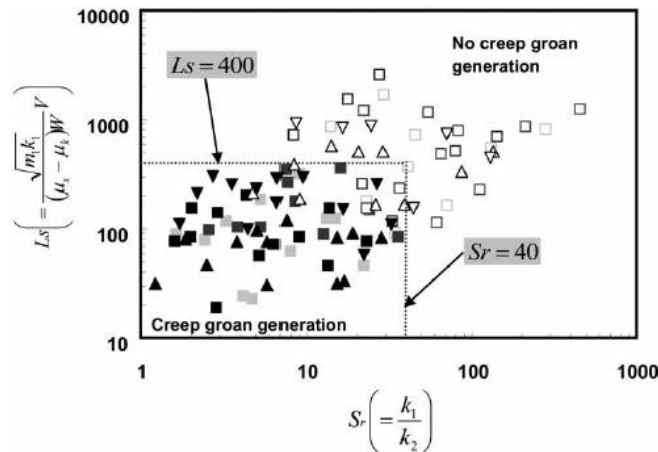


Figure 14 Map of creep groan events as a function of a stiffness ratio Ks and a dimensionless index Ls accounting for the main contact parameters affecting the stick-slip occurrence. More specific information in [157].

Consistently with other outcomes in the literature, it can be noted that a higher difference between the static and kinetic friction coefficient, as well as a higher normal load W and a lower sliding velocity V , promotes the onset of the instability. Moreover, a lower stiffness ratio, i.e. a higher contact stiffness with respect to the structure stiffness, is another non-negligible parameter that could lead to stick-slip phenomena.

Tonazzi et al. [105] investigated, through numerical analyses of two finite elastic media in frictional contact, how the same frictional system can switch from stable sliding to mode-coupling or stick-slip instabilities, as a function of the system and contact parameters. E.g., the structural damping affects the macroscopic frictional behavior leading to stick-slip or mode coupling. The study has been carried out introducing a proportional material damping consisting of a mass damping coefficient α and a stiffness damping coefficient β . The latter damps the local dynamics at the contact, i.e. the wave propagation at the contact interface [89], and it has been observed that lower values of β can lead to stick-slip phenomena. On the other hand, α plays a key role on the damping of the system response, reducing the amplitude of the stick-slip oscillation. In [87], a related work shows an experimental and numerical analysis aimed to investigate the transition of a system from a continuous sliding state to macroscopic stick-slip. Among the numerous works on the stick-slip motion [158-161], the examples provided here show that many parameters and operating conditions affect the onset of such friction instability. The mechanism driving the occurrence of stick-slip are clearly the result of several phenomena resulting from the strong interaction between the local contact dynamic (wave propagation), the overall frictional response at the interface (driven by the rheology and physicochemical characteristics of the interface) and the macroscopic vibrational response of the system.

The overall framework of the dynamic instabilities described so far provides an essential background to understand the complex dynamical response characterizing systems with C/C materials in frictional contact.

Finally, in the following section, some results from a preliminary work on the friction-induced vibrations obtained with C/C composite materials, under different boundary conditions, are presented.

1.2.3 Thermally driven instabilities on C/C materials

Despite being a key resource in many industrial fields, C/C materials are not exempt of frictional instabilities that may occur during the frictional contact. In [12], an experimental characterization on how different working temperatures affect the C/C material propensity to destabilize the dynamics of the system has been provided. Moreover, it has been shown a relationship between the frictional response, at different sliding velocities and temperature conditions, and the occurrence of unstable friction induced vibrations.

Tests have been performed by means of a suitable test rig, specifically designed for reproducing and measuring the frictional and vibrational response of C/C specimens, sliding one against the other, under controlled boundary conditions. In the study, a first set of measurements have been carried out at constant sliding velocities (0.2, 2, 20 mm/s) at both room temperature and 500 °C. A second set of measurements has been carried out with a decreasing sliding velocity (20 to 0 mm/s), in order to simulate braking, at 25, 100, 200, 300, 400 and 500 °C. All tests have been performed after that the C/C samples have been statically heated up to the target temperature.

Within the imposed heating protocol and boundary conditions, the first measurement campaign, at constant sliding velocities, has shown higher values of the friction coefficient at room temperature condition, compared to 500 °C. Furthermore, under different constant sliding velocities, the obtained friction coefficient at room temperature is almost the same. On the other hand, tests carried out at 500 °C have shown an increasing value of the friction coefficient with the decrease of the imposed constant sliding velocity.

Such trends have been confirmed in the second measurement campaign carried out at variable sliding velocity. As shown in Figure 15, the presence of a negative friction-velocity slope (i.e. increase of the friction coefficient with the decrease of the sliding velocity) has been observed for temperatures higher than 200 °C.

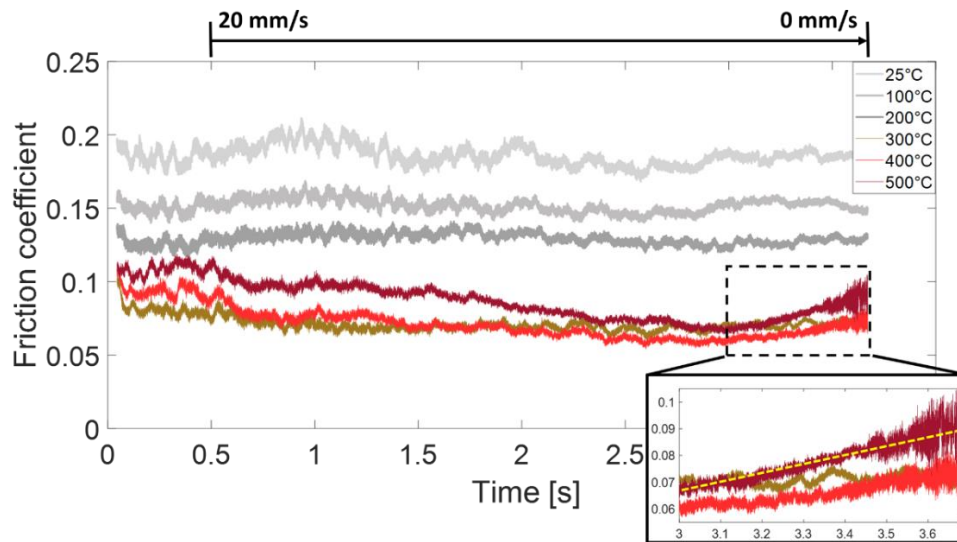


Figure 15 Friction coefficient behaviour, at different temperature conditions, during braking with an imposed sliding velocity varying from 20 to 0 mm/s. More specific information in [12].

The effect of the thermal conditions on the frictional response has a significant impact on the stability of the friction-induced vibrations generated by the sliding of C/C materials. As shown in Figure 15, a higher temperature leads to a negative friction-velocity slope, which, in turn, promotes the occurrence of a dynamic instability. The evolution of a typical C/C dynamic instability, observed for instance at 500 °C during a braking test, is shown in Figure 16.

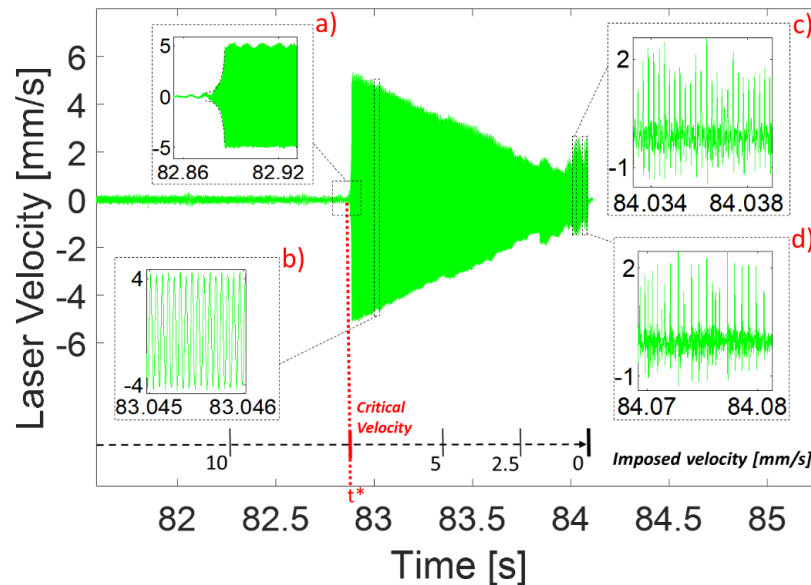


Figure 16 Evolution of a C/C dynamic instability in a single braking at 500 °C and with an imposed sliding velocity varying from 20 to 0 mm/s.

The main features of the observed instability are:

- First, at a critical velocity value, an increase of the amplitude of oscillation is observed, due to the negative friction-velocity slope, up to a limit cycle (inset a of Figure 16);
- Then, a decrease of the amplitude of the limit cycle of oscillation is obtained, as a result of a lower energy provided by the decreasing braking velocity (inset b of Figure 16);
- At lower velocities, the local surface reactivity leads to stick-slip instability, characterized by a periodic impulse-like excitation. The periodicity of the stick-slip phases is determined by the unstable mode (negative friction velocity-slope instability), which drives the stick-slip occurrence (inset c of Figure 16);
- Lastly, the further decrease in velocity entails a higher adherence time between local asperities, making the stick-slip sequence independent of the system mode. The stick-slip period is only related to the time needed to accumulate enough deformation energy to detach the interface (inset d of Figure 16).

These results provide an example of the different scenarios under which friction-induced vibrations, originated by C/C materials, may result in dynamic instabilities, with particular regard to the main contact parameters promoting the unstable vibrations.

1.3 PhD positioning

As shown in this Chapter, a huge amount of works deals with the characterization of the physicochemical and tribological features of carbon materials [1, 25, 54, 63]. Lately, the growing interest in C/C composites has led to many research studies aimed to understand the frictional and wear response of such materials, under different operative conditions [5, 6, 8, 9, 60]. Despite the extensive literature on this subject, the main mechanisms driving the occurrence of different unstable friction-induced vibrations, during frictional contact of C/C composites, are still poorly investigated and understood. A significant lack of information concerns the role played by the boundary conditions on the C/C material propensity to destabilize the dynamics of the system and its relationship with their frictional behavior. Moreover, the complex physicochemical and mechanical role of the C/C third body makes the rheological contribution an essential parameter to take into account when considering the overall frictional and vibrational response. Nevertheless, in the literature, most of the works focus on the physicochemical aspects of C/C particles, overlooking the effective rheological role in real contact interfaces and under different boundary conditions, especially in presence of metallic and non-metallic contaminants.

On the other hand, by a vibrational point of view, dynamic contact instabilities are often investigated separately, within specific industrial applications and boundary conditions [88, 90, 107]. Nevertheless, as proven by the recent literature [87, 89], the same mechanical system can be affected by different kinds of contact instabilities (macroscopic stick-slip, mode coupling, negative friction-velocity slope, etc.) as a function of the boundary conditions. Such unstable states of the system can compete or even coexist, leading to high amplitude vibrations.

Within this framework, the present work aims to provide a deep investigation of the main vibrational phenomena occurring during the frictional interaction of C/C materials, with and without impurities affecting the rheology at the contact interface.

The relationship between the frictional and vibrational response, under different boundary conditions, is examined closely. A deep dynamic analysis is combined with frictional tests, under a large panel of boundary conditions and third bodies, in order to reproduce and analyze the different dynamic and frictional responses. Furthermore, an approach for distinguishing the distinct dynamic contact instabilities, and their possible coexistence, is investigated. The analysis is carried out with a specific consideration of the rheological and physicochemical contributions at the interface, as a function of different operative conditions.

The goal of the PhD is then to combine and further develop the previous works in the literature, both on the physicochemical response of C/C materials and on the contact dynamic instabilities, contextualizing them to the effective tribological and dynamic response of mechanical systems equipped with such frictional composites.

Moreover, by an industrial point of view, large interest concerns the tribological response of C/C materials in harsh thermal conditions. In this respect, this work aims to offer a wider characterization of the frictional behavior of C/C composites with respect to different contact parameters and with particular regard to the effect of several working temperatures. The evolution of the friction coefficient, as well as the onset of dynamic instabilities, is studied up to 500 °C.

Chapter 2

Experimental characterization under controlled boundary conditions

In this Chapter, the tribological behaviour of C/C materials is investigated under controlled boundary conditions. Specimens machined from real disc brakes are tested in specifically designed test benches, where the influence of the main contact parameters on the frictional and vibrational response of the tested samples is investigated.

The analysis is focused on understanding how different boundary conditions affect the behavior of the friction coefficient and the onset of unstable friction-induced vibrations. The tribological and dynamic response is also investigated in presence of metallic and non-metallic contaminants on the contact interface of the C/C specimens. This experimental characterization allows taking into account the impact of the different parameters, including contaminating particles, affecting the frictional contact of C/C composites, in a significantly high range of temperature (up to 500 °C).

The specimens are tested through a dedicated test bench (*TriboAir*), which allows investigating the behavior of the friction coefficient and its relationship with the occurrence of dynamic instabilities. A specially developed protocol is used in order to study the role of the sliding velocity and temperature on the material tribological behavior. The effect of different contact atmospheres is then investigated through another test bench (*TriboWave*), by experiments carried out both in air and low oxygen environments. A critical discussion and comparison of the results obtained by testing the different specimens is provided as well.

2.1 Experimental setup and signal analysis

2.1.1 Dedicated test bench

In order to study the occurrence of unstable friction-induced vibrations and their relationship with the frictional response of C/C materials, under different operating conditions, a specifically designed tribometer has been used. The experimental test bench, named *TriboAir*, allows for the relative motion of two C/C specimens in contact and provides accurate measurement of friction-induced vibrations and contact forces originated by the frictional interactions between the tested samples. Moreover, thanks to the adopted test rig, boundary conditions such as sliding velocity, contact pressure and temperature of the frictional interface can be controlled. The experimental setup is shown in Figure 17.a. A simplified diagram of the test bench is presented in Figure 17.b.

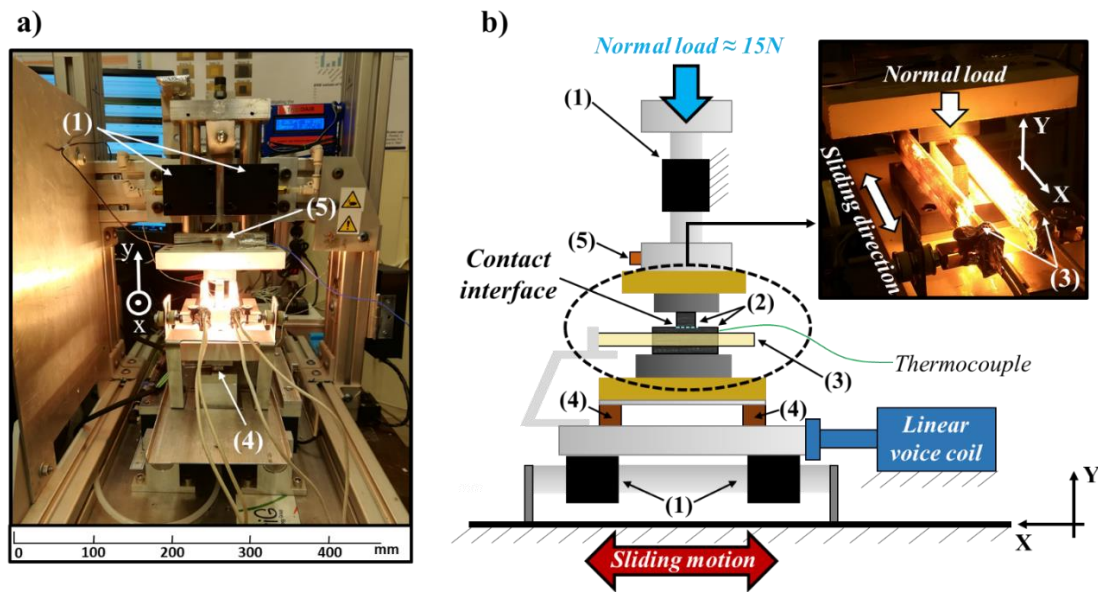


Figure 17 TriboAir experimental setup (a) and schematic diagram (b). (1) Air bearings; (2) C/C material specimens in frictional contact; (3) IR lamps; (4) 3-axial force transducers; (5) Uniaxial accelerometer.

High accuracy dynamic measurements are achieved thanks to the air bearings (1), which allow the relative motion of the tested samples without introducing parasitic noise affecting the measure of friction-induced vibrations and contact forces. The air bearing system consists of air guides placed on the upper and lower part of the setup. Four air bearings are assembled at the bottom of the moving base and allow the sliding motion of the lower C/C sample, with respect to the upper one, along the tangential direction (X direction). Other two air guides are placed along the normal direction to the contact (Y direction), allowing the load application by means of dead weights located at the top of the test bench. Thanks to this air bearing system, friction forces and vibrations that could affect the accuracy of the measurement at the contact interface are therefore prevented. In order to control the sliding velocity and the law of motion, a linear voice coil motor (BEI KIMCO LA30-75-001A), coupled to a linear optical encoder, drives the motion of the lower C/C specimen (2), while the upper C/C sample (2) is kept stationary and in frictional contact with the lower one. The temperature at the contact interface can be controlled by means of two IR lamps (3), placed alongside the tested samples. A specific thermal profile can be achieved thanks to a PID temperature controller (GEFRAN F650). Moreover, a ceramic insulation system has been specifically designed to best convey the heat to the contact interface. Temperature can be monitored thanks to a thermocouple placed inside a hole 3 mm deep, at 2 mm from the contact interface of the lower C/C sample, in order to be as close as possible to the contact interface. Before each test, the relative humidity of the environment is measured by a humidity sensor (SENSIRION SHT85).

As far as concern the measure of the contact forces, 3-axial force transducers (KISTLER 9017B) (4) are assembled on the moving base of the tribometer.

The vibrational response due to the frictional interaction between the samples is measured by a uniaxial accelerometer (5), placed in the tangential direction to the contact, on the upper part of the setup.

All data are recorded by an acquisition system, with a sample frequency equal to 40 kHz, and then post-processed by Matlab[®].

As regards the samples adopted for the analysis, C/C specimens of simple geometry have been machine from disc brakes. In the following, a description of the tested specimens is provided.

2.1.2 C/C material specimens

The samples of C/C materials consist of two blocks of simple geometries. The sample clamped on the mobile base of the test rig is a rectangular prism of 10x50x25 mm (contact surface 10x50 mm), while the sample clamped on the upper part of the tribometer is a cube of 10 mm side. Each stroke of the lower sample covers a sliding distance of 40 mm. Figure 18 shows, as an example, the sample clamped on the moving base (a) and the one clamped on the upper part of the setup (b). The frictional surface is also shown.

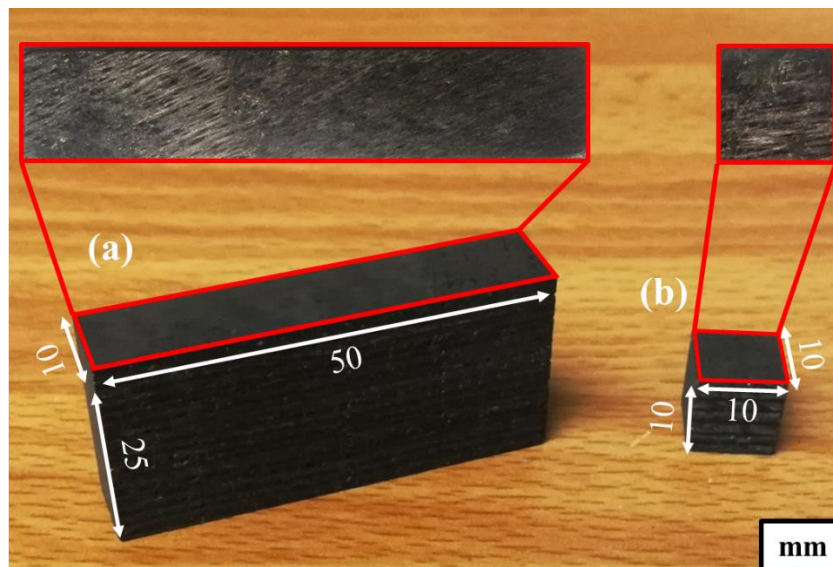


Figure 18 Example of C/C specimens adopted for the tests. a) Sample clamped on the moving base (10x50x25 mm) b) Sample clamped on the upper part of the setup (10x10x10 mm).

The experimental campaign has been carried out by using samples of C/C material machined from C/C brake discs. The specimens are referred to as MAT1, MAT2, MAT3 and MAT4. Analyses carried out by SEM (Scanning Electron Microscope) and EDX (Energy Dispersive X-ray Analysis) on different samples have shown the presence of metallic, semi-metallic and non-metallic elements on the contact interface of MAT1, MAT2 and MAT3, while MAT4 is characterized by only carbon (see Annex I) [162, 163]. Table 2 describes the different contaminants found on the friction surface of the C/C specimens.

Specimens	Contaminants
MAT1	Cont1, Cont2, Cont3, Cont4
MAT2	Cont3, Cont4, Cont2 (environment)
MAT3	Cont3, Cont4
MAT4	None

Table 2 Contaminants found on the contact surface of C/C specimens machine from brake discs with different contaminants.

It should be remarked that the amount of Cont2 found on MAT2 is significantly low, compared to MAT1, and probably due to impurities dispersed in the environment.

From Table 2, it can be noted that the main difference between the C/C specimens machined from MAT1, MAT2 and MAT3 is the presence of both Cont1 and Cont2 on MAT1. Figure 19 presents an example of SEM/EDX analysis carried out on MAT1. A SEM picture taken on the contact surface through secondary electrons is shown.

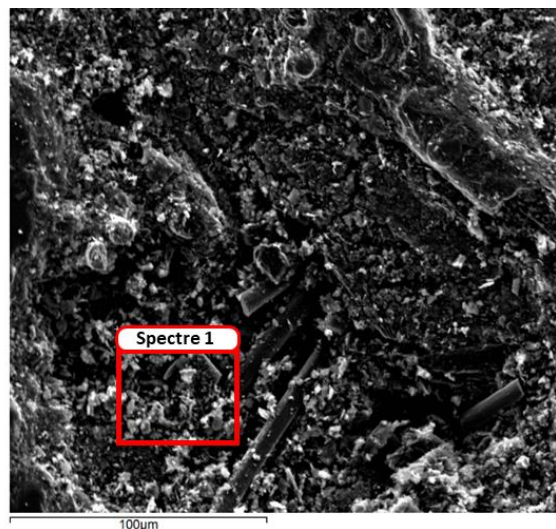


Figure 19 Example of SEM/EDX analysis carried out on the contact surface of a MAT1 specimen. SEM picture taken at a scale of 100 µm through secondary electrons.

MAT1, MAT2, MAT3 and MAT4 have been obtained from discs previously tested on a full disc brake setup. These specimens are referred to as “used”. Only one sample, called MAT5, has been machined from a new C/C disc without contaminants, in order to compare the material tribological and dynamical response in new and used states.

All the C/C specimens used for the analysis are tested according to a specific protocol mainly aimed to investigate the effect of different sliding velocities and temperatures on the frictional and vibrational behaviour of the C/C samples in frictional contact. In the following, the measurement protocol will be described.

2.1.3 Measurement protocol and definition of the boundary conditions

The experimental protocol for studying the tribological and dynamical response of the above-described C/C specimens provides for tests carried out with two different laws of motion. Variable velocity tests are used to investigate the material response during braking conditions. Constant velocity tests, by comparison with the variable velocity tests, allow investigating the effect of the variable sliding velocity on the frictional and vibrational behavior of the tested samples.

Figure 20 shows the imposed velocity profiles, during each cycle of back and forth of the moving sample, for the two types of tests.

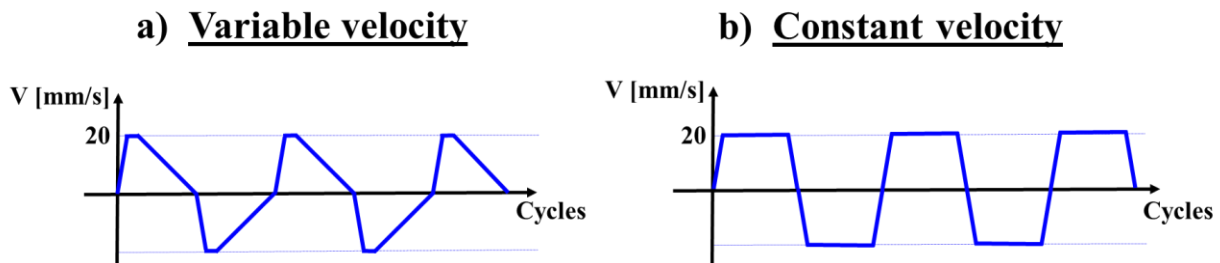


Figure 20. Example of variable and constant velocity profiles during the back-and-forth cycles of the lower C/C specimen. a) Decreasing velocity from 20 to 0 mm/s, with a deceleration of 6 mm/s² in each stroke; b) Constant velocity of 20 mm/s in each stroke.

As shown in Figure 20.a, tests carried out with a variable velocity profile are performed with an imposed sliding speed varying from 20 mm/s to 0 mm/s, with a deceleration of 6 mm/s². The maximum sliding speed of 20 mm/s is quickly reached with an acceleration of 100 m/s². In this way, most of the sliding distance, covered by the moving sample, is characterized by the imposed braking condition (decreasing velocity). Tests carried out at a constant velocity, shown in Figure 20.b, are performed with an imposed speed of 20 mm/s, kept constant in each cycle of the test. The increasing and decreasing speed ramps are carried out with an acceleration/deceleration equal to 100 mm/s².

The two laws of motions described above are used when imposing different heating profiles, through which C/C specimens are tested at different temperature conditions during frictional contact. As described in {1.1.3.2}, the frictional response of C/C materials is strongly affected by the increase of temperature, which can lead to a transition between two frictional regimes, one characterized by a lower friction coefficient and the other characterized by a higher friction coefficient. As a result, in order to study the evolution of the frictional response of the C/C materials at different temperature conditions, two heating methods have been preliminary adopted. The temperature trends, imposed respectively for the “sliding heating” method and the “static heating” one, are presented in Figure 21.

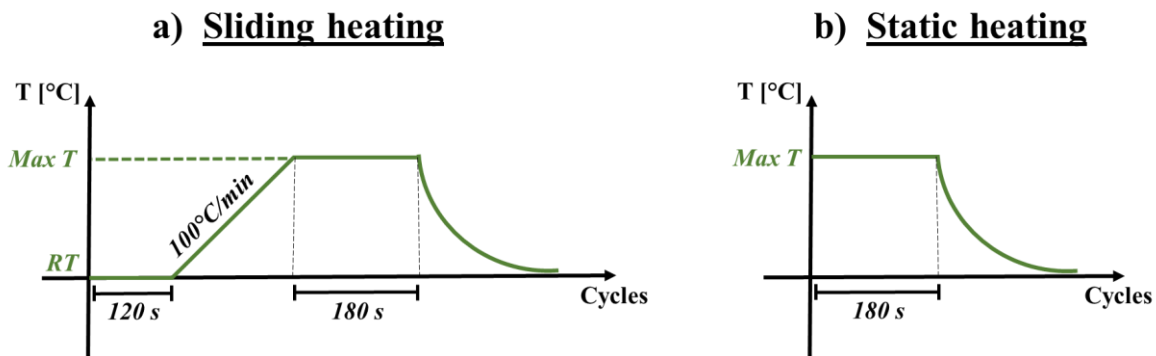


Figure 21 Heating methods preliminary adopted for the analysis. a) Sliding heating method; b) Static heating method.

Figure 21.a describes the *sliding heating* method. It provides for two minutes at room temperature, during which the lower sample slides again the upper one with either constant or variable velocity (law of motions shown in Figure 20). After that, the infrared emitters are turned on and the temperature regulator controls the increase of temperature with a gradient of $100\text{ }^{\circ}\text{C}/\text{min}$. In this case, the heating process takes place in parallel with the relative motion of the samples. The gradient has been chosen in order to have a reasonable amount of time for the temperature to increase and for studying the evolution of the material response during heating. When the maximum temperature of the test is reached, the temperature regulator keeps the temperature to the established value for 3 minutes. Then, the IR lamps are turned off and the sliding motion continues for other two minutes with a natural cooling. The maximum temperature of the test ($100, 200, 300, 400, 500\text{ }^{\circ}\text{C}$) varies for each different test.

While for the sliding heating method the sliding motion is maintained throughout the whole test, the *static heating* method, described in Figure 21.b, provides for a relative motion of the samples only when the maximum temperature is reached. Thus, once the two C/C samples are in contact, the IR lamps are turned on and increase the temperature up to the established value, while the lower sample is held in place and no relative motion occurs. When the maximum temperature is reached, the relative motion, with the desired law of motion, is imposed and the temperature regulator maintains the temperature for three minutes. Then, analogously to the *sliding heating* test, the samples are kept in relative motion for other two minutes while the system cools down. The *sliding heating* method allows studying the evolution of the friction coefficient and the onset of vibrational phenomena during the heating phase. On the other hand, the *static heating* method focuses only on the maximum temperature of the test, imposing the relative motion on the heated surfaces when they are still not in sliding contact. This heating method has been adopted only in a preliminary protocol where the C/C tribological response, in presence of the two different heating methods, has been investigated. The preliminary protocol is shown in Table 3.

DAY ONE		DAY TWO		DAY THREE		DAY FOUR	
<i>Sliding Heating</i>		<i>Static Heating</i>		<i>Sliding Heating</i>		<i>Sliding Heating</i>	
$V=const=20\text{ mm/s}$		$V=20\rightarrow 0\text{ mm/s}$		$V=20\rightarrow 0\text{ mm/s}$		$V=const=20\text{ mm/s}$	
1	RUN-IN	1	200°C	1	100°C	1	500°C
2	100°C	2	500°C	2	200°C		
3	200°C	3	200°C	3	300°C		
4	300°C			4	400°C		
5	400°C	$V=const=20\text{ mm/s}$		5	500°C		
6	500°C			6	300°C		
7	300°C	1	200°C	7	200°C		
8	200°C	2	500°C	8	100°C		
9	100°C	3	200°C				

Table 3 Preliminary protocol used for the experimental tests of the C/C specimens. Sliding heating tests are carried out in day one, three and four, while static heating tests are carried out in day two. Variable (20→0 mm/s) and constant (20 mm/s) imposed velocity tests are performed at different temperatures, up to a maximum temperature of 500 °C.

The first day of the protocol presented in Table 3 is characterized by *sliding heating* tests carried out at a constant velocity of 20 mm/s in each stroke. After an initial run-in of 15 minutes, where the samples are in relative motion and frictional contact, the protocol provides for a sequence of *sliding heating* tests, where different maximum temperatures are reached. The value of the maximum temperature reached during each test is shown in Table 3. First, a test with a maximum temperature of 100 °C is carried out. After that, the maximum temperature is progressively increased (100 °C more in each test) up to 500 °C. Then, the highest temperature of each sliding test is gradually decreased down to 100 °C, in order to verify the repeatability of the material response after the 500 °C test.

The second day of the protocol focuses on the *static heating* tests and consists of two sequences. The first sequence is carried out at variable velocity and it is characterized by a first test with a maximum temperature of 200 °C, to which follows a 500 °C test. Then, a test with a maximum temperature of 200 °C is again performed. On the other hand, the second sequence is characterized by the same series of tests of the previous one, but it is performed at constant velocity.

The third day of the protocol is characterized by *sliding heating* tests. It follows the same sequence of the first day, but each test is carried out at variable velocity in order to simulate a braking condition.

Lastly, the fourth day of the protocol verifies, with a single *sliding heating* test with a maximum temperature of 500 °C and at constant imposed velocity, if the material response of the C/C sample is the same as the day one (test at 500 °C).

The normal load applied in each test of the protocol is kept equal to almost 15 N, in order to have an average contact pressure of 0.15 MPa.

The preliminary protocol described above has been subsequently reduced, considering only the *sliding heating* tests. In fact, no remarkable differences of the C/C material response have been

observed between *static* and *sliding heating* methods (see Annex II), once the maximum temperature of the tests is reached and a steady state condition is achieved (usually after almost 2 minutes at constant maximum temperature). Moreover, also the fourth day of the preliminary protocol has been removed, because no differences have been observed between the tests carried out at the maximum temperature of 500 °C, at constant velocity, at the begin and at the end of the protocol (see Annex III).

Taking into account the previous considerations, the experimental protocol has been reduced to two days of *sliding heating* tests at constant and variable velocities, as shown in Table 4.

DAY ONE		DAY TWO	
<i>Sliding Heating</i>		<i>Sliding Heating</i>	
$V=const=20\text{ mm/s}$		$V=20\rightarrow 0\text{ mm/s}$	
1	RUN-IN	1	100°C
2	100°C	2	200°C
3	200°C	3	300°C
4	300°C	4	400°C
5	400°C	5	500°C
6	500°C	6	300°C
7	300°C	7	200°C
8	200°C	8	100°C
9	100°C		

Table 4 Final protocol used for the experimental tests of the C/C specimens. Sliding heating tests are carried out in day one and day two. The first day of the protocol is devoted to constant imposed velocity tests (20 mm/s) while the second day focuses on variable imposed velocity tests (20→0 mm/s).

In the following, a description of the analysis carried out on the signals retrieved from the experimental tests, performed according to the protocol described in Table 4, is provided.

2.1.4 Analysis of the outputs

The analysis of signals obtained from the experimental protocol described in the previous section focuses on the study of the friction coefficient, at different velocities and temperature conditions, and its relationship with the onset of dynamic instabilities. An example of retrieved data, obtained by *sliding heating* tests carried out on a MAT1 sample, at a maximum temperature of 500 °C, is provided in Figure 22. Figure 22.a shows the test carried out at constant imposed velocity ($V=20\text{ mm/s}$) while Figure 22.b shows the test carried out at variable imposed velocity ($V=20\rightarrow 0\text{ mm/s}$). Both Figure 22.a and Figure 22.b show the evolution of the friction coefficient (ratio between the tangential and normal force measured by the force transducers), in red, throughout

the whole *sliding heating* tests. The temperature of the samples, measured by the thermocouple located within the sample and near the contact interface, is in green.

In order to follow the evolution of the static friction coefficient (beginning of each stroke), an interpolation of all the static friction coefficient points are plotted in cyan. The blue lines show instead the interpolation of the friction coefficient points taken in the middle of each stroke, in order to have a reference value of the dynamic friction coefficient evolution during the test. In the insets of Figure 22.a and Figure 22.b, the behavior of the friction coefficient at room temperature, during a back-and-forth cycle of the moving sample, is shown respectively for constant and variable imposed velocities. The cyan markers denote the selected points for the interpolation of the static friction coefficient (SFC). The blue markers indicate instead the dynamic friction coefficient (DFC) points selected in the middle of each single stroke. The symmetric reversal of sign of the friction coefficient in each stroke is due to the back-and-forth motion of the lower sample with respect to the upper one. It should be also remarked that, while for the variable velocity test the dynamic friction coefficient points selected in the middle of each stroke are taken at an imposed speed of almost 11 mm/s, for the constant velocity test the dynamic friction coefficient is taken at 20 mm/s, being the velocity of each stroke constant.

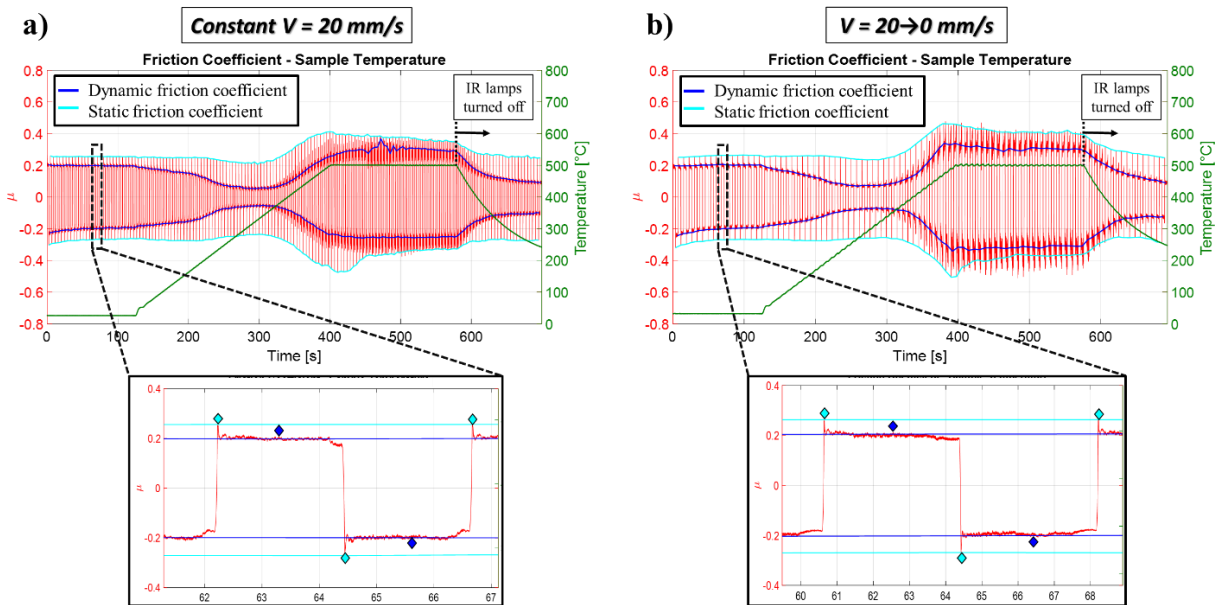


Figure 22 Example of friction coefficient analysis in sliding heating tests at constant (a) and variable (b) imposed velocity, with a maximum temperature of 500 °C, for the MAT1 specimens. In red the friction coefficient, in green the temperature, in cyan the interpolation of all the static friction coefficients (SFC) of each stroke and in blue the interpolation of the dynamic friction coefficient (DFC), considering its value in the middle of each stroke.

From both Figure 22.a and Figure 22.b, a characteristic behavior of the C/C frictional response, when the temperature increases, can be observed. At room temperature condition, the level of SFC and DFC is almost constant and respectively almost equal to 0.2 and 0.25. During the first two minutes of sliding no significant variation of the SFC and DFC is in fact observed. Moreover,

the trend of friction at both constant and variable velocities is similar during each back-and-forth stroke (insets in Figure 22).

When increasing the temperature up to 300 °C, a decrease of the dynamic friction coefficient can be noted on both the constant and variable imposed velocity tests. The static friction coefficient stays almost constant instead. Increasing further the temperature up to 500 °C, a growth of both the dynamic and static friction coefficient can be observed. Consequently, the SFC and the DFC result in higher values compared to the room temperature condition. When the IR lamps are turned off, the value of both the DFC and SFC decreases with the temperature.

The observed behavior is consistent with the occurrence of different frictional regimes when the temperature increases, as also shown in [24]. Compared to previous outcomes in the literature [24], this approach allows following the evolution of the DFC and SFC in a significantly higher temperature range and with a higher resolution with respect to the temperature variation, providing a clear description of the frictional response under controlled boundary conditions.

A more specific study of the frictional and vibrational response is also possible by investigating in further detail the single strokes of each test. As an example, Figure 23 shows a single stroke at room temperature condition (RT), taken from the test described in Figure 22.a. From the top to the bottom, the signals correspond to the absolute value of the friction coefficient measured during the frictional contact, the vibrational signal measured by the accelerometer and the velocity profile imposed on the lower moving sample by the linear voice coil motor.

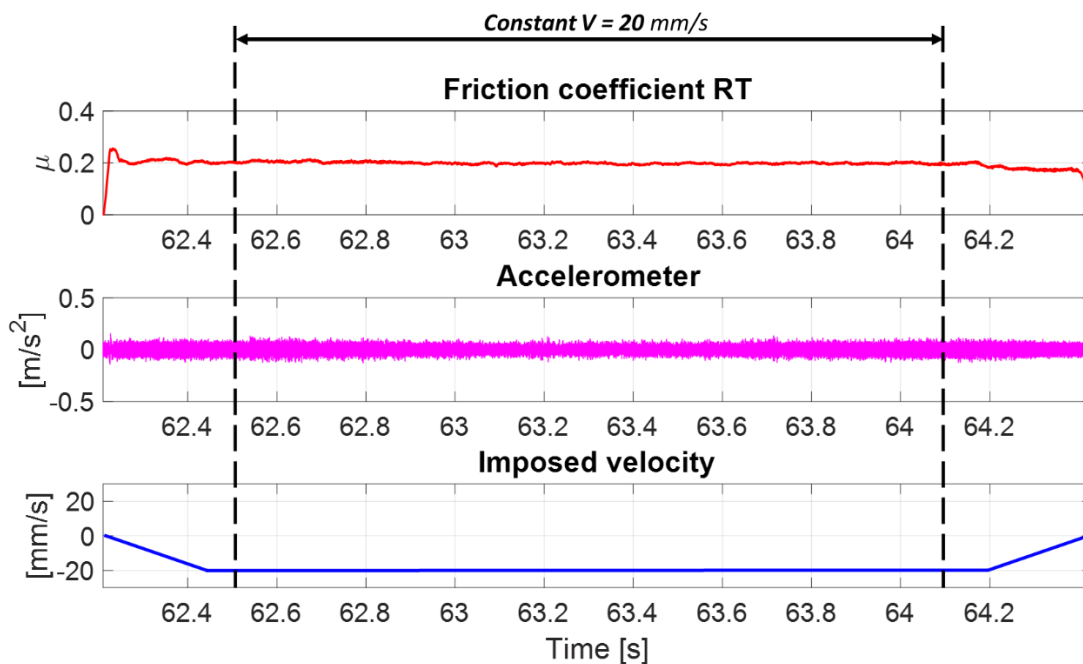


Figure 23 Example of signals recorded during a single stroke at room temperature condition ($\approx 25^\circ\text{C}$), in the constant sliding velocity test ($V=20\text{ mm/s}$) shown in Figure 22.a. From the top: the friction coefficient (ratio between tangential and normal force), the accelerometer signal and the imposed sliding velocity profile.

Figure 23 shows, within the range of the signal corresponding to constant velocity, a constant friction coefficient of almost 0.2. During the constant velocity sliding, the acceleration signal shows a low-amplitude noise, corresponding to friction noise when stable friction-induced vibrations occur [86, 95]. The imposed velocity profile is the one already described in Figure 20.b and characterized by a plateau at 20 mm/s and increasing/decreasing velocity ramps carried out at 100 mm/s². When comparing the friction coefficient behavior and the vibrational signals of different strokes, only the constant velocity part is taken into account, as shown in Figure 23 (signals in between the vertical dashed lines).

Similarly to the analysis described above for constant velocity tests, also for variable velocity tests the frictional and vibrational response of a single stroke is investigated in detail. An example of a single stroke at room temperature condition, taken from the test described in Figure 22.b, is shown in Figure 24. From the top to the bottom, the signals correspond to the absolute value of the friction coefficient, the vibrational signal measured by the accelerometer and the imposed sliding velocity profile. Because the tests are carried out with a decreasing imposed velocity (20 to 0 mm/s), the x (time) axes can be considered as inversely proportional to velocity.

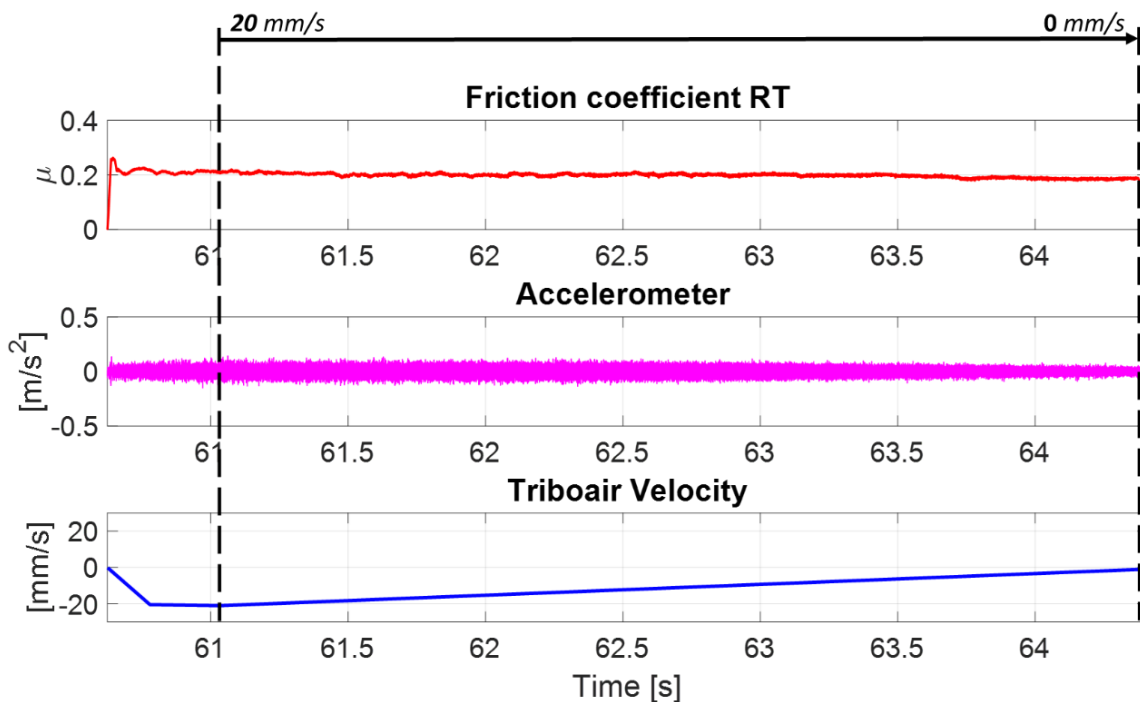


Figure 24 Example of signals recorded during a single stroke at room temperature condition ($\approx 25^\circ\text{C}$), in the variable sliding velocity test ($V=20 \rightarrow 0$ mm/s) shown in Figure 22.b. From the top: the friction coefficient (ratio between tangential and normal force), the accelerometer signal and the imposed sliding velocity profile.

As can be noted from Figure 24, at room temperature condition the friction coefficient is almost constant (slightly decreasing) during the braking part of the stroke. The vibrational response is characterized also in this case by low-amplitude stable friction-induced vibrations. The mean amplitude of the friction noise decreases slightly with the decrease of the sliding velocity, as

shown in [95]. The imposed velocity profile is the one already described in Figure 20.a and characterized by a fast acceleration (100 mm/s^2) up to 20 mm/s , to which follows a braking deceleration (6 mm/s^2) covering most of the stroke.

When comparing the friction coefficient behavior and the vibrational signals of different strokes during braking, only the decreasing velocity part of the signal, from 20 to 0 mm/s , will be considered, as shown in Figure 24 (signals in between the vertical dashed lines).

From the analysis and comparison of braking (decreasing velocity) tests, significant information about the effect of a decreasing sliding velocity on the friction coefficient evolution and on the onset of dynamic instabilities can be achieved. On the other hand, the analysis at constant velocity provides complementary information, in order to evaluate the material response regardless of the variable sliding velocity.

In the following, the main results obtained from the analysis of the signals retrieved from the experimental tests of the above-described C/C specimens are presented.

2.2 Frictional and vibrational characterization

The frictional response of the tested samples is here investigated and correlated with the occurrence of unstable friction-induced vibrations. The evolution of the friction coefficient under different temperatures and sliding velocities is analyzed for all the tested C/C specimens. First, the frictional and dynamical behavior of the samples machined from the MAT1 disc is described. The role played by the temperature and the sliding velocity on the frictional and vibrational response of C/C materials is shown. The obtained results are then compared with the ones retrieved from the MAT2 samples. Comparing these two materials, the different evolution of the friction coefficient and the occurrence of different vibrational phenomena are discussed. Then, a comparison between used and new C/C specimens machined from MAT4 and MAT5 discs is provided. Lastly, overall discussions concerning all constant and variable sliding velocities tests, carried out with all the C/C material specimens, are presented.

2.2.1 Role of temperature and imposed velocity profile

As already shown in Figure 22, the increase in temperature, with either constant or variable sliding velocities, significantly affects the behavior of the DFC. The different frictional response in presence of distinct boundary conditions (temperature, in this case) underlies the occurrence of specific vibrational phenomena. By investigating the single strokes of the MAT1 samples during braking, meaningful information can be obtained on the occurrence of unstable friction-induced vibrations and their relationship with the evolution of the friction coefficient when decreasing the sliding velocity. In this respect, Figure 25 shows an example of three single strokes at different temperatures, taken from the *sliding heating* test, at imposed variable speed, described in Figure 22.b. The friction coefficient behavior during braking and the vibration signal measured by the accelerometer at room temperature, at $300 \text{ }^\circ\text{C}$ and at $500 \text{ }^\circ\text{C}$ are shown in Figure 25.a, Figure 25.b and Figure 25.c, respectively.

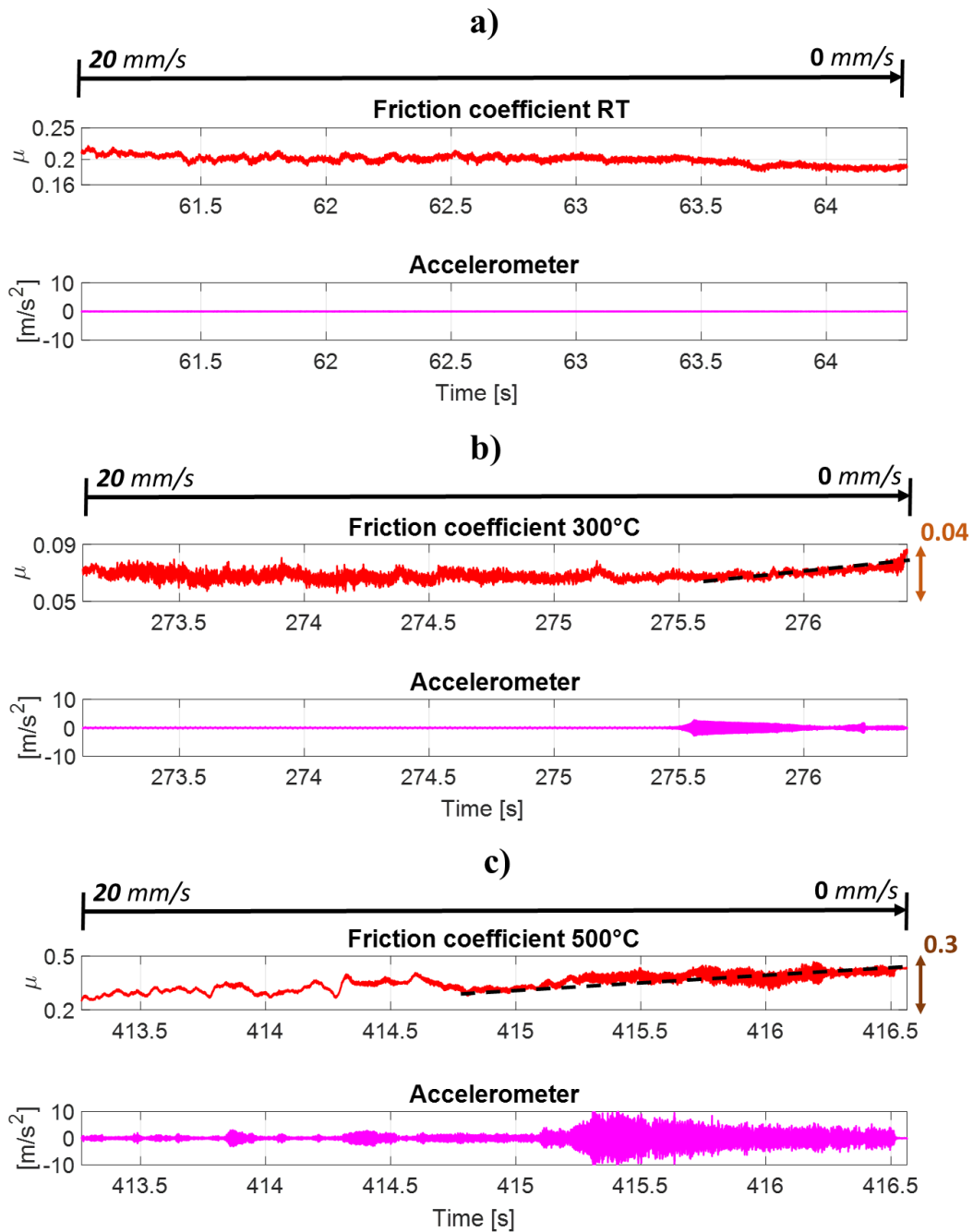


Figure 25 Singles strokes taken at different temperatures from the sliding heating test at variable imposed velocity (20→0 mm/s) described in Figure 22.b. From the top: friction coefficient and accelerometer signal during braking of singles strokes at room temperature (a), 300 °C (b) and 500 °C (c).

As shown in Figure 25.a, at room temperature condition, the friction coefficient is slightly decreasing with the decrease of the sliding velocity and no dynamic instabilities are observed. Conversely, in Figure 25.b, at almost 300 °C, a significant different behavior can be noted on both the frictional and vibrational responses. A considerably lower DFC, with respect to the room temperature, as well as a slight increase of the friction coefficient toward the end of braking, characterizes the frictional response observed during the stroke. The presence of a slight negative friction-velocity slope is well correlated with the onset of a dynamic instability detected by the accelerometer.

For higher temperatures, an overall increase of the friction coefficient has been observed in Figure 22. This phenomenon is due to a significant increase of the local reactivity at the contact interface (see {1.2.3}), which also leads to a steep negative friction-velocity slope toward the end of braking, as shown in Figure 25.c. Specifically, a decrease in velocity, at high temperature conditions, may promote the physiochemical interactions between dangling bonds of carbon at the contact interface, increasing therefore the overall macroscopic friction factor. The presence of a steeper negative slope and a higher level of friction, compared to 300 °C, favors the occurrence of sustained unstable friction-induced vibrations of higher amplitude, as shown by the accelerometer signal of Figure 25.c.

The effect of the variable sliding velocity on the frictional response, as well as the occurrence of the vibrational instability due to the negative friction-velocity slope, has been investigated in detail by comparing constant and variable sliding velocity tests. As an example, Figure 26 shows the comparison between the *sliding heating* tests, with a maximum temperature of 300 °C, carried out at both constant (Figure 26.a) and variable (Figure 26.b) imposed velocity.

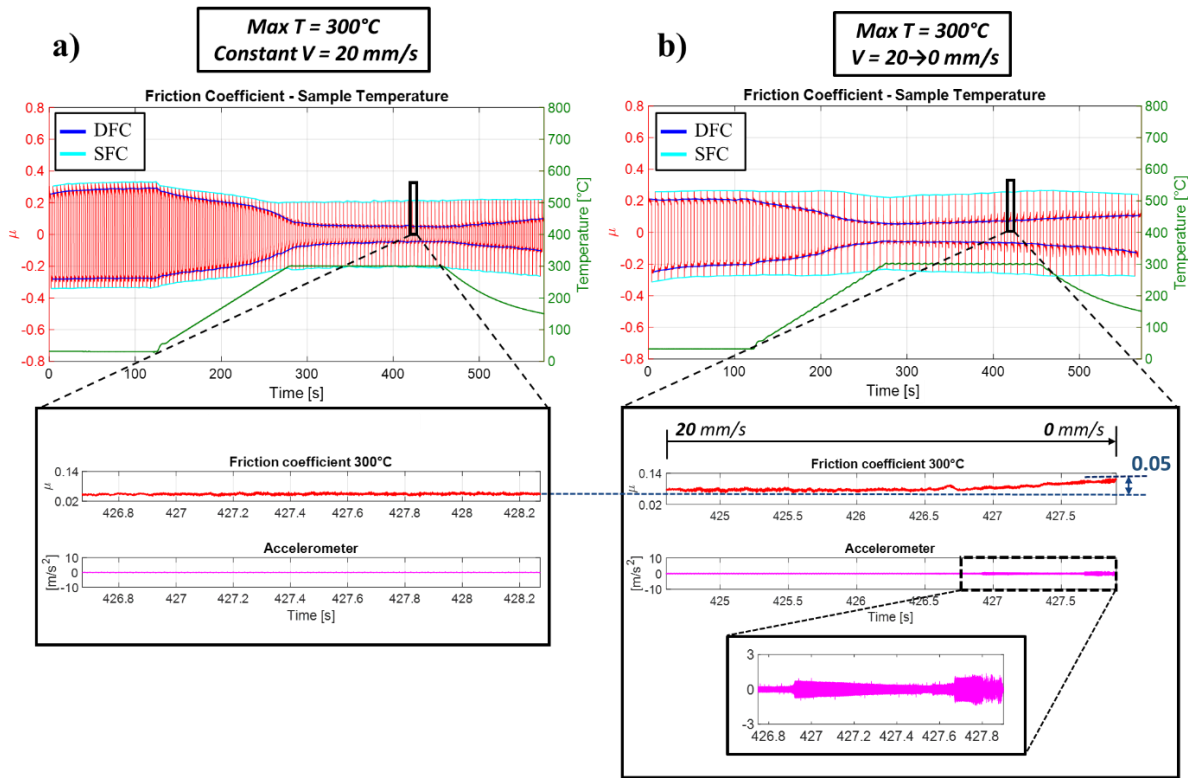


Figure 26 Comparison between the friction coefficient (in red) evolution during sliding heating tests carried out on MAT1 samples, at constant (a) and variable (b) sliding velocity, for tests at 300 °C. In blue the dynamic friction coefficient (DFC), in cyan the static friction coefficient (SFC) and in green the temperature. In the insets, a comparison between the friction coefficient and the accelerometer signal of two single strokes taken at 300 °C, at constant (inset in (a)) and variable velocity (inset in (b)). A detail of the accelerometer signal in correspondence of the dynamic instability is also shown in the inset in b).

Both constant and variable imposed velocity tests show a similar and consistent behavior of the SFC and the DFC. While the former remains almost constant when the temperature increases, the latter is characterized by a progressive decrease when the temperature rises. Once the maximum temperature of 300 °C is reached, the value of the DFC remains almost constant until the IR lamps are turned off and the temperature decreases again. The inset in Figure 26.a shows the behavior of the friction coefficient and the vibrational response recorded by the accelerometer for a single stroke at 300 °C and at a constant imposed velocity of 20 mm/s. The friction coefficient remains almost constant and equal to 0.06 throughout the whole stroke. No dynamic instabilities are observed.

Conversely, the frictional response shown in the inset of Figure 26.b, concerning a single stroke at 300 °C and variable imposed velocity (braking) from 20 to 0 mm/s, is characterized by a slight increase of the friction coefficient while the sliding velocity decreases. Analogously to the trends described in Figure 25.b, the presence of the slight negative friction-velocity slope triggers the onset of unstable friction-induced vibrations (zoom in the inset). It can be noted that the level of friction, at 300 °C, identified by the test at constant velocity, is almost equal to the friction

coefficient of the variable velocity stroke at the beginning of braking. The decrease of the sliding velocity subsequently leads to the increase of the friction coefficient and the occurrence of a dynamic instability.

The comparison between the frictional and vibrational response of the tested C/C specimens, at constant and variable velocity, highlights thus the role of the decreasing velocity on the occurrence of unstable friction-induced vibrations, when a negative friction-velocity slope is encountered.

So far, the frictional and vibrational response of the C/C materials have been described only for the MAT1 specimens. However, as a function of the tested material (i.e. the different contaminants on the contact surface), the dynamic and static friction coefficient behavior, at different temperature conditions, can differ significantly, leading to different vibrational responses as well. As an example, in the following, a comparison between the tribological and dynamical response of the MAT1 and the MAT2 is provided.

2.2.2 Comparison between MAT1 and MAT2

The tested C/C specimens differ for the presence of different contaminants on the contact surface. As it has been shown in Table 2, while the MAT1 specimens are characterized by the presence of Cont1, Cont2, Cont3 and Cont4 on the contact interface, only Cont3, Cont4 and a small amount of Cont2 (external pollution) have been found on the frictional surface of the MAT2. The effect of the particles (oxides) constituted by such contaminants, and taking part in the frictional contact of C/C composites, has been investigated by comparing the frictional and vibrational response of the tested materials.

The different behavior of the DFC and the SFC, between the MAT1 and the MAT2, in *sliding heating* tests carried out at imposed variable velocity (20→0 mm/s) and a maximum temperature of 500 °C, is shown in Figure 27.

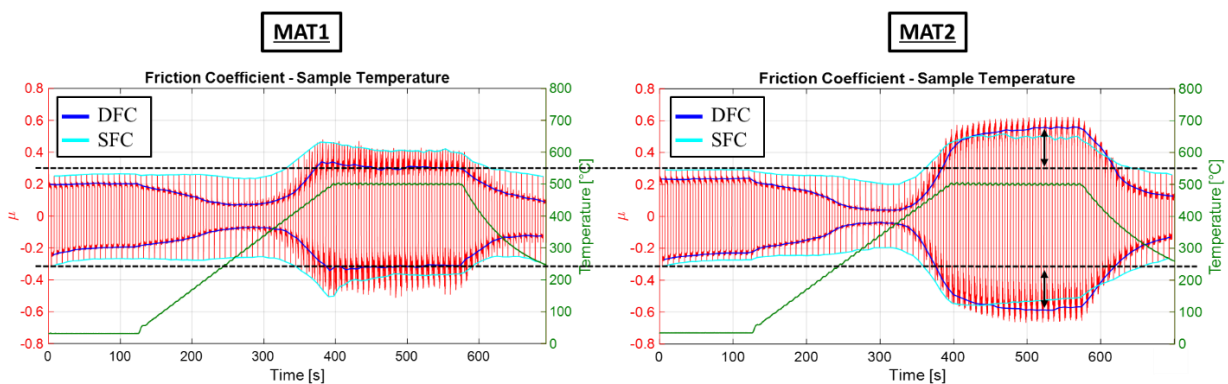


Figure 27. Comparison between the frictional responses of MAT1 (left) and MAT2 (right) specimens, during sliding heating tests carried out at variable sliding velocity (20→0 mm/s) and at a maximum temperature of 500 °C. In red the friction coefficient, in blue the DFC, in cyan the SFC and in green the temperature.

As can be seen from Figure 27, the behavior of both the SFC and the DFC of the MAT1 and the MAT2 is similar up to almost 400 °C. In both cases, the SFC remains almost constant while the DFC first decreases significantly compared to the room temperature value and successively increases again. For temperatures higher than 400 °C, remarkable differences can be observed between the tested samples. In both cases the SFC and the DFC increase, however a much higher increase of the DFC can be observed for the MAT2, which reaches a value of almost 0.6 (three times higher than the DFC at room temperature). In this case, the DFC at 500 °C becomes higher than the SFC. On the contrary, for the MAT1, the DFC remains always lower than the SFC. Such a different frictional response of the tested samples leads to different vibrational phenomena as well. In Figure 28, single strokes for both the MAT1 and the MAT2, taken from the *sliding heating* tests shown in Figure 27, at 500 °C, are compared.

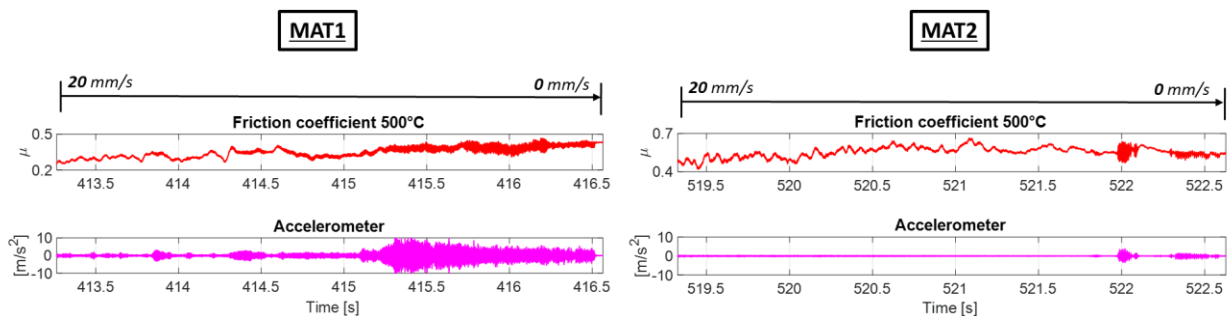


Figure 28 Comparison between the friction coefficient and the accelerometer signal of two single strokes taken at 500 °C from the sliding heating tests of the MAT1 (left) and MAT2 (right) shown in Figure 40.

As shown in Figure 28, while for the MAT1 the friction coefficient increases significantly toward the end of braking, leading to a steep negative-friction-velocity slope, for the MAT2 the friction coefficient remains almost constant at the end of braking. In this case, the higher value of the DFC, at 500 °C, for higher velocities seems to prevent the occurrence of a negative friction-velocity slope. Nevertheless, the onset of dynamic instabilities can be observed in both cases.

As also described in {1.2.2.1}, the onset of unstable friction-induced vibrations in presence of a sufficiently high constant friction coefficient can be attributed to the occurrence of a mode coupling instability [122, 133]. The comparison between the frictional and vibrational response of the MAT1 and MAT2 at 500 °C highlights therefore two different mechanisms at the basis of the observed unstable friction-induced vibrations. On the one hand, the MAT1 shows the presence of a significant negative friction-velocity slope and a relatively high level of friction, compared to the room temperature one, which favors the occurrence of a severe dynamic instability. In this case, the combined destabilizing effect of the steep negative friction-velocity slope with the mode coupling, due to the high level of friction coefficient, can be therefore hypothesized. It should be noticed that the same material at 300 °C shows a negative slope with lower values of friction. In this case only a negative slope contribution is provided to the instability and, therefore, lower amplitude of vibrations are observed.

On the other hand, for the MAT2 the instability can be attributed only to the high value of the DFC, reached at high temperature conditions, as no negative friction-velocity slope is observed.

In this case, being the friction coefficient almost constant, the unstable vibration can be attributed to the sole mode coupling.

Both the MAT1 and MAT2 specimens have been machined from discs already tested, i.e. “used”, on a full disc brake setup. In order to investigate the role of the material conditioning when braking, the tribological and dynamical response of C/C materials, both in new and used states, needs to be compared. For this purpose, a sample pair of C/C composites has been machined from MAT4 and MAT5 and tested on the TriboAir setup. In the following, the main results are presented.

2.2.3 Comparison between MAT4 and MAT5

The tribological and dynamical behavior of MAT4 and MAT5 has been investigated by comparing the tests at variable and constant sliding velocity, at different temperature conditions. Significant information can be obtained from the comparison between the evolution of the SFC and the DFC up to 500 °C. In this regard, Figure 29 shows the *sliding heating* tests carried out at variable imposed velocity (20→0 mm/s) and at a maximum temperature of 500 °C, for both MAT4 (Figure 29.a) and MAT5 (Figure 29.b).

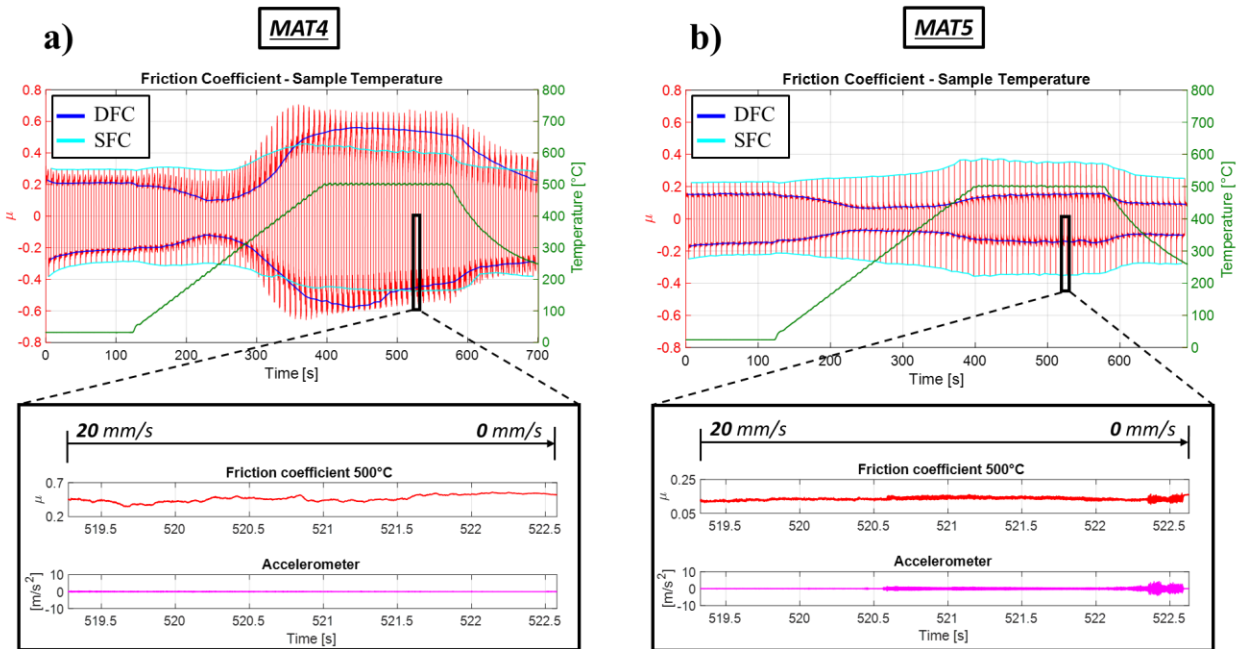


Figure 29 Comparison between the frictional responses of MAT4 (left) and MAT5 (right), during sliding heating tests carried out at variable sliding velocity (20→0 mm/s) and at a maximum temperature of 500 °C. In red the friction coefficient, in blue the DFC, in cyan the SFC and in green the temperature. In the insets, a comparison between the friction coefficient and the accelerometer signal of two single strokes, taken at 500 °C, of MAT4 (a) and MAT5 (b).

Similarly to the frictional response of the MAT2 described in Figure 27, the frictional response of the MAT4, shown in Figure 29.a, is characterized by a first decrease of the DFC, up to almost 200 °C, followed by a strong increase of the DFC for temperatures higher than 300 °C. At 500 °C, the DFC becomes higher than the SFC. As can be noted from the inset of Figure 29.a, related to a single braking stroke at 500 °C, the material response is characterized by an almost constant friction coefficient toward the end of braking and no dynamic instabilities occur.

A different scenario is the one shown in Figure 29.b and related to the MAT5. As for the used samples, a decrease of DFC is observed up to almost 200 °C. Nevertheless, the DFC increases again only for temperatures higher than 400 °C and it reaches, at 500 °C, values close to the room temperature ones (almost 0.2). In this case, the DFC remains considerably lower than the SFC, which increases slightly up to 500 °C. Unlike the MAT4, the inset of Figure 29.b, related to a single braking stroke at 500 °C, shows the presence of a slight negative friction-velocity slope toward the end of braking and the occurrence of unstable friction-induced vibrations.

By comparing the two described scenarios, it can be hypothesized that a lower DFC in the middle of the stroke can promote the occurrence of the negative friction-velocity slope and therefore the onset of dynamic instabilities. Moreover, the significant different evolution of the DFC, compared to the SFC, between the new and used state of the samples, highlights the key role played by the rheology (see {1.1.3.1}) at the contact interface. These results are consistent with the observations of the surfaces of new and used brake discs, which highlighted the formation of a compact third body layer on the surface and within the material porosities of the used discs [164].

It should be remarked that, despite the onset of a dynamic instability due to the negative friction-velocity slope, the increase of friction during braking at 500 °C of the MAT5 is significantly lower than the one observed for the MAT1. Consistently, a much weaker instability has been observed.

Complementary information, with respect to the considerations made so far, can be obtained from the comparison between the *sliding heating* tests at constant imposed velocity. Figure 30 shows the tests carried out at a maximum temperature of 500 °C and a constant imposed velocity of 20 mm/s of the MAT4 and MAT5.

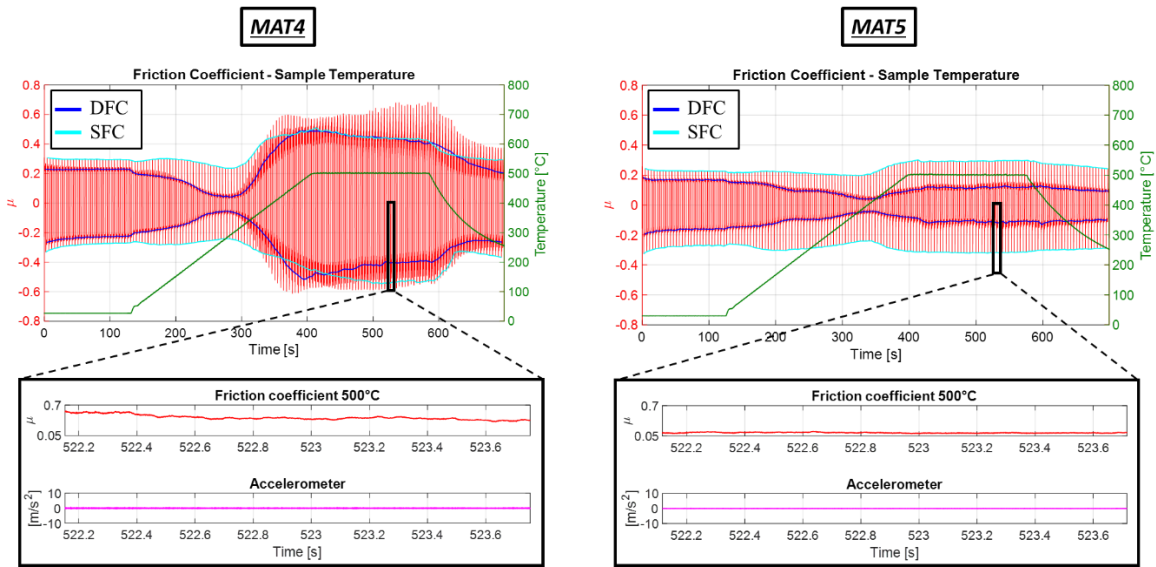


Figure 30 Comparison between the frictional responses of MAT4 (left) and MAT5 (right), during sliding heating tests carried out at constant sliding velocity (20 mm/s) and at a maximum temperature of 500 °C. In red the friction coefficient, in blue the DFC, in cyan the SFC and in green the temperature. In the insets, a comparison between the friction coefficient and the accelerometer signal of two single strokes, taken at 500 °C, of the MAT4 (a) and MAT5 (b).

Analogously to the tests carried out at variable velocity and presented in Figure 29, the behavior of the DFC between the used and the new samples differ significantly also at constant sliding velocity. While for the used sample the DFC decreases up to 200 °C and then increases significantly for temperatures higher than 300 °C, the new sample shows a mild increase of the DFC only for temperature higher than 400 °C. At 500 °C, the DFC reaches in this case values slightly lower than the room temperature ones.

The single strokes of the new and used samples, presented in the insets of Figure 30 and related to a temperature of 500 °C, show a constant friction coefficient and the absence of dynamic instabilities, for both the tested specimens. This behavior of the material response at constant velocity highlights the role played by the negative friction-velocity slope on the occurrence of the dynamic instability observed for the new samples, as it has been shown in Figure 29.b.

All the outcomes presented so far have shown considerable differences in the frictional and vibrational response of the tested samples, as a function of the contaminants on the contact interface and the new or used state of the specimens. Different regimes of friction, leading to different unstable friction-induced vibrations, have been identified as well. In the next section, the main results obtained from the comparison of all the used samples tested at variable imposed velocity and different temperatures, according to the protocol described in Table 4, are shown.

2.2.4 Overall discussion on tested materials (variable velocity tests)

The behavior of the friction coefficient and the onset of unstable friction-induced vibrations differ significantly as a function of the temperature conditions and the contaminants taking part in the rheology of the contact. In the previous sections of this Chapter, different dynamic instabilities due to either negative friction-velocity slope and/or mode-coupling have been hypothesized by investigating the frictional and vibrational response of the tested samples. In order to provide an overall description of the dynamic and static friction coefficient trends, at different temperatures, Figure 31 shows the frictional response of the tested specimens of the used C/C material. *Sliding heating* tests at variable imposed velocity, carried out at a maximum temperature of 100, 200, 300, 400 and 500 °C are compared. Each line of Figure 31 shows the sequence of tests provided for in the protocol, up to the maximum temperature test of 500 °C. The first line is the sequence of tests carried out on the MAT1. The second, third and fourth lines are related to the MAT2, MAT3 and MAT4, respectively. For each test, colored bars indicate the onset of dynamic instabilities. Peach-colored bars denoted the presence of a slight negative friction-velocity slope, when slight unstable friction-induced vibrations are observed (e.g. see Figure 25.b). Violet bars denote a dynamic instability in presence of an almost constant friction coefficient, which suggests the occurrence of a mode-coupling instability (e.g. see Figure 28, MAT2). Lastly, red bars indicate the occurrence of large unstable vibrations in presence of a strong negative friction-velocity slope, such as the one described in Figure 25.c. When the bars are bordered in black, the specific phenomenon is observed on both back-and-forth strokes. Otherwise, the phenomenon is observed only on single strokes.

It should be noticed that the identification of the mechanisms at the origin of the instability (negative friction-velocity slope or/and mode coupling) is mainly qualitative, thanks to the observation of the level and slope of the friction coefficient, together with the vibrational response. Nevertheless, the identification of the two possible mechanisms has been confirmed thanks to numerical analyses presented in Chapter 3.

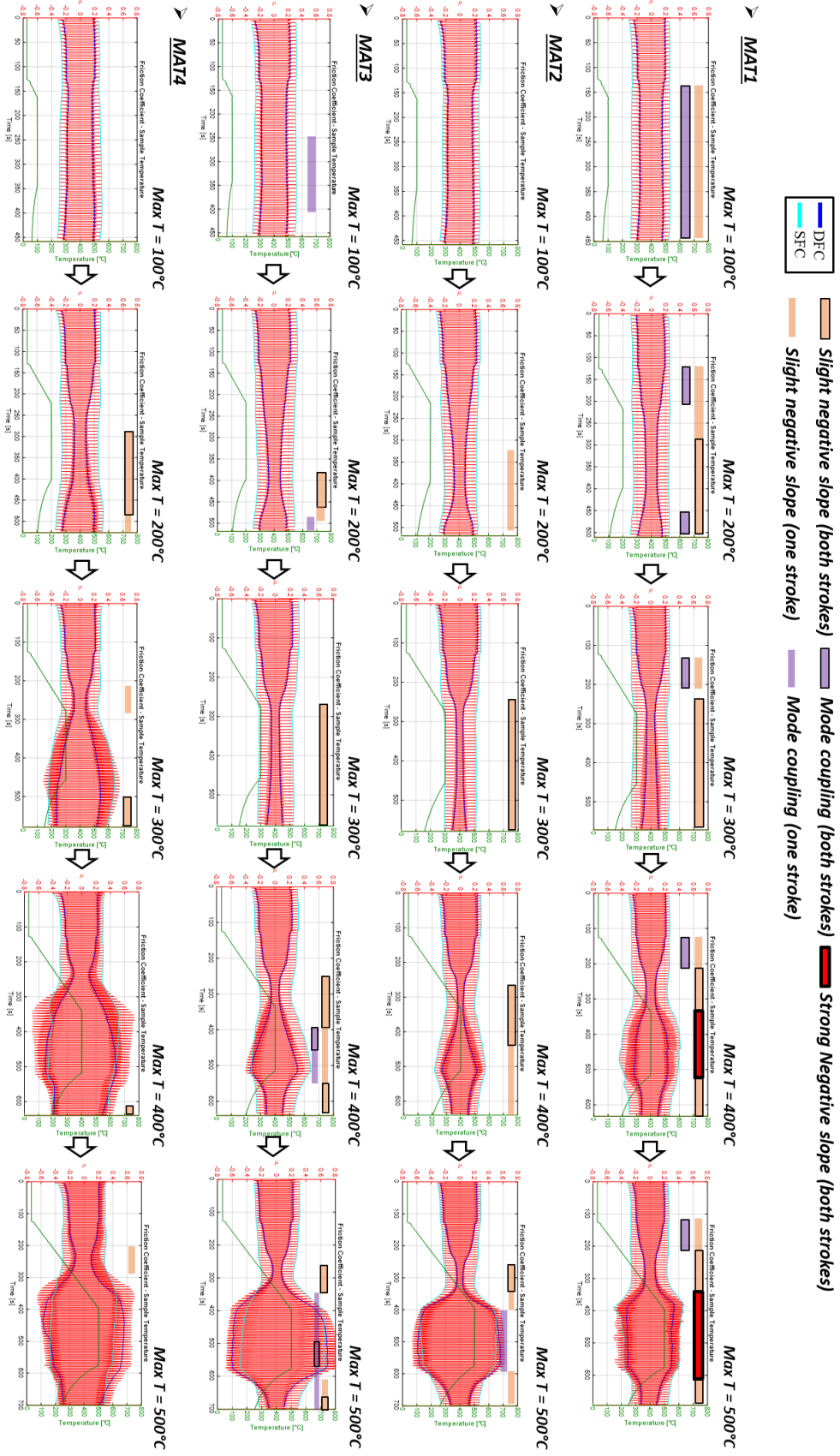


Figure 31 Comparison between sliding heating tests carried out at variable imposed velocity (20→0 mm/s) and at maximum temperatures of 100, 200, 300, 400, 500 °C. Each line shows a sequence of tests, up to the 500 °C maximum temperature test, for each used tested material. From the top: MAT1, MAT2, MAT3 and MAT4. The bars denote the occurrence of dynamic instabilities in presence of a slight negative friction-velocity slope (peach-colored bars), in presence of a constant friction coefficient (violet bars) and in presence of a strong negative friction-velocity slope (red bars). If the bars are bordered in black the phenomenon is observed on both back-and-forth strokes, otherwise it is observed only on single strokes. The friction coefficient is in red, the DFC is in blue, the SFC is in cyan and the temperature is in green.

From Figure 31 it is possible to notice that the onset of dynamic instabilities in presence of a significant negative friction-velocity slope, for both back-and-forth strokes, has been observed only for the MAT1 and for temperatures equal or higher than almost 400 °C.

At 500 °C, the MAT2 and the MAT3 show the presence of mode coupling instability and a DFC much higher than the one observed at room temperature conditions. A similar phenomenon is observed for the MAT4, but in this case, no dynamic instabilities have been detected.

It can be noticed that the MAT1 differs from the other tested samples for the presence of a DFC lower than the SFC at 500 °C. This distinctive feature of the frictional response seems to favor the occurrence of the steep negative friction-velocity slope observed for such material.

For lower temperatures, a similar trend of the DFC can be observed in all tested materials. For temperatures higher than the room temperature condition and up to 200-300 °C, the DFC decreases significantly while the SFC remains almost constant. In this case, dynamic instabilities in presence of a slight negative friction-velocity slope are always observed when the minimum DFC is reached. This condition occurs at almost 300 °C for all tested samples, except the MAT4, for which the minimum DFC is reached at almost 200 °C. A significantly higher SFC with respect to the DFC seems to promote the occurrence of the negative friction-velocity slope as well as the onset of dynamic instabilities. However, the significantly lower level of DFC does not allow for a high increase of the friction coefficient toward the end of braking and the resulting slope is always very small, compared to the one observed at 500 °C for the MAT1. Consequently, the amplitude of the unstable vibration is weaker as well.

In some cases, like for instance the MAT1 at 100 °C, the simultaneous presence of peached-colored and violet bars is shown. In this case, the presence of dynamic instabilities at relatively high sliding velocities (usually higher than almost 10 mm/s), where the friction coefficient is still almost constant, suggests the onset of the dynamic instability by mode coupling. However, in presence of a slight negative friction-velocity slope toward the end of braking, slight contributions to the dynamic instabilities due to the negative slope cannot be excluded. Its presence is therefore reported. This behavior must not be confused with the one observed for the MAT1 at 500 °C, where the negative friction-velocity slope leads to much higher values of the friction coefficient and the coexistence of both the negative friction-velocity slope and the mode coupling instability can be responsible for severe unstable friction-induced vibrations.

The main outcomes described in this section are summarized in Table 5.


	MAT1	MAT2	MAT3	MAT4
T=RT	SFC ≈0.25 DFC ≈0.2			
RT < T < ≈300 °C	Constant SFC (≈0.25) Decreasing DFC (<≈0.1)		Slight negative friction-velocity slope instability (when DFC << SFC)	
T > ≈300 °C	Increase of both SFC and DFC			
	Lower increase of DFC (<SFC at ≈500°C)		Higher increase of DFC (>SFC at ≈500°C)	
	Strong negative friction-velocity slope instability 	Mode coupling instability	No dynamic instabilities	

Table 5 Synthesis of the frictional and vibrational response of MAT1, MAT2, MAT3 and MAT4, at different temperature conditions.

2.2.5 Analysis of constant velocity tests

In order to obtain complementary information, the evolution of the DFC and SFC with the temperature has been also compared and investigated by tests carried out at constant sliding velocity. Being the behavior of the MAT2 and MAT3 very similar, and considering that no remarkable differences have been observed in the contaminants found on the contact interface, only the MAT2 will be considered in the following.

In this regard, Figure 32 shows the comparison between *sliding heating* tests of MAT1, MAT2 and MAT4, carried out at a maximum temperature of 500 °C and a constant sliding velocity of 20 mm/s.

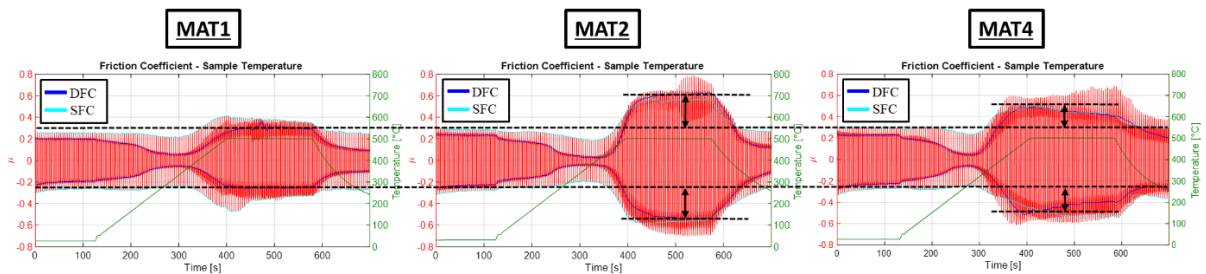


Figure 32 Comparison between the frictional responses of MAT1 (left), MAT2 (center) and MAT4 (right) specimens, during sliding heating tests carried out at constant sliding velocity (20 mm/s) and at a maximum temperature of 500 °C. In red the friction coefficient, in blue the DFC, in cyan the SFC and in green the temperature.

As can be seen from Figure 32, the behavior of the DFC and SFC of the tested samples is very similar for temperatures lower than almost 300-400 °C. In such a range of temperature all the specimens exhibit a significant decrease of the DFC, while the SFC remains almost constant. At higher temperatures, and up to 500 °C, MAT2 and MAT4 show a much higher increase of the DFC compared to the MAT1. Analogously to the tests at variable imposed velocity, the DFC of the MAT1 remains always lower than the SFC.

The behavior of the frictional response at constant sliding velocity, for temperature higher than almost 400 °C, is consistent with the outcomes obtained for variable velocity tests and similar trends of the DFC and SFC have been obtained. A further comparison at lower temperatures allows investigating in further details the decrease of the DFC observed in Figure 32. For this purpose, a comparison between the *sliding heating* tests of MAT1, MAT2 and MAT4, at constant imposed velocity (20 mm/s) and for a maximum temperature of 300 °C, is shown in Figure 33.

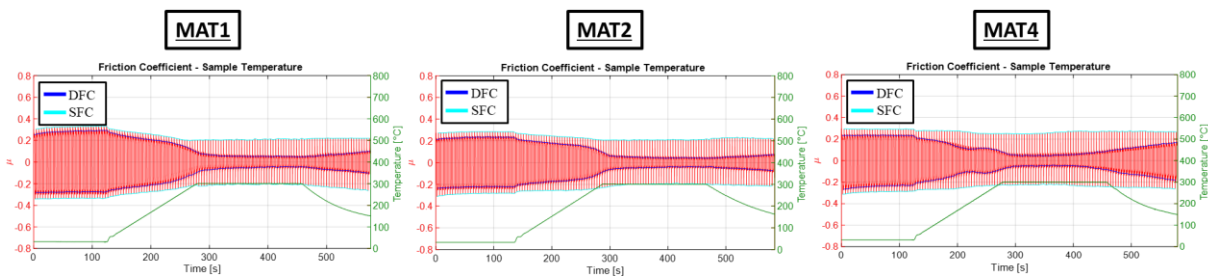


Figure 33 Comparison between the frictional responses of MAT1 (left), MAT2 (center) and MAT4 (right) specimens, during sliding heating tests carried out at a constant sliding velocity (20 mm/s) and at a maximum temperature of 300 °C. In red the friction coefficient, in blue the DFC, in cyan the SFC and in green the temperature.

As can be seen in Figure 33, also at constant sliding velocity, at 300 °C, a significantly low DFC is reached, for all tested samples. The SFC remains instead almost constant.

These results suggest that up to almost 300 °C the presence of the contaminants on the contact interface does not affect significantly the dynamic and static friction coefficient, which show common features in all the C/C specimens. Significant differences arise for higher temperatures, where the behavior of the DFC differs considerably as a function of the contaminants taking part in the frictional contact. On the contrary, the trend of the SFC is similar between all the tested materials.

The results shown so far highlight the significant contribution of the rheology in the frictional and dynamical response of the C/C materials. In presence of different contaminants, different frictional responses of the tested samples are observed mainly for the DFC, for which the rheology at the interface plays a key role, and at high temperatures, when the physicochemical reactivity of the materials is increased [24, 55]. The different trends of the SFC and DFC underlie then the occurrence of different unstable friction-induced vibrations.

Another important parameter to be considered for characterizing the tribological behaviour of C/C materials, according to the large amount of literature on the subject [8, 24, 25, 52], is the atmosphere surrounding the frictional contact. With the main aim of understanding how different

environments can affect the evolution of the dynamic and static friction coefficients described above, an experimental campaign has been carried out under controlled atmosphere. The experimental setup adopted for the analysis and the main outcomes are described in the following.

2.3 Experimental tests under controlled atmosphere

In the literature, it has been observed that different environments can affect the tribological behaviour of *C/C* materials [8, 25]. In particular, it has been shown that a low friction regime is possible when the active sites of the material are neutralized by water molecules contained in the environment and whose adsorption is favored by oxygen groups on the carbonaceous surface of the material [53, 58]. The experimental characterization presented in this section aims to investigate the evolution of the DFC and SFC, at different temperatures, in presence of both an air environment and a low oxygen atmosphere characterized by argon. Tests have been carried out by using samples of MAT1, whose frictional and vibrational response has been investigated on both the atmospheres and at different temperature conditions. The experimental campaign has been performed through a dedicated setup equipped with a chamber, inside which the gas is injected. In the following, a description of the test rig is first provided. Then the experimental protocol is presented and the main outcomes from the experimental campaign are discussed.

2.3.1 Description of the setup

Analogously to TriboAir, the setup adopted to perform tests under controlled atmosphere allows studying the frictional and dynamic response of specimens sliding in frictional contact under controlled boundary conditions. This test bench, named TriboWave, has been designed in order to guarantee the measurement reproducibility in a large range of contact forces. A dedicated chamber has been designed to measure the frictional and vibrational response of the tested samples in different environments. The experimental setup is shown in Figure 34.a. A simplified diagram of the test bench is presented in Figure 34.b.

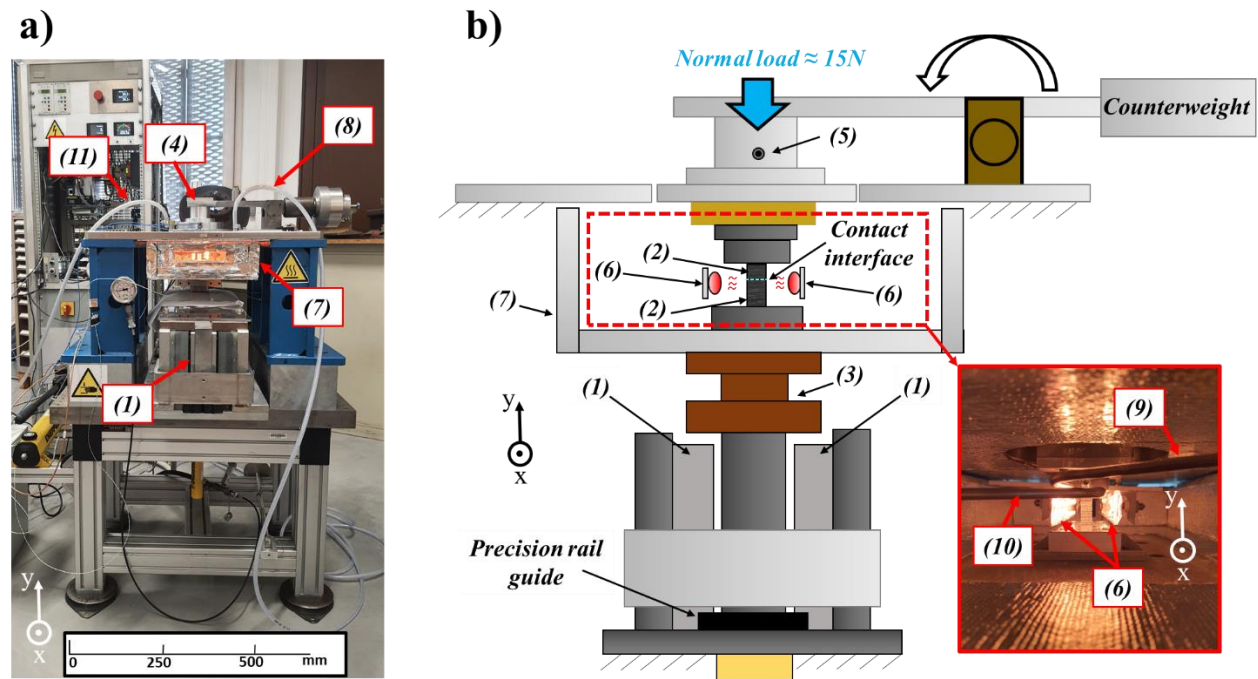


Figure 34 TriboWave experimental setup (a) and schematic diagram (b). (1) linear electromagnetic motors; (2) C/C material specimens in frictional contact; (3) 3-axial force transducer; (4) Mechanical arm for the load application by dead weights; (5) Uniaxial accelerometer; (6) IR lamps; (7) Chamber in Glashterm 220 for containing the gas; (8) Pipe for the gas inlet; (9) stainless steel cannula for the gas inlet; (10) Stainless steel cannula for the gas extraction; (11) Pipe for the gas extraction.

The same specimens of MAT1 adopted for the experimental campaign carried out on TriboAir have been used also in this setup (geometry and contact surface characteristics of the samples described in {2.1.2}). Four linear electromagnetic motors (ETEL of type LMA22-100) (1) guarantee the relative motion between the tested samples (2). Just like the Triboair setup, the cubic sample is clamped on the upper part of the setup while the other one moves with the desired law of motion, in the X direction, back and forth. The test bench allows cycles of back-and-forth of the moving sample with a maximum single stroke of 30 mm. The control of the relative motion is achieved thanks to a linear encoder (HEIDENHAIN of type LIP-200), a position controller (ETEL) and a precision rail guide (SKF), for having a relative imposed motion between the fixed and mobile parts of the motors.

In order to measure the orthogonal components of the dynamic forces acting between the two contact surfaces, a 3-axial force transducer (KISTLER of type 9067) (3) is assembled. The contact between the C/C samples and the normal load application is possible thanks to a mechanical arm (4) hinged on ball bearings, which support the tangential (X direction) thrust due to the frictional contact of the samples. A counterweight allow adjusting the normal load. Moreover, a uniaxial piezoelectric accelerometer (5) allows measuring the friction-induced vibrations on the tangential direction.

All data are recorded by an acquisition system (OROS), with a sample frequency equal to 51.2 kHz, and then post-processed by Matlab ©.

For performing tests under specific temperature conditions and under controlled atmosphere, the test bench is equipped with IR lamps (6), controlled by a temperature regulator (GEFRAN F650P), and a specifically designed chamber (7), for containing the gas injected in the environment and surrounding the contact surfaces of the samples. The chamber design consists of a composite material (Glastherm 220) frame with a ceramic insert to best convey the heat toward the area of the contact and to preserve the force transducer. Four Glastherm uprights are assembled around the frame. A specific insulation fabric covers all Glastherm components in order to reduce the increase of temperature due to the lamp irradiation. A borosilicate glass window is also included in the design in order to monitor the samples in frictional contact during the test.

The introduction of the gas (ALPHAGAZ 2 Argon, $\text{Ar} \geq 99,9999 \%$) in the chamber is possible thanks to a pipe (8) connected to a stainless steel cannula (9), which injects the argon in the close proximity of the contact surface. A similar configuration, consisting of a stainless steel cannula (10) connected to a pipe (11), is used to extract the gas around the contact. The collected gas is then analyzed through a gas analyzer (KANE 458s), which can measure concentrations of CO , CO_2 and O_2 . The relative humidity is instead measured by a humidity sensor (ALMEMO 2490). It should be remarked that the moving uprights of the chamber and the fixed upper plate of the setup are 2 mm apart, during the frictional contact of the C/C samples, in order to allow the relative motion without frictional interaction between the chamber and the frame of the test bench. However, in order to preserve the gas environment and compensate the gas leak, a constant flow (at a pressure of 1.2 bar) of injected gas is maintained throughout the whole tests in argon. The described setup has been used for characterizing the frictional and vibrational response of the MAT1 samples at different temperatures, sliding velocities and contact atmospheres. The experimental protocol for such characterization is described in the following.

2.3.2 Experimental protocol

The protocol adopted for the experimental characterization provides for two days of tests. The first day focuses on tests in air, while the second day is dedicated to tests in argon. In consideration of the results obtained in the previous experimental campaign on the TriboAir setup, the overall protocol has been reduced and focused on the tests of interest in order to investigate the role of the environment. All the tests are carried out with the sliding heating method (shown in Figure 21.a). The overall protocol is shown in Table 6.

DAY ONE (AIR)			DAY ONE (ARGON)		
<i>Sliding Heating</i>			<i>Sliding Heating</i>		
1	RUN-IN	$V=const=20\text{ mm/s}$			
2	500°C	$V=const=20\text{ mm/s}$	1	500°C	$V=const=20\text{ mm/s}$
3	500°C	$V=const=20\text{ mm/s}$	2	500°C	$V=const=20\text{ mm/s}$
4	500°C	$V=18\rightarrow 0\text{ mm/s}$	3	500°C	$V=18\rightarrow 0\text{ mm/s}$

Table 6 Protocol used for the experimental tests carried out on MAT1 samples and under controlled atmosphere. The first day of the protocol consists of a sequence of constant (20 mm/s) and variable (18→0 mm/s) velocity sliding heating tests at a maximum temperature of 500 °C, in air. The second day of the protocol provides for the same sequence of tests but in argon.

The sequence of tests carried out in the first day of protocol consists of 15 minutes of run-in performed at a constant velocity profile (already described in Figure 20.b), characterized by an imposed speed of 20 mm/s and kept constant in each cycle of the test. After the run-in, two *sliding heating* tests at constant velocity and at a maximum temperature of 500 °C are performed. The reason why two identical sequential tests are carried out is to evaluate if, after reaching 500 °C, some differences in the frictional response are observed in the subsequent identical test. These constant imposed velocity tests are followed by a variable imposed velocity test carried out at a maximum temperature of 500 °C. Braking strokes are performed with an imposed sliding speed varying from 18 mm/s to 0 mm/s, with a deceleration of 6 mm/s². The maximum sliding speed of 18 mm/s is reached with an acceleration ramp of 100 m/s². Compared to the variable velocity profile adopted for the experimental campaign performed on TriboAir (described in Figure 33.a), here the maximum sliding speed (18 mm/s) differs slightly from the one adopted for TriboAir variable velocity tests (20 mm/s). Such a difference is due to the maximum sliding distance that can be covered on TriboWave and TriboAir (30 mm for the former and 40 mm for the latter), which limits the maximum attainable speed.

The second day of protocol follows the same sequence of tests of the first day, but in presence of argon.

Before being tested in TriboWave setup, samples are kept in vacuum (0.2 mbar) in a chamber for 24h. The chamber is then reloaded with argon up to atmospheric pressure. This procedure allows significantly reducing water adsorbed on C/C specimen surfaces and potentially affecting the frictional response of the sample in a neutral environment. Then, for each test in argon, the following sequential operations are carried out:

1. The normal load is imposed and the samples are put in frictional contact;
2. The chamber is preheated up 100 °C. This allows decreasing the relative humidity presents in the test environment;
3. During the natural cooling, after the pre-heating, argon is injected in the chamber. It prevents the humidity to increase again during the cooling. A continuous flow of argon is then maintained throughout the whole test;
4. When the room temperature is achieved, the *sliding heating* test (shown in Figure 21.a) begins;

- When the test is finished, the load is removed and also the argon flow is stopped.

All the tests carried out in the experimental campaign are performed with a normal load almost equal to 15 N and an average contact pressure of 0.15 MPa.

The retrieved data are analyzed following the same procedure described in {2.1.4}. A discussion on the obtained outcomes is presented in the next section.

2.3.3 Discussion of the results

The frictional response of the MAT1 samples in air, obtained here on the TriboWave setup, has been first compared with the results obtained on the TriboAir setup and related to the same *sliding heating* tests, at a maximum temperature of 500 °C. This comparison allows verifying the consistency of the results obtained by using different test benches. As an example, Figure 35 shows the comparison between variable imposed velocity tests carried out on TriboWave (Figure 35.a) and TriboAir (Figure 35.b). In both cases, a relative humidity of the environment of almost 35% has been measured at room temperature condition.

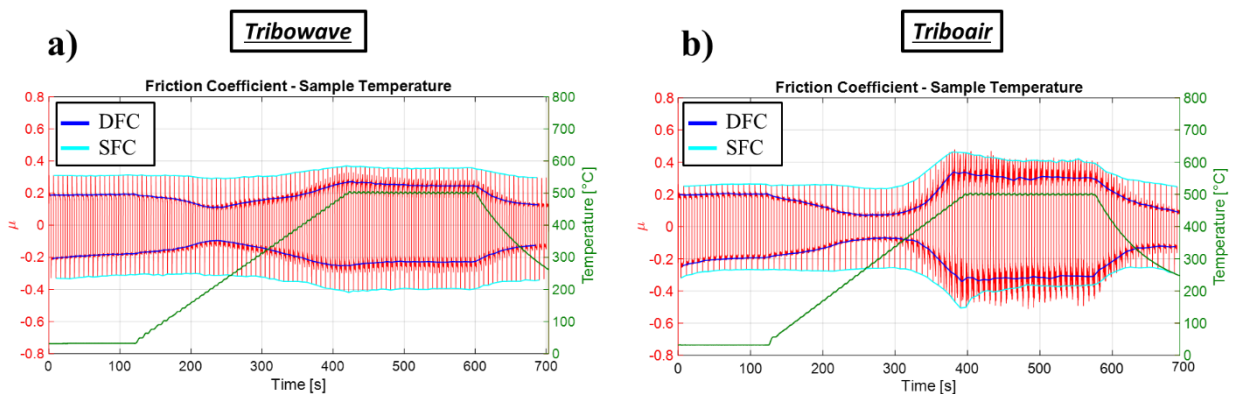


Figure 35 Comparison between the frictional responses of MAT1 samples tested on TriboWave (a) and TriboAir (b), during sliding heating tests carried out at variable sliding velocity (18→0 mm/s on TriboWave and 20→0 mm/s on TriboAir) and at a maximum temperature of 500 °C. In red the friction coefficient, in blue the DFC, in cyan the SFC and in green the temperature.

As can be seen from Figure 35.a, when increasing the temperature, the DFC decreases up to almost 200 °C while the SFC remains almost constant. For higher temperatures both the DFC and SFC increase and reach values slightly higher than the room temperature ones. The DFC remains always lower than the SFC.

As can be noticed by comparing Figure 35.a with Figure 35.b, the frictional response is very similar to the one observed when the samples have been tested on TriboAir. As expected, because the TriboAir setup is designed for being more sensitive on the specific range of the contact parameters (load, velocity and dynamic response), the overall frictional response shows a higher sensitivity when monitoring the response to a variation of the imposed parameter (temperature in Figure 35).

Along with the behavior of the dynamic and static friction coefficients, also the vibrational response shows similar features. As an example, Figure 36 shows the friction coefficient and the accelerometer signals, measured in the TriboWave setup, for the single strokes of Figure 35.a, at room temperature (a), 200 °C (b) and 500 °C (c).

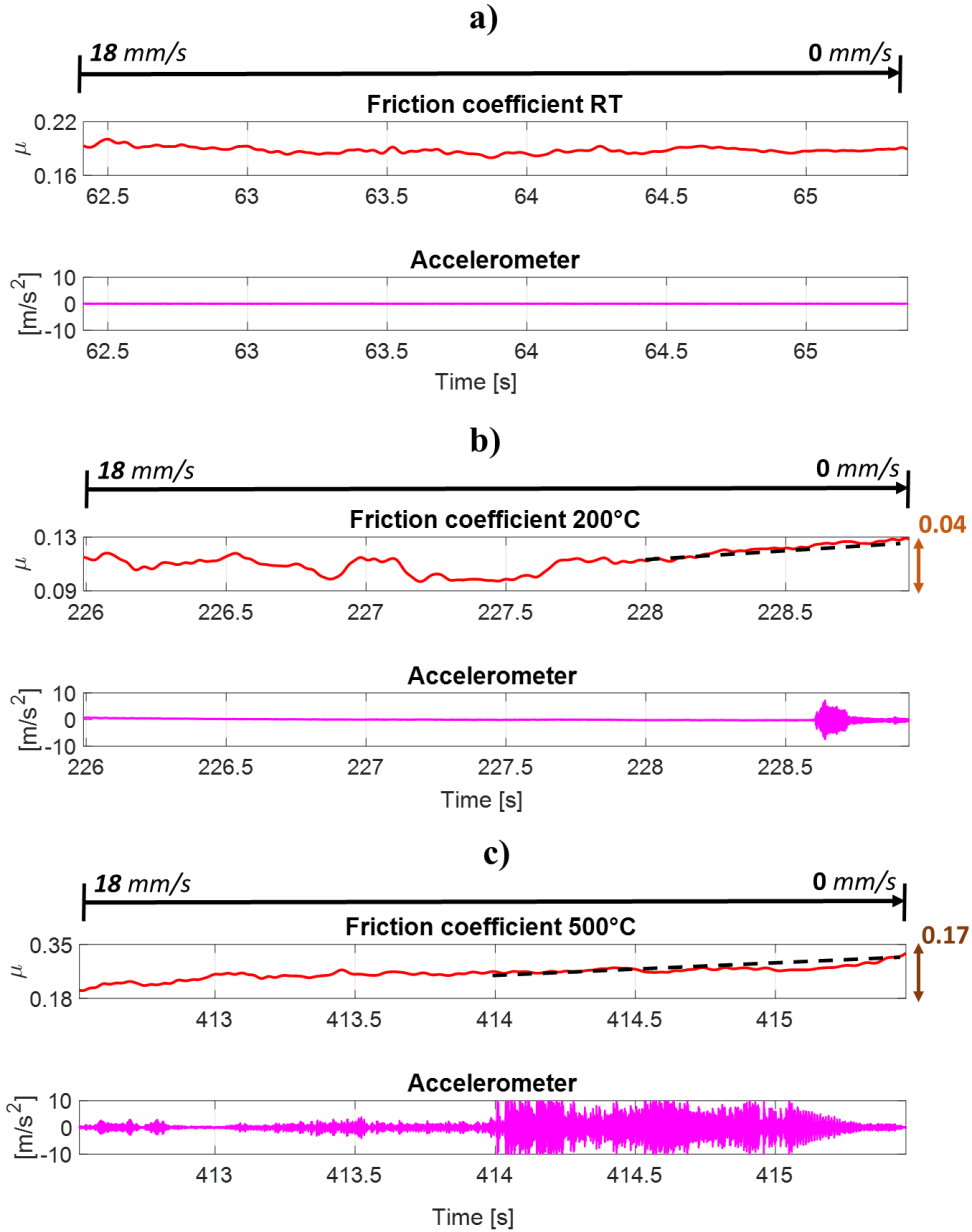


Figure 36 Singles strokes taken at different temperatures from the sliding heating test at variable imposed velocity (18→0 mm/s) described in Figure 35.a. From the top: friction coefficient and accelerometer signal during braking of singles strokes at room temperature (a), 200 °C (b) and 500 °C (c).

At room temperature (Figure 36.a), the friction coefficient is almost constant and no dynamic instabilities are observed. A slight negative friction-velocity slope, favored by the higher SFC, compared to the DFC, leads to the occurrence of a dynamic instability at almost 200 °C (Figure 36.b). At 500 °C, the presence of a steep negative friction-velocity slope leads to severe unstable friction-induced vibrations (Figure 36.c). A similar frictional and vibrational response has been observed on TriboAir (detailed description in {2.2.1}, Figure 25).

Being verified the consistency of the results obtained from testing the samples on TriboWave, the test sequence carried out in air (day one of the protocol) and in argon (day two of the protocol) have been compared. In this respect, Figure 37 shows the two sequences provided for in the protocol in Table 6. In the left column, the *sliding heating* tests carried out at constant (20 mm/s) and variable sliding imposed velocity (18→0 mm/s), at a maximum temperature of 500 °C, in air, are presented. In the right column, the same sequence of tests, but in argon, is shown.

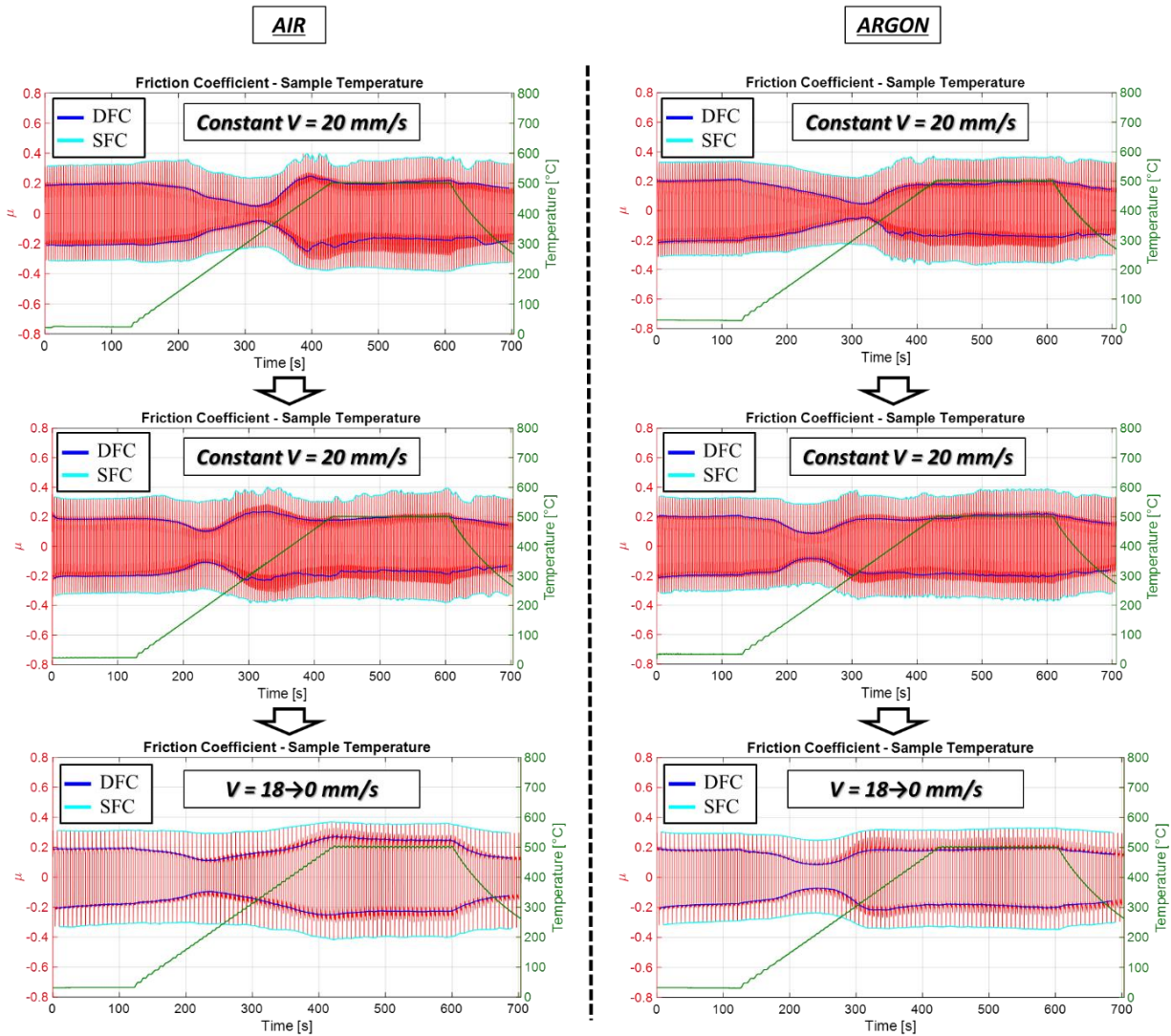


Figure 37 Comparison between the MAT1 frictional response of the sequences of sliding heating tests carried out at constant (20 mm/s) and variable (18→0 mm/s) imposed velocity and a maximum temperature of 500 °C. In the left column, the results obtained for the sequence of tests in air; in the right column, the results obtained for the same sequence of tests but in argon. In red the friction coefficient, in blue the DFC, in cyan the SFC and in green the temperature.

As can be noticed by comparing the tests in air and argon, no significant differences between the test sequences can be remarked. In both cases, the constant velocity tests show a consistent behavior with the variable velocity tests, characterized by the decrease/increase of the DFC while increasing the temperature up to 500 °C. Moreover, it has been observed that the similar frictional response between the two different test environments leads also to a similar vibrational response. In presence of argon, the same vibrational phenomena, described in Figure 36 at room temperature, 200 °C and 500 °C, are observed.

By comparing the repeated tests at constant imposed velocity, it can be also noticed that in both the environments a higher minimum value of the DFC can be observed in the second test, compared to the first one. Moreover, while for the first test at constant velocity the minimum value of the DFC is reached at 300 °C, for the repeated test the minimum value is reached at 200 °C. This trend could be explained by considering the hydrophilic behavior of the C/C third body, which allows retaining a considerable amount of water up to 300 °C [65]. During the first sliding heating test, it can be speculated that water adsorbed on the third body, acting as a lubricant, favors the decreasing trend of the DFC up to 300 °C. Being the first sliding heating test carried out at a maximum temperature of 500 °C, all water trapped in the third body is then desorbed. The subsequent sliding heating tests are therefore characterized by a lower lubricant contribution, given by the adsorbed water, and higher values of the DFC at 300 °C are observed.

During the tests carried out in air and argon, the volumes of gas extracted in the close proximity of the contact interface have been analyzed at different temperatures. The O₂ and CO₂ are measured by volume percentages of the total gas analyzed, with a resolution equal to 0.1%, while the CO is measured in ppm, with a resolution equal to 1 ppm. As an example, the results obtained for the first test at constant imposed velocity, for both air and low oxygen environments, are shown in Table 7.

	<i>Air</i>			<i>Argon</i>		
	O ₂ %	CO ₂ %	CO [ppm]	O ₂ %	CO ₂ %	CO [ppm]
RT	20.6	0	0	5.2	0	0
100°C	20.6	0	0	4.9	0	0
200°C	20.6	0	0	4.5	0	0
300°C	20.6	0	0	4.2	0	0
400°C	20.6	0	0	3.8	0	0
500°C	20.6	0	5	3.4	0	4

Table 7 Amount of O₂ (%), CO₂ (%) and CO (ppm) in the total analyzed volumes of gas extracted at different temperatures (room temperature, 100, 200, 300, 400, 500 °C). These data have been retrieved during the first sliding heating test at constant sliding velocity (20 mm/s).

As can be seen from Table 7, for the tests carried out in air the same level of oxygen, i.e. 20.6 % of the total analyzed volume, is observed at all the different temperatures. 0% of CO₂ and 0 ppm of CO are measured up to 400 °C. At 500 °C, 5 ppm of CO are detected by the gas analyzer. It should be remarked that the air atmosphere is characterized by about 0.04% of CO₂. However, the CO₂ resolution of the gas analyzer is equal to 0.1%, with an accuracy of ± 0.3%. It explains the 0% of CO₂ detected throughout the test.

In argon, the level of oxygen is significantly lower with respect to the tests carried out in air atmosphere. At room temperature a value of 6.7% of O₂ is measured. It decreases down to almost 3.5% at 500 °C. At such temperature, similarly to the tests carried out in air, a maximum of 4 ppm of CO is measured.

Despite the significant low level of oxygen in the atmosphere, for the tests carried out in argon, the same frictional and vibrational response have been obtained in both the air and low oxygen environments. By taking into account previous outcomes in the literature, where a high friction regime has been observed in neutral environments also at room temperature conditions [24, 25], these results suggest that even a very small amount of oxygen in the atmosphere can still favor the adsorption of water molecules on the contact interface, preventing a high friction regime at room temperature. As also hypothesized in [25], the presence of oxygen groups on the friction surface can favor the adsorption of water molecules even in dry air environment (100 ppm of water in [25]) and lead to a low friction regime (friction coefficient almost equal to 0.2) at room temperature.

Moreover, the significant small amount of CO released in the environment at 500 °C, probably due to gasification, for both air and low oxygen environments, suggest that the chemical reactions taking place at the contact interface require significantly low value of oxygen to occur.

2.4 Concluding remarks

Specimens of C/C materials machined from disc brakes have been tested in a dedicated test bench (TriboAir) in order to study their tribological and dynamical response, under controlled boundary conditions. The frictional and vibrational response has been investigated as a function of key role parameters, such as the relative contact velocity and temperature profiles.

Moreover, the presence of contaminants have been found on the contact surface of the tested samples. Specifically, particles of Cont1, Cont2, Cont3 and Cont4 contaminate the friction interface of the specimens machined from the MAT1 discs, while particle of Cont3 and Cont4 have been found on specimens derived from the MAT2 and MAT3. A small amount of Cont2 has been also found on the MAT2 samples.

Consequently, the analysis has been carried out by testing MAT1, MAT2, MAT3 and MAT4 at different temperatures, up to 500 °C, and constant (20 mm/s) and variable (from 20 to 0 mm/s) sliding velocities. The frictional response has been characterized by studying the evolution of both the dynamic and the static friction coefficients (DFC and SFC, respectively). The onset of unstable friction-induced vibrations has been correlated with the behavior of the DFC and SFC under the different operating conditions.

Up to almost 300 °C, some common features of the frictional response characterize all the tested samples:

1. At room temperature, all the tested samples show an almost constant DFC and SFC approximately equal to 0.2 and 0.25, respectively. No dynamic instabilities are observed;
2. When increasing the temperature up to 300 °C, while the SFC remains almost constant, the DFC decreases significantly and reaches values lower than 0.1. The considerable difference between the SFC and DFC favors the occurrence of a slight negative-friction velocity slope in variable velocity tests, which triggers, in turn, a low amplitude dynamic instability. A minimum value of the DFC is reached in all the C/C specimens at about 300 °C. Only the MAT4 shows a minimum value of the DFC at almost 200 °C.

For temperatures higher than almost 300-400 °C, all the C/C samples exhibit an increase of both the DFC and the SFC. Different behaviors, as a function of the tested specimens, are observed in the range of temperature from almost 400 to 500 °C. Therefore, the presence of different contaminants taking part in the rheology of the contact interface affects significantly the frictional and vibrational response of the tested materials. The MAT1 exhibits a lower increase of the DFC, compared to other materials, and it remains always lower than the SFC. The difference between the SFC and the DFC, for temperatures higher than almost 400 °C and up to 500 °C, promotes a pronounced negative friction-velocity slope, in variable velocity tests, leading to severe unstable friction-induced vibrations.

Conversely, in such a range of temperatures, for the MAT2, MAT3 and MAT4, a strong increase of the DFC, which becomes even higher than the SFC, prevents the occurrence of the steep negative friction-velocity slope observed for the MAT1. However, the high level of friction reached at 500 °C favors the occurrence of the mode coupling instability, observed for the MAT2 and MAT3 specimens. No dynamic instabilities occur for the MAT4.

All the outcomes described so far concern samples machined from discs already used on a full size test bench, where the contaminants migrate to the contact interfaces during braking. Then, an interesting comparison between new (MAT5) and used (MAT4) samples without contaminants, has shown that for temperatures higher than 300 °C the DFC of the new samples increases slightly, compared to the used one, and remains significantly lower than the SFC. In this case, the presence of a slight negative friction-velocity slope, in variable velocity tests, and low amplitude dynamic instabilities have been observed.

A further characterization of the frictional and dynamical response of the C/C materials has been finally achieved by tests carried out under controlled atmosphere. A dedicated test bench (TriboWave), equipped with a chamber for containing gas, has been used for the tests. Analogously to TriboAir, this setup allows reproducing friction phenomena under controlled boundary conditions (temperature, sliding velocity, contact pressure, etc.). Samples of MAT1 have been used for the experimental campaign. Tests carried out in air and argon have been compared. The behavior of the DFC and SFC, as well as the onset of dynamic instabilities, have been investigated. Despite having lowered considerably the level of oxygen in the atmosphere (≈ 3.5 % of O₂) a similar frictional and vibrational behavior has been retrieved in both the environments for the different tests. A small amount of CO released in the atmosphere at 500 °C (4-5 ppm) in both air and low oxygen environments suggests that a small amount of oxygen can still lead to gasification phenomena.

Overall, the obtained results have shown a significant sensitivity of the DFC, at the highest temperatures, to the presence of contaminants at the interface. On the other hand, the SFC has similar trends for all the tested materials. The propensity of each material to promote unstable vibrations is therefore mainly affected by the DFC.

These results indicate a fundamental contribution of the interface rheology (more significant on the DFC than on the SFC) to the frictional response of the C/C materials and, consequently, to the unstable vibrations. The presence of different contaminants at the interface leads in fact to considerable different scenarios for temperature higher than almost 300-400 °C and up to 500 °C.

In conclusion to this parametric analysis, the presence of a steep negative friction-velocity slope within a high friction range, leading to severe unstable friction-induced vibrations, has been observed only for the MAT1 for temperatures equal or higher than almost 400 °C. In this case the coexistence of negative friction-velocity slope and mode coupling has been so far

hypothesized. In order to validate such hypothesis and support the identification of the different instability scenarios, in the following, an experimental and numerical characterization has been carried out in order to reproduce and analyze the different unstable vibrations (mode coupling and negative friction-velocity slope).

Chapter 3

Experimental and numerical identification of unstable friction-induced vibrations through phase shift

The onset of different unstable friction-induced vibrations, as a function of the boundary conditions and the rheology of the contact, has been so far identified by investigating the behavior of the friction coefficient and the vibrational response during tests at either decreasing or constant sliding velocity. In order to provide further evidence to support the identified instability scenarios, both experimental and numerical analyses have been carried out. In this Chapter, the dynamic instabilities caused by C/C samples in frictional contact are first investigated in detail through specific experimental tests performed on the TriboAir setup. Then, a finite element analysis is carried out in order to further investigate the unstable modes identified experimentally. After that, a lumped-parameter numerical model is used to reproduce the different unstable vibrations and support the identification of the dynamic instabilities by analyzing the vibrational signals.

3.1 Experimental Analysis

The experimental characterization of the unstable friction-induced vibrations has been carried out by testing a C/C sample pair on the TriboAir setup. The frictional and dynamical response of the tested samples has been studied by defining a specific test protocol aimed to investigate the onset of mode coupling and negative friction-velocity slope instabilities, under different sliding velocities and a maximum temperature equal to 300 °C. In the following, the setup and the measurement protocol are described. Then, the main results concerning the occurrence of the dynamic instabilities at variable and constant sliding velocities are discussed in detail.

3.1.1 Setup and measurement protocol

The occurrence of unstable friction-induced vibrations and their correlation with the frictional response of C/C materials, under different operating conditions, has been studied through the TriboAir test bench, whose main characteristics have been already presented in {2.1.1}. For the analysis described in this section and aimed to investigate in detail the different instability scenarios, an additional uniaxial accelerometer has been assembled in the normal direction to the contact. A simplified diagram of the experimental setup is shown in Figure 38.

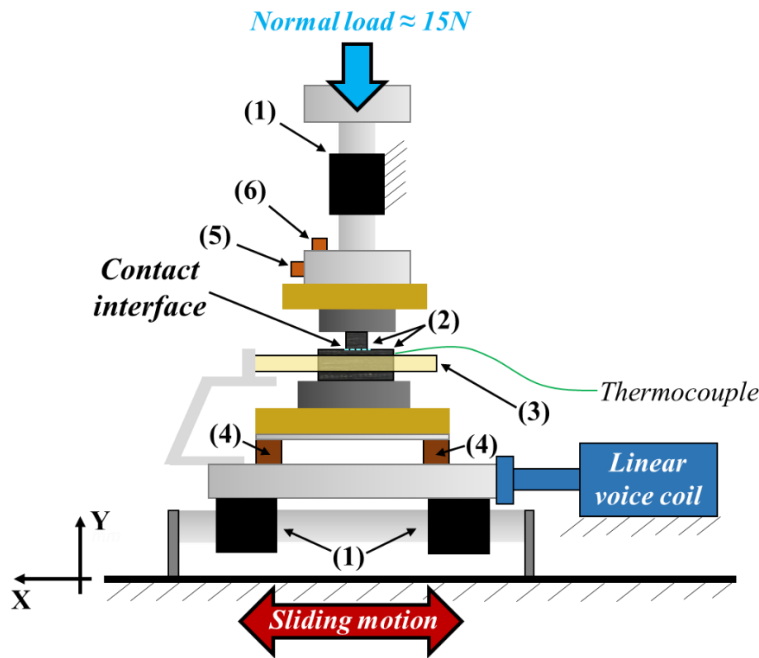


Figure 38 Schematic diagram of the TriboAir setup adopted for the experimental analysis. (1) Air bearings; (2) C/C material specimens in frictional contact; (3) IR lamps; (4) 3-axial force transducers; (5) Uniaxial accelerometer in the X direction; (6) Uniaxial accelerometer in the Y direction.

The uniaxial accelerometer placed in the Y direction (6), on the upper part of the test bench, allows measuring the vibrational response in the normal direction to the contact, providing further information for the characterization of the friction-induced vibrations.

With respect to the setup described in {2.1.1}, a different acquisition system has been used to increase significantly the sampling frequency and allow for a detailed analysis of the acceleration signals. Specifically, all data are recorded by the acquisition system SIRIUSi - DEWESOFT, based on the DualCoreADC technology with dual 24-bit delta-sigma analog to digital converter (ADC), with a sampling frequency equal to 200 kHz.

The C/C sample pair adopted for the analysis consists of the same used MAT1 specimens already tested in Chapter 2.

An experimental protocol has been specifically developed in order to investigate the onset of different dynamic instabilities and focus on their characterization. The sequence of tests of the protocol is presented in Table 8.

	Velocity [mm/s]	Max Temperature [°C]
1	Constant = 20	500
2	20→0	300
3	Constant = 15	300
4	Constant = 3	300

Table 8 Experimental protocol used for the characterization of the unstable friction-induced vibrations. A sequence of sliding heating tests are carried out at constant (20, 15, 3 mm/s) and variable imposed velocities (from 20 to 0 mm/s) and at different maximum temperatures (500 and 300 °C).

The experimental protocol consists of a sequence of *sliding heating* tests (see {2.1.3}, Figure 21.a), carried out according to the variable (from 20 to 0 mm/s) and constant (20, 15, 3 mm/s) imposed velocity profiles described in Figure 20.a and Figure 20.b, respectively (see {2.1.3}). The first *sliding heating* test is performed at a constant imposed velocity equal to 20 mm/s and a maximum temperature equal to 500 °C. This test has been carried out with the sole purpose of increasing the minimum value of the DFC on the subsequent tests carried at 300 °C. In fact, as shown in {2.3}, higher values of the minimum DFC, always reached at almost 300 °C for the MAT1, can be achieved by performing a preliminary *sliding heating* test at a maximum temperature higher than 300 °C, desorbing most of the water trapped in the third body [65]. A higher level of friction at 300 °C allowed investigating the onset of different dynamic instabilities (i.e. mode coupling and negative friction-velocity slope) at such a temperature, as shown in the following.

After the preliminary test at the maximum temperature of 500 °C, the sequence of *sliding heating* tests is carried out at a maximum temperature of 300 °C, with variable imposed velocity, from 20 to 0 mm/s, and constant imposed velocities equal to 15 and 3 mm/s. The analysis has been focused on these three tests.

As an example of the retrieved signals, Figure 39 shows two cycles of back-and-forth at room temperature condition, during the *sliding heating* test carried out at variable imposed velocity, from 20 to 0 mm/s, and a maximum temperature equal to 300 °C. From the top to the bottom, the signals correspond to the friction coefficient measured during the frictional contact, the vibrational signals on both the tangential and normal direction to the contact, X and Y respectively, and the velocity profile imposed on the moving lower sample. The symmetric reversal of sign of the friction coefficient in each stroke is due to the back-and-forth motion of the lower sample with respect to the upper one.

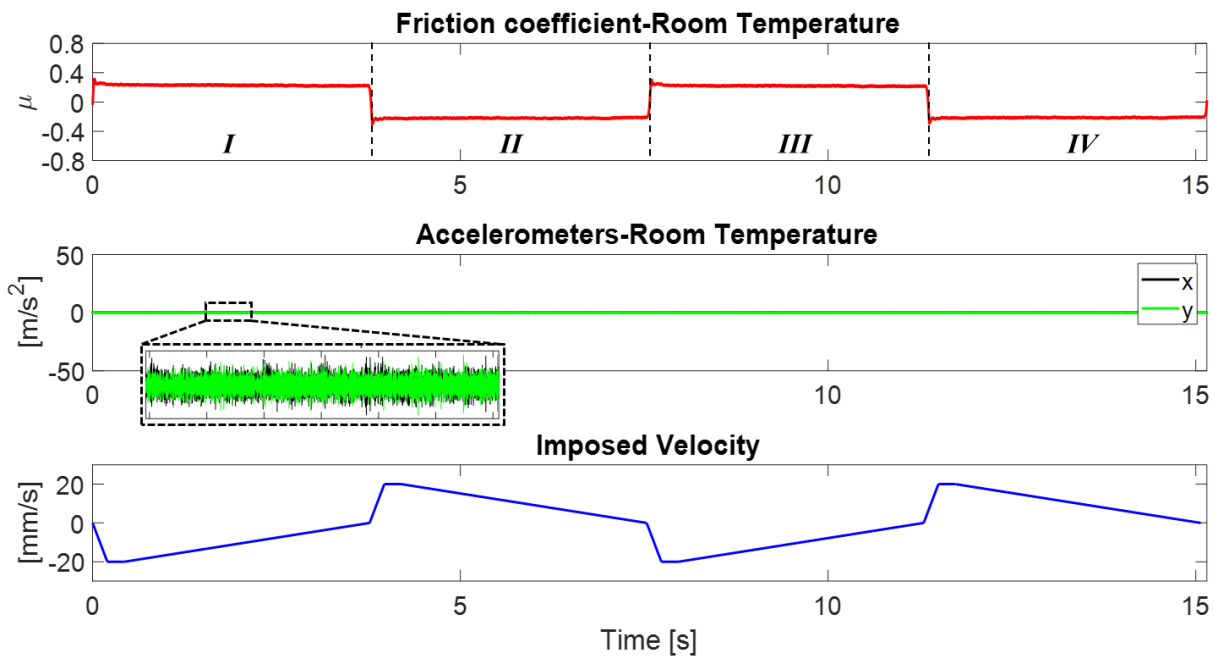


Figure 39 Example of signals recorded during two back-and-forth cycles (four strokes of the lower sample), at room temperature condition ($\approx 25^\circ\text{C}$), in the sliding heating test at variable imposed velocity ($20 \rightarrow 0$ mm/s) and a maximum temperature equal to 300°C . From the top: the friction coefficient, the accelerometer signals along the tangential (X, black) and normal direction (Y, green) to the contact and the imposed sliding velocity profile.

As can be noted from Figure 39, and consistently with the outcomes presented in Chapter 2, at room temperature condition the friction coefficient remains almost constant during each stroke. The vibrational response is characterized in this case by low-amplitude stable friction-induced vibrations, as also shown in the inset of Figure 39. The imposed velocity profile is the one already described in Figure 20.a and characterized by a fast acceleration (100 mm/s²) up to 20 mm/s, to which follows a braking deceleration (6 mm/s²) covering most of the stroke.

As also shown in Chapter 2, the frictional and vibrational response at 300°C differs significantly with respect to the room temperature condition. In particular, it has been observed, for all the tested C/C specimens, that the DFC decreases significantly up to almost 200 - 300°C (where it reaches a minimum value). On the other hand, the SFC remains almost constant in such a temperature range. The considerably lower DFC with respect to the SFC, at almost 300°C , favors the occurrence of a negative friction-velocity slope during braking, leading, in turn, to dynamic instabilities. It should be remarked that also at 300°C , if the DFC is enough high, mode-coupling instability can be observed.

In the following, the occurrence of unstable vibrations occurring during tests at 300°C is investigated for both the variable and constant imposed velocity tests provided for the protocol presented in Table 8. The different dynamic instabilities are described and discussed in detail.

3.1.2 Variable velocity test

While at room temperature condition and variable imposed velocity (from 20 to 0 mm/s) an almost constant friction coefficient and stable friction-induced vibrations are observed in each stroke (Figure 39), a significantly different scenario is observed at 300 °C. Figure 40 shows the frictional and vibrational response of two back-and-forth strokes recorded at 300 °C, during the same *sliding heating* tests of Figure 39.

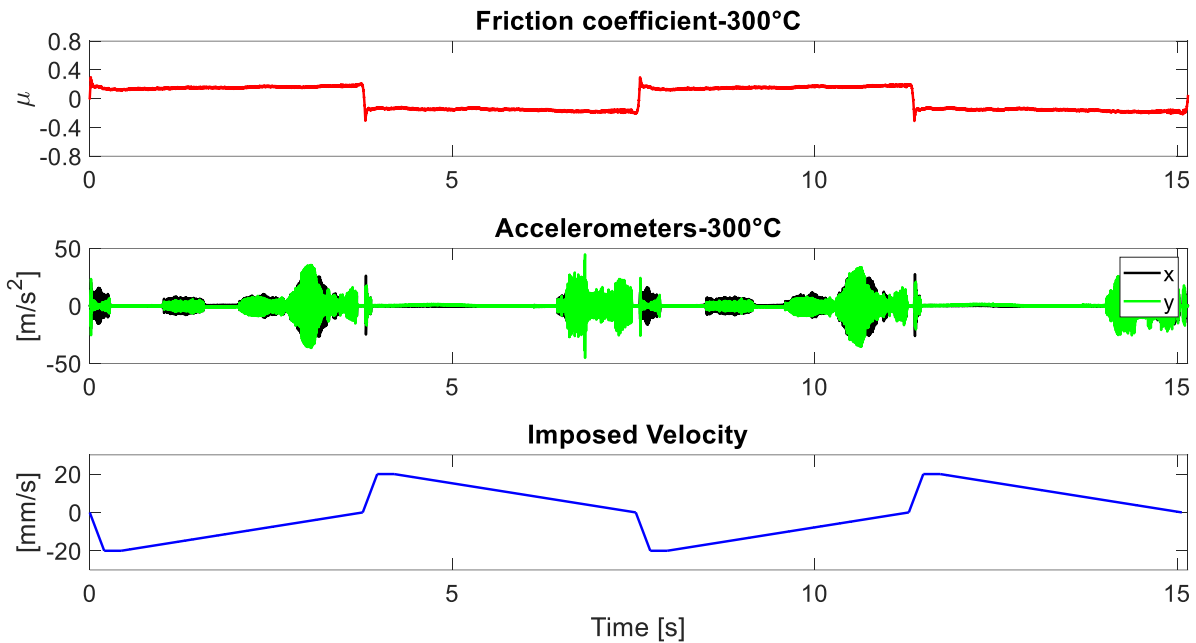


Figure 40 Example of signals recorded during two back-and-forth cycles (four strokes of the lower sample), at 300 °C, in the sliding heating test at variable imposed velocity (20→0 mm/s) and a maximum temperature equal to 300° C. From the top: the friction coefficient, the accelerometer signals along the tangential (X, black) and normal direction (Y, green) to the contact and the imposed sliding velocity profile.

Differently from braking carried out at room temperature condition, at 300 °C, an increase of the friction coefficient with the decrease of the sliding velocity can be observed. Moreover, the vibrational response of the C/C specimens is characterized, in this case, by the presence of unstable friction-induced vibrations. Further information can be obtained by analyzing the behavior of the friction coefficient and the dynamic response during one single stroke. As an example, Figure 41 shows the comparison between the signals (friction coefficient and acceleration along the X direction) acquired at room temperature and at 300 °C, in the third stroke of Figure 39 and Figure 40, respectively.

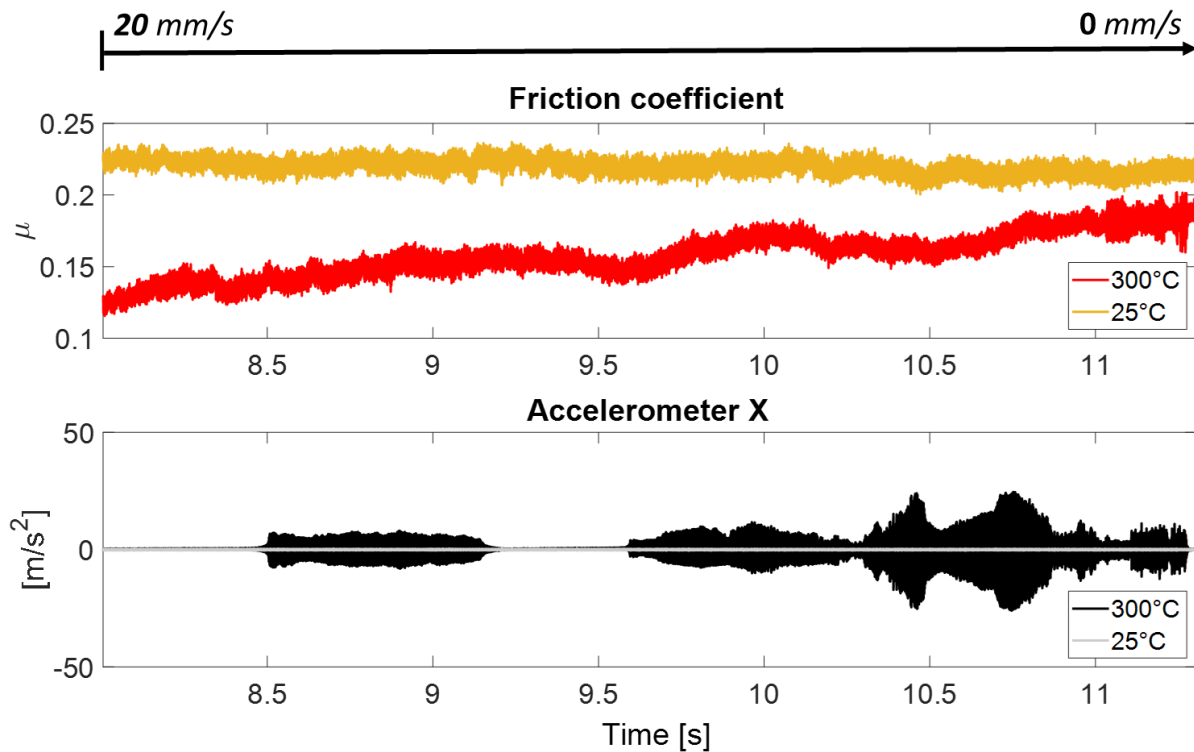


Figure 41 Comparison of the friction coefficient and the vibrational response along the X direction, measured at room temperature and at 300 °C (third stroke of Figure 39 and Figure 40, respectively).

It can be noticed that the friction coefficient observed during braking at 300 °C is characterized by lower values compared to those at 25 °C. The low DFC at higher sliding velocities promotes the occurrence of the negative friction-velocity slope toward the end of braking, where a significant increase of the friction coefficient, while lowering the imposed velocity, can be observed. Regarding the vibrational response, the comparison shows a clear difference between the stable response characterizing the material behavior at room temperature condition and the occurrence of dynamic instabilities during braking at 300 °C.

It should be remarked that the level of friction at 300 °C, shown in Figure 41, is slightly higher than the one shown in Figure 26.b at 300 °C (always lower than 0.14) and related to a *sliding heating* test at variable imposed velocity (from 20 to 0 mm/s), carried out on the same C/C specimen pair. Such a difference is due to the preliminary *sliding heating* test at 500 °C, which allows reaching higher values of the minimum DFC (see {2.3}), achieved at almost 300 °C, on the subsequent tests provided for the protocol presented in Table 8.

A detailed study of both the friction coefficient trend and the dynamic instabilities observed on the single stroke shown in Figure 41, at 300 °C, is presented in Figure 42. From the top, the friction coefficient, the measured accelerations along the X and Y directions and the spectrogram of the vibrational response along the X direction, normalized with respect to the maximum value of each Hamming window, in order to highlight the main frequency content.

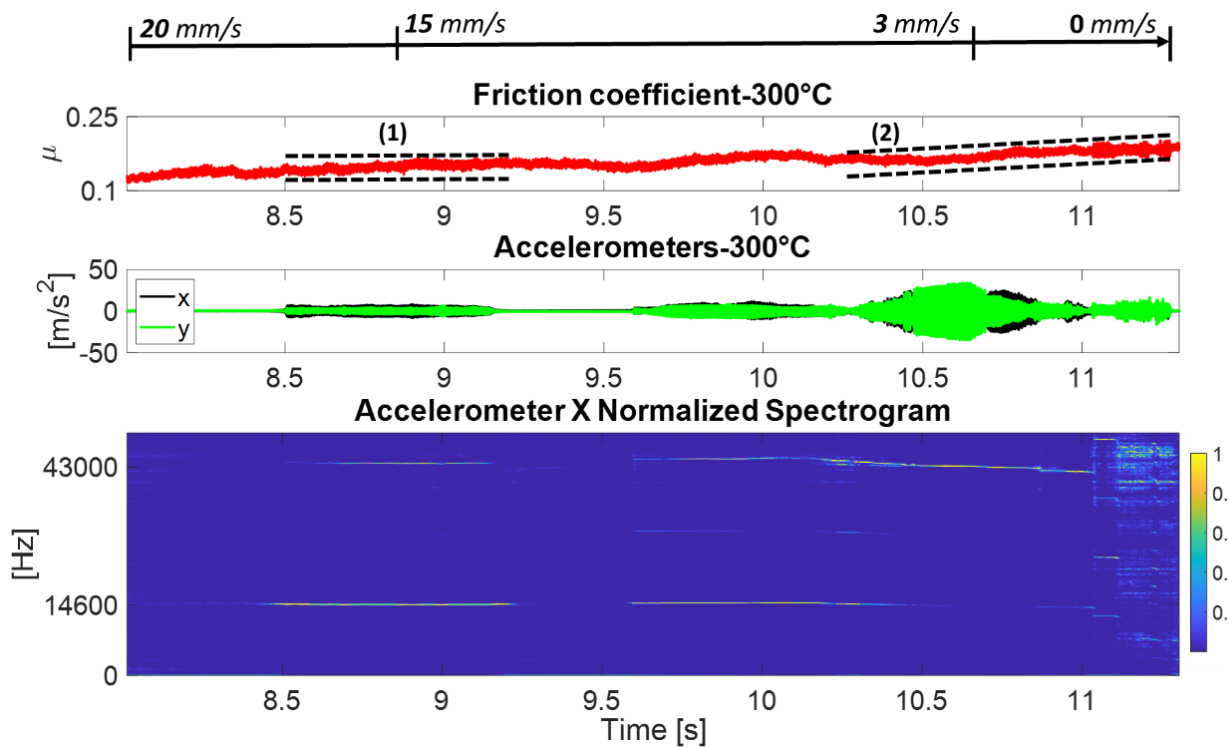


Figure 42 Example of signals recorded during a single stroke at 300 °C (third stroke of Figure 40) in the sliding heating test carried out at variable imposed velocity (from 20 to 0 mm/s). From the top: the friction coefficient, the accelerometer signals along the tangential (X, black) and normal (Y, green) direction to the contact and the normalized spectrogram of the acceleration along the X direction.

The scenario described in Figure 42 shows the occurrence of two different dynamic instabilities observed at different velocity ranges. The instabilities can be roughly distinguished, as a first attempt, thanks to the different amplitude and the different frequency content of the acceleration signals. A first dynamic instability can be noticed at the beginning of braking, when the sliding velocity is still relatively high and the friction coefficient is almost constant (Figure 42, friction coefficient range (1)). From the spectrogram, it can be observed that the main frequency content is almost equal to 14.6 kHz. On the other hand, toward the end of braking, the friction coefficient is no longer constant and an increase can be noticed (Figure 42, friction coefficient range (2)). Within this interval of decreasing velocity, where the friction coefficient increases (negative friction-velocity slope), the onset of a different dynamic instability can be observed. In this case, the main frequency content of almost 43 kHz can be detected by the spectrogram, highlighting a different unstable mode.

Meaningful information on the origin of the different unstable friction-induced vibrations can be retrieved by investigating in further detail the vibrational response of the C/C specimens in both the tangential and normal directions to the contact. Figure 43 shows magnifications of the vibrational response along the X and Y directions of both the first instability (Figure 43-up), detected at a sliding velocity of almost 15 mm/s, and the second instability (Figure 43-bottom), detected at almost 3 mm/s.

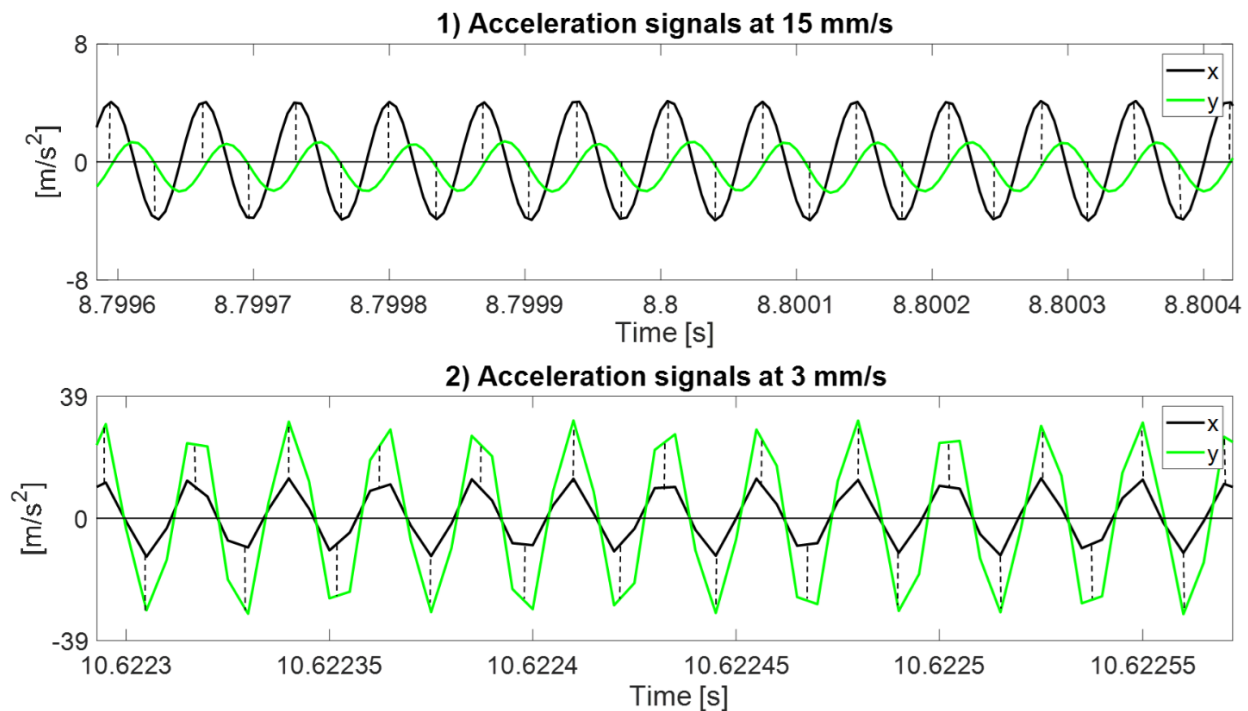


Figure 43 Detail of the vibrational response along the tangential (X) and normal (Y) directions for the mode coupling instability (up) and the negative friction-velocity slope (bottom) observed in Figure 42 at almost 15 mm/s and 3 mm/s, respectively.

In Figure 43-up, the vibrational response has been filtered by means of a low-pass filter with a cutoff frequency of 20 kHz, in order to focus on the main frequency content of the mode coupling. During this first contact instability, it can be noticed that the vibrational signals recorded in the tangential (X) and normal direction (Y) are phase-shifted by almost 90° . This is a typical feature retrieved in literature [15, 108, 165-167] when dealing with mode coupling instability. The coupling of two modes of vibrations brings to the establishment of a phase shift of about 90° between the tangential and normal directions to the contact [15, 108, 167]. Then, the observed shift in phase brings to the confirmation that the contact instability, observed within this range of velocities, where the friction is almost constant, is due to mode coupling.

On the other hand, Figure 43-bottom shows that, during the instability at lower velocities, the vibrational signals, along the X and Y directions, are in phase. This is well correlated with the trend of the friction coefficient, which shows a negative friction-velocity slope that can bring a single mode of the system to be unstable, explaining the in-phase behavior of the tangential and normal components of the acceleration.

This outcome provides a direct tool for distinguishing the two different types of dynamic instabilities and allows for a better characterization of the main features of the unstable vibrational response of C/C materials at high-temperature condition.

In order to investigate further the observed phenomena, decoupling the effect of the imposed velocity variation, *sliding heating* tests, at a maximum temperature of 300°C , have been carried out at constant imposed velocities equal to 15 mm/s and 3 mm/s. These tests have been performed

with the purpose of studying the main features of the instabilities caused by mode coupling and negative friction-velocity slope, respectively.

3.1.3 Constant velocity tests

The occurrence of the mode coupling instability has been reproduced through a *sliding heating* test performed at a constant sliding velocity equal to 15 mm/s. As an example, Figure 44 shows the behavior of the friction coefficient and the vibrational response on both X and Y directions for two cycles of sliding motion at 300 °C and at constant imposed velocity.

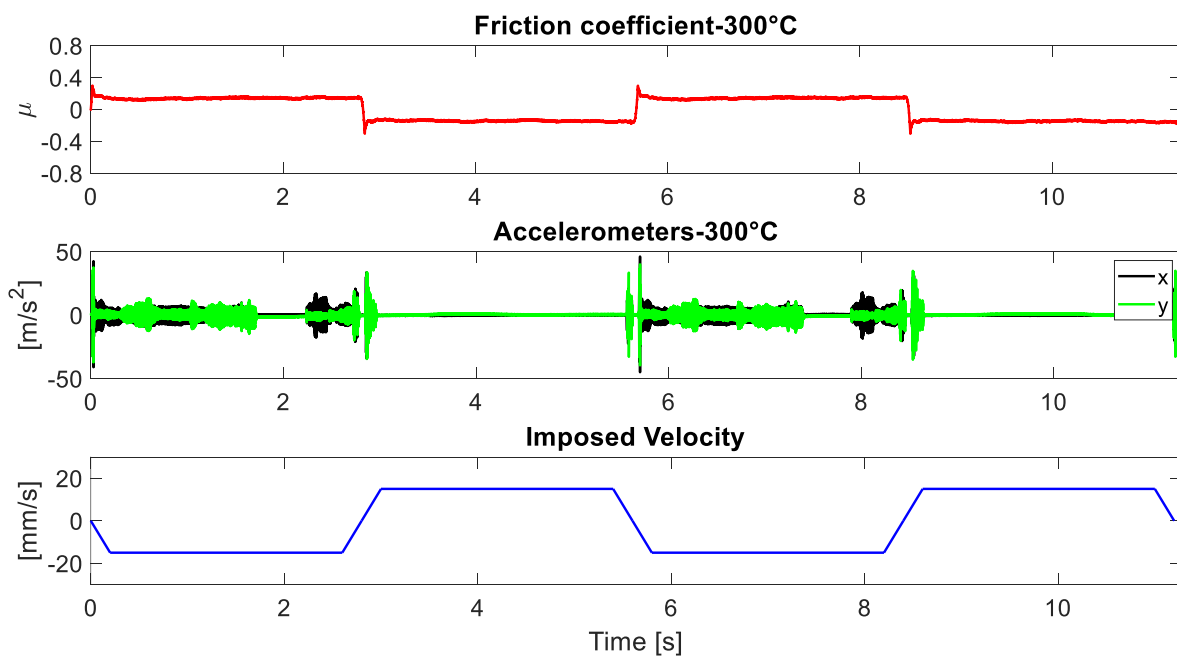


Figure 44 Example of signals recorded during two back-and-forth cycles, at 300 °C, in the sliding heating test at constant imposed velocity (15 mm/s) and a maximum temperature equal to 300° C. From the top: the friction coefficient, the accelerometer signals along the tangential (X , black) and normal (Y , green) direction to the contact and the imposed sliding velocity profile.

An almost constant friction coefficient in each stroke and the occurrence of unstable friction-induced vibrations can be observed in Figure 44. Further information on the main features of the dynamic instability, arising under a constant sliding velocity equal to 15 mm/s, can be retrieved by investigating the vibrational response along the X and Y directions in a single stroke. Figure 45 shows a detail of the frictional and vibrational response of the third stroke of Figure 44.

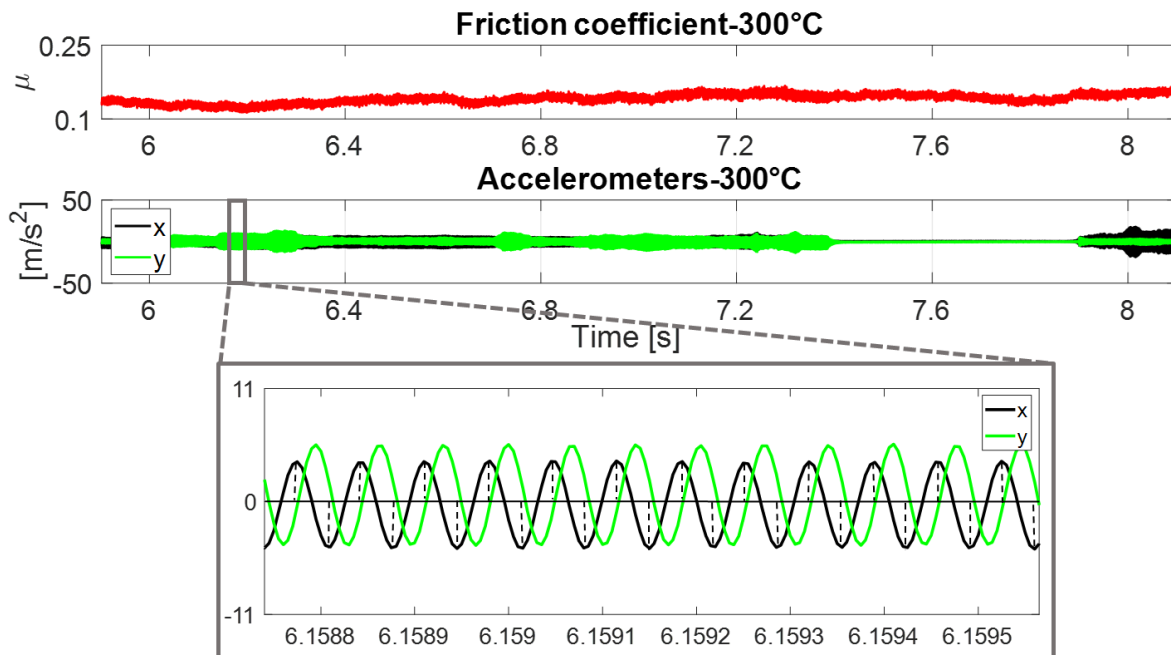


Figure 45. Detail of the friction coefficient and vibrational response of the third stroke of Figure 44. From the top: the friction coefficient and the accelerometer signals along the tangential (X) and normal (Y) direction to the contact.

Consistently with the dynamic instability observed during braking test at almost 15 mm/s (Figure 43-up), also at constant velocity the onset of unstable friction-induced vibrations is characterized by a phase shift of almost 90° between the X and Y direction, as shown in the zoom of Figure 45. Moreover, the main frequency content of the instability is almost 14.6 kHz, such as the one observed at 15 mm/s for the variable velocity test. The main features of the measured signals confirm the occurrence of a mode coupling instability.

A different scenario is the one retrieved under a constant sliding velocity equal to 3 mm/s. This test has been carried out in order to investigate the instability that arises in the range of sliding velocities where a negative friction-velocity slope is observed (detail (2) in Figure 42). In this range, the friction coefficient is no longer constant and, during the system vibration, an increase in the sliding velocity (due to its oscillation when vibrating) brings to a decrease of the friction coefficient, leading to negative friction-velocity slope instability. Figure 46 shows, as an example, the behavior of the friction coefficient as well as the vibrational response of a single stroke at 300 °C.

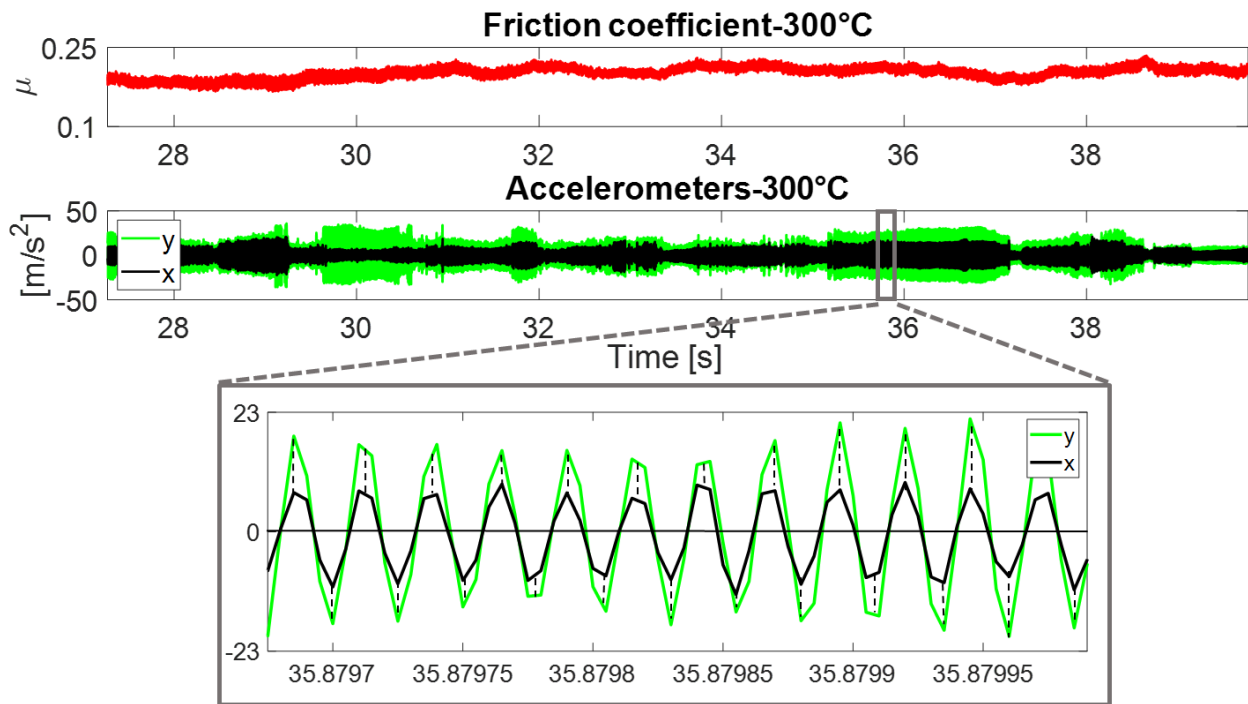


Figure 46. Detail of the friction coefficient and vibrational response of a single stroke at 300 °C, in the sliding heating test at constant imposed velocity (3 mm/s) and a maximum temperature equal to 300 °C. From the top: the friction coefficient and the accelerometer signals along the tangential (X) and normal (Y) direction to the contact.

Unstable friction-induced vibrations are observed during the whole stroke. Moreover, as can be seen from the zoom of Figure 46, in this case, the vibrational response is characterized by a higher frequency (almost 43 kHz), with respect to the mode coupling instability observed in Figure 45, and the acceleration signals along the tangential (X) and normal (Y) direction to the contact are in phase. This is consistent with the negative friction-velocity slope instability observed during braking test (Figure 43-bottom), within the same velocity range, where the oscillation of the sliding velocity (i.e. of the friction coefficient) brings to modal instability.

Further analyses on the unstable modes and the main features of the unstable friction-induced vibrations have been also carried out numerically. The following section aims then to support the experimental outcomes and provide additional information on the dynamic response and the identified instability scenarios.

3.2 Numerical Analysis

In order to confirm the different origins of the dynamic instabilities (either mode coupling or negative friction-velocity slope) observed experimentally in {3.1}, a numerical analysis has been carried out. First, the unstable modes at 14.6 kHz and 43 kHz have been numerically investigated

through a finite element analysis. This study allows supporting the experimental identification of the unstable modes and provides further information to characterize their mode shape. Then, a lumped-parameter numerical model has been developed to study the dynamic instabilities and correlate the observed features of the vibrational signals with the measured trends of the friction coefficient.

3.2.1 Finite element analysis of the unstable modes

In this section, the finite element numerical model, developed in order to investigate the unstable modes observed in {3.1}, is presented. The modes of the system are obtained through a pre-stressed modal analysis. A complex eigenvalue analysis is carried out in order to identify the mode coupling instability at 14.6 kHz. The mode at 43 kHz, triggered by negative friction-velocity slope, is investigated as well.

3.2.1.1 Numerical model

The different modes identified through the experimental characterization have been investigated numerically by finite element method (FEM). The commercial software through which the linear modal analysis has been carried out is ANSYS[®]. The geometry of the numerical model used for the analysis has been retrieved from the experimental one (see {2.1.1}). The finite element model is shown in Figure 47.

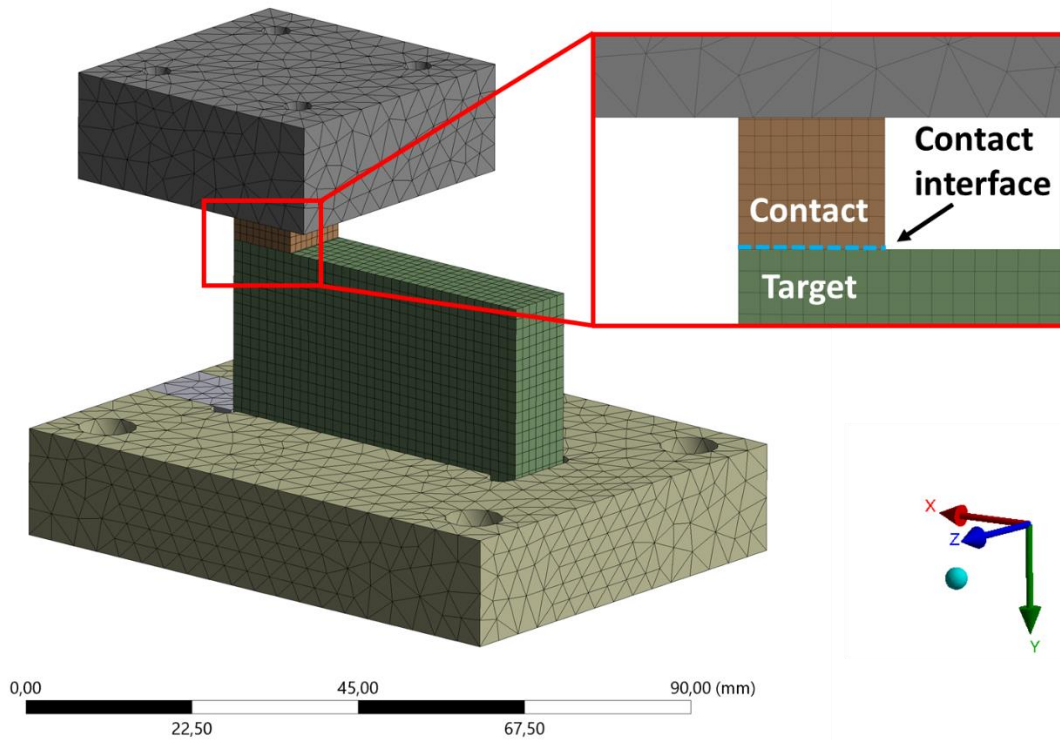


Figure 47 Finite element model of the two C/C samples in frictional contact. In the inset, a detail of the contact (upper sample) and target (lower sample) bodies.

As shown in Figure 47, the numerical model consists of a C/C specimen pair, such as those used for the experimental campaigns, with the steel mounting blocks that clamp and keep the samples in contact (see description of the experimental setup in {2.1.1}). A “Normal Lagrange” contact type has been set between the upper (contact body) and lower (target body) sample, as shown in the inset of Figure 47. The model has been developed with the material parameters obtained in [168]. Moreover, a mapped hexahedral (20 nodes) mesh and a free tetrahedral (10 nodes) mesh have been used to model the C/C specimens and the sample holders, respectively. The characteristics of the mesh are shown in Table 9.

Features	Upper sample	Lower sample	Upper sample holder	Lower sample holder
<i>Element Type</i>	Hex20	Hex20	Tet10	Tet10
<i>Geometry</i>	Hexahedron	Hexahedron	Tetrahedron	Tetrahedron
<i>Mesh</i>	Mapped	Mapped	Free	Free
<i>Element Size [mm]</i>	1,2	1,5	4	4
<i>No. Elements</i>	729	4046	4218	10907

Table 9 Mesh features of the finite element numerical model.

Before performing the modal analysis, a preliminary static analysis allows imposing the frictional contact forces at the contact nodes. As in the experiments, the loading conditions provides for a vertical total force equal to 15 N, applied to the upper sample holder along the normal direction to the contact (Y direction). Then, a displacement of 1 mm is applied along the tangential direction to the contact (X direction), on the lower surface of the bottom sample holder, bringing the interface in sliding condition.

Once the static structural analysis is carried out, the pre-stressed modal analysis is performed. Having introduced frictional contact forces, the stiffness matrix of the system is no longer symmetric and leads to complex eigenvalues and eigenvectors of the system [15]. A general eigenvalue can be therefore written as:

$$\lambda = \sigma \pm j\omega$$

where the real part is proportional to the modal damping factor of the mode, while the imaginary part is proportional to its angular frequency. A positive real part of the eigenvalue leads to an unstable mode of the system [135].

In the following, the unstable modes identified through the experimental tests, in {3.1}, are investigated. A complex eigenvalue analysis, as a function of the friction coefficient between the C/C sample pair in frictional contact, is carried out in order to investigate the unstable mode triggered by mode coupling (almost 14.6 kHz). The mode triggered by negative friction-velocity slope (almost 43 kHz) is studied as well.

3.2.1.2 Analysis of the experimental unstable modes

The unstable mode related to mode coupling has been numerically studied by performing a complex eigenvalue analysis as a function of the friction coefficient. This parametric analysis supports the experimental outcomes, shown in {3.1}, by reproducing the lock-in phenomenon leading to the mode-coupling unstable friction-induced vibrations. In order to perform the complex eigenvalues analysis, the modes of the systems obtained through pre-stressed modal analysis have been studied increasing the friction coefficient from 0.1 to 1. The friction coefficient is incremented by 0.1 at each iteration of the parametric analysis. Both the frequency and the stability (real part of the eigenvalues) of the modes have been investigated.

The results of the complex eigenvalue analysis are shown in Figure 48.

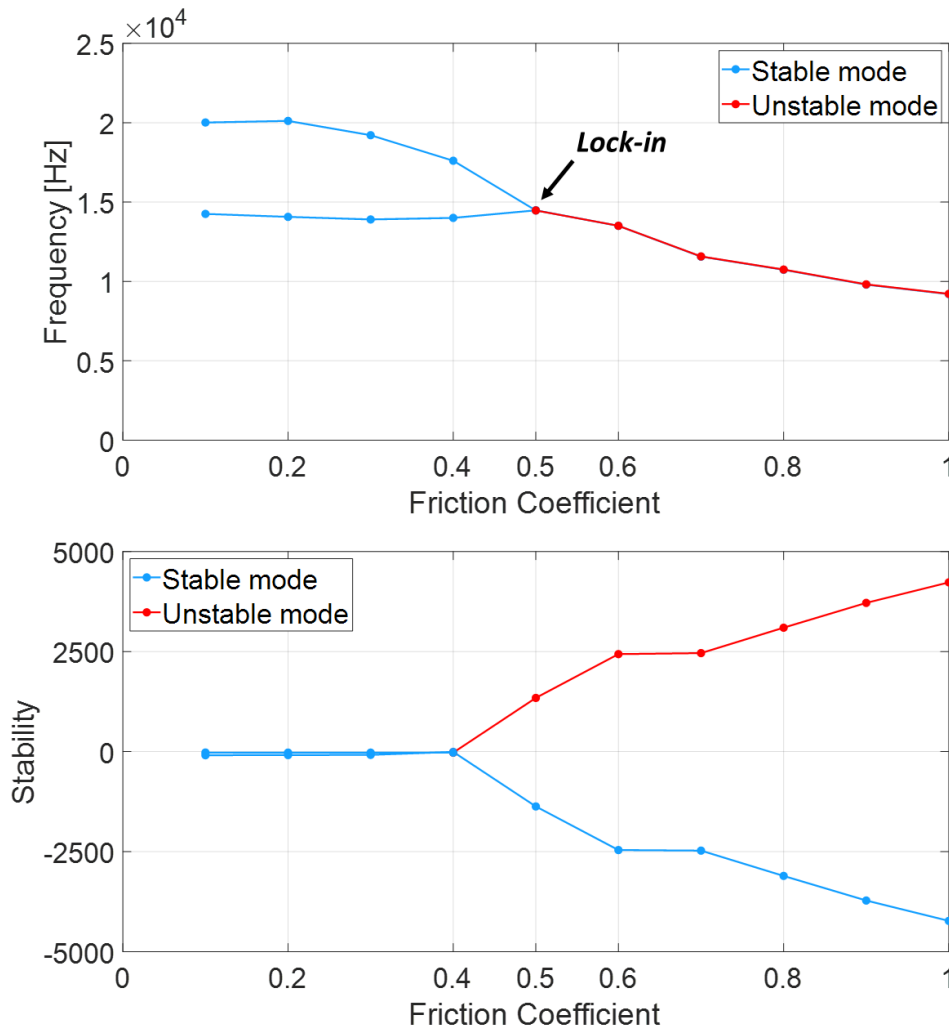


Figure 48 Complex eigenvalue analysis carried out as a function of the friction coefficient. The evolution of the frequency and the stability of the investigated modes are studied for a friction coefficient varying from 0.1 to 1 and increasing by 0.1 in each iteration of the parametric analysis.

In Figure 48, it can be noticed that, increasing the friction coefficient, the two modes of the system approach each other until they coalesce (lock-in). As a result, the real part of one of the eigenvalues becomes positive, leading to the mode coupling instability. Such phenomenon occurs for a frequency of the unstable mode almost equal to 14.6 kHz, which is the frequency retrieved also experimentally. The related mode shape is shown in Figure 49.

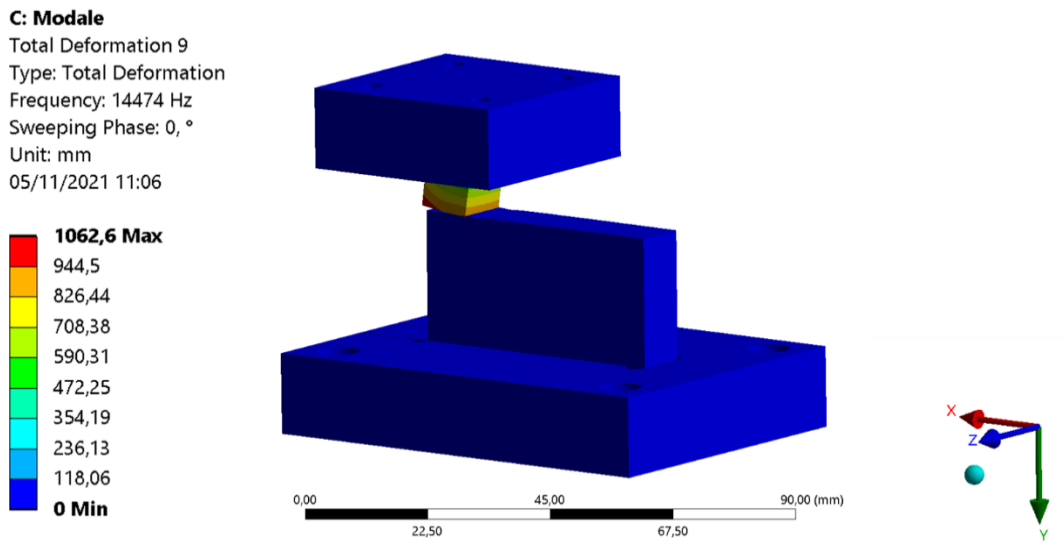


Figure 49. Mode shape of the unstable mode with a frequency of 14474 Hz.

As can be seen in Figure 49, the mode shape of the unstable mode deforms mainly in the tangential direction to the contact (X direction).

The pre-stressed modal analysis has been carried also with the aim of identifying the unstable mode triggered by the negative friction-velocity slope. A mode at almost 43 kHz, whose modal shape deforms along the tangential direction to the contact, has been identified and studied at different friction coefficients. Also in this case, a parametric analysis, carried out by increasing the friction coefficient by 0.1 in each iteration from 0.1 to 1, has been performed. Figure 50.a shows the evolution of the frequency related to the investigated mode, as a function of the friction coefficient. Figure 50.b shows the mode shape at almost 43 kHz.

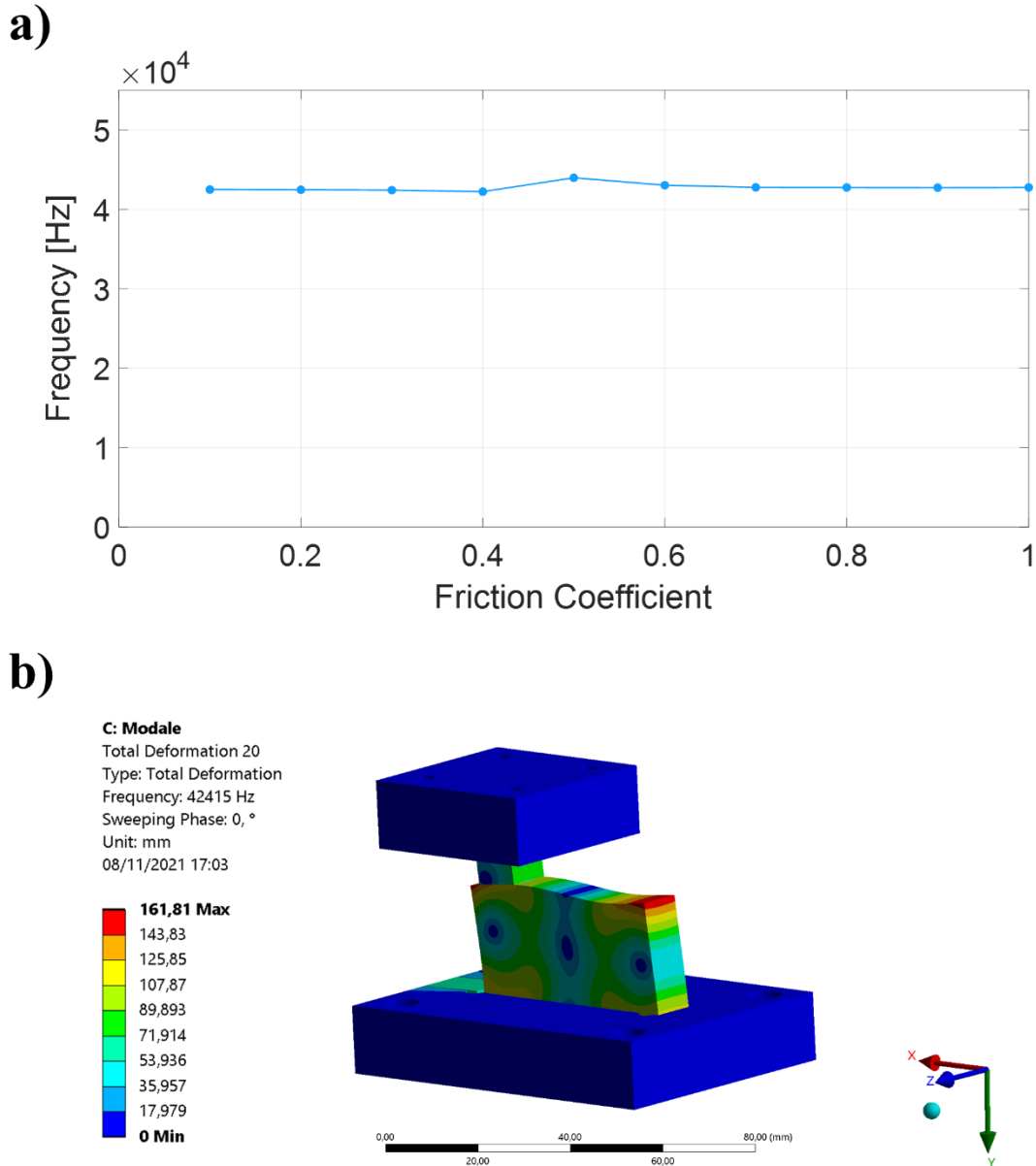


Figure 50 a) Evolution of the frequency of the mode at almost 43 kHz as a function of the friction coefficient varying from 0.1 to 1; b) Mode shape at 42415 Hz obtained for a friction coefficient equal to 0.3.

As can be seen from Figure 50.a, by increasing the friction coefficient no remarkable differences in the frequency of the mode at almost 43 kHz can be observed. The presence of a mode shape of the system, which deforms tangentially and with a frequency of almost 43 kHz (as shown in Figure 50.b), is in agreement with the experimental outcomes shown in {3.1}, where the dynamic

instability due to the negative friction-velocity slope is characterized by a frequency of almost 43 kHz.

Once the main features of the unstable modes, observed experimentally, have been retrieved through finite element analysis, the dynamic instabilities due to mode coupling and negative friction-velocity slope have been numerically reproduced by means of a lumped-parameter model. In the following, a description of the analysis is provided.

3.2.2 Numerical analysis through a lumped-parameter model

A numerical investigation of the mode coupling and negative friction-velocity slope instabilities, which are the dynamic response of the system generated by the C/C material interface, has been carried out by means of a lumped-parameter model. The analysis with such a simple, by a dynamic point of view, model allows decoupling the onset of the two different types of unstable friction-induced vibrations. In this way, it is possible to study the main features of the vibrational response, when either a mode coupling or a negative friction-velocity slope instability occurs. The coexistence of both phenomena has been investigated as well.

3.2.2.1 Description of the model

The analyzed model consists of two masses, one of which is in frictional contact with a rigid translating plane. Consistently with the existing literature, the presence of two masses allows considering both the dynamics at the contact and that of the bulk of the mechanical system, providing a tool for simulating the vibrational response of a frictional system [127]. Figure 51 shows a diagram of the developed model.

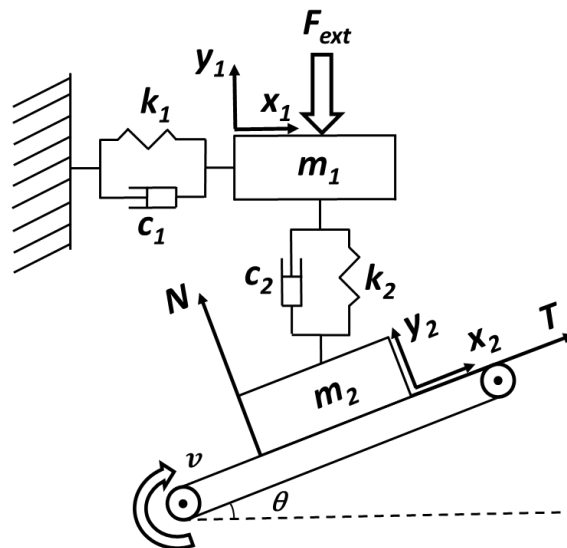


Figure 51 Diagram of the lumped-parameter model.

As shown in Figure 51, the mass m_2 is in frictional contact with a slider, inclined by an angle θ with respect to the horizontal plane and moving at a velocity v . The stiffness coefficients are indicated as k_1 and k_2 , while the damping coefficients are referred to as c_1 and c_2 . In the model, a preload is applied by means of an external force F_{ext} . The motion of the mass m_1 can be decomposed along the coordinates x_1 and y_1 , while the motion of the mass m_2 along the x_2 and y_2 directions. Moreover, the reaction force N , at the contact interface, between the mass m_2 and the slider, gives rise to a tangential force $T = \mu N$, where μ is the friction coefficient.

The model equations have been developed by considering two constrains. The first condition imposes $y_2=0$, preventing the detachment of the mass m_2 from the slider. The second constraint requires the coincidence between the horizontal motion of the mass m_1 and m_2 and it can be expressed as $x_1 = x_2 \cos\theta$. Then, the equations of motion describing the numerical model can be written as follows:

$$M\ddot{\underline{r}} + C\dot{\underline{r}} + K\underline{r} = \underline{F} \quad (1)$$

Where:

$$M = \begin{bmatrix} m_1 \cos^2 \theta + m_2 + \mu m_1 \cos\theta \sin\theta & 0 \\ 0 & m_1 \end{bmatrix} \quad (2)$$

$$C = \begin{bmatrix} c_1 \cos^2 \theta + c_2 \sin^2 \theta - \mu(c_2 - c_1) \sin\theta \cos\theta & c_2(\mu \cos\theta - \sin\theta) \\ -c_2 \sin\theta & c_2 \end{bmatrix} \quad (3)$$

$$K = \begin{bmatrix} k_1 \cos^2 \theta + k_2 \sin^2 \theta - \mu(k_2 - k_1) \sin\theta \cos\theta & k_2(\mu \cos\theta - \sin\theta) \\ -k_2 \sin\theta & k_2 \end{bmatrix} \quad (4)$$

$$\underline{F} = \begin{pmatrix} 0 \\ -F_{ext} \end{pmatrix} \quad (5)$$

$$\underline{r} = \begin{pmatrix} X \\ Y \end{pmatrix} \quad (6)$$

In particular, the unknown X and Y represent respectively x_2 and y_1 , which are the two degrees of freedom of the numerical model. The equations have been solved through Matlab/Simulink[®] with an ode23s solver.

The values of the parameters introduced for the numerical analysis are shown in Table 10. It should be noticed that the model parameters have no direct link with the physical system. Bearing in mind that such a simple model cannot be representative of a real frictional system, the parameters have been chosen only to reproduce qualitatively the different dynamic instabilities, in order to analyze their features of interest.

Parameter	Value
m_1	2.12 [kg]
m_2	0.18 [kg]
k_1	100000 [N/m]
k_2	101000 [N/m]
c_1	0.1 [kg/s]
c_2	0.1 [kg/s]
F_{ext}	500 [N]
θ	0.01 rad

Table 10 Parameters used in the numerical model for the analysis.

The significantly low value of θ allows considering the two degrees of freedom x_2 and y_1 as almost orthogonal. It is, therefore, reasonable to assume the vibrational response along X and Y as the tangential and normal vibrational components to the contact, respectively. As specified in the following sections, different trends of the friction coefficient μ , with respect to the sliding velocity, have been introduced in order to decouple the onset of the mode coupling and the negative friction-velocity slope instabilities, as observed experimentally. First, a complex eigenvalue analysis (CEA) has been carried out, as a function of μ , in order to characterize the overall dynamic response of the system.

3.2.2.2 Complex eigenvalues analysis

By computing the eigenvalues of the mechanical system, it is possible to predict the critical values of the friction coefficient leading to the occurrence of a mode coupling instability. The eigenvalues of a mechanical system characterized by a friction coefficient different from zero (asymmetric system matrices) can be found expressing the problem in the state space, as shown below:

$$\begin{cases} M\dot{\underline{r}} - M\dot{\underline{r}} = 0 \\ M\ddot{\underline{r}} + C\dot{\underline{r}} + K\underline{r} = \underline{F} \end{cases} \quad (7)$$

That can be written as:

$$A\dot{\underline{p}} + B\underline{p} = \underline{Q} \quad (8)$$

Where:

$$A = \begin{bmatrix} 0 & M \\ M & C \end{bmatrix}, \quad B = \begin{bmatrix} -M & 0 \\ 0 & K \end{bmatrix}, \quad \underline{p} = \begin{bmatrix} \dot{\underline{r}} \\ \underline{r} \end{bmatrix} \text{ and } \underline{Q} = \begin{bmatrix} 0 \\ \underline{F} \end{bmatrix} \quad (9)$$

The eigenvalues of this numerical model can be written as follow:

$$\lambda_i = -\omega_i \delta_i \pm j\omega_i \sqrt{1 - \delta_i^2} \quad (10)$$

where ω_i is the angular frequency, while δ_i is the modal damping factor. The value of the friction coefficient affects significantly the stability of the system, as it can be responsible for a negative modal damping factor and, therefore, a positive real part of the eigenvalues [123, 127, 140]. Such a condition leads to the onset of unstable friction-induced vibrations. In this respect, a value of μ higher than a specific threshold, depending on the parameters of the mechanical system, can lead to a mode coupling instability, where two different frequencies of the system coalesce together (lock-in) resulting in an unstable dynamical response [106, 169]. Figure 52 shows the complex eigenvalue analysis carried out as a function of the friction coefficient for the presented model.

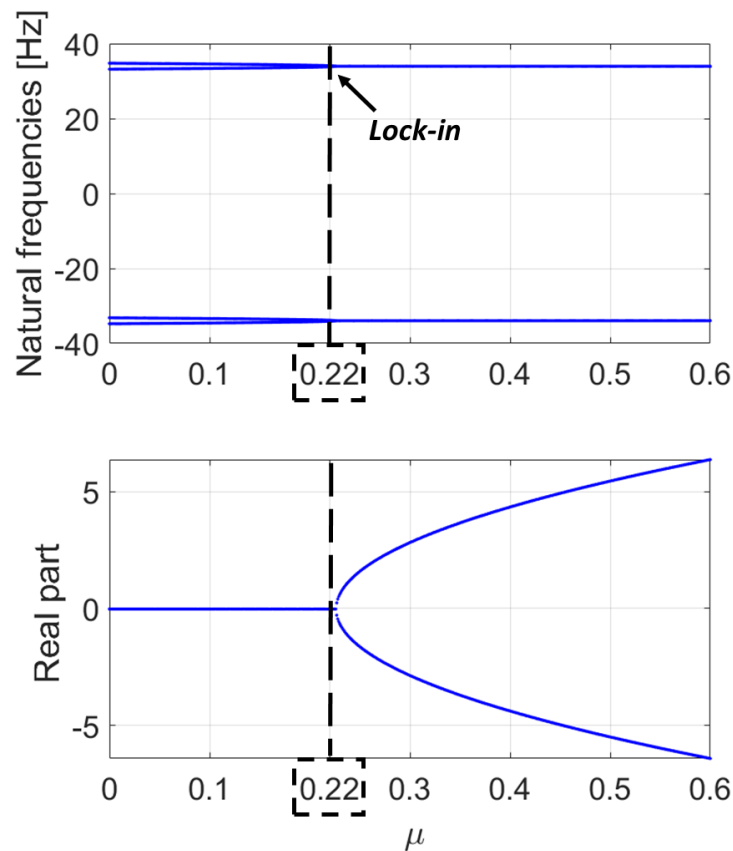


Figure 52 Real part and imaginary part (natural frequencies) of the eigenvalues as a function of the friction coefficient.

For a friction coefficient lower than 0.22, two separate modes of the system, characterized by different natural frequencies and positive damping, can be observed. As shown in Figure 52, the occurrence of a mode coupling instability arises for values of the friction coefficient higher than 0.22, where the initially separated frequencies merge together and one of the two real parts of the eigenvalues becomes positive (unstable mode).

Taking into account this preliminary stability analysis, in order to study the vibrational response related to the mode coupling, a constant friction coefficient equal to 0.5 will be imposed in the transient simulations. Being greater than 0.22, such a value of μ is in the range of friction coefficient where a positive real part of the eigenvalues can be observed and, therefore, a mode coupling dynamic instability is expected to occur.

On the other hand, an increasing μ from 0.05 to 0.15, while decreasing the relative velocity at the contact, will be imposed for simulating the onset of unstable friction-induced vibrations due to the negative friction-velocity gradient. Being in a range of friction coefficient lower than 0.22, the occurrence of unstable friction-induced vibrations during the simulation will be, in this case, not affected by the mode coupling phenomenon.

In this manner, the numerical decoupling of the mode coupling instability, from the negative friction-velocity slope instability, allows for their characterization separately. In the following paragraph, the main results achieved by the respective transient simulations are presented.

3.2.2.3 Transient analysis

The vibrational response for the two-degrees-of-freedom frictional system has been investigated for both the mode coupling and the negative friction-velocity slope instability. In order to simulate a braking condition, a variable velocity of the sliding belt has been imposed. In particular, the transient analysis has been carried out with a decreasing velocity of the slider from 7 m/s to 0 m/s and a deceleration equal to 1 m/s². According to the complex eigenvalue analysis described in {3.2.2.2}, a constant friction coefficient equal to 0.5 has been chosen to study the onset of the mode coupling instability. Figure 53 shows the vibrational response, in terms of acceleration, along the tangential (X) and normal (Y) direction to the contact, when the mode coupling instability arises. Only the exponential increase of the dynamic instability is taken into account, in order to avoid non-linear contribution in the dynamic response of the system (sticking and detachment from the belt).

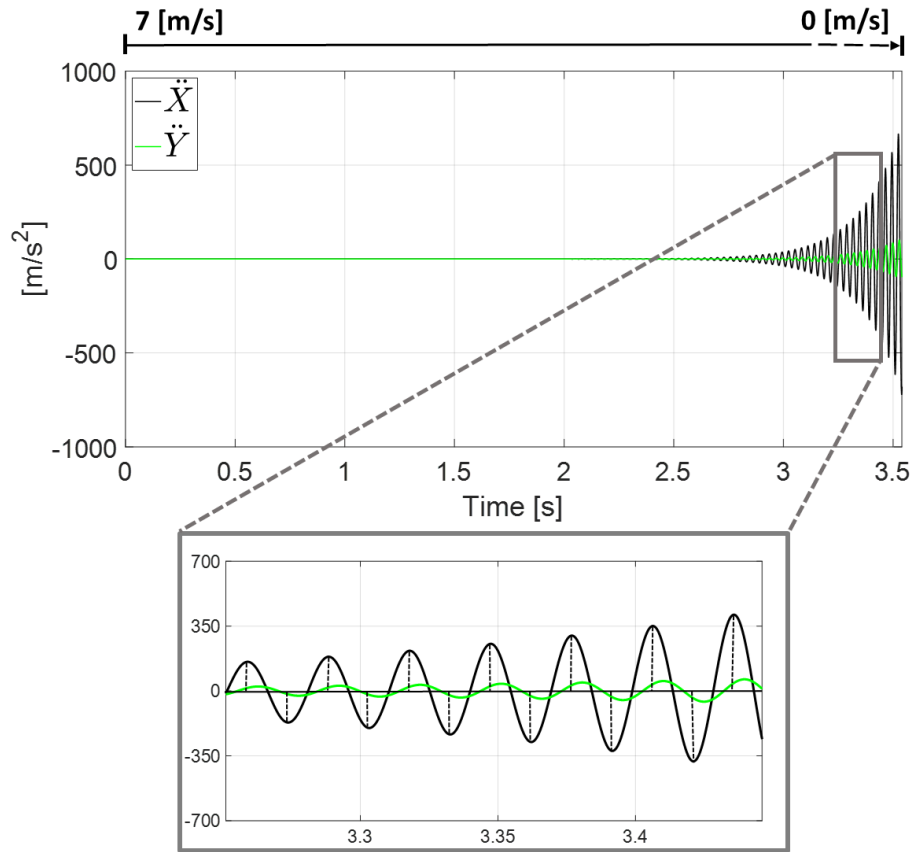


Figure 53 Onset of the mode coupling instability: acceleration \ddot{X} and \ddot{Y} with a constant friction coefficient equal to 0.5.

Consistently with the CEA, a constant friction coefficient higher than 0.22 leads to a mode coupling instability, with a frequency of the unstable mode equal to almost 34 Hz (Figure 52). The onset of the contact dynamic instability is characterized by an exponential increase in the amplitude of oscillation. Moreover, as can be seen from the zoom of Figure 53, the vibrational response along the X and Y directions shows a phase shift of the signals of almost 90° . This outcome is consistent with the experimental results related to the mode coupling instability, where a phase shift between the vibrational signals along the tangential and normal directions to the contact has been observed.

An analogous analysis has been also carried out, through the numerical model, on the negative friction-velocity slope instability. In this case, for the contact law at the contact interface between the mass m_2 and the slider, a linearly increasing friction coefficient with a decreasing relative velocity has been imposed. Figure 54 shows the trend of the friction coefficient as a function of the relative velocity at the contact, defined as $\dot{X} - v$.

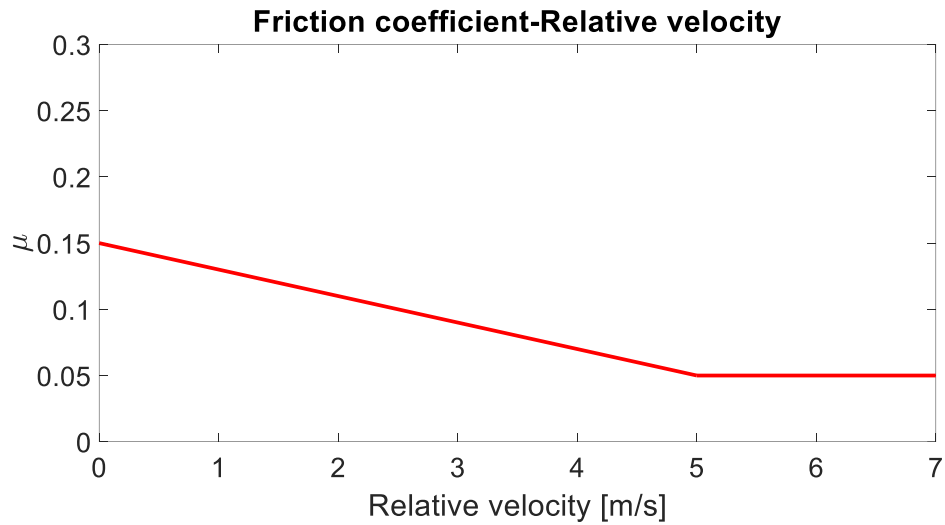


Figure 54 Friction coefficient vs relative velocity ($\dot{X} - v$), implemented at the contact interface between the mass m_2 and the sliding belt.

In this case, the friction coefficient increases from 0.05 to 0.15, while decreasing the relative velocity from 5 m/s to 0 m/s. Being the friction coefficient lower than 0.22, the occurrence of a dynamic instability can only be related to the negative friction-velocity gradient, because no mode coupling is observed (see Figure 52). The negative gradient leads to a negative apparent damping and consequently to an unstable dynamic response. The vibrational response in the X and Y directions, when the negative friction-velocity slope arises (exponential increase of the vibration amplitude), is shown in Figure 55.

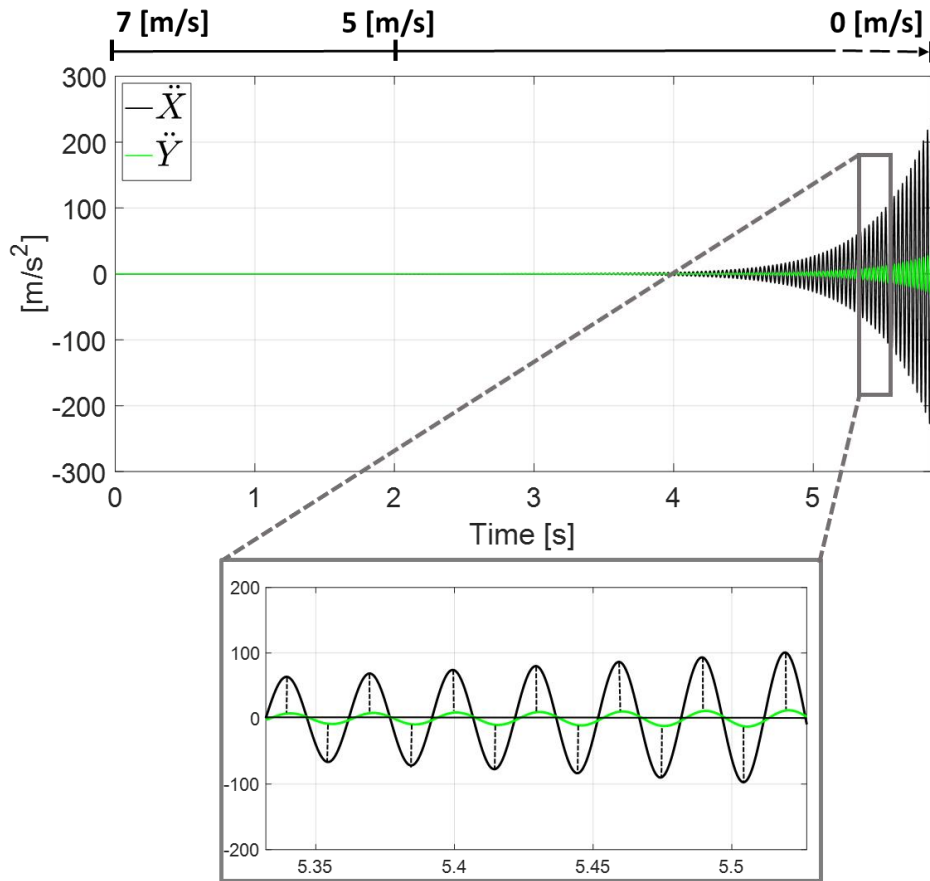


Figure 55 Onset of the negative friction-velocity slope instability: acceleration \ddot{X} and \ddot{Y} with a linearly increasing friction coefficient from 0.05 to 0.15 for a decreasing relative velocity from 5 m/s to 0 m/s.

The system is stable as long as the imposed velocity of the slider is higher than 5 m/s, being the friction coefficient constant in this range of sliding velocity. When the relative velocity decreases and becomes lower than 5 m/s, the system falls in the range of sliding velocities where the friction coefficient varies with the velocity, according to the law described in Figure 54. In this velocity range, the negative friction-velocity slope at the contact interface leads to the occurrence of the dynamic instability, characterized by an exponential increase of the amplitude of vibration. As can be seen from the zoom of Figure 55, in this case, the unstable vibrational response is characterized by acceleration components, along the tangential and normal directions to the contact, which are in phase. This result is coherent with the experimental outcomes and highlights a specific feature of the negative friction-velocity slope instability, distinguishing it from the mode coupling, which is instead characterized by a phase shift, between the normal and tangential system response, of about 90° .

So far, the dynamic instabilities have been studied taking into account only the exponential increase of the oscillation amplitude, in order to avoid non-linear contributions (sticking and

detachment at the contact) that could affect the phases of the dynamic response. With the aim of investigating the whole development of the instabilities, as well as comparing the overall dynamic response of the system in presence of different friction conditions, the numerical model has been upgraded including also the possibility to simulate stick-slip and the detachment of the mass m_2 from the sliding belt.

3.2.2.4 Lumped-parameter model with non-linear contributions (i.e. stick-slip and detachment)

The whole evolution of the dynamic instabilities has been studied by taking into account also the occurrence of non-linear phenomena occurring during braking. The model has been improved with the possibility of switching to a stick condition when the mass reaches the rigid plane speed $v = \dot{x}_2$ and $|T| \leq \mu N$. In this case, the system is reduced to only 1 degree-of-freedom in the Y direction. The equations of motion, presented in {3.2.2.1}, can be rewritten as:

$$M_{SS}\ddot{r} + C_{SS}\dot{r} + K_{SS}r = \underline{F} \quad (11)$$

Where

$$M_{SS} = \begin{bmatrix} 0 & 0 \\ 0 & m_1 \end{bmatrix} \quad (12)$$

$$C_{SS} = \begin{bmatrix} 0 & 0 \\ -c_2 \sin\theta & c_2 \end{bmatrix} \quad (13)$$

$$K_{SS} = \begin{bmatrix} 0 & 0 \\ -k_2 \sin\theta & k_2 \end{bmatrix} \quad (14)$$

$$\underline{F} = \begin{pmatrix} 0 \\ -F_{ext} \end{pmatrix} \quad (15)$$

$$\underline{r} = \begin{pmatrix} X \\ Y \end{pmatrix} \quad (16)$$

The increase of the oscillation amplitude, when the dynamic instabilities due to mode coupling or negative friction-velocity slope occur, can lead also to the detachment of the mass m_2 from the sliding belt. In particular, this condition arises when the conditions $N > 0$ and $y_2 = 0$ are no longer met. In this case, a third degree-of-freedom related to y_2 has to be considered. The model switches therefore to the following equations of motion:

$$M_D \ddot{\underline{r}} + C_D \dot{\underline{r}} + K_D \underline{r} = \underline{F} \quad (17)$$

$$M_D = \begin{bmatrix} m_1 \cos^2 \theta + m_2 & 0 & 0 \\ 0 & m_1 & 0 \\ -m_1 \cos \theta \sin \theta & 0 & m_2 \end{bmatrix} \quad (18)$$

$$C_D = \begin{bmatrix} c_1 \cos^2 \theta + c_2 \sin^2 \theta & -c_2 \sin \theta & c_2 \sin \theta \cos \theta \\ -c_2 \sin \theta & c_2 & -c_2 \cos \theta \\ (c_2 - c_1) \sin \theta \cos \theta & -c_2 \cos \theta & c_2 \cos^2 \theta \end{bmatrix} \quad (19)$$

$$K_D = \begin{bmatrix} k_1 \cos^2 \theta + k_2 \sin^2 \theta & -k_2 \sin \theta & k_2 \sin \theta \cos \theta \\ -k_2 \sin \theta & k_2 & -k_2 \cos \theta \\ (k_2 - k_1) \sin \theta \cos \theta & -k_2 \cos \theta & k_2 \cos^2 \theta \end{bmatrix} \quad (20)$$

$$\underline{F} = \begin{pmatrix} 0 \\ -F_{ext} \\ 0 \end{pmatrix} \quad (21)$$

$$\underline{r} = \begin{pmatrix} X \\ Y \\ y_2 \end{pmatrix} \quad (22)$$

The evolution of the dynamic instabilities during braking, along the tangential (X) direction to the contact, has been investigated by imposing different friction laws. This analysis has been carried out with the same parameters of the model shown in Table 10. As a result, the same mode

coupling threshold (hereafter called “*MC threshold*”) of the friction coefficient, equal to almost 0.22, has been retrieved from the CEA (see Figure 52).

Such as for the transient analysis described in {3.2.2.3}, a decreasing velocity of the slider from 7 m/s to 0 m/s and a deceleration equal to 1 m/s^2 has been used.

In Figure 56, four different friction laws, as a function of the relative velocity (left column), have been investigated. For each friction law, the acceleration \ddot{X} (in black) and the status of the contact (in blue dots) during braking are plotted (right column). When the system is in sliding condition the status of the system is set equal to 1. The occurrence of either sticking or detachment is instead identified by a status equal to 0 or 2, respectively.

The evolution of the dynamic instabilities have been analyzed in presence of the sole negative friction-velocity slope (μ increases from 0.05 to 0.15), mode coupling (μ constant and equal to 0.3) and when both of them coexist. Regarding this latter condition, simulations have been performed when μ increases either from 0.05 (below the *MC threshold*) or from 0.3 (above the *MC threshold*) up to 0.5. In all cases, the negative slope is imposed for values of the relative velocities lower than 5 m/s.

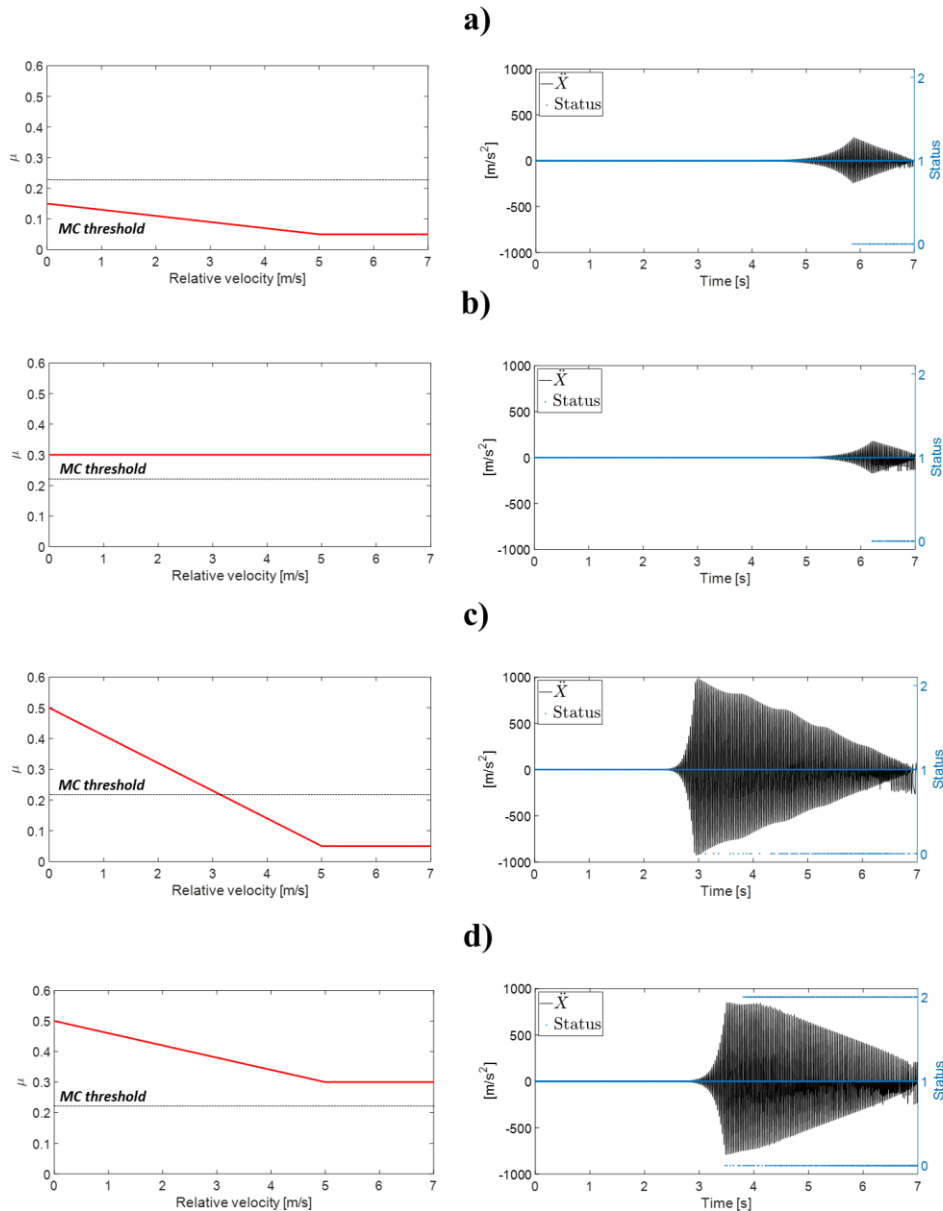


Figure 56 Comparison between different friction laws as a function of the relative velocity (left column) and the respective vibrational response of the mechanical system along the X direction (right column). Both the acceleration \ddot{X} and the status of the contact are shown. When the mass m_2 is in sliding condition the status of the system is set equal to 1. The occurrence of either sticking or detachment of the mass m_2 from the sliding belt is identified by a status equal to 0 or 2, respectively. The onset of four different dynamic instabilities is numerically reproduced: a) negative friction-velocity slope instability (μ varies from 0.05 to 0.15); b) mode coupling instability (μ constant and equal to 0.3); c) coexistence of negative friction-velocity slope and mode coupling with μ varying from 0.05 to 0.5; d) coexistence of negative friction-velocity slope and mode coupling with μ varying from 0.3 to 0.5. A MC threshold equal to 0.22 has been used for the analysis.

As can be noticed from Figure 56, when the dynamic instability arises in presence of either negative friction-velocity slope or mode coupling (Figure 56.a and Figure 56.b) the maximum vibration amplitude is significantly lower compared to the case where mode coupling and negative friction-velocity slope coexist (Figure 56.c and Figure 56.d). Such a result is consistent with the experimental outcomes presented in Chapter 2 and provides further support to the assumptions made in the previous Chapter.

In all cases shown in Figure 56, the occurrence of stick-slip can be noticed once the limit cycle is achieved. The detachment of the mass m_2 from the sliding belt occurs only in the case where both the negative slope and mode coupling coexist and the friction coefficient varies from 0.3 to 0.5 (Figure 56.d). Moreover, it can be observed that between the two cases shown in Figure 56.c and Figure 56.d, higher amplitude of vibrations are achieved when the friction coefficient varies from 0.05 up to 0.5 and leads, therefore, to a steeper negative slope compared to the case where the friction coefficient varies from 0.3 to 0.5.

Nevertheless, it should be kept in mind that the relative weight of the two kind of instabilities is strongly related to the dynamics of the frictional system. As a function of the involved system modes and the damping distribution within the system, the mode coupling and the negative friction-velocity slope phenomena could lead to completely different amplitude contributions.

3.3 Concluding remarks

The analysis of the contact dynamic instabilities, investigated here experimentally and simulated numerically, has provided meaningful information to distinguish the occurrence of the mode coupling from the negative friction-velocity slope instability.

The experimental characterization has been carried out by means of the TriboAir setup and C/C samples machined from a MAT1 disc. *Sliding heating* tests, with a maximum temperature of 300 °C, have been performed at variable (from 20 to 0 mm/s) and constant (15 and 3 mm/s) velocity profiles.

The onset of different dynamic instabilities at 300 °C has been identified. In particular, the *sliding heating* test at variable imposed velocity (from 20 to 0 mm/s) has shown the occurrence of a mode coupling instability at higher velocities (almost 15 mm/s), where the friction coefficient is almost constant, and a negative friction-velocity slope instability toward the end of braking, where the friction coefficient increases while decreasing the sliding velocity. By studying the main features of the two different dynamic instabilities, it has been observed a significant difference in the vibrational response along the tangential (X) and normal (Y) directions to the contact. While for the mode coupling instability the vibrational signals along the X and Y directions are almost 90° out of phase, for the negative friction-velocity slope instability the signals are in phase. Different frequencies of the unstable modes triggered by either mode coupling or negative friction-velocity slope have been identified. Specifically, 14.6 kHz for the former and 43 kHz for the latter.

Constant velocity tests are in agreement with the variable velocity test. The *sliding heating* test carried out at a higher imposed velocity (15 mm/s), at 300 °C, has shown the onset of a dynamic instability characterized by a frequency of almost 14.6 kHz and a phase shift of almost 90° between the vibrational signals along the X and Y directions (i.e. mode coupling instability). On the other hand, the *sliding heating* test carried out at lower imposed velocity (3 mm/s), at 300

°C, has shown the occurrence of a dynamic instability characterized by a frequency of almost 43 kHz and vibrational signals in phase between the X and Y directions (i.e. negative friction-velocity slope instability).

The unstable modes related to the mode coupling and the negative slope have been investigated numerically through a finite element analysis. Consistently with the experimental outcomes, both the modes at almost 14.6 kHz and 43 kHz have been numerically identified.

The main features of the two different unstable friction-induced vibrations have been studied also by means of a lumped-parameter numerical model consisting of two masses, one of which in frictional contact with a sliding belt. A complex eigenvalue analysis, carried out as a function of the friction coefficient, has allowed decoupling the friction conditions for the negative friction-velocity slope instability from those for the mode coupling instabilities, in order to simulate the two phenomena separately. The obtained results are consistent with the experimental outcomes. The vibrational signals along the tangential and normal directions to the contact are in phase in presence of the sole negative friction-velocity slope. On the other hand, a phase shift of almost 90° is observed in presence of mode coupling. Moreover, it has been shown that when both the mode coupling and the negative slope coexist, higher amplitude of vibrations are reached, compared to the sole mode coupling or negative slope instability.

On the one hand, the overall outcomes presented in this Chapter allows characterizing more in detail the tribological and dynamic behavior of C/C composite materials. On the other hand, by investigating the phase shift between tangential and normal accelerations to the contact, a useful means has been proposed in order to distinguish the nature of the unstable friction-induced vibrations, which is of main interest for several industrial applications. In fact, whenever frictional contact occurs, different contact instabilities can arise and identifying the origin of the encountered unstable vibrations can help in determining solutions for their suppression.

As also shown in this Chapter, the presence of the steep negative friction-velocity slope at high friction regimes, leading to the coexistence of mode coupling and negative slope instabilities, underlies the occurrence of the worst vibrational scenario, as it results in severe unstable friction-induced vibrations. As shown in Chapter 2, this phenomenon has been observed only for the MAT1, for temperature higher than almost 300-400 °C.

Being the presence of Cont1 and Cont2 on the contact surface of the MAT1 the difference between all the tested specimens, the analysis has been focused on such contaminants. In particular, oxygen in the areas of the friction surface where Cont1 and Cont2 have been detected by EDX (see {2.1.2}) suggests the presence of oxides [162]. Therefore, in the following, the material response of C/C composites has been investigated in presence of different coatings made up of Cont1 and Cont2 oxides, hereafter referred to as Ox and Oy respectively.

Chapter 4

Experimental analysis of the C/C material response with different third bodies

In Chapter 2, it has been observed that the combined presence of Cont1 and Cont2 on the frictional interface of C/C specimens affects significantly their tribological and dynamic response, for temperatures higher than almost 300-400 °C. Compared to C/C samples without such contaminants, the MAT1 specimens, characterized by both Cont1 and Cont2 on the friction surface, have shown the occurrence of a strong negative friction-velocity slope and severe unstable friction-induced vibrations. In order to investigate in detail the role of these specific contaminants, taking part in the rheology of the contact, C/C specimens machined from C/C brake discs have been painted on the contact surface with specific quantities of Ox and Oy colloidal suspensions. After that, the samples have been tested on the TriboAir setup, under controlled boundary conditions. In the following, a description of the specimens used for the analysis and the experimental protocol is first provided. Then, the main outcomes are discussed in detail for all the different tested samples. A SEM/EDX analysis carried out on the frictional surfaces of the painted samples, after being tested on TriboAir, is presented as well.

4.1 Materials and methods

The frictional surfaces of the C/C specimens adopted for the analysis have been coated with different paints made up of Ox and/or Oy. Some coatings have been realized with either the Ox colloidal suspension or the Oy colloidal suspension alone. Some other coatings have been realized with weighted mixtures of Ox and Oy. In this section, the samples coated with only Ox or Oy are described. After that, a description of the samples painted with the Ox/Oy mixtures is provided as well. Lastly, the experimental protocol used for testing all the coated samples on TriboAir setup is presented.

4.1.1 C/C material with either Ox or Oy coatings

The C/C specimens used for the analysis have been machined from new C/C brake discs, without contaminants on the friction surface. Two pairs of C/C specimens have been painted with Ox and other two pairs have been painted with Oy. The coatings have been obtained from colloidal suspensions of either Ox or Oy.

An example of C/C specimens coated with Ox, before being tested on TriboAir, is shown in Figure 57. In the insets, the frictional surfaces of both samples are shown.

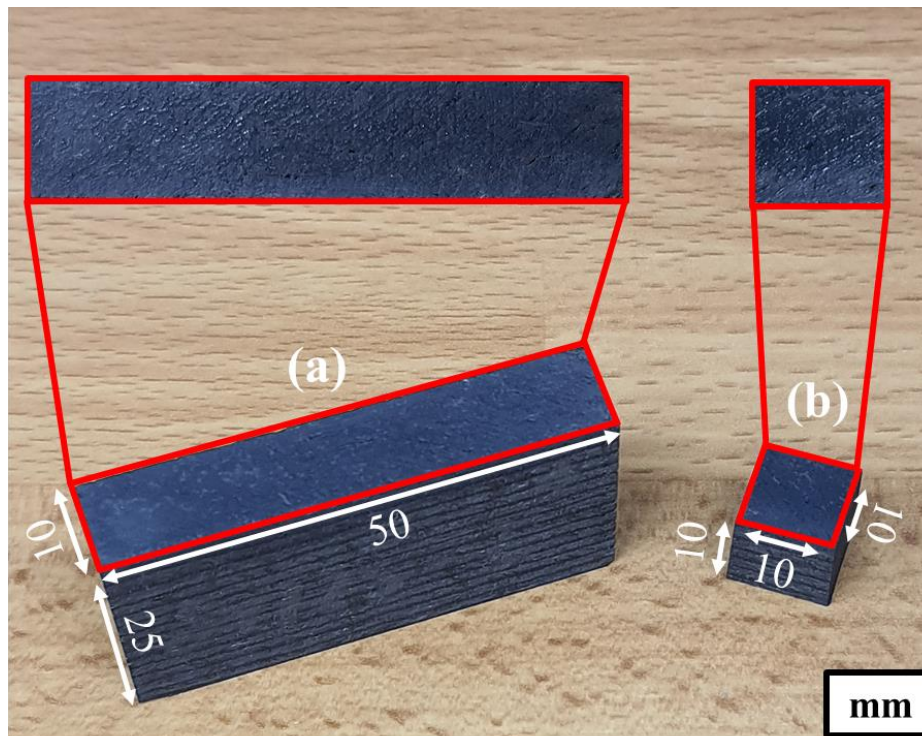


Figure 57 Example of C/C specimens coated with colloidal suspension of Ox. a) Sample clamped on the moving base (10x50x25 mm) b) Sample clamped on the upper part of the setup (10x10x10 mm).

The geometry of the samples has been maintained such as the one shown in Figure 18. Each pair of specimens consists of a rectangular prism of 10x50x25 mm (a), clamped on the moving base of the test-bench and a cube of 10 mm side, clamped on the upper part of the setup (b) and kept fixed throughout the tests.

A different mass per unit of area (mg/cm^2) of paint is deposited onto the contact surfaces (either $50 \times 10 \text{ mm}^2$ or $10 \times 10 \text{ mm}^2$) of the C/C specimens. Table 11 shows the different amount of Cont1 and Cont2 on each sample.

<i>Ox</i>		
Specimens	Contact surface [mm ²]	Mass per unit of area of Cont1 [mg/cm ²]
Ox1	50x10	1.04
Ox2	10x10	1.04
Ox3	50x10	0.12
Ox4	10x10	0.30
<i>Oy</i>		
Specimens	Contact surface [mm ²]	Mass per unit of area of Cont2 [mg/cm ²]
Oy1	50x10	2.50
Oy2	10x10	2.40
Oy3	50x10	2.10
Oy4	10x10	2.10

Table 11 Mass per unit of area (mg/cm²) of Cont1 and Cont2 deposited on the contact surfaces of the samples coated with either Ox or Oy.

The analysis has been focused on the C/C pairs with the highest amount of Ox (Ox1 and Ox2) and Oy (Oy1 and Oy2). As shown in Annex IV, in order to verify the repeatability and robustness of the results, complementary tests have been carried out also with the C/C pairs characterized by a lower amount of Ox (Ox3 and Ox4) and Oy (Oy3 and Oy4).

In addition to the above described specimens of C/C materials, other samples of C/C composite have been coated with paints characterized by a mixture of Ox and Oy. These samples are described in the following.

4.1.2 C/C material coated with Ox/Oy mixtures

In order to investigate the combined presence of Cont1 and Cont2 on the frictional surface of C/C composites, some specimens of C/C material, machined from new discs, have been painted with Ox/Oy mixtures characterized by different percentage of the oxides. In particular, three mixtures have been used:

- **80x20y**. Coating characterized by 80% of Ox and 20% of Oy;
- **50x50y**. Coating characterized by 50% of Ox and 50% of Oy;
- **20x80y**. Coating characterized by 20% of Ox and 80% of Oy.

Table 12 shows the total mass per unit of area (mg/cm²) of paint deposited on the frictional surface of the samples. The theoretical mass per unit of area (mg/cm²) of Ox and Oy, depending on the mixture, has been computed as well. Each sample is named as a function of the mixture. As an example, the samples coated with the 80x20y paint are called 80x20y-1 and 80x20y-2, where the former is the rectangular prism with contact surface 10x50 mm² while the latter is the cube with contact surface 10x10 mm².

80x20y						
Specimens	Contact surface [mm²]	Total mass per unit of area [mg/cm²]	Ox%	Oy%	Ox [mg/cm²]	Oy [mg/cm²]
80x20y-1	50x10	1.12	80%	20%	0.90	0.22
80x20y-2	10x10	1.56	80%	20%	1.25	0.31
50x50y						
Specimens	Contact surface [mm²]	Total mass per unit of area [mg/cm²]	Ox%	Oy%	Ox [mg/cm²]	Oy [mg/cm²]
50x50y-1	50x10	2.18	50%	50%	1.09	1.09
50x50y-2	10x10	2.16	50%	50%	1.08	1.08
20x80y						
Specimens	Contact surface [mm²]	Total mass per unit of area [mg/cm²]	Ox%	Oy%	Ox [mg/cm²]	Oy [mg/cm²]
20x80y-1	50x10	1.60	20%	80%	0.32	1.28
20x80y-2	10x10	1.56	20%	80%	0.31	1.25

Table 12 Total mass per unit of area (mg/cm²) of Ox/Oy mixtures deposited on the frictional surfaces of the tested samples. According to the composition of the mixtures (80% Ox-20% Oy, 50% Ox-50% Oy, 20% Ox-80% Oy), the theoretical mass per unit of area of Ox and Oy on each sample is shown as well.

After having applied the coating, a SEM/EDX analysis has been carried out for each sample in order to verify the proper distribution of the mixture all over the frictional surface. As an example, Figure 58 shows the pictures taken by SEM (Z-contrast) at the left, in the middle and at the right of the rectangular contact surfaces of the 50x10x25mm samples. Each row of Figure 58 shows a sequence of images taken through backscattered electrons, at the scale of 1 mm for each sample. From the top to the bottom, the sequences of pictures are related to the 80x20y-1, 50x50y-1 and 20x80y-1 samples.

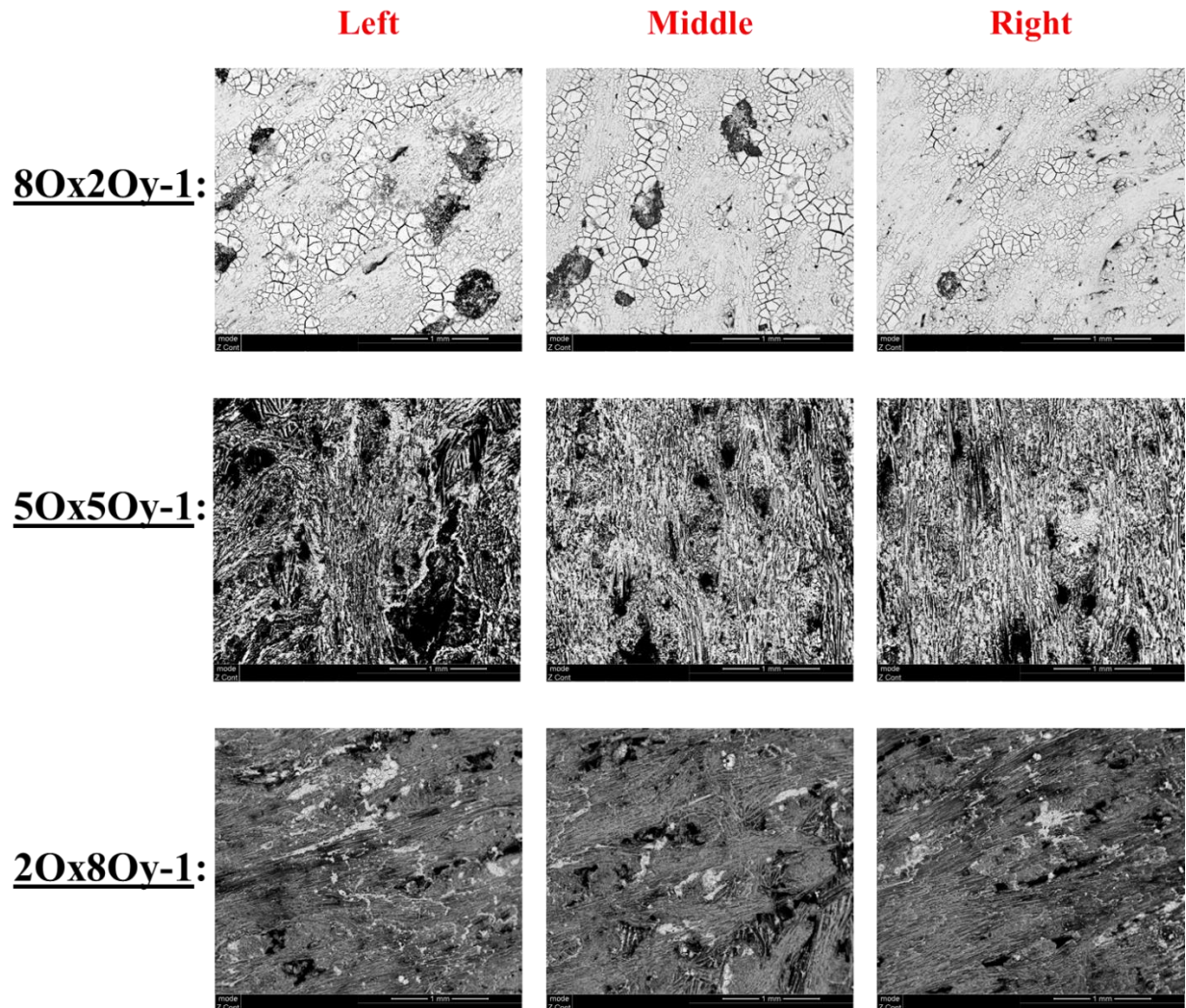


Figure 58 SEM pictures (Z-contrast) of the 80x20y-1, 50x50y-1 and 20x80y-1 specimens taken through backscattered electrons, at the scale of 1 mm. For each sample, the photos are taken at the left, in the middle and at the right of the contact surface of the samples. The whiter areas indicate a higher amount of Cont1, the grey areas indicate a higher amount of Cont2 while the black areas are the carbon substratum.

By using backscattered electron imaging it is possible to identify the areas where a higher amount of either Ox or Oy have been deposited. In particular, the heavier the element, the brighter it appears. In this case, white areas highlight the presence of a higher amount of Cont1, while grey areas indicate the presence of a higher amount of Cont2. The C substratum appears in black. This approach has been preliminarily verified by EDX measurements of the different areas.

In Figure 58, all the three pictures of the 80x20y-1 sample surface are characterized by a significant amount of Ox (white areas), which is greatly predominant with respect to Oy (grey areas). Conversely, the 20x80y-1 sample shows predominant Oy grey areas compared to the Ox

white ones. An almost equal distribution of grey and white areas is instead observed in the 5Ox5Oy-1 pictures, characterized by 50% of Ox and 50% of Oy. A proper and homogeneous distribution of the mixtures, in all the observed areas of the samples, can be therefore assumed.

4.1.3 Experimental protocol

Both the samples coated with only Ox or Oy (described in {4.1.1}) and the samples coated with the Ox/Oy mixtures (described in {4.1.2}), have been tested with the same experimental protocol presented in Table 13.

DAY ONE		DAY TWO	
<i>Sliding Heating</i>		<i>Sliding Heating</i>	
<i>V=const=20 mm/s</i>		<i>V=20→0 mm/s</i>	
1	RUN-IN		
2	100°C	1	100°C
3	300°C	2	300°C
4	500°C	3	500°C

Table 13 Protocol used for the experimental tests of the C/C specimens coated with either Ox or Oy and Ox/Oy mixtures. The first day of the protocol is devoted to constant imposed velocity tests (20 mm/s), while the second day focuses on variable imposed velocity tests (20→0 mm/s). Tests at different temperatures are carried out at the maximum temperatures of 100, 300 and 500 °C.

The sequence of tests carried out in the first day of protocol consists of 15 minutes of run-in, performed with a constant velocity profile characterized by an imposed constant speed of 20 mm/s (see Figure 20.b). After the run-in, sliding heating tests (see Figure 21.a) at constant velocity (20 mm/s) and at maximum temperatures of 100, 300 and 500 °C are performed. The second day of the protocol consists of the same sequence of tests of the first day (except for the run-in), but with a variable velocity profile characterized by an imposed speed varying from 20 to 0 mm/s (see Figure 20.a) for each cycle of the test.

As can be noticed, the protocol is similar to the one shown in {2.1.3, Table 4}. However, in this case, only the most significant tests (i.e. at 100, 300 and 500 °C) for characterizing the frictional and vibrational response of the tested samples have been carried out.

The analysis of the outputs has been performed as described in {2.1.4}.

All the specimens coated with Ox and/or Oy have been tested according to the above described protocol. The main outcomes obtained from the analysis of data retrieved from the experimental campaigns are shown in the next section.

4.2 Main experimental outcomes

The rheological contribution given by the presence of Ox or Oy on the frictional interface has been here investigated by performing two experimental campaigns on TriboAir. The first one has been devoted to the analysis of the C/C samples coated with only Ox or Oy. The second one focuses on different combinations of Ox and Oy on the contact surface. The main results obtained at variable (20 to 0 mm/s) and constant (20 mm/s) sliding velocities and at different temperature conditions (100, 300, 500 °C) are discussed in the following. Particular attention is addressed to temperatures higher than 400 °C, where the experimental tests carried out on samples of MAT1, contaminated with both Cont1 and Cont2, have shown a significant different frictional and vibrational response of the C/C composite, compared to the other tested samples.

First, the main outcomes obtained from the tests carried out on C/C specimens coated with either Ox or Oy are discussed. Then, the results obtained from the experimental campaign performed with C/C samples coated with Ox/Oy mixtures are shown. A SEM/EDX analysis on the friction surface of the 8Ox2Oy-1 and 2Ox8Oy-1 specimens is shown as well.

4.2.1 Third body with either Ox or Oy contaminants

The experimental campaigns performed with C/C samples coated with Ox and Oy have been focused on understanding the role played by such contaminants into the tribological response of C/C materials. The onset of different vibrational phenomena arising when only Ox or Oy take part in the rheology of the contact have been investigated as well. In the following, the main results obtained from variable velocity tests (*day two* of the protocol described in Table 13) are first discussed in order to show the frictional and dynamical response of the samples in braking conditions. Then, the outcomes obtained from constant velocity tests are presented as well (*day one* of the protocol described in Table 13).

4.2.1.1 Discussion on variable velocity tests

In order to understand the C/C material response in presence of either Ox or Oy during braking, a comparison between tests performed at variable imposed velocity has been carried out. Major attention has been paid for temperatures higher than 300-400 °C, where the different contaminants, taking part in the rheology of the contact, affect significantly the tribological and dynamical behaviour of the C/C material (see Chapter 2). In this respect, Figure 59 shows the evolution of the DFC and SFC, up to 500 °C and at variable imposed velocity (20 to 0 mm/s), of the C/C specimen pairs coated with Ox (left) and Oy (right). The results are related to the experimental tests carried out with the specimens named Ox1-Ox2 and Oy1-Oy2, respectively.

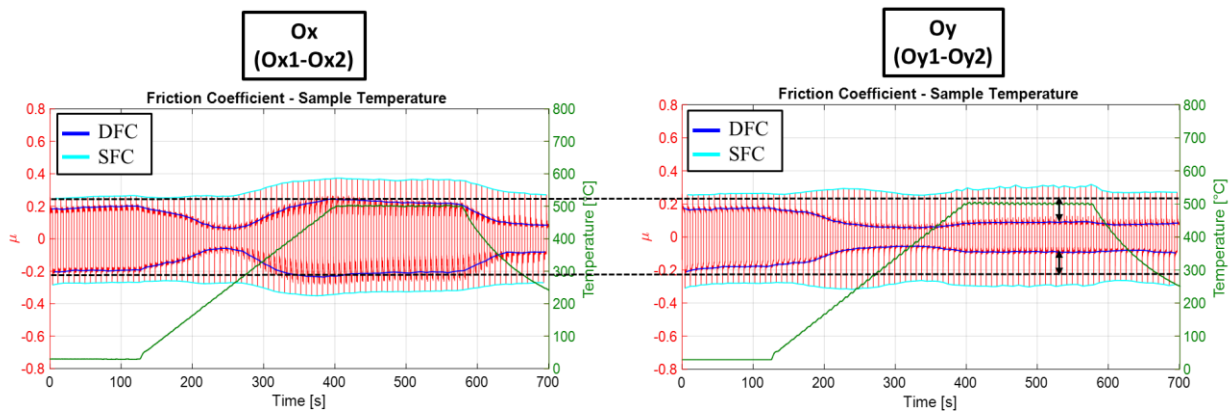


Figure 59 Comparison between the frictional responses of the Ox1-Ox2 (left) and Oy1-Oy2 (right), during sliding heating tests carried out at variable sliding velocity (20→0 mm/s) and at a maximum temperature of 500 °C. In red the friction coefficient, in blue the DFC, in cyan the SFC and in green the temperature.

Consistently with the C/C frictional response described in Chapter 2, the DFC decreases up to 200-300 °C and then increases for temperature higher than 300-400 °C for both the C/C samples coated with Ox and Oy. However, while for the C/C material with Ox the DFC at 500 °C becomes slightly higher than the DFC at room temperature, for the C/C material with Oy the increase of DFC, for temperatures higher than 400 °C, is barely noticeable and leads to values of the DFC considerably lower than the room temperature ones. In both cases, the SFC shows only slight variations at all temperature conditions (a slight increase can be noticed at temperatures higher than 300 °C, for the C/C material with Ox).

It should be remarked that, being the samples machined from a new C/C disc, the increase of DFC for temperatures higher than 400 °C is, for both the C/C samples with Ox and Oy, significantly lower than the one obtainable with used C/C specimens, as also shown in {2.2.3}. However, by using new samples for the analysis it is possible to investigate the effective role of a third body contaminated with Ox and Oy, regardless of the specimen status.

The significant different behavior of the DFC observed for temperatures higher than 300 °C, in presence of Ox and Oy, leads also to a different vibrational response. As an example, Figure 60 shows the comparison between the friction coefficient and the accelerometer signal of two braking strokes taken from Figure 59, at 500 °C, and related to the C/C specimens coated with Ox (left) and Oy (right).

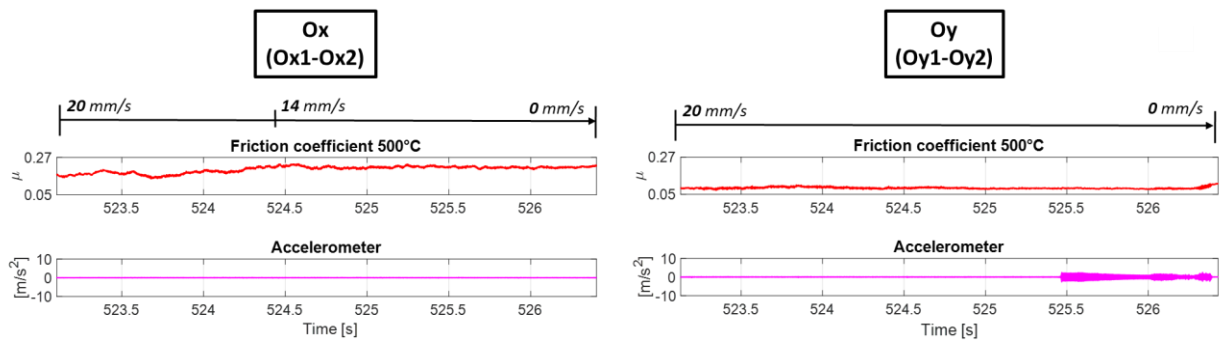
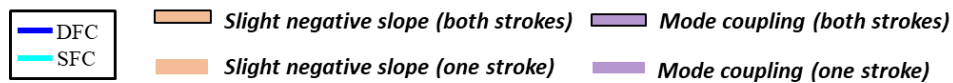


Figure 60. Comparison between the friction coefficient and the accelerometer signal of two single strokes taken at 500 °C from the sliding heating tests of the Ox1-Ox2 (left) and Oy1-Oy2 (right), shown in Figure 59.

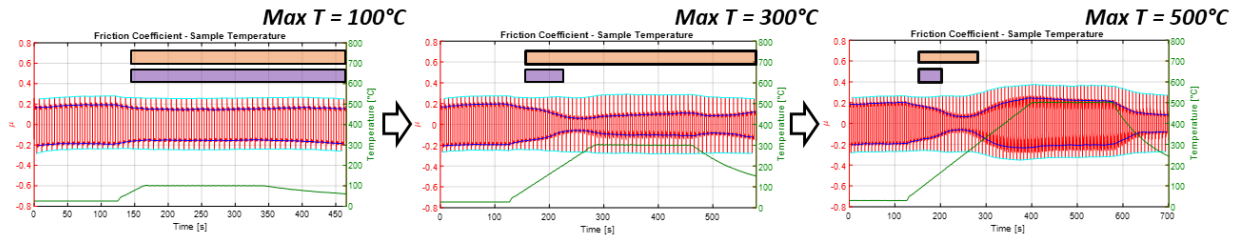
As can be noticed from Figure 60, the behavior of the friction coefficient and the vibrational phenomena observed during braking differ significantly between the two pairs. While for the C/C material with Ox the friction coefficient toward the end of braking remains almost constant and no dynamic instabilities occur, the C/C material with Oy shows a considerably lower DFC, which increases rapidly at the very end of the stroke. Such phenomenon leads to a negative friction-velocity slope and the occurrence of dynamic instabilities.

The presence of Oy, within the third body at the interface, seems to reduce the capability of the carbon dangling bonds to recombine between antagonist contact surfaces and lead, therefore, to a lower friction during the relative sliding. On the contrary, when no sliding occurs, the SFC is not affected by the presence of these contaminants. This observation leads to the assumption that a main role is played by the contribution of the Oy particles in the rheology of the third body (modifying the response only during the sliding), which consequently modifies the physiochemical reactivity at the interface reducing the overall dynamic friction. The particles of Ox seems to bring a completely different contribution, by increasing the dynamic friction and thus promoting the increase of the interface reactivity during the relative motion. It can be noticed that higher values of the friction coefficient of the C/C samples with Ox are reached only for sliding velocities lower than almost 14 mm/s. It can be hypothesized that at lower sliding velocities (lower than 14 mm/s in this case) the dangling bonds between the antagonist surfaces have enough time to react. This phenomenon leads to higher friction.

Further information concerning the frictional and vibrational response of the samples coated with Ox and Oy can be achieved by investigating all the experimental tests at variable imposed velocity, provided for the protocol. For this purpose, Figure 61 shows the behavior of the friction coefficient of the Ox1-Ox2 and Oy1-Oy2 pairs of C/C samples, in *sliding heating* tests at different maximum temperatures (100, 300 and 500 °C) and variable imposed velocity (20 to 0 mm/s). The first row of Figure 61 shows the sequence of tests of C/C samples with Ox, carried out according to the *day two* of the protocol described in Table 13. The second row is related to the same sequence of tests performed on the C/C samples with Oy. For each test, colored bars indicate the onset of dynamic instabilities. Such as in Figure 31, peach-colored bars denote the presence of dynamic instabilities in presence of a slight negative friction-velocity slope. Violet bars indicate the occurrence of dynamic instabilities with a constant friction coefficient (mode coupling). When the bars are bordered in black, the specific phenomenon is observed on both back-and-forth strokes. Otherwise, the phenomenon is observed only on single strokes.



➤ Ox (Ox1-Ox2)



➤ Oy (Oy1-Oy2)

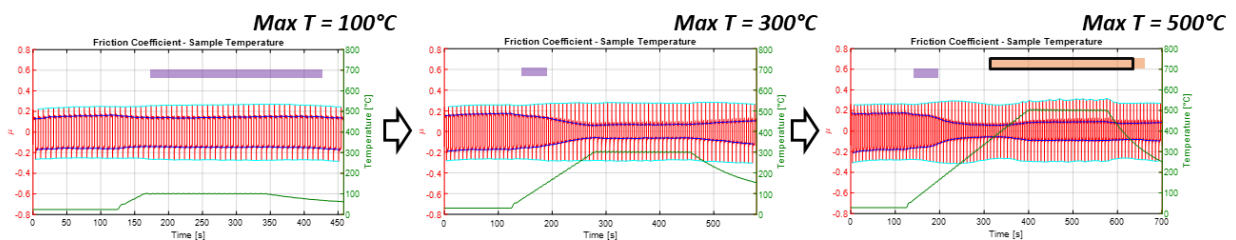


Figure 61 Sliding heating tests carried out at variable imposed velocity (20→0 mm/s) and at maximum temperatures of 100, 300 and 500 °C. The first row shows the sequence of tests carried out for the Ox1-Ox2 sample pair. The second row shows the same sequence of tests but for the Oy1-Oy2 sample pair. The bars denote the occurrence of dynamic instabilities in presence of a slight negative friction-velocity slope (peach-colored bars) and in presence of a constant friction coefficient (violet bars). If the bars are bordered in black the phenomenon is observed on both back-and-forth strokes, otherwise it is observed only on single strokes. The friction coefficient is in red, the DFC is in blue, the SFC is in cyan and the temperature is in green.

From Figure 61, it can be noticed that significant differences in terms of DFC and SFC, between the C/C specimens coated with Ox and Oy, arise only for temperatures higher than almost 300 °C (as also shown in Figure 59). For lower temperatures, the *sliding heating* tests carried out at 300 °C show a very similar frictional response, characterized by a significant decrease of the DFC when increasing the temperature. Analogously, a similar frictional response between the sample pairs is observed also in *sliding heating* tests with a maximum temperature of 100 °C, where a slight decrease of the DFC is observed. The SFC remains instead almost constant (about 0.3 on average) at all temperatures and for both the C/C specimens with Ox and Oy.

The significant evolution of the DFC, as a function of the temperatures and the sample coatings, highlights the role played by the rheology in presence of a third body characterized by the presence of contaminants.

The onset of dynamic instabilities for the C/C material with Ox is observed up to 300 °C, where the difference between the SFC and the DFC seems to favor the occurrence of a slight negative friction-velocity slope, leading to unstable friction-induced vibrations. The presence of dynamic

instabilities occurring also at a constant friction coefficient (mode coupling) is observed at 100 °C and up to 200 °C.

On the other hand, for the C/C material with Oy, the presence of a negative friction-velocity slope able to trigger the dynamic instability is observed only for temperature higher than 300 °C.

At 100 °C, dynamic instabilities with a constant friction coefficient are detected as well.

Additional tests on C/C specimens painted with a lower amount of Ox and Oy have shown consistent results with those described above. A comparison between the *sliding heating* tests carried out with the Ox3-Ox4 and Oy3-Oy4 pairs, at 500 °C and variable imposed velocity, is shown in the Annex IV.

The main outcomes described in this section are summarized in Table 14.

	C/C + Ox	C/C + Oy
T=RT	SFC≈0.25 DFC≈0.2	
RT < T < ≈300 °C	Constant SFC (≈0.25) and decreasing DFC (<≈0.1)	
	Slight negative friction-velocity slope instability (when DFC << SFC)	Negative friction-velocity slope not steep enough to trigger dynamic instability
T > ≈300 °C	DFC increases (but always DFC < SFC)	
	Higher DFC at higher velocities	Lower DFC at higher velocities
	Negative friction-velocity slope prevented ↓ No dynamic instabilities	Slight negative friction-velocity slope instability

Table 14 Synthesis of the frictional and vibration al response of C/C specimens coated with either Ox or Oy, at different temperature conditions.

The behavior of the DFC and SFC in presence of Ox and Oy has been studied also at constant sliding velocity. The main results are shown in the next section.

4.2.1.2 Discussion on constant velocity tests

According to the protocol described in Table 13, *sliding heating* tests at constant imposed velocity (20 mm/s) have been carried out for both the C/C materials coated with Ox and Oy. Such as for the variable velocity tests, particular attention has been given to temperatures higher than 400 °C. In this respect, Figure 62 shows a comparison between *sliding heating* tests of C/C specimens with Ox (Ox1-Ox2) and Oy (Oy1-Oy2) carried out at constant imposed velocity and at a maximum temperature of 500 °C. In the insets, the friction coefficient and the accelerometer signal of single strokes taken at 500 °C, for both the tested C/C sample pairs, are shown as well.

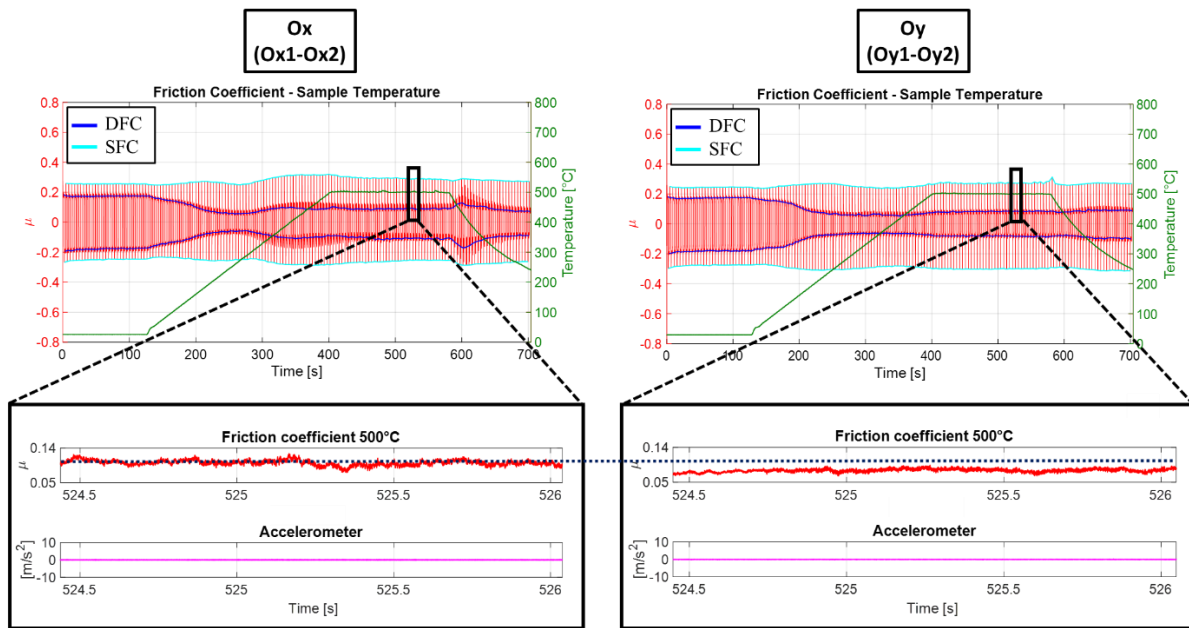
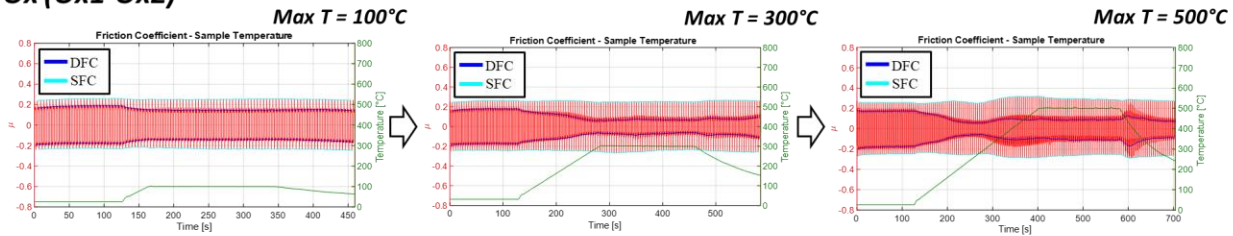


Figure 62 Comparison between the frictional responses of Ox1-Ox2 (left) and Oy1-Oy2 (right), during sliding heating tests carried out at constant sliding velocity (20 mm/s) and at a maximum temperature of 500 °C. In red the friction coefficient, in blue the DFC, in cyan the SFC and in green the temperature. In the insets, a comparison between the friction coefficient and the accelerometer signal of two single strokes, taken at 500 °C, of the Ox1-Ox2 (left) and Oy1-Oy2 (right) sample pairs.

As shown in Figure 62, the SFC remains almost constant for both the C/C materials with Ox and Oy, at all temperature conditions. Consistently with the variable imposed velocity tests (Figure 59), the DFC is characterized by a decrease up to about 200 °C. For temperatures higher than 300 °C a small increase of DFC is observed for both the C/C materials coated with Ox and Oy. As also shown in the insets of Figure 62, a higher dynamic friction coefficient can be noticed for the C/C samples with Ox, compared to the C/C samples with Oy. The higher value of the DFC at 500 °C, in presence of Ox, is consistent with the outcomes presented in the previous section {4.2.1.1}. Moreover, it can be observed that no dynamic instabilities occur at 500 °C in both cases. This outcome is in agreement with the hypothesis of a dynamic instability due to the negative friction-velocity slope (Figure 60) observed for the C/C material with Oy. It can be noticed that the increase of the DFC in presence of Ox, for temperatures higher than 300 °C, is smaller than the one observed in the variable velocity test carried out at the maximum temperature of 500 °C (Figure 59 and Figure 60). This result is consistent with the behavior of the friction coefficient shown in Figure 60, where higher values of the dynamic friction coefficient are achieved for sliding velocities lower than almost 14 mm/s. In this case, being the constant imposed velocity equal to 20 mm/s, lower values of the DFC are observed at 500 °C. An overall comparison of all the *sliding heating* tests at constant imposed velocity, for the Ox1-Ox2 and Oy1-Oy2 pairs is shown in Figure 63. The first row of Figure 63 shows the sequence of tests of C/C samples with Ox, carried out according to the *day one* of the protocol described in Table 13. The second row shows the same sequence of tests, but for the C/C samples with Oy.

➤ Ox (Ox1-Ox2)



➤ Oy (Oy1-Oy2)

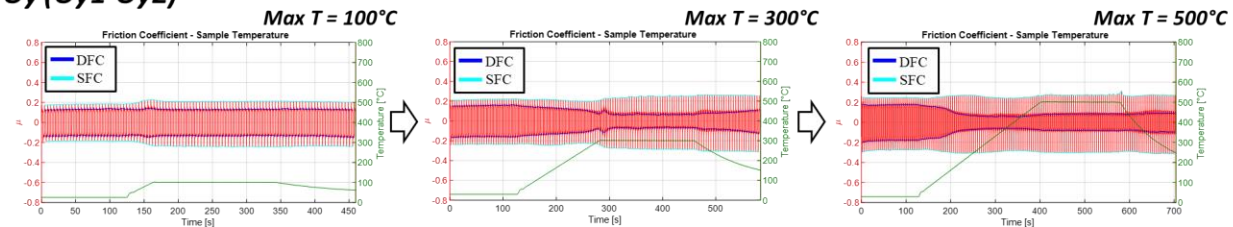


Figure 63 Sliding heating tests carried out at constant imposed velocity (20 mm/s) and at maximum temperatures of 100, 300 and 500 °C. The first row shows the sequence of tests carried out for the Ox1-Ox2 sample pair. The second row shows the same sequence of tests but for the Oy1-Oy2 sample pair. The friction coefficient is in red, the DFC is in blue, the SFC is in cyan and the temperature is in green.

The frictional response of the tested samples in *sliding heating* tests carried out at constant imposed velocity is similar to the one obtained in the variable imposed velocity tests. The DFC decreases for both the Ox1-Ox2 and Oy1-Oy2 pairs, up to almost 300 °C. For higher temperatures, the behavior of the friction coefficient is the one already shown and described in Figure 62. It can be noticed that the SFC remains almost constant in all tests and at all temperature conditions, with a slight increase after about 300 °C.

After having investigated separately the role of Ox and Oy on the tribological and dynamical behavior of C/C specimens in frictional contact, further studies have been carried out in order to understand how the simultaneous presence of Ox and Oy in the third body of the contact affects the material behavior. New C/C specimens coated with the Ox/Oy mixtures have been tested with the protocol described in Table 13. The main outcomes obtained from the experimental campaign carried out with such C/C specimens are discussed in the following.

4.2.2 Third body with Ox/Oy mixtures

As shown in the previous section, the presence of either Ox or Oy in the third body of the contact leads to a different tribological behaviour of the C/C composites. For temperatures higher than almost 400 °C, the evolution of the DFC of the tested samples differs as a function of the Ox or Oy contaminants. Specifically, while the presence of Ox seems to favor the increase of the DFC, preventing the occurrence of the negative friction-velocity slope, the presence of Oy seems to be

responsible for a low DFC favoring the negative friction-velocity slope toward the end of braking. The combined effect of both Ox and Oy is here studied in order to understand how the co-presence of both the contaminants can affect the frictional response of the C/C materials and, in turn, the occurrence of unstable friction-induced vibrations. In the following, a comparison between the main results obtained from the tests carried out with different Ox/Oy mixtures is presented. First, data retrieved from the variable imposed velocity tests are discussed, with particular attention to the temperatures higher than 400 °C. Then, constant velocity tests are discussed as well.

4.2.2.1 Discussion on variable velocity tests

With a view to understanding how the frictional and vibrational response of the tested samples is affected by the co-presence of Ox and Oy at high temperature conditions, a first comparison is carried out between all the *sliding heating* tests performed at a maximum temperature of 500 °C and variable imposed velocity (20 to 0 mm/s). In this respect, Figure 64 shows the comparison of the frictional response of the specimens coated with the mixture 8Ox2Oy (left), 5Ox5Oy (center) and 2Ox8Oy (right).

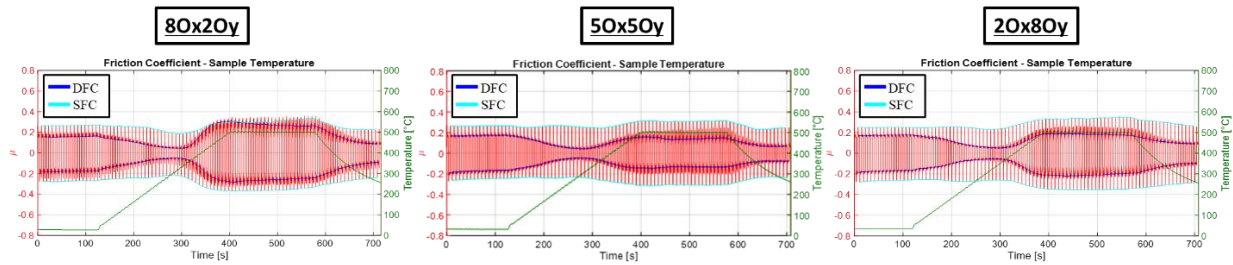


Figure 64 Comparison between the frictional responses of the specimens coated with 8Ox2Oy (left), 5Ox5Oy (center) and 2Ox8Oy (right), during sliding heating tests carried out at variable imposed velocity (20→0 mm/s) and at a maximum temperature of 500 °C. In red the friction coefficient, in blue the DFC, in cyan the SFC and in green the temperature.

As can be seen from Figure 64, up to almost 300 °C the behavior of the DFC and SFC is similar in all tested samples and consistent with the results shown in {4.2.1}. Specifically, the DFC decreases up to almost 200-300 °C while the SFC remains almost constant.

For higher temperatures, namely higher than almost 300-400 °C, a different frictional response can be observed between the tested samples. It can be noticed that in such a range of temperature, the specimens coated with 8Ox2Oy show a higher increase of the DFC compared to the specimens with 5Ox5Oy and 2Ox8Oy. It can be also observed that the difference between the SFC and the DFC is lower for the samples with 8Ox2Oy. Being the amount of Ox considerably higher than that of the Oy in the 8Ox2Oy paint, a predominant effect of the Ox seems to be responsible for the higher values of the DFC at 500 °C. More detailed information can be achieved by investigating both the friction coefficient and the accelerometer signal in single strokes taken at 500 °C from the three *sliding heating* tests presented in Figure 64. Such a comparison is shown in Figure 65.

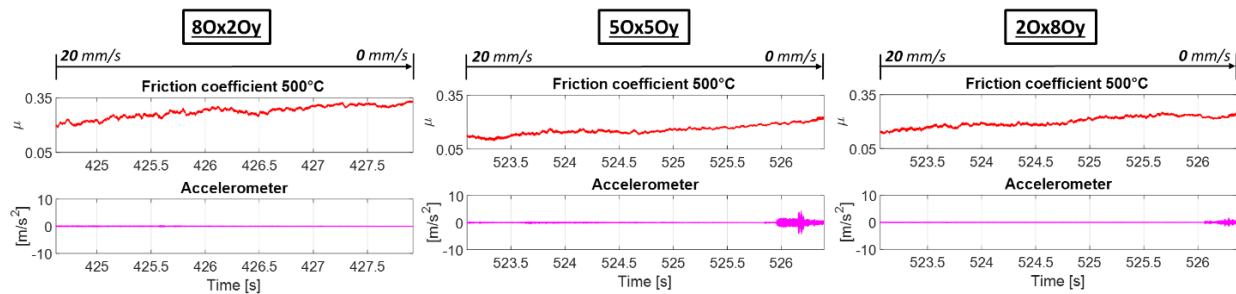


Figure 65 Comparison between the friction coefficient and the accelerometer signal of single strokes taken at 500 °C from the sliding heating tests of the specimens coated with 8Ox2Oy (left), 5Ox5Oy (center) and 2Ox8Oy (right), shown in Figure 64.

As can be seen from Figure 65, all single strokes taken at 500 °C show an increase of friction coefficient during braking. The presence of a negative friction-velocity slope is consistent with the friction coefficient behavior observed for temperatures higher than 400 °C for the MAT1 (see {2.2.1}). The presence of both Cont1 and Cont2 seems to be responsible for the occurrence of this phenomenon. In fact, as it has been shown in {4.2.1}, while the presence of Oy lowers the DFC at high velocities, Ox particles lead instead to higher values of the DFC. The simultaneous presence of both contaminants results in a progressive increase of the friction coefficient during braking. This phenomenon can lead to the occurrence of a negative friction-velocity slope toward the end of braking that can trigger unstable friction-induced vibrations.

It can be noticed in Figure 65 that, despite the presence of an increasing friction coefficient with the decrease of the sliding velocity in all tested samples, dynamic instabilities occur only for the specimens coated with 5Ox5Oy and 2Ox8Oy. By comparing the frictional response, it can be observed that the C/C samples coated with 8Ox2Oy are characterized by a DFC that reaches a higher range of friction before the end of braking. On the other hand, the DFC of the other C/C pairs with 5Ox5Oy and 2Ox8Oy increases progressively, with a higher slope toward the end of braking. Consistently with the results shown in {4.2.1}, overall higher values of the DFC prevent the occurrence of a negative slope steep enough to trigger unstable friction-induced vibrations.

It should be also remarked that all the C/C specimens, whose frictional and dynamic response is discussed in this Chapter, are machined from new discs. As shown in {2.2.3}, these samples are characterized by a lower increase of DFC, for temperatures higher than 400 °C, compared to the used ones. As a result, in all the samples coated with the Ox/Oy mixtures, the level of friction during braking is lower than the one observed for the samples machined from the used MAT1 disc, where, similarly, particles of Cont1 and Cont2 take part in the rheology of the contact (Figure 22 and Figure 25.c). In the case of new C/C specimens with Ox and Oy contaminants on the contact surface, for temperatures higher than 400 °C, a less steep negative-friction velocity slope, as well as lower values of the friction coefficient, compared to the used MAT1, are observed. When the negative friction-velocity slope toward the end of braking is steep enough to trigger the dynamic instability, such as for the C/C materials with 5Ox5Oy and 2Ox8Oy, also the amplitude of vibrations is lower compared to the one shown in Figure 25.c.

An overall comparison of the *sliding heating* tests carried out at variable imposed velocity (20 to 0 mm/s) and at different maximum temperatures (100, 300, 500 °C), for all the samples coated

with Ox/Oy paints, is shown in Figure 66. From the top to the bottom, each row of Figure 66 is related to the sequence of variable imposed velocity tests, described in Table 13 (*day two*), carried out on C/C specimens with 8Ox2Oy, 5Ox5Oy and 2Ox8Oy. The onset of dynamic instabilities is indicated with colored bars, bordered in black if the instability is observed on both the back and forth strokes. Peach-colored bars indicate the occurrence of a dynamic instability in presence of a slight negative friction-velocity slope (such as the one shown in Figure 25.b), while violet bars indicate the onset of unstable friction-induced vibrations with a constant friction coefficient (mode coupling). Red bars have been used to show the occurrence of dynamic instabilities in presence of negative friction-velocity slopes such as those shown in Figure 65.

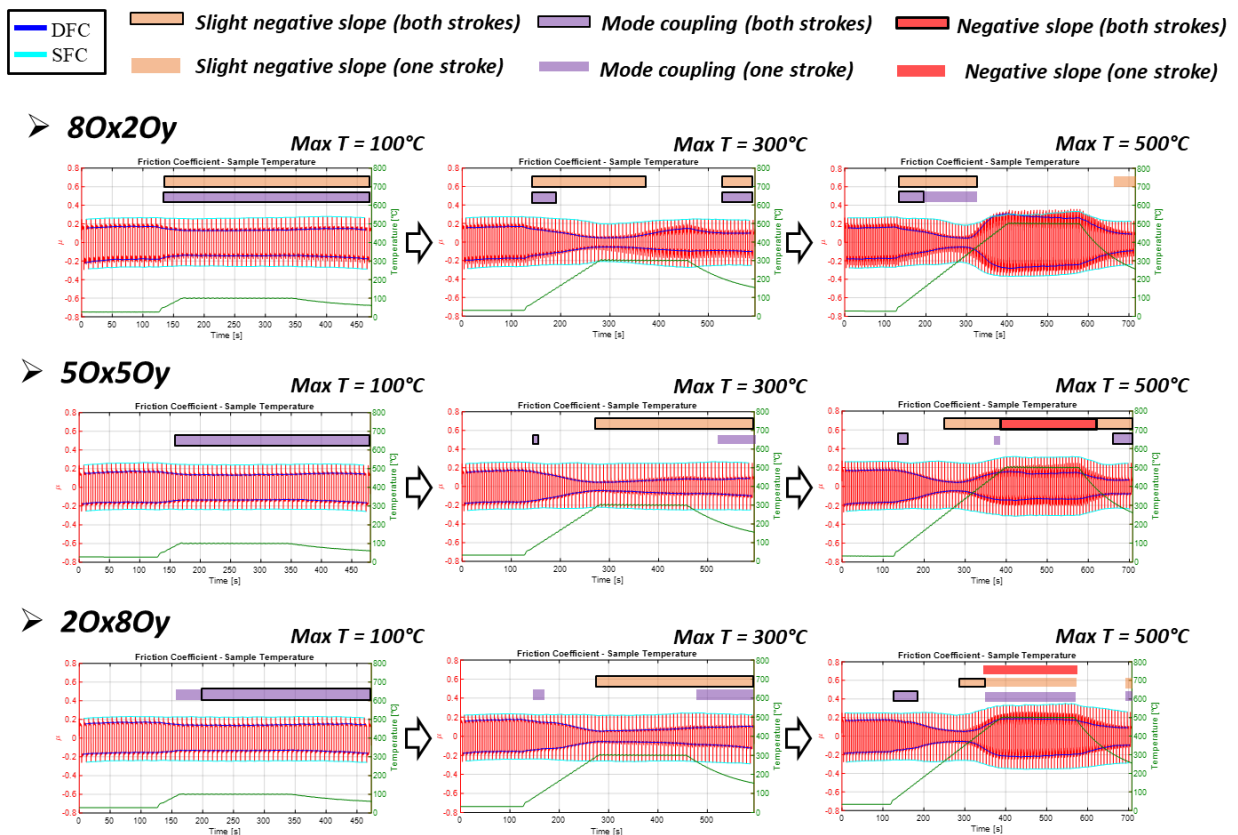


Figure 66 Sliding heating tests carried out at variable imposed velocity (20→0 mm/s) and at maximum temperatures of 100, 300 and 500 °C, for each sample pair coated with the Ox/Oy mixtures. From the top: C/C specimens with 8Ox2Oy, 5Ox5Oy and 2Ox8Oy. The bars denote the occurrence of dynamic instabilities in presence of a slight negative friction-velocity slope (peach-colored bars) and in presence of a constant friction coefficient (violet bars). The red bar indicates the onset of dynamic instability in presence of a steeper negative friction-velocity slope. If the bars are bordered in black the phenomenon is observed on both back-and-forth strokes, otherwise it is observed only on single strokes. The friction coefficient is in red, the DFC is in blue, the SFC is in cyan and the temperature is in green.

As can be seen in Figure 66, the frictional response of all the tested samples is characterized by a minimum value of the DFC, reached at almost 200-300 °C. Consistently with previous outcomes on C/C specimens, up to this temperature the SFC remains almost constant. Significant differences in terms of DFC arise only for temperatures higher than almost 300-400 °C. In such a range of temperature, the presence of different contaminants in the contact interface affects strongly both the frictional and vibrational response of the samples. As also shown in Figure 64 and Figure 65, at 500 °C, the higher amount of Ox in the 8Ox2Oy coating leads to higher values of the DFC, compared to the other Ox/Oy mixtures, which are characterized by a lower increase of the DFC. Moreover, at 500 °C, slightly higher values of the SFC can be observed in all tested samples.

Regarding the vibrational response of the specimens, it can be noticed that, around 100 °C, mode coupling is always observed. At 300 °C, the significant lower values of the DFC with respect to the SFC lead to the occurrence of a slight negative friction-velocity slope instability such as the one shown, for instance, in Figure 25.b. At 500 °C, only the 5Ox5Oy and 2Ox8Oy coatings lead to a negative friction-velocity slope steep enough to trigger a dynamic instability toward the end of braking.

The main results presented in this section are summarized in Table 15.

	C/C + 8Ox2Oy	C/C + 5Ox5Oy	C/C + 2Ox8Oy
T=RT	SFC≈0.25 DFC≈0.2		
RT < T < ≈300 °C	Constant SFC (≈0.25) and decreasing DFC (< ≈0.1)		
	Slight negative friction-velocity slope instability (When DFC << SFC)		
T > ≈300 °C	Increase of both SFC and DFC (but always DFC ≤ SFC)		
	Negative friction-velocity slope observed at 500 °C in all samples (favored by the co-presence of TiO ₂ and SiO ₂)		
	Higher DFC at higher velocities	Lower DFC at higher velocities	
	No dynamic instabilities	Negative friction-velocity slope instability at 500 °C	

Table 15 Synthesis of the frictional and vibrational response of C/C specimens coated with 8Ox2Oy, 5Ox5Oy, 2Ox8Oy, at different temperature conditions.

The frictional response of the tested samples has been investigated also with *sliding heating* tests at constant imposed velocity. The main outcomes are described in the following.

4.2.2.2 Discussion on constant velocity tests

Sliding heating tests at constant imposed velocity (20 mm/s) have been carried out for all the specimens coated with the Ox/Oy mixtures, in order to evaluate the tribological response of the samples without the effect of the decreasing sliding velocity. The evolution of the DFC and SFC have been studied at all temperature conditions up to 500 °C. In this respect, Figure 67 shows the comparison between all the *sliding heating* tests carried out at constant imposed velocity and at different maximum temperatures. From the top to the bottom, each row of Figure 67 shows the sequence of *sliding heating* tests, performed at the maximum temperature of 100, 300 and 500 °C, of the samples coated with 8Ox2Oy, 5Ox5Oy and 2Ox8Oy.

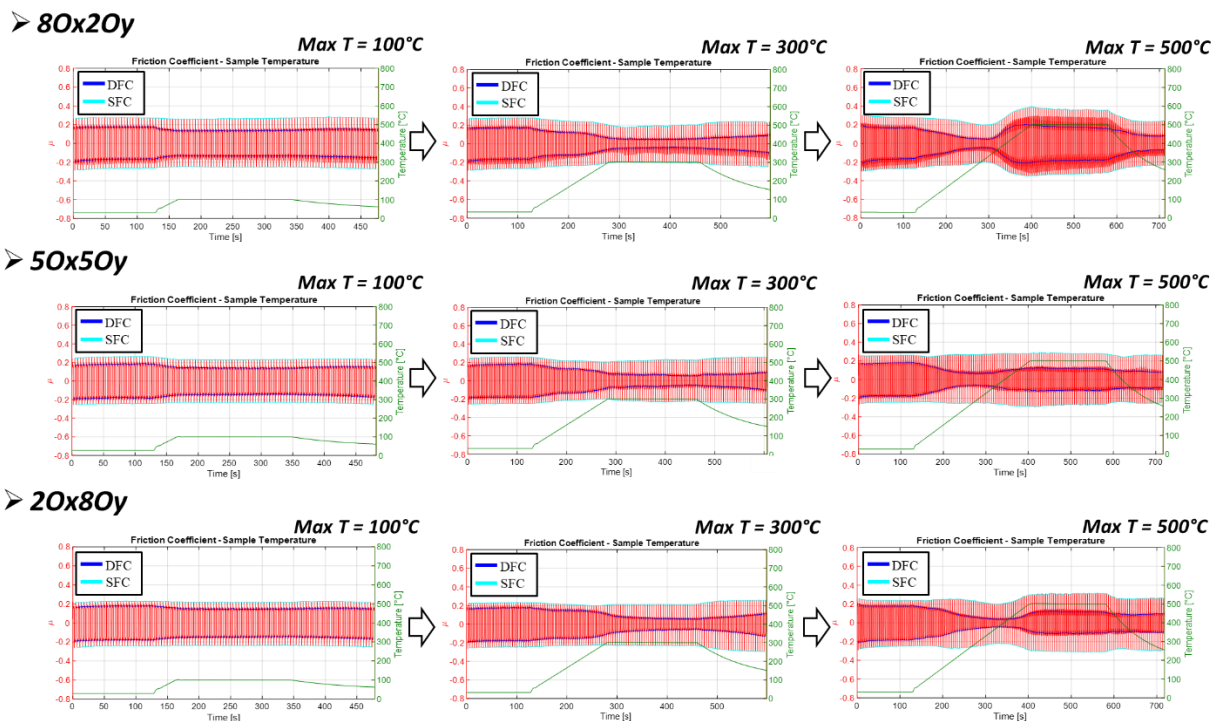


Figure 67 Sliding heating tests carried out at constant imposed velocity (20 mm/s) and at maximum temperatures of 100, 300 and 500 °C, for each sample pair coated with the Ox/Oy mixtures. From the top: C/C specimens with 8Ox2Oy, 5Ox5Oy and 2Ox8Oy. The friction coefficient is in red, the DFC is in blue, the SFC is in cyan and the temperature is in green.

As shown in Figure 67, the behavior of the DFC and SFC is almost the same for all the tested specimens up to almost 300 °C. In particular, consistently with the previous outcomes, up to such temperature the SFC remains almost constant while the DFC decreases.

For higher temperatures, the DFC increases for all the samples. However, a higher increase of the DFC can be noticed for the C/C material with 8Ox2Oy. This behavior of the friction coefficient is consistent with the results presented in {4.2.2.1}, where a higher DFC at 500 °C has been observed for the C/C samples coated with the 8Ox2Oy mixture. The higher amount of

Ox with respect to the Oy seems to be responsible for the different frictional response observed for the C/C samples with 8Ox2Oy, for temperatures higher than almost 300-400 °C.

Further information on the behavior of the friction coefficient at 500 °C can be obtained from the comparison of single strokes taken from the *sliding heating* tests shown in Figure 67. In this respect, Figure 68 shows a comparison of the friction coefficient and accelerometer signal of single strokes at 500 °C and at constant imposed velocity of the specimens coated with 8Ox2Oy, 5Ox5Oy and 2Ox8Oy.

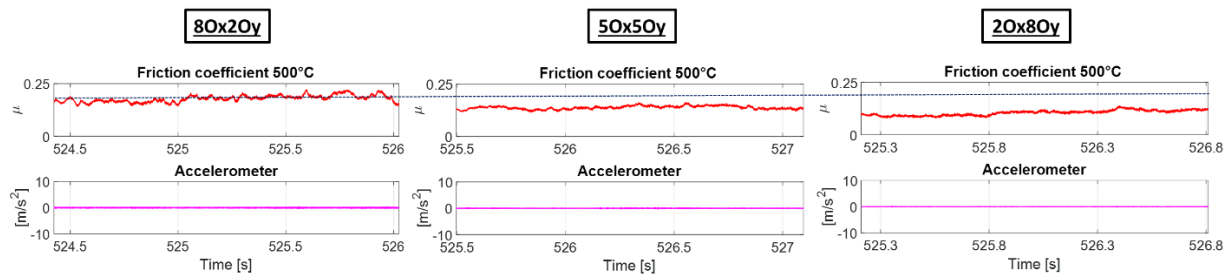


Figure 68 Comparison between the friction coefficient and the accelerometer signal of single strokes taken at 500 °C from the sliding heating tests of the specimens coated with 8Ox2Oy (left), 5Ox5Oy (center) and 2Ox8Oy (right) shown in Figure 67.

It can be noticed that in all the single strokes of Figure 68, the friction coefficient remains almost constant and no dynamic instabilities occur, independently of the Ox/Oy mixture. Such frictional and vibrational behavior of the tested samples at constant imposed velocity differs significantly from the one observed at variable imposed velocity (shown in Figure 65), where the negative friction-velocity slope can trigger the instability at 500 °C. This phenomenon further highlights the role of the decreasing velocity and the negative slope on the onset of dynamic instabilities. Consistently with Figure 67, the level of friction of the C/C material with 8Ox2Oy is higher than the ones obtained with the other sample pairs at 500 °C.

In the following, in order to investigate the main features of the third body affecting the frictional response and the occurrence of unstable friction-induced vibrations, SEM/EDX analysis have been carried out on the C/C materials with 8Ox2Oy and 2Ox8Oy after being tested on TriboAir. The main results are discussed in the next section.

4.3 SEM/EDX analysis on C/C materials with 8Ox2Oy and 2Ox8Oy

With similar values of the static friction coefficient, the different behavior of the dynamic friction coefficient observed in presence of a higher amount of either Ox or Oy in the contact interface, for temperatures higher than almost 300-400 °C, highlights the key role of the rheology of the third body in such a range of temperature. The rheological phenomena taking place during the contact underlies the occurrence of different frictional and vibrational responses of the C/C

materials. With a view to characterize the third body and understand the mechanisms leading to the different tribological scenarios described above, SEM/EDX analyses have been carried out on the contact surfaces of the specimens 8Ox2Oy and 2Ox8Oy, after being tested on TriboAir. To this end, Figure 69 shows a comparison between two photos taken on the friction surface of the 8Ox2Oy-1 (a) and 2Ox8Oy-1 (b) samples, through secondary electrons and at a scale of 200 μm .

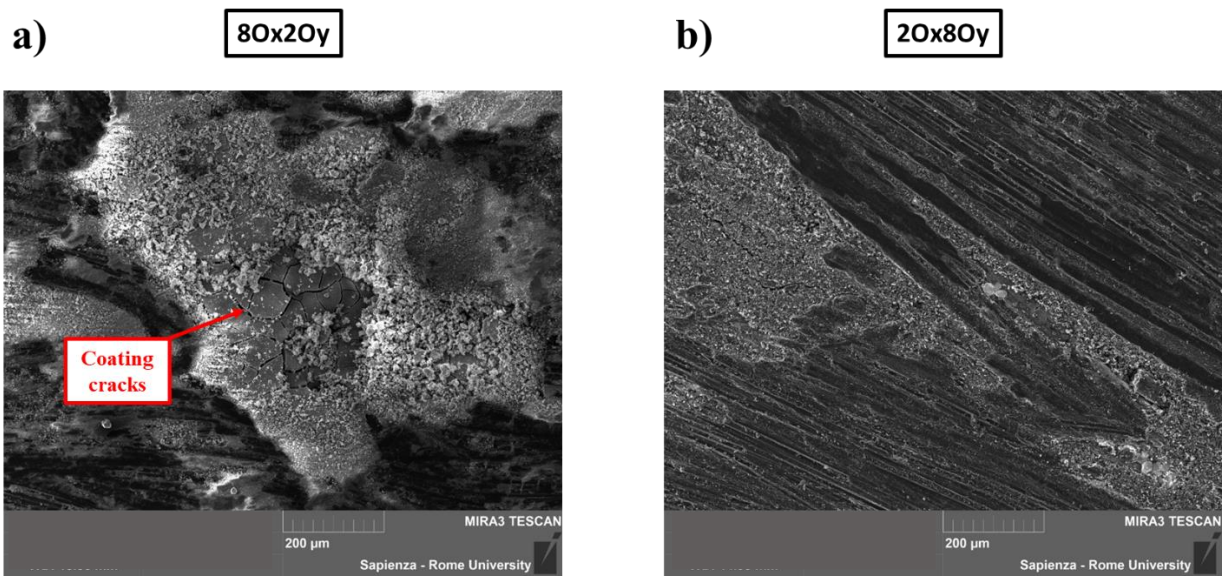


Figure 69 SEM pictures of the 8Ox2Oy-1 (a) and 2Ox8Oy-1 (b) samples, after being tested on TriboAir setup. The photos are taken through secondary electrons, at the scale of 200 μm .

As can be noticed in Figure 69, significant differences between the third bodies of the C/C materials with 8Ox2Oy and 2Ox8Oy can be observed. Figure 69.a (8Ox2Oy) shows a powdery third body characterized by larger size of the particles (micrometric) compared to the third body of Figure 69.b (2Ox8Oy), characterized instead by a compact agglomeration of fine particles (submicrometric) filling the porosities of the friction surface. Moreover, in Figure 69.a, cracks on the coating layer, from which the particles detach and take part in the rheology of the contact, suggest the presence of a brittle third body.

The EDX analysis allows investigating the composition of the observed third body particles. In this respect, Figure 70 shows the EDX mapping analysis carried out on the area shown in Figure 69.a and related to the 8Ox2Oy-1 sample. C, O, Cont2 and Cont1 particles are indicated in blue, yellow, green and red, respectively.

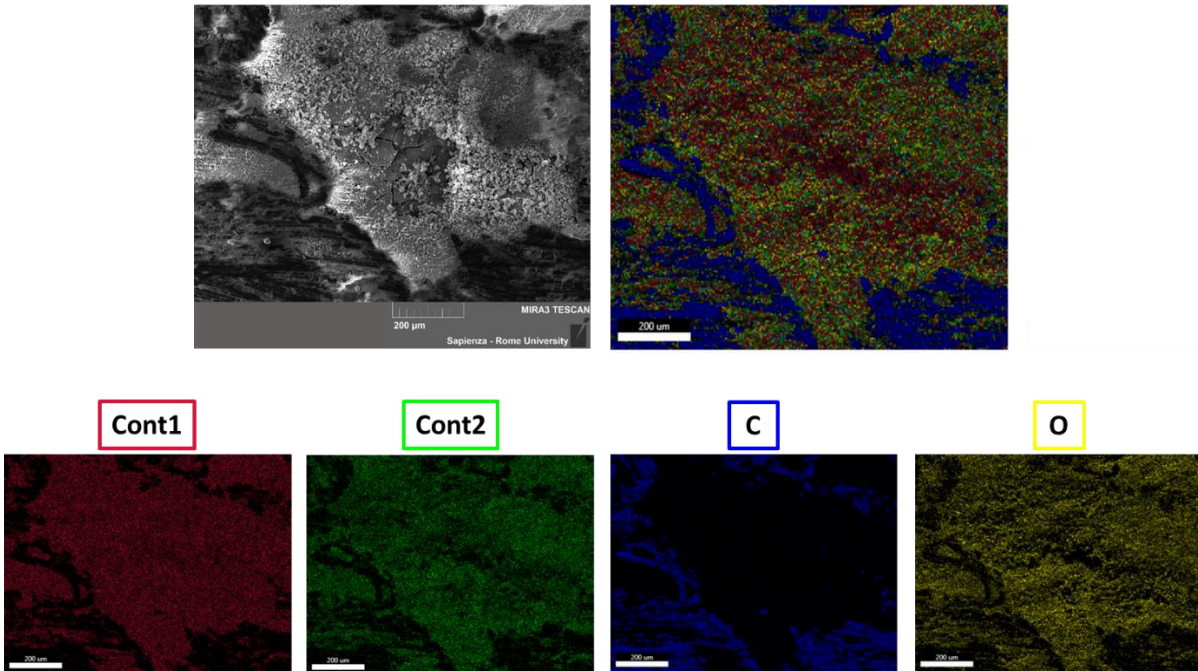


Figure 70. EDX cartography of the area shown in Figure 69.a and related to the 80x20y-1 specimen. Cont1, Cont2, C and O are in red, green, blue and yellow respectively.

Figure 70 shows the presence of Cont1 where the third body particles lie. The presence of Cont2 is observed as well. The substratum of carbon can be clearly seen in the areas where a lower distribution of Cont1 and Cont2 particles is detected. Moreover, the presence of oxygen, in the areas where Cont1 and Cont2 are observed, suggests a third body characterized by Cont1 and Cont2 oxides.

The EDX mapping analysis has been performed also for the 20x80y-1 sample. As an example, Figure 71 shows the mapping of Figure 69.b. C, O, Cont2 and Cont1 particles are in blue, yellow, green and red, respectively.

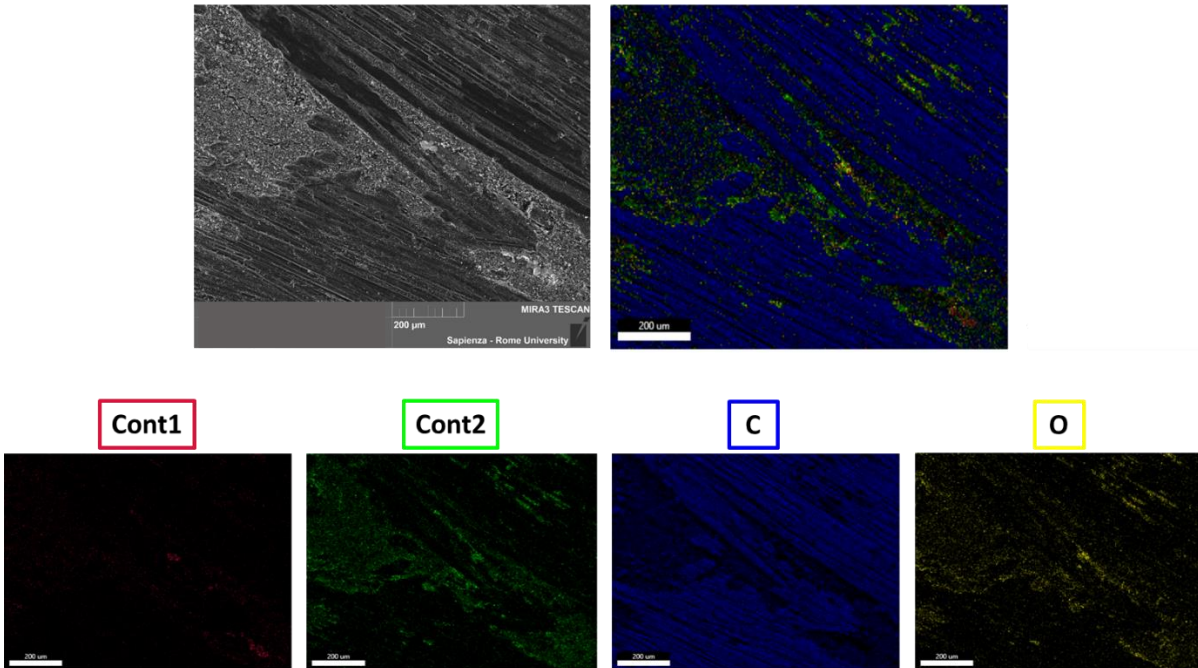


Figure 71. EDX cartography of the area shown in Figure 69.b and related to the 2Ox8Oy-1 specimen. Cont1, Cont2, C and O are in red, green, blue and yellow respectively.

From Figure 71, it can be noticed that the agglomeration of small particles characterizing the third body of the 2Ox8Oy sample is mainly composed of Cont2 and C particles. A very small distribution of Cont1 can be found in the areas where the third body is agglomerated. The carbon substratum around the agglomerated particles is shown in blue. Moreover, the presence of O in the areas where Cont2 particles are detected suggests the presence of Cont2 oxide.

From the SEM/EDX analysis, it can be assumed that in presence of a higher amount of Ox (samples coated with 8Ox2Oy) the third body is mainly characterized by large (micrometric) and brittle particles which take part in the rheology of the contact. The hard particles bring to accommodation mechanisms dominated by a continuous breaking of the third body layer and local abrasion of the contacting surfaces of the first bodies, with a supposed renewing of the dangling bonds. This effect could justify the higher dynamic friction coefficient observed in the frictional tests.

Conversely, a higher amount of Oy (samples coated with 2Ox8Oy) leads to smaller third body particles agglomerated and mixed with carbon particles. It can be hypothesized that the compacted third body on the surface brings to lower reactivity of the interface when sliding at higher velocities. The decrease of the relative velocity provides more time for the dangling bonds on the contact surfaces to react with the counterparts, leading therefore to an increase of friction at lower velocities (negative friction-velocity slope).

4.4 Concluding remarks

In this Chapter, the role of Ox and Oy contaminants on the contact surface of C/C specimens machined from new brake discs has been investigated. The analysis has been carried out by coating several C/C samples with different paints characterized by different content of Ox and Oy. Two experimental campaigns have been performed. The first one has been carried out with samples coated with colloidal suspensions of either Ox or Oy, in order to investigate how the individual contaminants affect the frictional and vibrational response of the C/C material.

The second experimental campaign has been instead carried out with C/C samples coated with different Ox/Oy mixtures. Three different combinations of Ox and Oy have been adopted for the analysis:

- 8Ox2Oy. Coating with 80% of Ox and 20% of Oy;
- 5Ox5Oy. Coating with 50% of Ox and 50% of Oy;
- 2Ox8Oy. Coating with 20% of Ox and 80% of Oy.

Both the experimental campaigns have been performed according to the same protocol, consisting of *sliding heating* tests at constant (20 mm/s) and variable (20 to 0 mm/s) velocity and at the maximum temperatures of 100, 300 and 500 °C.

The tests related to the C/C samples coated with either Ox or Oy have shown a similar frictional behavior up to almost 300 °C. Specifically, the DFC decreases and reaches its minimum around 200-300 °C, while the SFC remains almost constant and equal to the room temperature value (almost 0.25). Similarly to the results discussed in Chapter 2, the lower DFC, with respect to the SFC, favors the occurrence of a slight negative friction-velocity slope. The samples coated with Oy, differently from those coated with Ox, in such a temperature range, do not show the occurrence of low-amplitude unstable vibrations triggered by the slight negative slope. The onset of mode coupling instability has been always observed at 100 °C for both the pairs coated with Ox and Oy.

Significant differences in terms of frictional and vibrational response of the C/C materials with Ox and Oy have been observed for temperatures higher than almost 300-400 °C. In such a range of temperature, in presence of Ox contaminants, the DFC increases up to values slightly higher than the room temperature ones. On the other hand, in presence of Oy particles in the contact interface, the DFC remains significantly low and close to the minimum values reached at almost 300 °C. While the evolution of the DFC differs significantly for temperatures higher than 400 °C, the SFC remains almost constant for both the C/C pairs with Ox and Oy.

In presence of Oy contaminants, the considerably low DFC with respect to the SFC, for temperatures higher than almost 300 °C and up to 500 °C, leads to the occurrence of a negative friction-velocity slope resulting in unstable friction-induced vibrations. Conversely, for temperatures higher than 400 °C and in presence of Ox particles, higher values of the DFC prevent the occurrence of the negative friction-velocity slope as well as the onset of dynamic instabilities.

Regarding the experimental campaign carried out with the C/C specimens coated with Ox/Oy mixtures, independently of the coating, a similar frictional behavior has been observed up to 300 °C. In particular, the DFC decreases and reaches the minimum value around 200-300 °C, while the SFC remains almost constant and equal to the room temperature value (almost 0.25).

Analogously to previous outcomes, in presence of a low DFC, with respect to the SFC, the onset of a slight negative friction-velocity slope, leading to a weak dynamic instability, has been observed in all tested samples at 200-300 °C. Mode coupling instability around 100 °C has been also observed for all the specimen pairs.

For temperatures higher than almost 300-400 °C, the DFC increases for all the tested samples. However, a higher increase of the DFC has been observed for the C/C material with 8Ox2Oy, compared to the C/C materials with 5Ox5Oy and 2Ox8Oy. The SFC, in such a range of temperatures, increases slightly in all the specimen pairs.

It has been observed that for temperatures higher than 400 °C, the co-presence of Ox and Oy leads to a negative friction-velocity slope in all the tested samples. This phenomenon is consistent with the frictional response of the MAT1 (shown in {2.2.1, Figure 25.c}), where a steep negative friction-velocity slope has been observed for temperatures higher than 400 °C. Also for the MAT1 specimens, the co-presence of Cont1 and Cont2 contaminants characterizes the third body of the frictional contact.

Even if the presence of the negative friction-velocity slope has been observed in all the tested samples for temperatures higher than 400 °C, dynamic instabilities due to such phenomenon arise only for the specimens coated with 5Ox5Oy and 2Ox8Oy. Also in this case, the higher increase of the DFC of the C/C material with 8Ox2Oy seems to prevent the occurrence of a negative friction-velocity slope steep enough to trigger the dynamic instability toward the end of braking. In order to investigate the third body of C/C materials contaminated with Ox and Oy, SEM/EDX analyses have been carried out on the contact surface of the C/C samples with 8Ox2Oy and 2Ox8Oy. In presence of a higher amount of Ox with respect to Oy, large (micrometric) and brittle particles of third body, characterized mainly by Ox, have been found on the friction surface of the sample. On the other hand, a higher amount of Oy with respect to Ox leads to smaller third body particles, mainly characterized by Oy, agglomerated and mixed with carbon particles. The difference of the third body morphology has allowed hypothesizing the effect of the different contaminants in the interface rheology. While brittle and hard particles of Ox bring to a continuous renewal of the dangling bonds, increasing the dynamic friction, the compacted third body, promoted by the Oy, brings to smoother surfaces with a reactivity that increases when the sliding velocity decreases.

In conclusion to this analysis, the presence on the friction surface of Ox, for temperatures higher than 400 °C, modifies the rheology of the third body at the interface and leads to values of the DFC sufficiently high to prevent the occurrence of a negative friction-velocity slope leading to dynamic instabilities. However, the co-presence of an equal or higher amount of Oy can lead to a negative friction-velocity slope able to trigger unstable friction-induced vibrations. These results are consistent with the outcomes presented in Chapter 2, where the analysis carried out on used MAT1 specimens, characterized by the presence of Cont1 and Cont2 on the contact surface, has shown the occurrence of a steep negative friction-velocity slope leading to severe dynamic instabilities, for temperatures higher than almost 300-400 °C.

Chapter 5

General conclusions

This thesis work aimed to investigate and characterize the frictional and vibrational response of C/C materials in frictional contact. The research has been carried out by means of test rigs intended to study the tribological behavior of such materials under different operating conditions. The evolution of the frictional response as a function of temperature, sliding velocity and rheology of the contact has been investigated and correlated to the occurrence of unstable friction-induced vibrations. The onset of dynamic instabilities (i.e. mode coupling, negative friction-velocity slope and macroscopic stick-slip) under different boundary conditions has been studied. The main features of the unstable vibrations have been retrieved experimentally and further characterized through specifically developed numerical models. Particular attention has been paid to the role of the temperature, up to 500 °C, and the presence of metallic and non-metallic contaminants taking part in the rheology of the contact. SEM/EDX analyses, carried out on the contact surface of C/C specimens, have provided supporting data for the interpretation of the results.

The main outcomes are summarized and described in the following. The overall scenario obtained from the analyses carried out in this PhD thesis is then discussed in detail. Lastly, the main outlines for future works are presented.

5.1 Original contributions

The works presented in this thesis have allowed investigating the C/C material response on many levels. In the following, all the main results and contributions presented in the manuscript are synthesized, leading to the reconstruction of the overall scenario, and reorganized in four sections:

- Analysis of the C/C frictional and vibrational response under controlled boundary conditions;
- Numerical investigation of C/C unstable friction-induced vibrations;
- C/C material response in presence of either Ox and/or Oy at the contact interface.

5.1.1 Analysis of the C/C frictional and vibrational response under controlled boundary conditions

The tribological and dynamical behavior of C/C materials in frictional contact has been investigated as a function of different operating conditions and rheologies at the contact. Specimens have been machined from used (i.e. already tested on a full brake setup) and new brake discs, with different contaminants, and tested in dedicated test benches. The TriboAir setup, characterized by air bearings that avoid parasitic noise affecting the measure, has been used in order to investigate the relationship between the frictional response and the occurrence of specific vibrational phenomena, under controlled boundary conditions. The analysis has been carried out at different temperatures, up to 500 °C, and constant (20 mm/s) and variable (from 20 to 0 mm/s) sliding velocities. Both the dynamic and static friction coefficient, referred to as

DFC and SFC respectively, have been studied and correlated with the occurrence of unstable friction-induced vibrations.

Regardless of the contaminants and the status of the friction surface, a similar behavior of the tested C/C specimens has been observed up to almost 200-300 °C:

- At room temperature condition, with both constant and variable sliding velocity, the DFC is almost constant and equal to almost 0.2, while the SFC is equal to almost 0.25. The dynamic response is characterized by stable friction-induced vibrations;
- Between room temperature and 200-300 °C, the DFC decreases significantly and reaches values lower than 0.1. Conversely, the SFC remains almost constant. Such a difference between the SFC and the DFC favors the occurrence of a slight negative friction-velocity slope during braking, which can lead in turn to low-amplitude dynamic instabilities.

For temperatures higher than almost 300-400 °C, all used C/C specimens have shown an increase of both the DFC and the SFC, which reach values higher than those retrieved at room temperature condition. As a function of the contaminants, found on the friction surfaces of the tested samples (see Annex I and [162, 163]), different frictional and vibrational responses are obtained:

- *MAT1*. In this case, particles of Cont1, Cont2, Cont3 and Cont4 contaminate the contact surfaces of the specimens. Compared to other materials, a smaller increase of the DFC, which remains lower than the SFC, has been observed. The difference between the SFC and the DFC, promotes a steep negative friction-velocity slope. As opposed to the slight negative friction-velocity slope observed at almost 300 °C, high values of the friction coefficient (up to almost 0.4) are reached during braking. The coexistence of mode coupling and negative friction-velocity slope instability has been assumed. Severe unstable friction-induced vibrations have been observed as well as a final phase of macroscopic stick-slip instability;
- *MAT2 and MAT3*. Particles of Cont3 and Cont4 have been mainly found on the contact surfaces. These specimens are characterized by a strong increase of the DFC, which becomes even higher than the SFC. The high level of DFC, with respect to the SFC, prevents the occurrence of the negative friction-velocity slope observed when also Cont1 and Cont2 particles take part in rheology of the contact (*MAT1*). However, the high level of friction reached at 500 °C (from 0.6 up to almost 0.8) favors the onset of mode coupling instability, observed during some braking strokes;
- *MAT4*. Samples machined from used discs without contaminants exhibit a strong increase of the DFC, which becomes higher than the SFC at 500 °C. In contrast to the C/C specimens with only Cont3 and Cont4 particles on the contact interface, in this case, even in presence of a high level of friction (up to almost 0.6), no dynamic instabilities are observed.

In the range of temperature from 300 °C to 500 °C, a significant different tribological and dynamical scenario has been also observed by comparing used (*MAT4*) and new (*MAT5*) specimens machined from discs without contaminants. With respect to the used C/C samples, the

new ones have shown very little increase of the DFC, which remains significantly lower than the SFC. The presence of a slight negative friction-velocity slope and low-amplitude dynamic instabilities have been observed.

The analysis carried out on the tested C/C specimens has shown the occurrence of different dynamic instabilities during braking, as a function of the temperature and contaminants within the contact. In order to further characterize the different vibrational phenomena (i.e. mode coupling and negative friction-velocity slope instabilities), specific tests, with a dedicated protocol, have been carried out on TriboAir. The onset of two different unstable modes at almost 14.6 kHz and 43 kHz, triggered respectively by mode coupling and negative friction-velocity slope, has been observed. In case of mode coupling, a phase shift of almost 90° between the tangential and normal vibrational response, with respect to the contact surface, has been shown. Unlike the mode coupling, the negative friction-velocity slope instability has shown instead in-phase vibrational signals between the tangential and normal direction to the contact. Such results have been positively correlated with the experimental tests.

The frictional and dynamic response of the C/C materials has been also investigated by means of a dedicated setup, named TriboWave, in order to perform friction tests, such as those carried out through TriboAir, under controlled atmosphere. Despite having lowered considerably the level of oxygen in the atmosphere (almost 3.5 % of O₂), C/C samples tested in argon have shown a similar frictional and vibrational response of the same C/C samples tested in air. Moreover, a small amount of CO, detected at 500 °C (4-5 ppm), suggests the occurrence of gasification phenomena even in presence of a very small amount of oxygen.

All the main outcomes obtained from the analysis of the frictional and vibrational response of the C/C specimens have been summarized in the diagram of Figure 72.

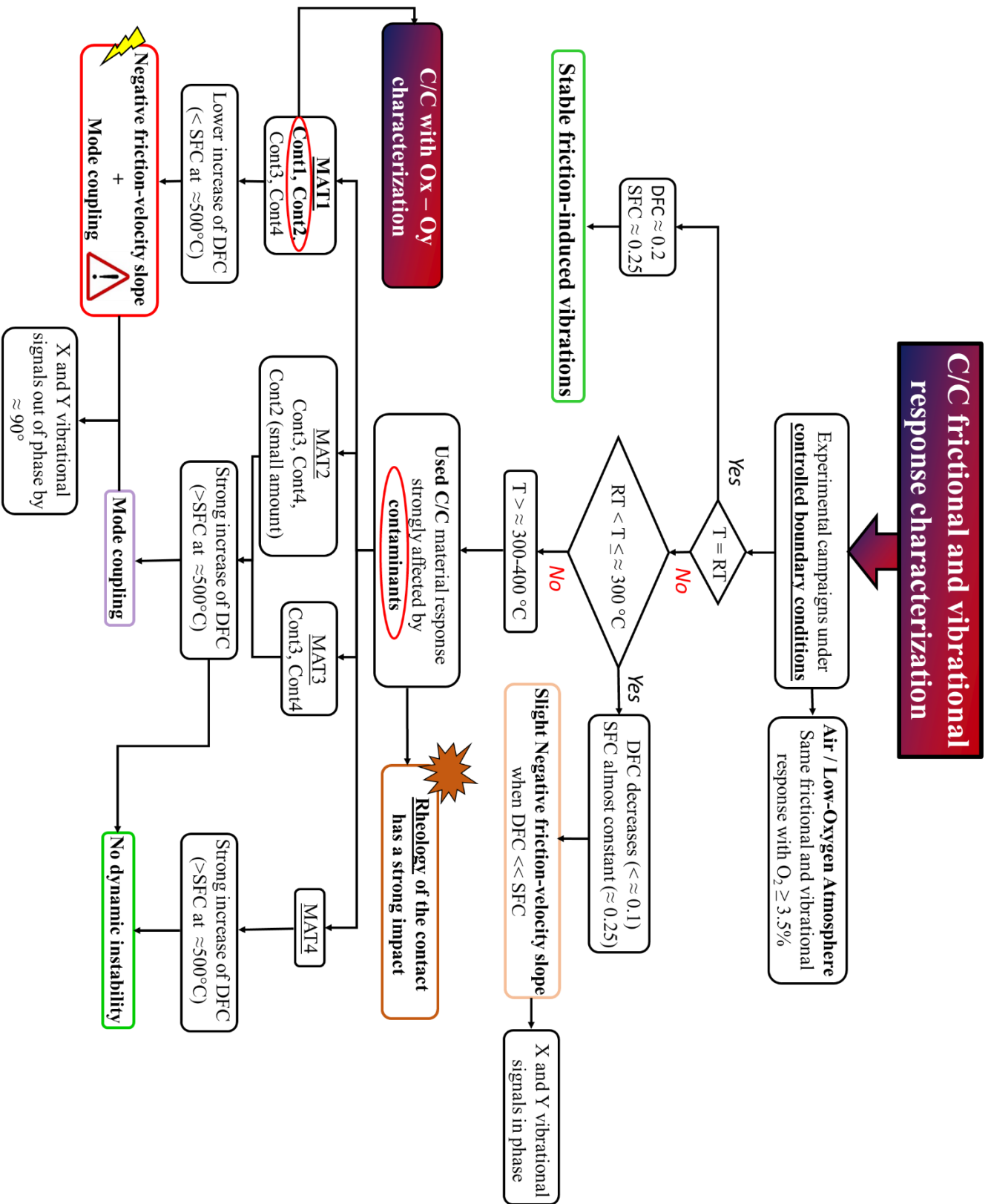


Figure 72 Comprehensive diagram of the C/C material frictional and vibrational response.

From the experimental campaigns, the tribological and dynamical behavior of C/C specimens has been described and specific features of the dynamic instabilities have been retrieved. In order to further characterize the different vibrational phenomena and support the interpretation of the outcomes obtained experimentally, numerical analyses have been carried out.

5.1.2 Numerical characterization of the dynamic instabilities

With a view to investigate the unstable modes related to mode coupling and negative friction-velocity slope, observed experimentally on TriboAir, a finite element analysis has been carried out. A pre-stressed modal analysis has been performed in order to identify the unstable mode triggered by mode coupling at almost 14.6 kHz. It has been observed that, increasing the friction coefficient, two stable modes of the system approach each other until they coalesce in an unstable mode, causing the mode coupling instability. In agreement with the experience, a frequency of the unstable mode at almost 14.6 kHz, at which the lock-in phenomenon occurs, has been identified. The finite element analysis has also shown a high-frequency mode, at almost 43 kHz, whose modal shape deforms along the tangential direction to the contact. Such a mode has been identified as the one triggered by the negative friction-velocity slope.

The main features of the mode-coupling and negative-slope instabilities have been further investigated by means of a lumped-parameter numerical model, which has allowed reproducing and decoupling the different vibrational phenomena, as a function of the friction coefficient behavior during braking. Such a model, consisting of two masses, one of which in frictional contact with a sliding belt, allows considering also non-linear contributions arising during the contact (i.e. stick-slip and detachment of the mass from the sliding belt). The vibrational response, when the different dynamic instabilities arise, has been investigated along the tangential and normal directions to the contact. The obtained results are consistent with the experimental outcomes obtained on the TriboAir test bench. In particular, it has been observed that vibrational signals along the tangential and normal directions to the contact are in phase in presence of the sole negative friction-velocity slope. On the other hand, a phase shift of almost 90° is observed in presence of mode coupling. The model has allowed also investigating the coexistence of both the mode coupling and negative friction-velocity slope. It has been observed that when both the dynamic instabilities coexist, higher amplitude of vibrations are reached with respect the sole mode-coupling or negative-slope instabilities.

The numerical analysis has provided a supporting tool for validating the hypothesis related to the different vibrational scenarios speculated in presence of unstable friction-induced vibrations. From the analysis of the phase shift between in-plane and out-of-plane vibrational signals it is therefore possible to identify the onset of different dynamic instabilities.

In agreement with the experimental results, the worst vibrational scenario, in terms of high-amplitude vibrations, has been identified when a steep negative friction-velocity slope and a high level of friction (higher than the mode coupling threshold value) coexist. The experimental tests, carried out on the TriboAir test bench, have shown the occurrence of such phenomenon for temperatures higher than almost 300°C and when both Cont1 and Cont2 particles take part in the rheology of the contact. As a result, the strong impact of such contaminants on the rheology

at the contact, and consequently on the overall frictional response, has required a thorough analysis of how Ox and Oy particles on the friction contact affect the tribological and dynamical response of the C/C materials.

5.1.3 C/C material response in presence of Ox and Oy on the contact interface

New C/C samples have been coated with colloidal suspensions of either Ox or Oy, in order to investigate the effect of each contaminant within the third body. Up to almost 300 °C, the DFC and SFC evolve similarly to all the other used and new tested samples, regardless of the coating and the contaminants. Specifically, the DFC decreases and reaches its minimum around 200-300 °C, while the SFC remains almost constant and equal to the room temperature value (almost 0.25). When the DFC reaches its minimum, a slight negative friction-velocity slope is observed. Significant differences in terms of both the frictional and dynamical response, between the samples coated with Ox and Oy, have been observed in the range of temperature from almost 300-400 °C up to 500 °C. Being the coated samples new, in both cases the increase of the DFC, in this temperature range, is lower than the one observed for the used samples and the DFC is always no higher than the SFC. However, while for the samples coated with Ox the increase of the DFC is enough to prevent the occurrence of a negative friction-velocity slope, for the samples coated with Oy a considerably lower DFC leads to a negative friction-velocity slope (high difference between the DFC and the SFC) resulting in unstable friction-induced vibrations. The different contaminants affect thus differently the DFC, while maintaining a similar SFC, highlighting how the contact rheology, for temperature higher than about 300 °C, plays a key role in the frictional and dynamical behavior of C/C materials.

With the main purpose of understanding how the co-presence of Ox and Oy affect the material response, an experimental campaign has been carried out also with samples coated with different Ox and Oy mixtures:

- 8Ox2Oy. Coating with 80% of Ox and 20% of Oy;
- 5Ox5Oy. Coating with 50% of Ox and 50% of Oy;
- 2Ox8Oy. Coating with 20% of Ox and 80% of Oy.

As usual, regardless of the coating, up to 300 °C, a similar behavior is observed.

For higher temperatures, the rheology of the contact plays again a significant role. The DFC increases for all the tested samples, however a higher increase is observed in presence of a higher amount of Ox with respect to the Oy (i.e. for the C/C samples with 8Ox2Oy). Consistently with the experimental tests carried out on MAT1 specimens, the presence of both Ox and Oy leads to a negative friction-velocity slope in all tested samples. However, a higher amount of Ox with respect to Oy allows reaching a higher range of friction toward the end of braking (lower difference between the DFC and SFC), preventing the occurrence of a negative-slope steep enough to trigger the unstable vibrations. Conversely, the 5Ox5Oy and 2Ox8Oy, characterized by a higher amount of Oy, lead to a progressively increasing friction coefficient during braking and the occurrence of dynamic instabilities due to the negative friction-velocity slope. It should

be remarked that, being the samples new, the level of friction at 500 °C is lower than the one observed for the MAT1, where the coexistence of both negative friction-velocity slope and mode coupling has been assumed.

In order to investigate further the third body of both the samples pairs coated with 8Ox2Oy and 2Ox8Oy, SEM/EDX analyses have been carried out on the friction surfaces. The study has allowed observing the main features of the third body when Ox or Oy oxides take part in the contact rheology. Specifically, it has been observed that in presence of a higher amount of Ox, with respect to Oy, large (micrometric) and brittle particles, characterized mainly by Ox, lie on the friction surface of the examined samples and the third body appears fragmented, by the action of such particles, and less cohesive. Conversely, a higher amount of Oy lead to a third body mainly characterized by smaller and agglomerated particles of Oy, mixed with carbon and filling the porosities of the material.

All the obtained results synthesized in this section, related to the effect of a C/C third body contaminated by Cont1 and Cont2 particles, are schematically represented in Figure 73.

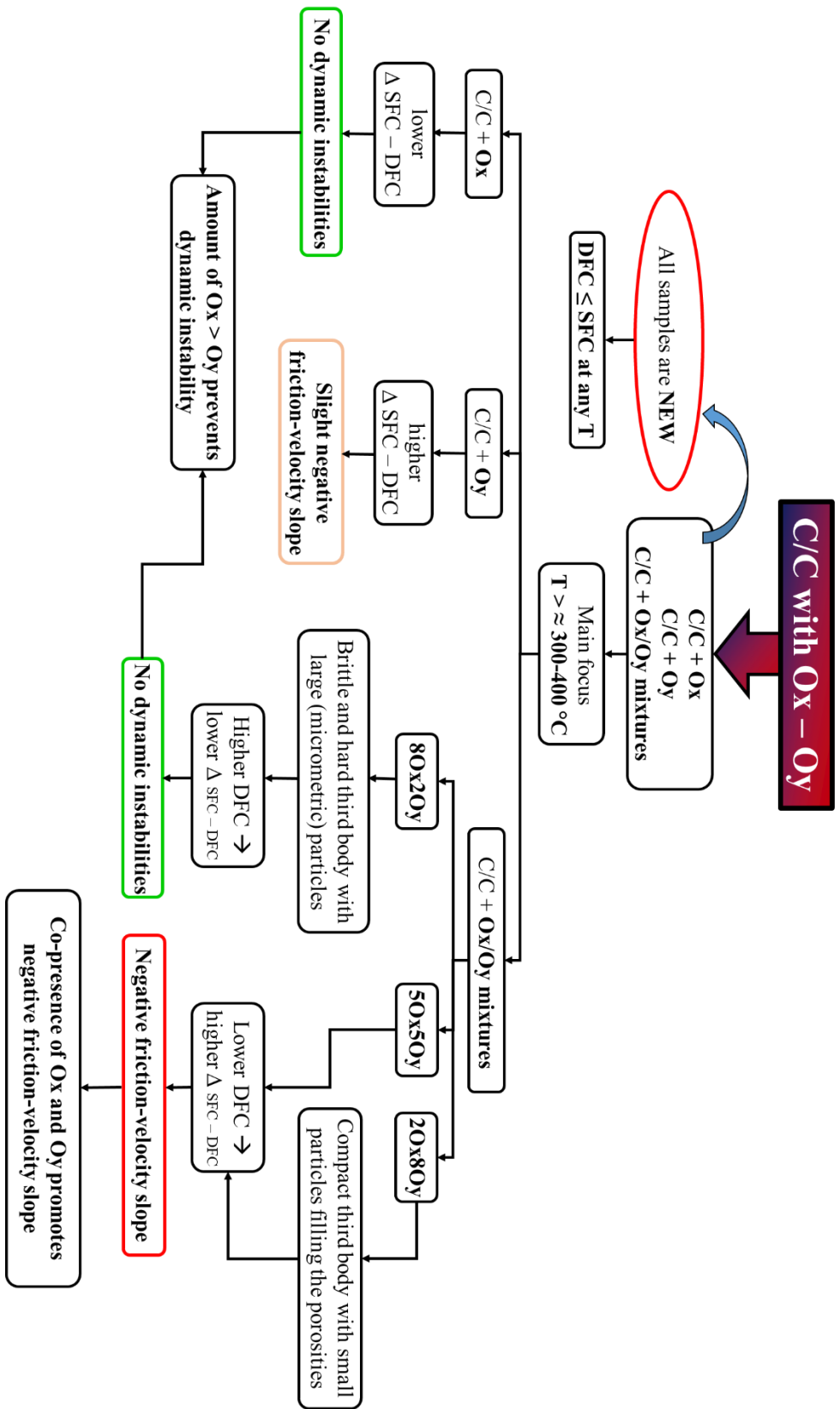


Figure 73 Comprehensive diagram of the C/C material response in presence of either Ox and/or Oy in the contact interface.

The synthesis of the overall findings, summarized in the above sections, allowed developing a comprehensive scenario for helping to understand the tribological and dynamical behavior of the C/C composites, as detailed in the following.

5.2 Overall scenario

This PhD thesis has highlighted the close relationship between the frictional response of C/C materials in sliding contact and the occurrence of unstable friction-induced vibrations. Among all the investigated parameters, it has been observed a strong evolution of the friction coefficient as a function of the temperature and the rheology of the contact. Different frictional responses underlie the occurrence of distinct dynamic instabilities, which can result in high-amplitude vibrations and be therefore undesired in industrial applications. The outcomes obtained by this study allow defining comprehensive scenarios in order to explain the occurrence of the observed tribological and dynamic phenomena. In the following, the hypothesized mechanisms driving different behaviors of the friction coefficient and unstable friction-induced vibrations are described in two different ranges of temperatures. The C/C material response is first discussed for temperatures lower than almost 300 °C, then for temperatures up to 500 °C.

5.2.1 Frictional and vibrational response for $T < 300$ °C

The results obtained from this thesis work have shown the occurrence of different vibrational scenarios occurring as a function of the operating temperature.

It has been observed that as long as C/C specimens are in frictional contact at room temperature condition, the friction coefficient is almost constant during braking and no dynamic instabilities occur. In this case, the dynamic response is characterized by low-amplitude stable friction-induced vibrations. Consistently with the existing literature, in normal water-containing environment, a low friction regime, characterized by a dynamic friction coefficient almost equal to 0.2, has been retrieved [6, 25]. At room temperature condition, the carbon dangling bonds, which favor the adhesion of the contacting surfaces, are neutralized by water molecules in the atmosphere [53-55].

When increasing the temperature, up to almost 200-300 °C, regardless of the status (i.e. either new or used) of the friction surfaces or the presence of metallic/non-metallic contaminants, the DFC decreases significantly and reaches values lower than about 0.1. Conversely, the SFC remains almost constant and preserves the room temperature value (almost 0.25).

Even if the response of C/C materials within this temperature range is not the main object of this thesis, which is focused on higher temperatures, the works in the literature allow hypothesizing that the occurrence of this phenomenon is due to concurrent causes, which affect the frictional response of the material:

- In [6, 21, 24], it has been observed that with the increase of temperature the contact atmosphere is enriched with water vapor. The equilibrium of absorption of the water

molecules is therefore modified and a higher lubricating effect can take place, leading to lower values of the friction coefficient;

- The increase of temperature can increase the mobility of the carbon active sites and lead to a local recombination of the dangling bonds on the contact surface of each first body [170, 171]. This mechanism favors a decrease of the friction coefficient, as the interactions between active sites of antagonist surfaces are reduced.

It has been shown that the significantly lower DFC with respect to the SFC favors the occurrence of a slight negative friction-velocity slope during braking. Being the level of friction particularly low, the dynamic instability is due, in this case, to the sole negative slope and low-amplitude vibrations are usually observed.

For temperatures higher than almost 300 °C, up to 500 °C, the recombination between the carbon dangling bonds of the antagonist surfaces and within the third body becomes predominant with respect to the deactivation of the active sites by water molecules. An increase of the DFC is usually observed. Moreover, the gasification process favors wear and creation of new active sites, promoting the increase of the friction coefficient. The work carried out in this thesis has shown that in addition to these phenomena, widely known and discussed in the literature, the rheological contribution of the third body to the frictional response has a strong impact in such a range of temperature. Specifically, it has been observed that, as a function of the status and the contaminants taking part in the frictional contact, very different frictional and vibrational responses of the C/C materials can be obtained. These outcomes are discussed in the following.

5.2.2 Frictional and vibrational response for $T > 300$ °C: role of the third body and rheology of the contact

In the range of temperature between 300 °C and 500 °C, a significant different frictional response has been observed between new and used C/C specimens. Without contaminants on the contact surface, while for the used (already tested on a real brake apparatus) sample pairs the DFC increases significantly (up to almost 0.6) and becomes higher than the SFC, for the new samples the DFC increases slightly and reaches values lower than the room temperature ones.

The significant different evolution of the DFC with respect to the SFC, which shows a similar behavior regardless of the status of the contact surfaces, highlights the key role played by the rheology on the frictional response of the C/C materials.

Observations aimed to characterize the third body, between the new and used status of the contact interface [164], have shown the presence of a compact layer of carbon particles on the friction surfaces and inside the porosities of the used material. It can be assumed that such a different feature of the interface underlies the occurrence of the different frictional response observed experimentally between new and used samples. In order to discuss the hypothesized scenario, Figure 74 shows a simplified representation of a contact interface of new (Figure 74.a) and used (Figure 74.b) C/C specimen pairs.

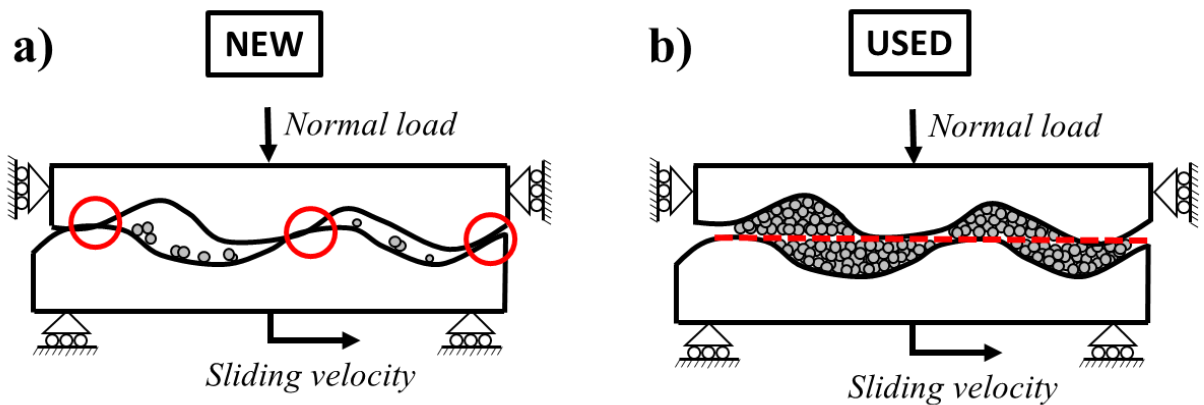


Figure 74 Schematic representation of a contact interface of new (a) and used (b) C/C specimen pairs. In grey, third body of carbon particles.

The main difference, between the new (a) and used (b) sample pairs, is the presence of carbon particles (in grey) filling the porosities and leading to a compact third body for the used specimens. As shown in Figure 74.b, the presence of such third body layer leads to a significantly higher real contact area with respect to the new samples. Moreover, as observed in [21], C/C wear and third body particles are characterized by an active surface area larger than that of the bulk material and physicochemical characteristics similar to the activated carbons. It can be hypothesized that the significantly higher DFC increase of the used material is due to the highly reactive third body, which participates in the rheology of the frictional contact and favors adhesion (dangling bond recombination) between the antagonist surfaces, at high temperature conditions (namely higher than 300 °C).

It should be remarked that such a different frictional response leads also to different vibrational scenarios. No dynamic instabilities are observed for the used specimens, while the new specimens show the presence of a slight negative friction-velocity slope, favored by the low DFC with respect to the SFC, and the occurrence of low-amplitude unstable friction-induced vibrations. As a result, it can be noticed how the rheological contribution of the third body can drive different behaviors of the friction coefficient which, in turn, can lead to the onset of different vibrational phenomena.

By taking into account the rheology of the contact, it is possible to hypothesize how the presence of different contaminants on the third body affects the frictional response and lead to significantly different scenarios, for temperatures higher than almost 300 °C.

By SEM/EDX analyses, it has been observed that in presence of a higher amount of Ox, the third body is characterized by brittle and large particles of Ox, which take part in the contact rheology. On the other hand, a higher amount of Oy brings to small and agglomerated particles, mixed with carbon, which fill the porosity of the material. A schematic representation of a contact interface of new samples (such as those tested on TriboAir), characterized by the presence of Ox and Oy, is shown in Figure 75. Ox (in brown) and Oy (in cyan) contaminate the contact surfaces in Figure 75.a and Figure 75.b, respectively. Carbon particles (in grey) are also represented. The trend of the corresponding macroscopic friction coefficient of the two rheological conditions, as a function of the sliding velocity, is shown as well.

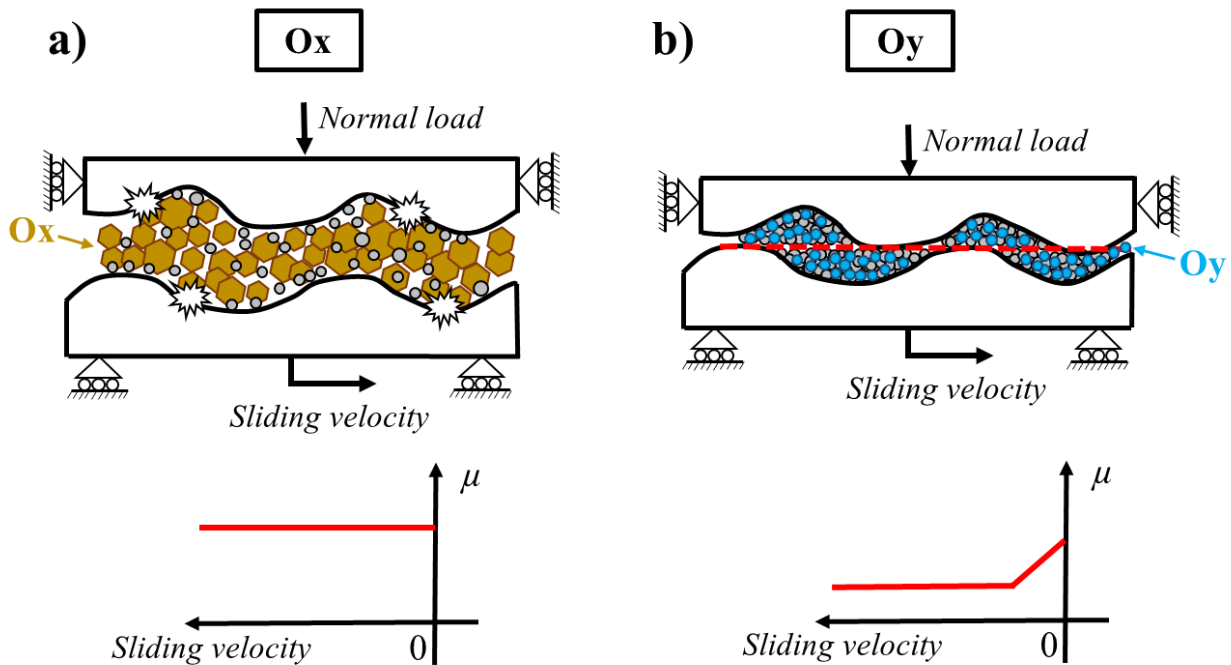


Figure 75 Above, schematic representation of a contact interface in presence of Ox (a) and Oy (b) contaminants. In brown, cyan and grey, the Ox, Oy and carbon particles, respectively. Below, simplified representation of the trend of the macroscopic friction coefficient, as a function of the sliding velocity, in presence of Ox (a) and Oy (b) contaminants.

In presence of large and hard particles of Ox within the frictional interface (Figure 75.a), it can be assumed that the local abrasion of the contacting surfaces of the first bodies is increased, as well as the renewal of the dangling bonds during the frictional interaction, both at the surfaces and within the third body layer. For temperatures higher than almost 300 °C, the recombination of the dangling bonds on the antagonist surfaces and the increase of the active sites caused by such a third body lead then to a higher increase of the DFC. Moreover, a larger size of the third body particles hinders the relative motion between sliding surfaces, favoring therefore the increase of the friction coefficient. It can be also hypothesized that higher and lower sliding velocities can be equally affected by a higher friction coefficient, as the abrasive third body favors the renewal of the active sites at any sliding speed.

A different scenario is assumed in presence of Oy particles within the contact interface (Figure 75.b). The observed compact third body, characterized by a small size of the particles, leads to smooth contacting surfaces of the first bodies, with material porosities filled by both Oy and C. In this case, the compact third body reduces the numbers of dangling bonds, which are not renewed, such as in case of large abrasive particles. Moreover, the relative motion is favored and a lower friction coefficient is obtained at higher sliding velocity, where the dangling bonds of the surfaces in contact have shorter time to react and recombine. However, lower sliding velocities increase the time for the dangling bonds to react and favor therefore the adherence between the contacting surfaces. As a result, an increase of the friction coefficient with the

decrease of the velocity can be observed. The described scenario is in agreement with the frictional response, at 500 °C, retrieved in presence of only Oy contaminants on the friction surfaces, where a negative friction-velocity slope, leading to dynamic instability, has been observed only at the very end of braking.

Considering the above-described scenarios, it is reasonable to assume that the co-presence of Ox and Oy on the contact surface is a possible root cause for the steep negative friction-velocity slope, in a high friction range, observed for the MAT1, characterized by the presence of both Cont1 and Cont2 within the contact interface. While the presence of Ox leads to an overall increase of the friction level, the Oy lowers the friction coefficient at higher velocities and favors the occurrence of a steep negative friction-velocity slope toward the end of braking. The combined effect of both contaminants leads to a high increase of the friction coefficient when lowering the sliding velocity, resulting in unstable friction-induced vibrations. This assumption has been validated by the experimental campaign carried out with the new C/C samples coated with Ox and Oy mixtures, where the presence of a negative friction-velocity slope has been always observed for temperatures higher than almost 300-400 °C. Moreover, it has been also observed that a higher amount of Ox on the friction surface, with respect to Oy (sample pair coated with 8Ox2Oy), can lead to a predominant effect of such oxide on the contact rheology. The higher friction coefficient at higher sliding velocities can prevent the occurrence of the negative slope toward the end of braking.

The overall scenario described for temperatures higher than almost 300 °C is summarized in the diagram of Figure 76.

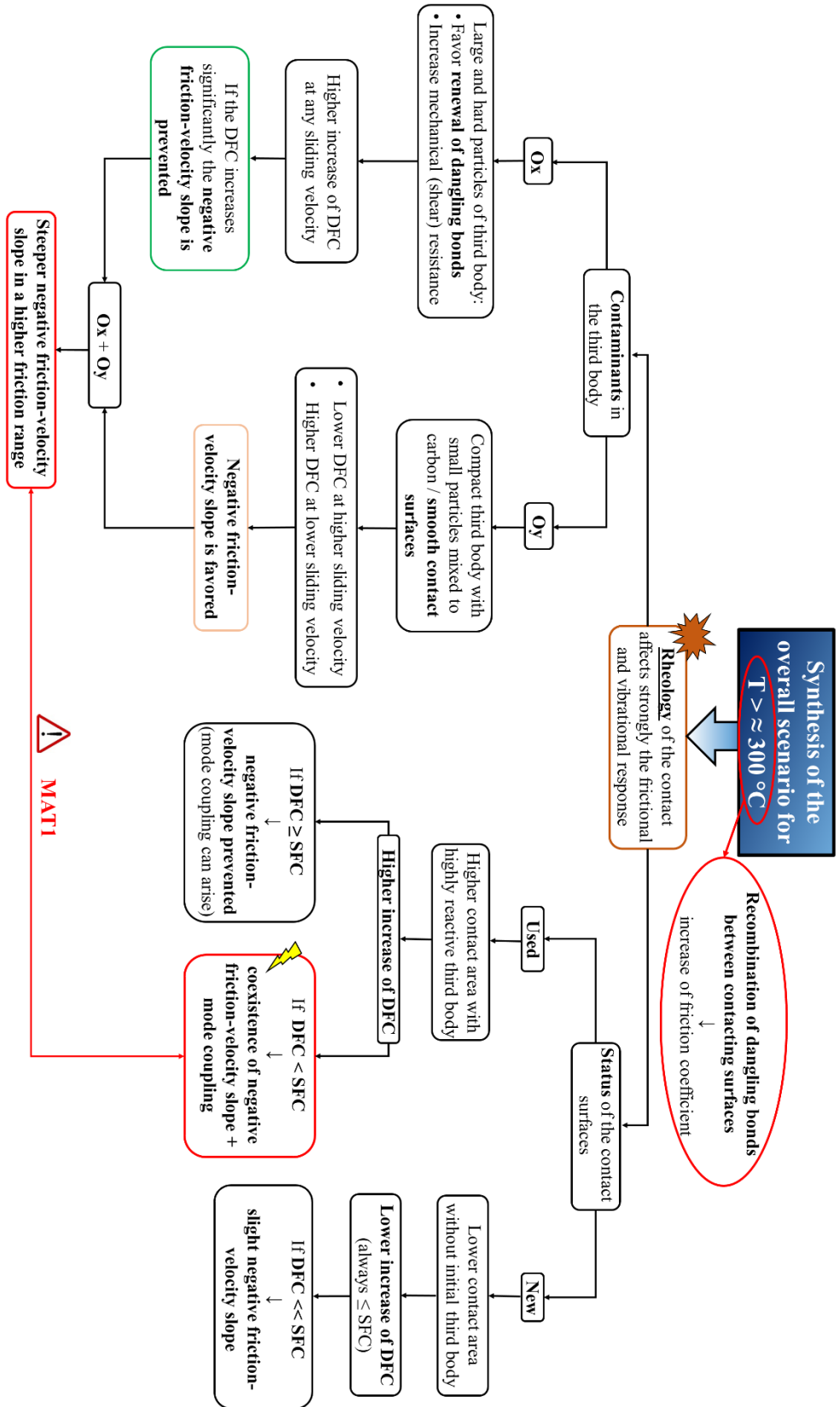


Figure 76 Comprehensive diagram of the overall scenario for $T \geq 300 \text{ }^\circ\text{C}$.

5.3 Future works

This thesis work highlighted the complexity of the rheological and physicochemical phenomena affecting the C/C material response. Many different tribological and dynamic aspects have been taken into account in order to develop comprehensive scenarios aimed to explain the occurrence of specific frictional and vibrational responses of the C/C composites. Nevertheless, future developments can be taken into considerations in order to further investigate the tribological and dynamical behaviors of such materials in presence of contaminants:

- Even if the analysis has been carried out in presence of different metallic and non-metallic contaminants in the contact interface, major attention has been paid to the effect of Cont1 and Cont2 particles taking part in the contact rheology. In fact, for temperatures higher than almost 300 °C, the worst vibrational scenario, characterized by the coexistence of the negative friction-velocity slope and mode coupling, has been always observed for the MAT1. This material differs from the others for a consistent amount of Cont1 and Cont2 found on the friction surfaces of the examined specimens. As a result, an in-depth analysis has been carried out in order to understand how such contaminants bring to the occurrence of the steep negative friction-velocity slope leading to high-amplitude vibrations. Nevertheless, it must be taken into consideration that a certain percentage of Cont3 and Cont4 has been also detected on the MAT1 as well as on the MAT2 and MAT3. With respect to the other tested materials, both the MAT2 and MAT3 have shown a significant increase of the DFC (up to even 0.8) for temperatures higher than almost 300-400 °C. It can be hypothesized that the MAT3 oxide has a similar role to the Ox and leads to an abrasive third body, which favors the renewal of the carbon dangling bonds during the frictional interaction. At high temperature condition, the recombination of the dangling bonds between the contacting surfaces could lead to the strong increase of the DFC observed for the MAT2 and MAT3. In order to fully understand the role of different contaminants on the rheology of the contact, and thus on the overall frictional and dynamic response, further analyses with C/C samples coated with other contaminants, and specifically with MAT3 oxides, can be carried out in order to investigate such hypothesis. Moreover, a finer characterization of the third body, both by a mechanical and physicochemical point of view, should be developed, in order to fully understand the rheology at the contact and its impact on the macroscopic frictional response of the system;
- Different dynamic instabilities have been investigated. The onset of mode coupling and negative friction-velocity slope instabilities have been studied as a function of the friction coefficient evolution under different operating conditions. However, the occurrence of unstable friction-induced vibrations is also affected by other phenomena. As shown in [103], the friction noise provides a source of broadband dynamical excitation, which can trigger an unstable mode of the system and lead to self-excited unstable vibrations. As a result, a higher energy content of the friction noise can favor the occurrence of dynamic instabilities. Further studies can be carried out in order to investigate such phenomenon and how the presence of contaminants affect the friction noise at different temperatures. Moreover, other mechanical properties of the C/C materials, such as material damping

and stiffness, could be affected by temperature. The effect of their variations on the vibrational response should be taken into account;

- The vibrational response of the material is related to the elastic energy released by the local impacts taking place at the contact interface. Waves propagating until the boundaries of the mechanical system lead to friction-induced vibrations. The relationship between the local contact dynamic excitation and the system response is a relevant parameter when investigating the occurrence of dynamic instabilities due to the frictional interactions. To date, few information exists on how wave propagation is affected by the mechanical properties of the third body, the superficial layer and the bulk of the first bodies. Further analyses should be focused on understanding how different material properties, both at the interface and within the bulk of the first bodies, affect the wave propagation and then the onset of unstable vibrations.

Overall, looking further into the effective rheology of the contact, as well as investigating how the dynamic material response (wave propagation) is affected by different third bodies and material properties, can lead to a deeper understanding of the tribological phenomena and to design robust solutions to prevent the occurrence of undesired unstable vibrations.

References

- [1] E. Savage, *Carbon-carbon composites*. Springer Science & Business Media, 2012.
- [2] L. M. Manocha, "High performance carbon-carbon composites", *Sadhana*, vol. 28, no. 1, pp. 349-358, 2003.
- [3] T. Windhorst and G. Blount, "Carbon-carbon composites: a summary of recent developments and applications", *Materials & Design*, vol. 18, no. 1, pp. 11-15, 1997.
- [4] G. R. Devi and K. R. Rao, "Carbon-Carbon Composites -An Overview", *Defence Science Journal*, vol. 43, pp. 369-383, 1993.
- [5] J. R. Gomes, O. M. Silva, C. M. Silva, L. C. Pardini, and R. F. Silva, "The effect of sliding speed and temperature on the tribological behaviour of carbon-carbon composites", *Wear- Proceedings of the ninth Nordic Symposium on Tribology*, vol. 249, no. 3, pp. 240-245, 2001.
- [6] M. Gouider, Y. Berthier, P. Jacquemard, B. Rousseau, S. Bonnamy, and H. Estrade-Szwarcckopf, "Mass spectrometry during C/C composite friction : carbon oxidation associated with high friction coefficient and high wear rate", (in French), *Wear*, pp. 1082-1087, 2004.
- [7] B. K. Yen, T. Ishihara, and I. Yamamoto, "Influence of environment and temperature on "dusting" wear transitions of carbon-carbon composites", *Journal of Materials Science*, vol. 32, no. 3, pp. 681-686, 1997.
- [8] J. D. Chen, J. H. Chern Lin, and C. P. Ju, "Effect of humidity on the tribological behavior of carbon-carbon composites", *Wear*, vol. 193, no. 1, pp. 38-47, 1996.
- [9] H. Kasem, S. Bonnamy, Y. Berthier, P. Dufrénoy, and P. Jacquemard, "Tribological, physicochemical and thermal study of the abrupt friction transition during carbon/carbon composite friction", *Wear*, vol. 267, no. 5, pp. 846-852, 2009.
- [10] J. Lancaster and J. Pritchard, "On the 'dusting' wear regime of graphite sliding against carbon", *Journal of Physics D: Applied Physics*, vol. 13, no. 8, p. 1551, 1980.
- [11] R. Gilmore, "La friction des composites carbone-carbone : étude des mécanismes contrôlant le comportement tribologique des matériaux carbonés dans les freins d'avion", 1994.

- [12] M. Di Bartolomeo, A. Lazzari, M. Stender, Y. Berthier, A. Saulot, and F. Massi, "Experimental observation of thermally-driven frictional instabilities on C/C materials", *Tribology International*, vol. 154, 2021.
- [13] D. Tonazzi, F. Massi, L. Baillet, J. Brunetti, and Y. Berthier, "Interaction between contact behaviour and vibrational response for dry contact system", *Mechanical Systems and Signal Processing*, vol. 110, pp. 110-121, 2018.
- [14] G. Chen and Z. R. Zhou, "Correlation of a negative friction–velocity slope with squeal generation under reciprocating sliding conditions", vol. 255, pp. 376-384, 2003.
- [15] N. Hoffmann, M. Fischer, R. Allgaier, and L. Gaul, "A minimal model for studying properties of the mode-coupling type instability in friction induced oscillations", *Mechanics Research Communications*, vol. 29, no. 4, pp. 197-205, 2002.
- [16] A. Meziane, L. Baillet, and B. Laulagnet, "Experimental and numerical investigation of friction-induced vibration of a beam-on-beam in contact with friction", *Applied Acoustics*, vol. 71, no. 9, pp. 843-853, 2010.
- [17] A. Lazzari, D. Tonazzi, G. Conidi, C. Malmassari, A. Cerutti, and F. Massi, "Experimental Evaluation of Brake Pad Material Propensity to Stick-Slip and Groan Noise Emission", *Lubricants*, vol. 6, no. 4, 2018.
- [18] J. Behrendt, C. Weiss, and N. P. Hoffmann, "A numerical study on stick–slip motion of a brake pad in steady sliding", *Journal of Sound and Vibration*, vol. 330, no. 4, pp. 636-651, 2011.
- [19] P. Vielsack, "Stick–slip instability of decelerative sliding", *International Journal of Non-Linear Mechanics*, vol. 36, no. 2, pp. 237-247, 2001.
- [20] T. Richard and E. Detournay, "Stick–slip motion in a friction oscillator with normal and tangential mode coupling", *Comptes Rendus De L Academie Des Sciences Serie Ii Fascicule B-mecanique - C R ACAD SCI SER IIB-MEC*, vol. 328, pp. 671-678, 2000.
- [21] J. Rietsch *et al.*, "Characterizations of C/C composites and wear debris after heavy braking demands", *Carbon*, vol. 47, pp. 85-93, 2009.
- [22] H. Kasem, S. Bonnamy, B. Rousseau, H. Estrade-Szwarckopf, Y. Berthier, and P. Jacquemard, "Interdependence between wear process, size of detached particles and CO₂ production during carbon/carbon composite friction", *Wear*, vol. 263, pp. 1220-1229, 2007.
- [23] J.-C. Rietsch, R. Gadiou, C. Vix-Guterl, and J. Dentzer, "The influence of the composition of atmosphere on the mechanisms of degradation of graphite in planetary ball millers", *Journal of Alloys and Compounds*, vol. 491, no. 1, pp. L15-L19, 2010.

- [24] M. Gouider, "Tribologie des composites Carbone/Carbone: échelles et contributions relatives de la mécanique et de la physico-chimie", Lyon, INSA, 2004.
- [25] B. Yen, "Influence of water vapor and oxygen on the tribology of carbon materials with sp² valence configuration", *Wear*, vol. 192, pp. 208-215, 1996.
- [26] X. Bertran, "Comportement en milieu oxydant d'un composite carbone/carbone pour applications structurales entre 150 et 400° c dans l'aéronautique civile", Université Sciences et Technologies-Bordeaux I, 2013.
- [27] H. O. Pierson, "3 - Graphite Structure and Properties." Oxford: William Andrew Publishing, pp. 43-69, 1993.
- [28] J. J. Zuckerman and J. D. Atwood, *Inorganic Reactions and Methods, Formation of Ceramics*. Wiley, 2009.
- [29] T. Badosz and C. Ania, "Chapter 4 Surface chemistry of activated carbons and its characterization", vol. 7, pp. 159-229, 2006.
- [30] F. Robert, "Study of the tribological behaviour of graphite under inert gases environment Etude du comportement tribologique du graphite sous gaz inertes", Institut National Polytechnique de Lorraine, 1993.
- [31] N. R. Laine, F. J. Vastola, and P. L. Walker, "THE IMPORTANCE OF ACTIVE SURFACE AREA IN THE CARBON-OXYGEN REACTION^{1,2}", *The Journal of Physical Chemistry*, vol. 67, no. 10, pp. 2030-2034, 1963.
- [32] H. P. Boehm, "Some aspects of the surface chemistry of carbon blacks and other carbons", *Carbon*, vol. 32, no. 5, pp. 759-769, 1994.
- [33] S. Ahmed and M. H. Back, "The role of the surface complex in the kinetics of the reaction of oxygen with carbon", *Carbon*, vol. 23, no. 5, pp. 513-524, 1985.
- [34] C. Vix-Guterl, G. Bekri, J. Dentzer, S. Manocha, L. M. Manocha, and P. Ehrburger, "Reactivity in wet air of carbon-carbon composites with treated pitches", *Journal of Analytical and Applied Pyrolysis*, vol. 67, no. 2, pp. 341-357, 2003.
- [35] O. L. Blakslee, D. G. Proctor, E. J. Seldin, G. B. Spence, and T. Weng, "Elastic Constants of Compression-Annealed Pyrolytic Graphite", *Journal of Applied Physics*, vol. 41, no. 8, pp. 3373-3382, 1970.
- [36] P. Bernier and S. Lefrant, *Le Carbone Dans Tous Ses Eacutetats*. Taylor & Francis, 1997.

- [37] D. K. L. Tsang, B. J. Marsden, S. L. Fok, and G. Hall, "Graphite thermal expansion relationship for different temperature ranges", *Carbon*, vol. 43, no. 14, pp. 2902-2906, 2005.
- [38] D. B. Schuepfer *et al.*, "Assessing the structural properties of graphitic and non-graphitic carbons by Raman spectroscopy", *Carbon*, vol. 161, pp. 359-372, 2020.
- [39] M. Alexandre, "Optimization of mechanical behavior of PEKK / Carbon fibers structural composites by PEKK oligomers sizing", 2017.
- [40] N. Yusof and A. Ismail, "Post spinning and pyrolysis processes of polyacrylonitrile (PAN)-based carbon fiber and activated carbon fiber: A review", *Journal of Analytical and Applied Pyrolysis - J ANAL APPL PYROL*, vol. 93, 2011.
- [41] J. Neumeister, S. Jansson, and F. Leckie, "The effect of fiber architecture on the mechanical properties of carbon/carbon fiber composites", *Acta materialia*, vol. 44, no. 2, pp. 573-585, 1996.
- [42] M. Zhang, Z. Su, Z. Xie, J. Chen, and Q. Huang, "Microstructure of pyrocarbon with chemical vapor infiltration", *Procedia Engineering*, vol. 27, pp. 847-854, 2012.
- [43] M. Godet, "The third-body approach: A mechanical view of wear", *Wear*, vol. 100, no. 1, pp. 437-452, 1984.
- [44] M. Godet, "Third-bodies in tribology", *Wear*, vol. 136, no. 1, pp. 29-45, 1990.
- [45] Y. Berthier, "Mécanismes et tribologie", Lyon, INSA, 1988.
- [46] Y. Berthier, "Experimental evidence for friction and wear modelling", *Wear*, vol. 139, no. 1, pp. 77-92, 1990.
- [47] J. Denape, "Third body concept and wear particle behavior in dry friction sliding conditions", in *Key Engineering Materials*, 2015, vol. 640: Trans Tech Publ, pp. 1-12.
- [48] S. Descartes and Y. Berthier, "Rheology and flows of solid third bodies: Background and application to an MoS_{1.6} coating", *Wear*, vol. 252, pp. 546-556, 2002.
- [49] W. Bragg, "An Introduction to Crystal Analysis (Bell, London)", 1928.
- [50] R. H. Savage, "Graphite Lubrication", *Journal of Applied Physics*, vol. 19, no. 1, pp. 1-10, 1948.
- [51] R. H. Savage, "Physically and chemically adsorbed films in the lubrication of graphite sliding contacts", *Annals of the New York Academy of Sciences*, vol. 53, no. 4, pp. 862-869, 1951.

- [52] R. H. Savage and D. L. Schaefer, "Vapor Lubrication of Graphite Sliding Contacts", *Journal of Applied Physics*, vol. 27, no. 2, pp. 136-138, 1956.
- [53] J. K. Lancaster, "A review of the influence of environmental humidity and water on friction, lubrication and wear", *Tribology International*, vol. 23, no. 6, pp. 371-389, 1990.
- [54] J. K. Lancaster and J. R. Pritchard, "The influence of environment and pressure on the transition to dusting wear of graphite", *Journal of Physics D: Applied Physics*, vol. 14, no. 4, pp. 747-762, 1981.
- [55] J. K. Lancaster, "Transitions in the Friction and Wear of Carbons and Graphites Sliding Against Themselves", *A S L E Transactions*, vol. 18, no. 3, pp. 187-201, 1975.
- [56] I. C. Roselman and D. Tabor, "The friction of carbon fibres", *Journal of Physics D: Applied Physics*, vol. 9, no. 17, pp. 2517-2532, 1976.
- [57] B. Yen, "Roles of oxygen in lubrication and wear of graphite in "dusting "and ambient conditions", *Journal of materials science letters*, vol. 14, no. 21, pp. 1481-1483, 1995.
- [58] P. J. M. Carrott, "Adsorption of water vapor by non-porous carbons", *Carbon*, vol. 30, no. 2, pp. 201-205, 1992.
- [59] P. J. Bryant, P. L. Gutshall, and L. H. Taylor, "A study of mechanisms of graphite friction and wear", *Wear*, vol. 7, no. 1, pp. 118-126, 1964.
- [60] J. Chen and C. Ju, "Effect of sliding speed on the tribological behavior of a PAN-pitch carbon-carbon composite", *Materials chemistry and physics*, vol. 39, no. 3, pp. 174-179, 1995.
- [61] B. K. Yen and T. ishihara, "An investigation of friction and wear mechanisms of carbon-carbon composites in nitrogen and air at elevated temperatures", *Carbon*, vol. 34, no. 4, pp. 489-498, 1996.
- [62] H. W. Chang and R. M. Rusnak, "Contribution of oxidation to the wear of carbon-carbon composites", *Carbon*, vol. 16, no. 5, pp. 309-312, 1978.
- [63] C. Blanco, J. Bermejo, H. Marsh, and R. Menendez, "Chemical and physical properties of carbon as related to brake performance", *Wear*, vol. 213, no. 1, pp. 1-12, 1997.
- [64] J.-C. Rietsch, P. Brender, J. Dentzer, R. Gadiou, L. Vidal, and C. Vix-Guterl, "Evidence of water chemisorption during graphite friction under moist conditions", *Carbon*, vol. 55, pp. 90-97, 2013.

- [65] J.-C. Rietsch, J. Dentezer, A. Dufour, F. Schnell, L. Vidal, P. Jacquemard, R. Gadiou and C. Vix-Guterl., "Characterizations of C/C composites and wear debris after heavy braking demands", ed: *Carbon* 47, 2009.
- [66] T. J. Hutton, B. McEnaney, and J. C. Crelling, "Structural studies of wear debris from carbon-carbon composite aircraft brakes", *Carbon*, vol. 37, no. 6, pp. 907-916, 1999.
- [67] K. Peszynsk-Bialczyk, M. Krkoska, A. Pawliczek, P. Filip, and K. Anderson, "Study of Adsorption/Desorption Phenomena on Friction Debris of Aircraft Brakes", 2008.
- [68] M. François, J.-P. Joly, P. Kapsa, and P. Jacquemard, "A temperature-programmed desorption and oxidation investigation of wear debris from carbon/carbon composite aircraft brakes", *Carbon*, vol. 45, pp. 124-131, 2007.
- [69] M. François, "Matériaux composites C/C pour le freinage aéronautique: Elements de compréhension des régimes de frottement et d'usure haut et bas", Ecully, Ecole centrale de Lyon, 2003.
- [70] C. Pevida, P. Jacquemard, and J.-P. Joly, "Physicochemical properties of debris ejected from C/C brakes with different structural orders", *Carbon*, vol. 46, no. 7, pp. 994-1002, 2008.
- [71] I. M. K. Ismail, "Structure and active surface area of carbon fibers", *Carbon*, vol. 25, no. 5, pp. 653-662, 1987.
- [72] H. Amariglio and X. Duval, "Etude de la combustion catalytique du graphite", *Carbon*, vol. 4, no. 3, pp. 323-332, 1966.
- [73] D. W. McKee, "Metal oxides as catalysts for the oxidation of graphite", *Carbon*, vol. 8, no. 5, pp. 623-635, 1970.
- [74] D. W. McKee, "The oxidation of dispersed refractory metal compounds and their behavior as carbon oxidation catalysts", *Carbon*, vol. 24, no. 3, pp. 331-336, 1986.
- [75] A. Yamaguchi, S. Zhang, and J. Yu, "Effect of Refractory Oxides on the Oxidation of Graphite and Amorphous Carbon", *Journal of the American Ceramic Society*, vol. 79, pp. 2509-2511, 2005.
- [76] J. Lee, L. Yun, and J. Park, "Anisotropic properties of needle punched carbon/carbon composites", in *Proceedings of the 18th International Conference on Composite Materials*, 2011.
- [77] G. Peillex, L. Baillet, and Y. Berthier, "Homogenization in non-linear dynamics due to frictional contact", *International Journal of Solids and Structures*, vol. 45, no. 9, pp. 2451-2469, 2008.

- [78] C. Mbodj, "Rôle des paramètres matériaux et structuraux dans l'homogénéisation numérique des composites C/C. Cas des sollicitations tribologiques de freinage", INSA de Lyon, 2011.
- [79] C. Mbodj, G. Peillex, M. Renouf, L. Baillet, Y. Berthier, and P. Jacquemard, "Influence du «contraste» des propriétés élastiques des composites carbone/carbone (C/C) sous conditions dynamiques de contact frottant", *Mechanics & Industry*, vol. 11, no. 3-4, pp. 289-294, 2010.
- [80] M. Champagne, M. Renouf, and Y. Berthier, "Modeling wear for heterogeneous bi-phasic materials using discrete elements approach", *Journal of Tribology*, vol. 136, no. 2, 2014.
- [81] J. Rivière, M. Renouf, and Y. Berthier, "Thermo-Mechanical Investigations of a Tribological Interface", *Tribology Letters*, vol. 58, no. 3, p. 48, 2015.
- [82] J. Brunetti, W. D'Ambrogio, and A. Fregolent, "Friction-induced vibrations in the framework of dynamic substructuring," *Nonlinear Dynamics*, vol. 103, no. 4, pp. 3301-3314, 2021.
- [83] R. A. Ibrahim, "'Friction-Induced Vibration, Chatter, Squeal, and Chaos—Part I: Mechanics of Contact and Friction'," *Applied Mechanics Reviews*, vol. 47, no. 7, pp. 209–226, Jul. 1994.
- [84] M. Stender, M. Di Bartolomeo, F. Massi, and N. Hoffmann, "Revealing transitions in friction-excited vibrations by nonlinear time-series analysis", *Nonlinear Dynamics*, vol. 98, no. 4, pp. 2613-2630, 2019.
- [85] İ. M. Koç and T. Eray, "Modeling frictional dynamics of a visco-elastic pillar rubbed on a smooth surface", *Tribology International*, vol. 127, pp. 187-199, 2018.
- [86] G. Lacerra, M. Di Bartolomeo, S. Milana, L. Baillet, E. Chatelet, and F. Massi, "Validation of a new frictional law for simulating friction-induced vibrations of rough surfaces", *Tribology International*, vol. 121, pp. 468-480, 2018.
- [87] D. Tonazzi, F. Massi, L. Baillet, A. Culla, M. Di Bartolomeo, and Y. Berthier, "Experimental and numerical analysis of frictional contact scenarios: from macro stick–slip to continuous sliding", *Meccanica*, vol. 50, no. 3, pp. 649-664, 2015.
- [88] A. Akay, "Acoustics of friction", *The Journal of the Acoustical Society of America*, vol. 111, no. 4, pp. 1525-1548, 2002.
- [89] M. Di Bartolomeo, F. Massi, L. Baillet, A. Culla, A. Fregolent, and Y. Berthier, "Wave and rupture propagation at frictional bimaterial sliding interfaces: From local to global dynamics, from stick-slip to continuous sliding", vol. 52, pp. 117-131, 2012.

- [90] N. P. Hoffmann and L. Gaul, "Friction Induced Vibrations of Brakes: Research Fields and Activities", SAE Technical Paper, 2008.
- [91] A. Papangelo, M. Ciavarella, and N. Hoffmann, "Subcritical bifurcation in a self-excited single-degree-of-freedom system with velocity weakening–strengthening friction law: analytical results and comparison with experiments", *Nonlinear Dynamics*, vol. 90, no. 3, pp. 2037-2046, 2017.
- [92] J.-J. Sinou, O. Dereure, G. B. Mazet, F. Thouverez, and L. Jezequel, "Friction-induced vibration for an aircraft brake system—Part 1: Experimental approach and stability analysis", vol. 48, no. 5, pp. 536-554, 2006.
- [93] J.-J. Sinou, F. Thouverez, L. Jezequel, O. Dereure, and G. B. Mazet, "Friction induced vibration for an aircraft brake system—Part 2: Non-linear dynamics", *International Journal of Mechanical Sciences*, vol. 48, no. 5, pp. 555-567, 2006.
- [94] J. Brunetti, F. Massi, A. Saulot, M. Renouf, and W. D'Ambrogio, "System dynamic instabilities induced by sliding contact: A numerical analysis with experimental validation", *Mechanical Systems and Signal Processing*, vol. 58-59, pp. 70-86, 2015.
- [95] M. Di Bartolomeo, G. Lacerra, L. Baillet, E. Chatelet, F. Massi, "Parametrical experimental and numerical analysis on friction-induced vibrations by a simple frictional system", *Tribology International*, vol. 112, pp. 47-57.
- [96] P. Xing, L. Guobin, H. Gao, and G. Wang, "Experimental investigation on identifying friction state in lubricated tribosystem based on friction-induced vibration signals", *Mechanical Systems and Signal Processing*, vol. 138, 2020.
- [97] N. S. Eiss, "Frictional Instabilities", Dordrecht, 1998: Springer Netherlands, in *Tribology Issues and Opportunities in MEMS*, pp. 149-156.
- [98] G. Ouenzerfi, F. Massi, E. Renault, and Y. Berthier, "Squeaking friction phenomena in ceramic hip endoprosthesis: Modeling and experimental validation", *Mechanical Systems and Signal Processing*, vol. 58-59, pp. 87-100, 2015.
- [99] F. Massi, Y. Berthier, and L. Baillet, "Contact surface topography and system dynamics of brake squeal", *Wear*, vol. 265, no. 11, pp. 1784-1792, 2008.
- [100] A. Le Bot, "Noise of sliding rough contact", *Journal of Physics: Conference Series*, vol. 797, 2017.
- [101] H. Ben Abdelounis, A. Le Bot, J. Perret-Liaudet, and H. Zahouani, "An experimental study on roughness noise of dry rough flat surfaces", *Wear*, vol. 268, no. 1, pp. 335-345, 2010.

- [102] M. O. Othman, A. H. Elkholy, and A. A. Seireg, "Experimental investigation of frictional noise and surface-roughness characteristics", *Experimental Mechanics*, vol. 30, no. 4, pp. 328-331, 1990.
- [103] A. Lazzari, D. Tonazzi, and F. Massi, "Squeal propensity characterization of brake lining materials through friction noise measurements", *Mechanical Systems and Signal Processing*, vol. 128, pp. 216-228, 2019.
- [104] J.-J. Sinou and L. Jézéquel, "Mode coupling instability in friction-induced vibrations and its dependency on system parameters including damping", *European Journal of Mechanics - A/Solids*, vol. 26, no. 1, pp. 106-122, 2007.
- [105] D. Tonazzi, F. Massi, A. Culla, L. Baillet, A. Fregolent, and Y. Berthier, "Instability scenarios between elastic media under frictional contact", *Mechanical Systems and Signal Processing*, vol. 40, no. 2, pp. 754-766, 2013.
- [106] J. Brunetti, F. Massi, W. d'Ambrogio, and Y. Berthier, "Numerical investigation on the mode coupling contact dynamic instabilities", in *XXI Congresso Associazione Italiana di Meccanica Teorica e Applicata (AIMETA 2013)*, 2013.
- [107] R. A. Ibrahim, "Friction-induced vibration, chatter, squeal, and chaos—part II: dynamics and modeling", 1994.
- [108] A. Akay, O. Giannini, F. Massi, and A. Sestieri, "Disc brake squeal characterization through simplified test rigs", *Mechanical systems and signal processing*, vol. 23, no. 8, pp. 2590-2607, 2009.
- [109] B. Hervé, J.-J. Sinou, H. Mahé, and L. Jézéquel, "Analysis of squeal noise and mode coupling instabilities including damping and gyroscopic effects", *European Journal of Mechanics - A/Solids*, vol. 27, no. 2, pp. 141-160, 2008.
- [110] Y. K. Wu, B. Tang, Z. Y. Xiang, H. H. Qian, J. L. Mo, and Z. R. Zhou, "Brake squeal of a high-speed train for different friction block configurations", *Applied Acoustics*, vol. 171, 2021.
- [111] A. H. Dweib and A. F. D'Souza, "Self-excited vibrations induced by dry friction, part 1: Experimental study", *Journal of Sound and Vibration*, vol. 137, no. 2, pp. 163-175, 1990.
- [112] Y. Yuan, "A Study of the Effects of Negative Friction-Speed Slope on Brake Squeal", in *ASME 1995 Design Engineering Technical Conferences collocated with the ASME 1995 15th International Computers in Engineering Conference and the ASME 1995 9th Annual Engineering Database Symposium*, 1995, vol. Volume 3A: 15th Biennial Conference on Mechanical Vibration and Noise — Vibration of Nonlinear, Random, and Time-Varying Systems, pp. 1153-1162.

- [113] G. X. Chen and Z. R. Zhou, "Correlation of a negative friction–velocity slope with squeal generation under reciprocating sliding conditions", *Wear, 14th International Conference on Wear of Materials*, vol. 255, no. 1, pp. 376-384, 2003.
- [114] H. Hetzler, "On the effect of nonsmooth Coulomb friction on Hopf bifurcations in a 1-DoF oscillator with self-excitation due to negative damping", *Nonlinear Dynamics*, vol. 69, no. 1, pp. 601-614, 2012.
- [115] Y. Ida, "Analysis of stick-slip and earthquake mechanism", *Physics of the Earth and Planetary Interiors*, vol. 11, no. 2, pp. 147-156, 1975.
- [116] R. E. Goodman and P. N. Sundaram, "Fault and system stiffnesses and stick-slip phenomena", *pure and applied geophysics*, vol. 116, no. 4, pp. 873-887, 1978.
- [117] S. Casado, "Studying friction while playing the violin: exploring the stick-slip phenomenon", *Beilstein journal of nanotechnology*, vol. 8, pp. 159-166, 2017.
- [118] D. W. Lee, X. Banquy, and J. N. Israelachvili, "Stick-slip friction and wear of articular joints", *Proceedings of the National Academy of Sciences*, vol. 110, no. 7, p. E567, 2013.
- [119] W. Owen and E. Croft, "The reduction of stick-slip friction in hydraulic actuators", *Mechatronics, IEEE/ASME Transactions on*, vol. 8, pp. 362-371, 2003.
- [120] S. W. Yoon, M. Shin, W. G. Lee, and H. Jang, "Effect of surface contact conditions on the stick–slip behavior of brake friction material", *Wear*, vol. s 294–295, pp. 305–312, 2012.
- [121] H. Jang, J. S. Lee, and J. W. Fash, "Compositional effects of the brake friction material on creep groan phenomena", *Wear, 13th International Conference on Wear of Materials*, vol. 251, no. 1, pp. 1477-1483, 2001.
- [122] M. North, *Disc brake squeal: a theoretical model*. MIRA Nuneaton, 1972.
- [123] N. Hoffmann and L. Gaul, "Effects of damping on mode-coupling instability in friction induced oscillations", *ZAMM-Journal of Applied Mathematics and Mechanics/Zeitschrift für Angewandte Mathematik und Mechanik: Applied Mathematics and Mechanics*, vol. 83, no. 8, pp. 524-534, 2003.
- [124] U. von Wagner, D. Hochlenert, and P. Hagedorn, "Minimal models for disk brake squeal", *Journal of Sound and Vibration*, vol. 302, no. 3, pp. 527-539, 2007.
- [125] L. Charroyer, O. Chiello and J.-J. Sinou, "Parametric study of the mode coupling instability for a simple system with planar or rectilinear friction", *Journal of Sound and Vibration*, vol. 384, pp. 94-112, 2016.

- [126] K. Popp, "Modelling and control of friction-induced vibrations", *Mathematical and Computer Modelling of Dynamical Systems*, vol. 11, no. 3, pp. 345-369, 2005.
- [127] J. Brunetti, F. Massi, W. D'Ambrogio, and Y. Berthier, "Dynamic and energy analysis of frictional contact instabilities on a lumped system", *Meccanica*, vol. 50, no. 3, pp. 633-647, 2015.
- [128] M. North, "Disc brake squeal. Braking of Road Vehicles, Automobile Division of the Institution of Mechanical Engineers", ed: Mechanical Engineering Publications Limited, London, England, 1976.
- [129] F. Massi, A. Saulot, M. Renouf, and G. Messenger, "Simulation of dynamic instabilities induced by sliding contacts", in *DINAME 2013*, Brazil, 2013.
- [130] A. Meziane, S. D'Errico, L. Baillet, and B. Laulagnet, "Instabilities generated by friction in a pad-disc system during the braking process", *Tribology International*, vol. 40, no. 7, pp. 1127-1136, 2007.
- [131] S. W. E. Earles and C. K. Lee, "Instabilities Arising From the Frictional Interaction of a Pin-Disk System Resulting in Noise Generation", *Journal of Engineering for Industry*, vol. 98, no. 1, pp. 81-86, 1976.
- [132] R. Allgaier, L. Gaul, W. Keiper, and K. Willner, "Mode Lock-in And Friction Modelling", *WIT transactions on engineering sciences*, vol. 24, 1970.
- [133] A. Tuchinda, N. Hoffmann, D. Ewins, and W. KELPER, "Mode lock-in characteristics and instability study of the pin-on-disc system", in *Proceedings of SPIE, the International Society for Optical Engineering*, 2001, vol. 4359: Society of Photo-Optical Instrumentation Engineers, pp. 71-77.
- [134] F. Massi and O. Giannini, "slightEffect of damping on the propensity of squeal instability: An experimental investigation", *The Journal of the Acoustical Society of America*, vol. 123, no. 4, pp. 2017-2023, 2008.
- [135] F. Cantone and F. Massi, "A numerical investigation into the squeal instability: Effect of damping", *Mechanical Systems and Signal Processing*, vol. 25, no. 5, pp. 1727-1737, 2011.
- [136] C. Weiss, P. Gdaniec, N. P. Hoffmann, A. Hothan, G. Huber, and M. M. Morlock, "Squeak in hip endoprosthesis systems: An experimental study and a numerical technique to analyze design variants", *Medical Engineering & Physics*, vol. 32, no. 6, pp. 604-609, 2010.
- [137] H. Mills, *Brake squeak*. Institution of Automobile Engineers, 1938.

- [138] D. Sinclair, "Frictional vibrations", *Journal of Applied Mechanics*, 1955.
- [139] R. Fosberry and Z. Holubecki, *Disc brake squeal: its mechanism and suppression*. Motor Industry Research Association, 1961.
- [140] K. Shin, M. J. Brennan, J. E. Oh, and C. J. Harris, "ANALYSIS OF DISC BRAKE NOISE USING A TWO-DEGREE-OF-FREEDOM MODEL", *Journal of Sound and Vibration*, vol. 254, no. 5, pp. 837-848, 2002.
- [141] J. Kang, "Parametric study on friction-induced coupled oscillator", *Proceedings of The Institution of Mechanical Engineers Part C-journal of Mechanical Engineering Science - PROC INST MECH ENG C-J MECH E*, vol. 222, pp. 1381-1387, 2008.
- [142] H. Ouyang, J. E. Mottershead, M. P. Cartmell, and M. I. Friswell, "FRICTION-INDUCED PARAMETRIC RESONANCES IN DISCS: EFFECT OF A NEGATIVE FRICTION-VELOCITY RELATIONSHIP", *Journal of Sound and Vibration*, vol. 209, no. 2, pp. 251-264, 1998.
- [143] I. Ghezzi, D. Tonazzi, M. Rovere, C. Le Coeur, Y. Berthier, and F. Massi, "Tribological investigation of a greased contact subjected to contact dynamic instability", *Tribology International*, vol. 143, 2020.
- [144] I. Ghezzi, D. Tonazzi, M. Rovere, C. Le Coeur, Y. Berthier, and F. Massi, "Frictional behaviour of a greased contact under low sliding velocity condition", *Tribology International*, vol. 155, p. 106788, 2021.
- [145] S. M. Rubinstein, G. Cohen, and J. Fineberg, "Dynamics of Precursors to Frictional Sliding", *Physical Review Letters*, vol. 98, no. 22, p. 226103, 2007.
- [146] G. G. Adams, "Self-Excited Oscillations of Two Elastic Half-Spaces Sliding With a Constant Coefficient of Friction", *Journal of Applied Mechanics*, vol. 62, no. 4, pp. 867-872, 1995.
- [147] G. G. Adams, "Steady Sliding of Two Elastic Half-Spaces With Friction Reduction due to Interface Stick-Slip", *Journal of Applied Mechanics*, vol. 65, no. 2, pp. 470-475, 1998.
- [148] Y. Ben-Zion, "Dynamic ruptures in recent models of earthquake faults", *Journal of the Mechanics and Physics of Solids*, vol. 49, no. 9, pp. 2209-2244, 2001.
- [149] H. Blok, "Fundamental aspects of boundary friction", *J. SAE*, vol. 46, p. 275, 1940.
- [150] B. C. Derjagin, V. E. Push and D. M. Tolstoi, "A Theory of Stick-Slip Sliding of Solids", ed: Proc. Conference on Lubrication and Wear, London, 1957.

- [151] A. K. Banerjee, "Influence of kinetic friction on the critical velocity of stick-slip motion", vol. 12, no. 2, pp. 107-116, 1968.
- [152] B. R. Singh, "Study of Critical Velocity of Stick-Slip Sliding", *Journal of Engineering for Industry*, vol. 82, no. 4, pp. 393-398, 1960.
- [153] J. Brecht, W. Hoffrichter, and A. Dohle, "Mechanisms of Brake Creep Groan", *SAE Transactions*, vol. 106, pp. 3405-3411, 1997.
- [154] X. C. Wang, B. Huang, R. L. Wang, J. L. Mo, and H. Ouyang, "Friction-induced stick-slip vibration and its experimental validation", vol. 142, 2020.
- [155] M. T. Bengisu and A. Akay, "Stick-slip oscillations: Dynamics of friction and surface roughness", *The Journal of the Acoustical Society of America*, vol. 105, no. 1, pp. 194-205, 1999.
- [156] F. Van De Velde and P. De Baets, "Mathematical approach of the influencing factors on stick-slip induced by decelerative motion", *Wear*, vol. 201, no. 1, pp. 80-93, 1996.
- [157] Z. Fuadi, S. Maegawa, K. Nakano, and K. Adachi, "Map of low-frequency stick-slip of a creep groan", *Proceedings of the Institution of Mechanical Engineers, Part J: Journal of Engineering Tribology*, vol. 224, no. 12, pp. 1235-1246, 2010.
- [158] B. Feeny, A. Guran, N. Hinrichs, and K. Popp, "An historical review on friction in nonlinear dynamics", *App. Mech. Rev.*, vol. 51, no. 5, pp. 321-341, 1998.
- [159] R. Nachane, G. Hussain, and K. Iyer, "Theory of stick-slip effect in friction", *Indian Journal of Fibre & Textile Research*, 1998.
- [160] J. Juel Thomsen and A. Fidlin, "Analytical approximations for stick-slip vibration amplitudes", *International Journal of Non-Linear Mechanics*, vol. 38, no. 3, pp. 389-403, 2003.
- [161] X. C. Wang, B. Huang, R. L. Wang, J. L. Mo, and H. Ouyang, "Friction-induced stick-slip vibration and its experimental validation", *Mechanical Systems and Signal Processing*, vol. 142, 2020.
- [162] A. Lazzari and A. Bessette, *Rapport d'Expertise (DEx 2020-06)*, 2020.
- [163] L. Hamza, *Note technique (WB/TMF 21-011)*, 2020.
- [164] M. D. Bartolomeo, D. Tonazzi, F. Massi, and Y. Berthier, *RESEARCH PROJECT*, 2016.

- [165] F. Massi, O. Giannini, and L. Baillet, "Brake squeal as dynamic instability: an experimental investigation", *The Journal of the Acoustical Society of America*, vol. 120, no. 3, pp. 1388-1398, 2006.
- [166] B. Ding, G. Squicciarini, D. Thompson, and R. Corradi, "An assessment of mode-coupling and falling-friction mechanisms in railway curve squeal through a simplified approach", *Journal of Sound and Vibration*, vol. 423, pp. 126-140, 2018.
- [167] O. Giannini, A. Akay, and F. Massi, "Experimental analysis of brake squeal noise on a laboratory brake setup", *Journal of Sound and Vibration*, vol. 292, no. 1, pp. 1-20, 2006.
- [168] M. D. Bartolomeo, D. Tonazzi, F. Massi, and Y. Berthier, *RESEARCH PROJECT* 2017.
- [169] F. Massi, L. Baillet, O. Giannini, and A. Sestieri, "Brake squeal: Linear and nonlinear numerical approaches", *Mechanical Systems and Signal Processing*, vol. 21, no. 6, pp. 2374-2393, 2007.
- [170] K. Urita, K. Suenaga, T. Sugai, H. Shinohara, and S. Iijima, "In situ observation of thermal relaxation of interstitial-vacancy pair defects in a graphite gap", *Physical review letters*, vol. 94, no. 15, 2005.
- [171] Y. A. Zarifyanz, V. F. Kiselev, N. N. Lezhnev, and O. V. Nikitina, "Interaction of graphite fresh surface with different gases and vapours", *Carbon*, vol. 5, no. 2, pp. 127-135, 1967.

Annexes

I. SEM/EDX analysis of C/C specimens

The friction surfaces of C/C samples machined from used C/C brake discs with and without contaminants have been analyzed through SEM/EDX. An example of analysis carried out on a MAT1 sample has been already shown in {2.1.2}. Figure 77, Figure 78 and Figure 79 show examples of SEM pictures for the MAT4, MAT2 and MAT3, respectively. Each SEM picture has been obtained through secondary electrons.



Figure 77. Example of SEM/EDX analysis carried out on the contact surface of a specimen machined from a MAT4. SEM picture taken at a scale of 1 mm through secondary electrons.

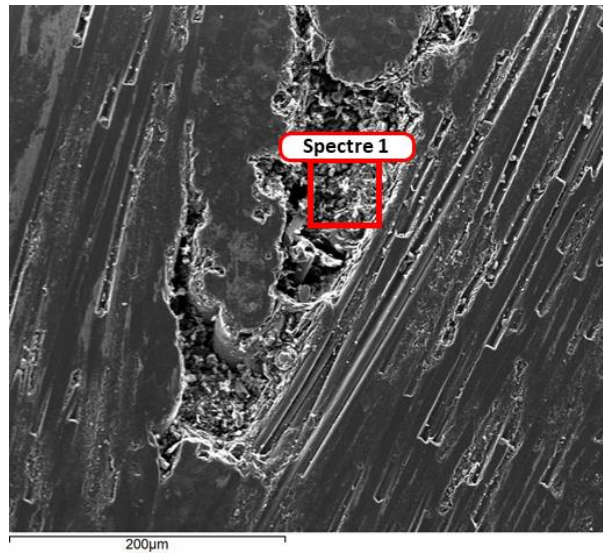


Figure 78. Example of SEM/EDX analysis carried out on the contact surface of a specimen machined from a MAT2 disc. SEM picture taken at a scale of 200 μm through secondary electrons.

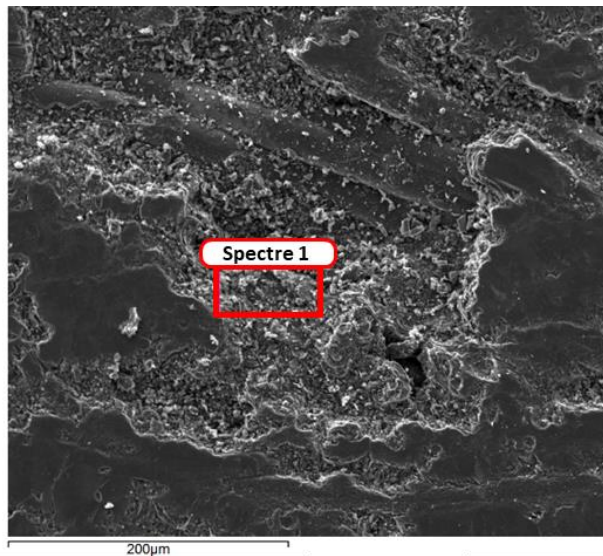


Figure 79. Example of SEM/EDX analysis carried out on the contact surface of a specimen machined from a MAT3 disc. SEM picture taken at a scale of 200 μm through secondary electrons.

The contaminating particles found on the friction surface of the specimens are consistent with those described in {2.1.2, Table 2}.

Moreover, no contaminants have been found on the MAT4. Further details on the analysis of the contaminants found on the contact surface of C/C specimens machined from the brake discs can be found in [162, 163].

II. Comparison between *sliding* and *static heating* tests

As stated in {2.1.3}, *static heating* tests have been considered only in the preliminary protocol, as no significant differences between the *static heating* and *sliding heating* tests have been observed under the same imposed velocity profile and once the maximum temperature of the test is achieved. In this respect, Figure 80 shows an example of comparison between *sliding* (left) and *static* (right) *heating* tests carried out at variable imposed velocity (20 to 0 mm/s) and at a maximum temperature of 500 °C, for the samples machined from a MAT2 disc. Colored bars indicate the onset of dynamic instabilities. Peach-colored bars denoted the presence of a slight negative friction-velocity slope when the unstable friction-induced vibrations are observed. Violet bars denote a dynamic instability in presence of an almost constant friction coefficient, which suggests the occurrence of a mode coupling. When the bars are bordered in black, the specific phenomenon is observed on both back-and-forth strokes. Otherwise, the phenomenon is observed only on single strokes.

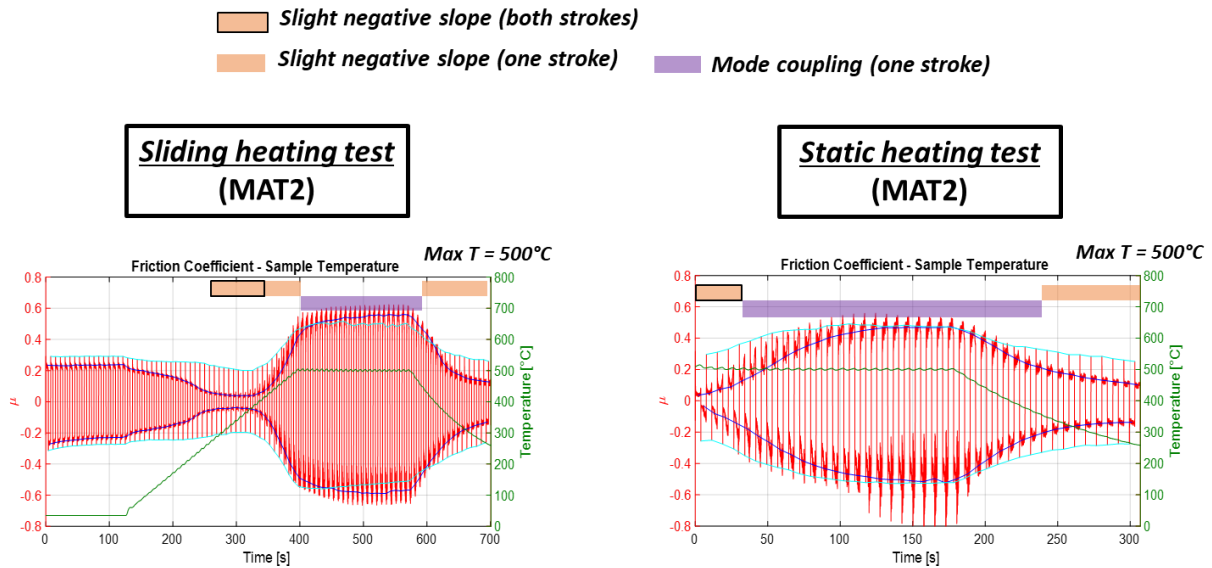


Figure 80. Comparison between sliding (left) and static (right) heating tests carried out at variable imposed velocity ($20 \rightarrow 0$ mm/s) and at a maximum temperature of 500 °C, for the sample pairs machined from a MAT2 disc. The bars denote the occurrence of dynamic instabilities in presence of a slight negative friction-velocity slope (peach-colored bars) and in presence of a constant friction coefficient (violet bars). If the bars are bordered in black, the phenomenon is observed on both back-and-forth strokes, otherwise it is observed only on single strokes. The friction coefficient is in red, the DFC is in blue, the SFC is in cyan and the temperature is in green.

As can be seen from Figure 80, in the *sliding heating* test, once the maximum temperature of 500 °C is reached, the high level of DFC with respect to the SFC prevents the occurrence of the negative friction-velocity slope instability. However, the occurrence of mode coupling, favored by the high friction coefficient, is observed. A detailed description of the DFC and SFC evolution as a function of the different temperatures is provided in {2.2.2}.

A similar behavior of both the frictional and vibrational response of the tested material, at 500 °C, can be noticed in the *static heating* test. In this case, the sliding motion starts only after that the maximum temperature of 500 °C is reached. It can be observed that, at the beginning of the test, the DFC is significantly lower than the SFC and a dynamic instability due to a slight negative friction-velocity slope is promoted. While the temperature is kept constant at 500 °C, the DFC increases progressively and after almost 2 minutes it reaches a steady state condition. It can be noticed that after only about 30 s of sliding motion, the high level of the DFC prevents the onset of the negative friction-velocity slope instability. Such as for the *sliding heating* test, the presence of mode coupling is observed. The significant increase of the DFC at 500 °C, before reaching the steady state condition, highlights the significant role played by the rheology, which strongly affect the frictional response of the C/C material. However, once the steady state condition is achieved, no remarkable differences can be observed between the *static* and *sliding heating* tests. A similar behavior of both the frictional and vibrational response can be observed also during the natural cooling.

III. Comparison between first and fourth day of the preliminary protocol

The fourth day of the preliminary protocol adopted for the TriboAir experimental campaign has been removed, because no differences have been observed between the tests carried out at the maximum temperature of 500 °C, at constant velocity, at the begin (first day) and at the end (fourth day) of the protocol. As an example, in Figure 81, a comparison between the sliding heating tests at 500 °C and constant imposed velocity (20 mm/s), related to a MAT1 sample pair, is shown.

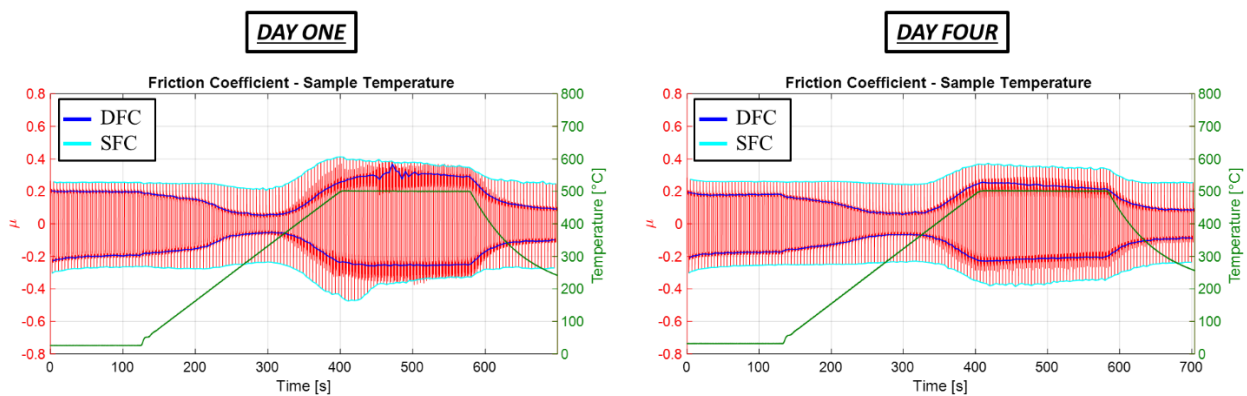


Figure 81. Comparison between the frictional responses of the MAT1 during sliding heating tests carried out at constant sliding velocity (20 mm/s) and at a maximum temperature of 500 °C, at the first and fourth day of the preliminary protocol. In red the friction coefficient, in blue the DFC, in cyan the SFC and in green the temperature.

As can be seen in Figure 81, the evolution of the frictional response is almost equal at the different temperature conditions in both day one and four of the protocol. At room temperature condition the DFC and the SFC are equal to about 0.2 and 0.25, respectively. Increasing the temperature up to around 300 °C, the SFC remains almost constant while the DFC decreases significantly and becomes lower than 0.1. For higher temperatures, both the SFC and DFC increase and becomes higher than the room temperature values. However, the DFC remains always lower than the SFC. These results are consistent with the variable imposed velocity tests (from 20 to 0 mm/s in each stroke) and also prove a good repeatability of the measurement.

IV. Comparison between C/C specimens coated with a lower amount of Ox and Oy

Further tests on C/C specimens painted with a lower amount of Ox and Oy have been carried out in order to investigate the frictional and vibrational response of the C/C samples also in presence

of a different amount of contaminants taking part in the rheology of the contact interface. A comparison between the *sliding heating* tests carried out at variable imposed velocity (20→0 mm/s) and at a maximum temperature of 500 °C, for both the Ox3-Ox4 and Oy3-Oy4 pairs (see {4.1.1}, Table 11), is shown in Figure 82. The insets are related to the friction coefficient and the accelerometer signal recorded during single strokes at 500 °C of the C/C samples with Ox (left) and with Oy (right).

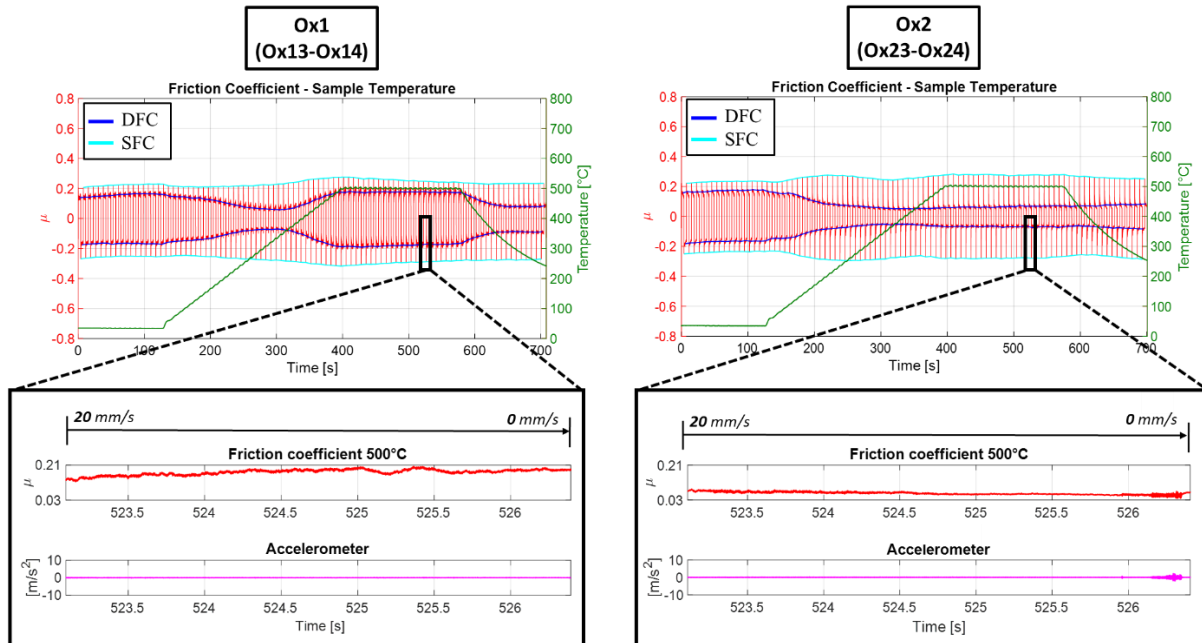


Figure 82. Comparison between the frictional responses of Ox3-Ox4 (left) and Oy3-Oy4 (right), during sliding heating tests carried out at variable imposed velocity (20→0 mm/s) and at a maximum temperature of 500 °C. In red the friction coefficient, in blue the DFC, in cyan the SFC and in green the temperature. In the insets, a comparison between the friction coefficient and the accelerometer signal of two single strokes, taken at 500 °C, of the Ox3-Ox4 (left) and Oy3-Oy4 (right) sample pairs.

The frictional response of the tested materials is characterized by a decrease of the DFC up to almost 200-300 °C. For temperatures higher than almost 300-400°C, only the C/C samples with Ox shows a significant increase of the DFC, which reaches value slightly higher than the room temperature ones. Conversely, the increase of the DFC for the C/C samples with Oy is barely noticeable and the friction coefficient remains significantly lower compared to the room temperature condition. Moreover, by looking at the insets of Figure 82, a similar behavior to the one described in Figure 60 is observed. Specifically, for the C/C material with Ox no dynamic instabilities occur and the friction coefficient is almost constant toward the end of braking. On the other hand, a slight negative friction-velocity slope is observed for the C/C material with Oy as well as the onset of a dynamic instability.

The obtained results are consistent with those shown for the Ox1-Ox2 and Oy1-Oy2 pairs. This outcome not only proves a good repeatability of the measurements, but also demonstrates that a lower amount of contaminants can equally affect the tribological behavior of C/C materials.



FOLIO ADMINISTRATIF

THESE DE L'UNIVERSITE DE LYON OPEREE AU SEIN DE L'INSA LYON

NOM : LAZZARI DATE de SOUTENANCE : 28/02/2022

Prénoms : Alessandro

TITRE : Vibrational and frictional aptitude of C/C materials in presence of a rheological and physico-chemical active interface

NATURE : Doctorat Numéro d'ordre : 2022LYSEI009

Ecole doctorale : MEGA

Spécialité : Génie Mécanique

RESUME :

Nowadays, the growing interest in carbon-carbon (C/C) composites, in a significant number of industrial contexts, has led to a major increase of research works aimed to investigate such materials. Being C/C composites used in many industrial applications, such as high-performance disc brakes, considerable numbers of studies focus on their tribological properties. Nevertheless, despite the large amount of works dealing with this topic, very few researches have been carried out so far on the relationship between the C/C frictional response and the onset of unstable friction-induced vibrations, as a function of the main contact parameters (e.g. sliding velocity, temperature, contact pressure, etc.). However, understanding and predicting the occurrence of undesired vibrational phenomena, taking place during frictional contact of C/C composites, is one of the greatest challenges in order to improve the overall braking performance.

In this regard, the study of friction-induced vibrations involves multiple scientific fields, especially considering the complex physiochemical characteristics of C/C composites and the strong influence of the operating conditions on the frictional response of such materials. Moreover, the significant impact of the third body on their tribological behavior requires a deep insight of the rheological mechanisms affecting the friction coefficient and the occurrence of contact dynamic instabilities.

Within this research framework, the present PhD thesis aims to investigate and characterize the onset of unstable friction-induced vibrations of C/C materials, under different contact conditions. Their frictional response and its relationship with the occurrence of dynamic instabilities have been investigated on linear tribometers aimed to characterize C/C specimens, under controlled boundary conditions. The specifically designed test benches have allowed studying the frictional and vibrational response of C/C samples, with particular attention on the role of temperature, up to almost 500 °C,

sliding velocity and test environment. Meaningful information, so far missing in the literature, concerning the nature and the main characteristics of the dynamic instabilities caused by C/C materials in frictional contact, are presented in this work. Moreover, numerical models have been developed, in order to investigate the main features of the different vibrational phenomena. In this respect, the present work proposes a novel approach, based on the analysis of the phase shift between vibrational signals, in order to distinguish the onset of mode coupling or negative friction-velocity slope instabilities, as well as the coexistence of both phenomena.

Particular attention is also given to the role of the third body and its rheological contribution. The effect of metallic and non-metallic contaminants has been investigated as well, by contaminating the frictional surface of C/C material samples, tested under controlled boundary conditions. The relationship between the rheological contribution to the frictional response and the onset of dynamic instabilities in presence of distinct boundary conditions has been then investigated. The obtained results have allowed developing different scenarios describing the C/C tribological behavior and the occurrence of unstable friction-induced vibrations, taking into account the rheology of the contact during braking.

This PhD thesis has been carried out in collaboration between the Sapienza University of Rome, at the Department of Mechanical and Aerospace Engineering (Rome, Italy) and the Institut National des Sciences Appliquées (INSA) of Lyon, at the laboratory LaMCoS (Lyon, France).

MOTS-CLÉS : C/C materials, Friction-induced vibrations, Contact instabilities, Contact rheology

Laboratoire (s) de recherche :

- Laboratoire de Mécanique de Contact et des Structures (LaMCoS) UMR CNRS 5259-INSA de Lyon, France

- Dipartimento di Ingegneria Meccanica e Aerospaziale (DIMA), La Sapienza-Università di Roma, Rome, Italy

Directeur de thèse:

SAULOT Aurélien, Professeur, Insa de Lyon

MASSI Francesco, Professeur, Sapienza University of Rome

Président de jury :

BUENO Marie-Ange, Professeure, Université de Haute-Alsace

Composition du jury :

Bueno, Marie-Ange	Professeure	Université de Haute-Alsace	Présidente
Meziane, Anissa	Professeure	Université de Bordeaux	Rapporteuse
Renouf, Mathieu	Chargé de Recherche	Université de Montpellier	Rapporteur
Baillet, Laurent	Professeur	Université Grenoble Alpes	Examineur
Gadiou, Roger	Professeur	Université de Haute-Alsace	Examineur
Akay, Adnan	Professeur	Bilkent University	Examineur

Saulot, Aurélien	Professeur	Insa de Lyon	Directeur de thèse
Massi, Francesco	Professeur	Sapienza University of Rome	Directeur de thèse
Dubois, Sandra	Ingénieure	Safran Landing Systems	Invitée